CONFORMATIONAL STUDIES OF THE DOMAINS AND SUBUNITS OF THE HIGH AFFINITY IgE RECEPTOR BY NMR AND MOLECULAR MODELLING

by

Mire Zloh

A thesis submitted in partial fulfilment of the requirements for the degree of

DOCTOR OF PHILOSOPHY

(Faculty of Science)

at the

SCHOOL OF PHARMACY, UNIVERSITY OF LONDON

1999

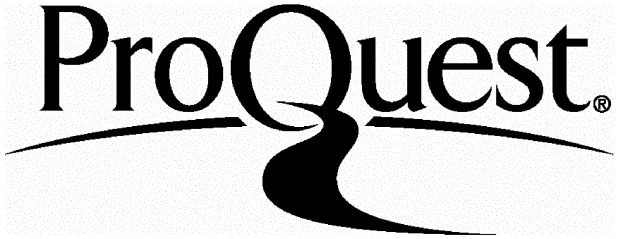

ABSTRACT

The sequence of the high affinity integral membrane receptor for immunoglobulin E, designated as FcεRI, led to the proposal that it was an $\alpha\beta\gamma_2$ with seven transmembrane helices. The latter were connected by three loop peptides. FcεRI had five cytoplasmic and one extracellular domain peptides. Except for the seven transmembrane helices most of these peptides were synthesized and their solution structure determined, whole or in part, by a combination of circular dichroism, Fourier transform infrared and multidimensional nuclear magnetic resonance spectroscopy. This experimentally-derived structural data base then served as a basis for calculating the structures of subunits, especially the β-subunit of FcεRI.

To improve these determinations of the 3D structure, the arrangement of the transmembrane helices of the FcεRI was studied using molecular modelling. Specifically, protein docking methods were used to study the interaction between all transmembrane helices of the FcεRI and to establish the favourable helix surfaces for helix - helix contacts. This objective procedure led to the proposal that the transmembrane domain of the β-subunit consisted of a four helix bundle.

Further information was needed to determine the 3D structure of the receptor and its subunits, specifically which helix surfaces favoured hydrophobic interactions with membrane lipids. Molecular mechanics was used to predict the relative lipid - transmembrane helix interacting surfaces. The interaction of dodecane and palmitic fatty acid with transmembrane helices led to mapping of the relative hydrophobic surfaces on these helices. This type of experiment successfully predicted the lipid-helix interaction surfaces which were in agreement with those found in the crystal structure of the *Bacteriorhodopsin.* It fully supported mapping of the hydrophobic surfaces and fatty acid interaction sites of all six different transmembrane helices of the IgE receptor.

By experimentally elucidating the conformational components of domain peptides within the FcεRI, it has therefore been possible to have an improved understanding of the structural interactions between receptor peptides, and between receptor peptides and lipids, and to model the conformation of the receptor subunits. The final 3D structures of the β-subunit were calculated by molecular dynamics using: a) NMR-based loop peptide structure; b) calculated helix-helix interactions; and c) mapping of lipid-helix interactions. The proposed structure of the β-subunit had the repeated conformational motif (transmembrane helix - turn - loop helix - bend - transmembrane helix).

Мама, тата,
Верона,
Ања и Оља
хвала вам
за сву љубав и
бескрајну подршку.

To Mum and Dad,
Verona,
Anja and Olja
thank you for
all your love and
everlasting support.

ACKNOWLEDGEMENT

First of all I would like to thank to my supervisor Professor William A. Gibbons for his constant help, advice and support throughout the whole period of my studies. I would also like to thank to the School of Pharmacy for accepting me as a part-time student. Many people from the School helped me during this long, but never boring period. Andy, Gill, Viv, David, Derek, Kevin, Keith, Lionel, Mac, Malcolm, Roy, Rob, were always helpful. Colin, remember the responsibility, we are not allowed to be too funny.

My colleagues in basement deserve a special place, Jelena, Jo, Lily, Manuela, Pascale, Arturo, Dave, Diego, Mark, Mike, Paul, thanks a lot for coffee, help, friendship and hours and hours of fun. Wilf, thank you for all your help and trouble that you have had with me.

I am grateful to Dr Harold Toms and Peter Haycock for the help with the 600 MHz NMR, Dr Alex Drake and Dr Guilliano Siligardi for the use of the CD spectroscopy facility

Advice for the PhD survival - go to the UCL Aikido Club. Most of my stress was released on the mat, while practicing with Barbara Sensei, Chin-Tao, Barry, Keith, Mark, Raja, Rob, and many others who were willing to be thrown around. My deepest respect to Mr Smith Sensei, and all friends in United Kingdom Aikikai. Mark, thanks again for sorting out all my hardware problems at home.

I have to mentioned friends here in London, Dejana, Emina, Tamara, Drago, Jova and Koya, and people in Belgrade who kept in touch, while I am so far away from home, Zdenko, Jovana, Nemanja, Višnja, my in-laws, Professor Ivan Juranić, Ivanka, Aca, Joca, Saša, and many others that are in my heart.

TABLE OF CONTENTS

Abstract 2

Table of contents 5

List of figures 9

List of tables 15

List of abbreviations 17

1. Introduction 20

1.1 Immune system and allergy 21

1.2 High affinity IgE receptor 24

1.3 Membrane protein structure determination 27

1.3.1 Domains and subunits 31

1.3.2 CD spectroscopy 33

1.3.3 NMR spectroscopy 36

1.4 Molecular modelling 40

1.4.1 Molecular mechanics 41

1.4.2 Molecular dynamics 43

1.4.3 Protein docking 45

1.5 Aim of the work 46

2. Conformational studies of the connecting loop 2-3 peptide of the β-subunit of the high affinity IgE receptor 47

2.1 Background 48

2.2 Material and Methods 51

2.2.1 Circular Dichroism 51

2.2.2 NMR Spectroscopy 51

2.2.3 Structure Calculations 53

2.3 Results and Discussion 54

2.3.1 Circular dichroism spectroscopy of loop 2-3 54

2.3.2 NMR Spectroscopy of loop 2-3 60
2.4 NMR Based Molecular Modelling 79
2.4.1 Loop 2-3 in 90 % H_2O / 10 % D_2O - Conformational State I 79
2.4.2 Loop 2-3 in 40 % H2O / 60 % TFE-d2 - Conformational State II 83
2.4.3 Loop 2-3 in TFE - Conformational State III 84
2.4 Summary 92
3.Conformational studies of the connecting loop 1-2 peptide of the β-subunit of the high affinity IgE receptor 96
3.1 Background 97
3.2 Material and Methods 99
3.2.1 CD Spectroscopy 99
3.2.2 NMR Spectroscopy 99
3.2.3 NMR Based Molecular Modelling 100
3.3 Results and Discussion 101
3.3.1 Electronic Circular Dichroism Studies on Loop 1-2 101
3.3.2 NMR Studies of the Loop 1-2 105
3.3.3 NMR Based Structure Calculations of the Loop 1-2 120
3.3.4 Overall Structures of the Loop 1-2 in Different Solvents 122
3.4 Summary 125
4. Interaction of transmembrane helices with dodecane: mapping of hydrophobic surfaces by molecular modelling 127
4.1 Background 128
4.2 Methods 134
4.3 Results 136
4.3.1 Interaction of poly-alanine with dodecane 136
4.3.2 Interaction of the transmembrane helices of *Bacteriorhodopsin* with dodecane 139
4.3.3 Interaction of transmembrane helices of FcεRI with dodecane 156

4.4 Discussion 175

4.5 Summary 180

5. Interaction of transmembrane helices of the high affinity IgE receptor with palmitic fatty acid studied by molecular modelling 182

5.1 Background 183

5.2 Methods 185

5.3 Results and Discussion 187

5.3.1 Interaction of transmembrane helix of α-subunit with palmitic acid. 187

5.3.2 Interaction of the four transmembrane helices of β-subunit with palmitic acid 189

5.3.3 Interaction of transmembrane helix of the γ-subunit with palmitic fatty acid. 207

5.3.4 Homology and similarity studies 211

5.4 Summary 215

6. Docking of the TM helices of the high affinity IgE receptor 218

6.1 Background 219

6.2 Methods 223

6.2.1 Docking of the TM helices of the high affinity IgE receptor 223

6.3 Results and Discussion 225

6.3.1 Docking the TM helices of the β-subunit into helix pairs 225

6.3.2 Docking the TM helices of the β-subunit into four helix bundle. 240

6.3.3 Analysis of the four helix bundle 25 of the β-subunit of high affinity IgE receptor 256

6.3.4 Interaction between other TM helices of the high affinity IgE receptor 261

6.4 Summary 264

7. Modelling the 3D structure of the β-subunit of the high affinity IgE receptor 266

7.1 Background 267

7.2 Methods 270

7.2.1 Molecular modelling of the β-subunit. Model I - use of the hydrophobic moments. 271

7.2.2 Molecular modelling of the β-subunit. Model II - use of the docked four-helix bundle and the addition of the loops and tails in two stages. 272

7.2.3 Molecular modelling of the β-subunit. Model III - use of the four helix bundle and the addition of the loops and tails in one stage. 275

7.3 Results and discussion 280

7.3.1 Molecular modelling of the β-subunit. Model I - using the hydrophobic moments. 280

7.3.2 Molecular Modelling of the β-subunit. Model II -use of the docked four-helix bundle and the addition of the loops and tails in two stages 288

7.3.3 Molecular modelling of the β-subunit. Model III - use of the docked four helix bundle and the addition of the loops and tails in one stage. 301

7.4 Summary 309

8. Conclusions 311

8.1 Introduction 312

8.2 Integrated results summary 313

8.3 Future work 318

8.4 Summary 312

References 322

Appendix 1. Protein structure prediction 353

Appendix 2. Publications resulting from this thesis 359

LIST OF FIGURES

Chapter 1.

Figure 1.1 Activation of mast cells. 23

Figure 1.2 The proposed topology for the FcεRI.. 25

Figure 1.3 Circular dichroism spectra of "pure" secondary structures. 34

Chapter 2.

Figure 2.1 CD spectra for loop 2-3 of the FcεRIβ at different TFE/water compositions. 56

Figure 2.2 Changes in Δε in the CD spectra of loop 2-3 during TFE/water titration. 57

Figure 2.3 CD spectra of loop 2-3 in water and SDS micelles. 58

Figure 2.4 1D proton NMR spectrum of the loop 2-3 of the FcεRIβ in TFE. 61

Figure 2.5 The NH/sidechain region of a 600 MHz TOCSY spectrum of the loop 2-3 of the FcεRIβ in TFE . 62

Figure 2.6 NH/α and NH/NH region of a 600 MHz NOESY spectrum of the loop 2-3 of the FcεRIβ in TFE. 64

Figure 2.6C Summary of sequential and medium range NOE connectivities observed for the loop 2-3 in the TFE. 66

Figure 2.7 1D proton NMR spectrum of the loop 2-3 of the FcεRIβ H_2O/TFE. 67

Figure 2.8 NH/sidechain region of the of a 600 MHz TOCSY spectrum of the loop 2-3 of the FcεRIβ in H_2O/TFE. 68

Figure 2.9 NH/NH region of the of a 600 MHz NOESY spectrum of the loop 2-3 of the FcεRIβ in H_2O/TFE. 69

Figure 2.10 1D proton NMR spectrum of the loop 2-3 of the FcεRIβ in H_2O/D_2O. 74

Figure 2.11 Chemical shift index (CSI) plot of αH for the loop 2-3 of the FcεRIβ in H_2O/D_2O. 75

Figure 2.12 Residual chemical shift plot of NH and αH protons for the loop 2-3 of the FcεRIβ in H_2O/D_2O. 75

Figure 2.13 Chemical shifts vs sequence A) NH and B) αH for loop 2-3 of the FcεRIβ in water, water/TFE and TFE 77

Figure 2.14 Number of the distance constraints versus sequence of the loop 2-3 of the FcεRIβ in H_2O/D_2O. 80

Figure 2.15 Ten lowest energy structures obtained from the NMR data for the loop 2-3 of the FcεRIβ in H_2O/D_2O. 81

Figure 2.16 Ramachandran ϕ,ψ plot for the lowest energy NMR based structure of the loop 2-3 peptide of the FcεRIβ in H_2O/D_2O. 82

Figure 2.17 Number of the distance constraints versus sequence of the loop 2-3 of the FcεRIβ in H_2O/TFE. 83

Figure 2.18 Ten lowest energy structures obtained from the NMR data for the loop 2-3 of the FcεRIβ in H_2O/TFE. 85

Figure 2.19 Lowest energy NMR based structure of the loop 2-3 of the FcεRIβ in H2O/TFE. 86

Figure 2.20 Number of the distance constraints versus sequence of the loop 2-3 of the FcεRIβ in TFE. 87

Figure 2.21 Seven structures from the first cluster obtained from the NMR data for the loop 2-3 of the FcεRIβ in TFE. 88

Figure 2.22 Lowest energy NMR based structure for the loop 2-3 of the FcεRIβ in TFE. 89

Figure 2.23 Ten structures from the second cluster obtained from the NMR data for the loop 2-3 of the FcεRIβ in TFE. 90

Figure 2.24 Ten structures from the third cluster obtained from the NMR data for the loop 2-3 of the FcεRIβ in TFE. 91

Figure 2.25 Conformational motif in the FcεRI. 95

Chapter 3.

Figure 3.1 CD spectrum of the loop 1-2 peptide of the FcεRIβ in water. 103

Figure 3.2 CD spectrum of the loop 1-2 peptide of the FcεRIβ in water + SDS micelles. 104

Figure 3.3 1D proton NMR spectrum of the loop 1-2 of the FcεRIβ in methanol. 106

Figure 3.4 NH/sidechain region of the of a 600 MHz TOCSY spectrum of the loop 1-2 of the FcεRIβ in methanol. 110

Figure 3.5 NH/αH and NH/NH region of the of a 600 MHz NOESY spectrum of the loop 1-2 of the FcεRIβ in methanol. 114

Figure 3.6 1D proton NMR spectrum of the loop 1-2 of the FcεRIβ in DMSO. 115

Figure 3.7 NH/sidechain region of the of a 600 MHz TOCSY spectrum of the loop 1-2 of the FcεRIβ in DMSO. 117

Figure 3.8 NH/αH and NH/NH region of the of a 600 MHz NOESY spectrum of the loop 1-2 of the FcεRIβ in DMSO. 119

Figure 3.9 Four structures obtained from the NMR data for the loop 1-2 of the FcεRIβ in methanol. 121

Figure 3.10 Averaged NMR based structure for the loop 1-2 of the FcεRIβ in methanol and DMSO. 124

Figure 3.11 Average structures of the loop 1-2 of the FcεRIβ in methanol and DMSO 125

Chapter 4.

Figure 4.1 Schematic representation of five different moieties of the phospholipid (PC). 131

Figure 4.2 Schematic representation of the study of TM helix and dodecane hydrophobic interaction. 133

Figure 4.3 Interaction energy between Poly-alanine and Dodecane as a function of the rotation of dodecane around helical axis. 137

Figure 4.4 The most stable complexes between poly-alanine helix and dodecane as a result from minimization and simulation protocol. 138

Figure 4.5 7 helix bundle of *Bacteriorhodopsin*. 141

Figure 4.6 The hydrophobic surface mapping of the TM helix 1 of the *Bacteriorhodopsin*. 143

Figure 4.7 The hydrophobic surface mapping of the TM helix 2 of the *Bacteriorhodopsin*. 146

Figure 4.8 The hydrophobic surface mapping of the TM helix 3 of the *Bacteriorhodopsin*. 149

Figure 4.9 The hydrophobic surface mapping of the TM helix 4 of the *Bacteriorhodopsin*. 151

Figure 4.10 The hydrophobic surface mapping of the TM helix 5 of the *Bacteriorhodopsin*. 152

Figure 4.11. The hydrophobic surface mapping of the TM helix 6 of the *Bacteriorhodopsin*. 153

Figure 4.12 The hydrophobic surface mapping of the TM helix 7 of the *Bacteriorhodopsin*. 154

Figure 4.13 The hydrophobic surface mapping of the TM helix of the α-subunit of the FcεRI . 158

Figure 4.14 The complexes of TM helix of the α-subunit of the FcεRI and dodecane. 159

Figure 4.15 The hydrophobic surface mapping of the TM helix 1 of the β-subunit of the FcεRI. 161

Figure 4.16 The complexes of TM helix 1 of the β-subunit of the FcεRI and dodecane. 162

Figure 4.17 The hydrophobic surface mapping of the TM helix 2 of the β-subunit of the FcεRI. 164

Figure 4.18 The complexes of TM helix 2 of the β-subunit of the FcεRI and Dodecane. 165

Figure 4.19 The hydrophobic surface mapping of the TM helix 3 of the β-subunit of the FcεRI. 168

Figure 4.20 The complexes of TM helix 3 of the β-subunit of the FcεRI and Dodecane. 169

Figure 4.21 The hydrophobic surface mapping of the TM helix 4 of the β-subunit of the FcεRI. 171

Figure 4.22 The complexes of TM helix 4 of the β-subunit of the FcεRI and Dodecane. 172

Figure 4.23 The hydrophobic surface mapping of the TM helix of the γ-subunit of the FcεRI. 173

Figure 4.24 The complexes of TM helix of the γ-subunit of the FcεRI and Dodecane. 174

Figure 4.25 The time averaged distribution of the principal structural of the lipid projected onto axis normal to the bilayer plane. 175

Figure 4.26 The amino acid composition of *Bacteriorhodopsin* (BR) and *Rhodob. Sphaeroides* (RC) residues involved in A) lipid -TM helix and B) TM helix - TM helix contacts. 178

Figure 4.27 The schematic representation of the dodecane favourable surfaces of TM helix. 179

Chapter 5.

Figure 5.1 The schematic representation of the study of TM helix and PFA interaction. 186

Figure 5.2 The PFA favourable surface mapping of the TM helix of the α-subunit of the FcεRI 190

Figure 5.3 The lowest energy complex of TM helix of the α-subunit of the FcεRI and PFA at rotational angle 270°. 191

Figure 5.4 The least stable complex of TM helix of the α-subunit of the FcεRI and PFA at rotational angle 0°. 191

Figure 5.5 The PFA favourable surface mapping of the TM helix 1 of the β-subunit of the FcεRI. 195

Figure 5.6 The lowest energy complex of TM helix 1 of the β-subunit of the FcεRI and PFA at rotational angle 270°. 196

Figure 5.7 The least stable complex of TM helix 1 of the β-subunit of the FcεRI and PFA at rotational angle 0°. 196

Figure 5.8 The PFA favourable surface mapping of the TM helix 2 of the β-subunit of the FcεRI 197

Figure 5.9 The lowest energy complex of TM helix 2 of the β-subunit of the FcεRI and PFA at rotational angle 225°. 198

Figure 5.10 The least stable complex of TM helix 2 of the β-subunit of the FcεRI and PFA at rotational angle 45°. 198

Figure 5.11 The PFA favourable surface mapping of the TM helix 3 of the β-subunit of the FcεRI 203

Figure 5.12 The lowest energy complex of TM helix 3 of the β-subunit of the FcεRI and PFA at rotational angle 135°. 204

Figure 5.13 The least stable complex of TM helix 3 of the β-subunit of the FcεRI and PFA at rotational angle 0°. 204

Figure 5.14 The PFA favorable surface mapping of the TM helix 4 of the β-subunit of the FcεRI . 205

Figure 5.15 The lowest energy complex of TM helix 4 of the β-subunit of the FcεRI and PFA at rotational angle 180°. 206

Figure 5.16 The least stable complex of TM helix 4 of the β-subunit of the FcεRI and PFA at rotational angle 0°. 206
Figure 5.17 The PFA favorable surface mapping of the TM helix of the γ-subunit of the FcεRI 209
Figure 5.18 The lowest energy complex of TM helix of the γ-subunit of the FcεRI and PFA at rotational angle 90°. 210
Figure 5.19 The least stable complex of TM helix of the γ-subunit of the FcεRI and PFA at rotational angle 135°. 210
Figure 5.20 The schematic representation of the amphiphatic TM helix surrounded by phospholipids. 216

Chapter 6.

Figure 6.1 Some examples of the possible arrangements of the TM helices of the high affinity IgE receptor. 221
Figure 6.2 Definition of the helix packing parameters. 224
Figure 6.3 The helical wheel of the complex between TM helix 1 and TM helix 2 of the FcεRIβ. 226
Figure 6.4 The overlap of the complexes between TM helix β1 (green) and TM helix β3 (red) of the FcεRIβ. 227
Figure 6.5 The helical wheel presentation of the complex between TM helix β1 and TM helix β4 of the FcεRIβ. 229
Figure 6.6A The helical wheel presentation of the first complex between TM helix β2 and TM helix β3 of the FcεRIβ. 231
Figure 6.6B The helical wheel presentation of the second complex between TM helix β2 and TM helix β3 of the FcεRIβ. 231
Figure 6.6C The helical wheel presentation of the third complex between TM helix β3 of the β-subunit of the FcεRIβ. 232
Figure 6.6D The helical wheel presentation of the fourth complex between TM helix β2 and TM helix β3 of the FcεRIβ. 232
Figure 6.7A The helical wheel presentation of the first complex between TM helix β2 and TM helix β4 of the FcεRIβ. 235
Figure 6.7B The helical wheel presentation of the second complex between TM helix β2 and TM helix β4 of the FcεRIβ. 235
Figure 6.8 The helical wheel presentation of the complex between TM helix β3 and TM helix β4 of the FcεRIβ. 237

Figure 6.9 The schematic representation of the strategy for building the four helix bundle, using the TM helix β2 and TM helix β3 as a starting helix pair in this example. 241

Figure 6.10 The appearance of the residues in all docked four helix bundles of the FcεRIβ. 254

Figure 6.11 The orientation of the helix hydrophobic moments in the anticlockwise and clockwise four helix bundles. 257

Figure 6.12 Four helix bundle 25 of the FcεRIβ. 259

Chapter 7.

Figure 7.1 The calculated four-helix bundle conformation for the β subunit TM domains of $Fc_{\epsilon}RI$. 281

Figure 7.2 Diagram of the four β TM domains where inter-helix interactions are indicated with full lines (residues up to 4 Å apart). 283

Figure 7.3 The conformation of the four-helix bundle and three loops of the FcεRIβ. 284

Figure 7.4 Helical wheel representation of connecting loop helices based on the model I of the FcεRIβ. 287

Figure 7.5 Three truncated models overlap of the FcεRIβ based on the bundle 18. 292

Figure 7.6 Geometric analysis of the whole FcεRIβ based on bundle 18, at each 0.25 ps of the molecular dynamics run at 300 K. 294

Figure 7.7 Geometric analysis of the helical moieties of the FcεRIβ based on bundle 18, at each 0.25 ps of the molecular dynamics run at 300 K. 296

Figure 7.8 FcεRIβ models (II) based on the bundle 18. 297

Figure 7.9 The van der Waals surface presentation of the cytoplasmic tails of the β-subunit model II based on the bundle 18. 298

Figure 7.10 Geometric analysis of the whole FcεRIβ based on the bundle 25, at each 0.25 ps of the molecular dynamics run at 300 K. 302

Figure 7.11 Geometric analysis of the helical moieties of the FcεRIβ based on the bundle 25, at each 0.25 ps of the molecular dynamics run at 300 K. 303

Figure 7.12 FcεRIβ models (III) based on the bundle 25. 306

Figure 7.13 The van der Waals surface presentation of the cytoplasmic tails of the β-subunit model III based on the bundle 25. 307

LIST OF TABLES

Chapter 2.

Table 2.1 The calculated secondary structure of the loop 2-3 of the FcεRIβ based on the CD spectra. 59

Table 2.2 Assignment of spin systems of the ^{1}H NMR spectra of loop 2-3 major component in TFE. 65

Table 2.3: Assignment of spin systems of the ^{1}H NMR spectra of the minor component of the loop 2-3 in TFE. 70

Table 2.4. Assignment of spin systems of the ^{1}H NMR spectra of the loop 2-3 in H_2O/TFE. 72

Table 2.5 Assignment of spin systems of the ^{1}H NMR spectra of the loop 2-3 in H_2O/D_2O 76

Chapter 3.

Table 3.1. Secondary structure content of the loop 1-2 of the FcεRIβ calculated from far UV CD spectra. 102

Table 3.2 Assignment of spin systems of the ^{1}H NMR spectra of the loop 1-2 of the FcεRIβ in methanol. 107

Table 3.3 Assignment of spin systems of the ^{1}H NMR spectra of the loop 1-2 of the FcεRIβ in DMSO. 116

Chapter 4.

Table 4.1 The amino acid colour scheme in Rasmol. 135

Table 4.2 The interaction energies between TM helices of BR and dodecane. 142

Chapter 5.

Table 5.1. TM helix residues of the FcεRI involved in forming stable complexes with PFA. 212

Table 5.2. TM helix residues of the FcεRI involved in forming least stable complexes with PFA. 213

Table 5.3. Sequence alignment of the four parallel TM helices of the FcεRI. 214

Table 5.4. Sequence alignment of the four parallel TM helices of the *Bacteriorhodopsin*. 214

Chapter 6.

Table 6.1 Interaction energies and contact surfaces between TM helices of the FcεRIβ. 238

Table 6.2 Energetic and orientation analysis of the four helix bundles of the FcεRIβ 244

Table 6.3 Analysis of interactions in the four helix bundles of the FcεRIβ. 247

Table 6.4 Interaction energies and contact surfaces between α- and γ-TM helices and TM helices of the FcεRIβ. 263

Chapter 7.

Table 7.1 Model building and MM/MD protocol for the β-subunit without cytoplasmic tails - model I. 271

Table 7.2 Model building and MM/MD protocol for the β-subunit - model II. 277

Table 7.3 Model building and MM/MD protocol for the β-subunit - model III. 279

Table 7.4 Geometric and energetic analysis of TM helix - TM helix packing in the partially truncated model of the FcεRIβ. 285

Table 7.5 The interaction energies between the TM helices of the lowest energy four helix bundles of the partially truncated FcεRIβ. 291

LIST OF ABBREVIATIONS

2D J-res	J resolved spectroscopy
BR	*Bacteriorhodopsin*
CD	Circular Dichroism
CMC	Critical micellar concentration
COSY	Correlated spectroscopy
CPK	Corey-Pauling-Koltun; space filling representation of a molecule
CSI	Chemical shift index
DDA	dodecane
DMSO	dimethylsulfokside
DOPC	Dioleoylphosphocholine
dαN	distance between protons αCH_i and NH_{i+1}
dβN	distance between protons βCH_i and NH_{i+1}
dNN	distance between protons NH_i and NH_{i+1}
FcεRI	High affinity IgE Receptor
IgE	Immunoglobulin E
J	scalar coupling constant
MD	Molecular dynamics
NE	Number of experiments
ni	Number of increments
NMR	Nuclear magnetic resonance
NOESY	Nuclear Overhauser effect spectroscopy
ns	number of scans
PFA	palmitic fatty acid
ppm	part per milion
PSRC	Photosynthetic reaction centre
rd	relaxation delay

RMSD	Root mean square deviation
ROESY	Rotating frame overhauser effect spectroscopy
SA	Simulated annealing
SASA	Solvent accessible surface area
SDS	Sodium dodecyl sulfate
SI	Size of the NMR spectrum
t1	time dimension, acquisition time
T1	spin-lattice relaxation
t2	time dimension
T2	spin-spin relaxation
TD	time domain points
TFE	Trifluoroethanol
TM	Transmembrane
TOCSY	Total correlation spectroscopy
T_s	Transition during solvent titration
UV	Ultra violet

Amino acids:

A, Ala	Alanine
C, Cys	Cysteine
D, Asp	Aspartic acid
E, Glu	Glutamic Acid
F, Phe	Phenylalanine
G, Gly	Glycine
H, His	Histamine
I, Ile	Isoleucine
K, Lys	Lysine
L, Leu	Leucine

M, Met	Methionine
P, Pro	Proline
Q, Gln	Glutamine
R, Arg	Arginine
S, Ser	Serine
T, Thr	Threonine
V, Val	Valine
W, Trp	Tryptophan
Y, Tyr	Tyrosine

Chapter 1.

INTRODUCTION

1. INTRODUCTION

1.1 Immune system and allergy

A whole series of the cells defend the body against microbial and viral invaders. The main properties of the immune system are: specific recognition of foreign entities, the ability to destroy them and mechanism of memorizing those process for the future rapid reaction. The range of cells on which immune system depends are many specialized lineages - B cells, macrophages, killer T cells, helper T cells, inflammatory T cells and others.

Mutual recognition of proteins is crucial for the immune system response. The sites on foreign molecules (antigens) recognized by the immune system are named antigenic determinants. Recognition is mediated mainly by two protein families: immunoglobulin like molecules, and proteins of major histocompatibility complex.

Immunoglobulins, which are also known as antibodies, act as a antigen receptor on the surface of B cells, they recognize and bind intact soluble molecules (or molecules on the surface of the invading entity). This activates the B cells to multiply, differentiate, then to synthesize and to secrete more copies of antibodies into blood stream. The soluble antibodies bind to the antigen and the complexes are then recognized and removed by macrophages.

The T cell receptor acts as a antigen receptor for the T cell, whose principal function is to recognize and destroy virus infected cells. T cells directly destroy infected cells. Their

receptors recognize the antigen only when is bound to the major histocompatibility complex or MHC. The T cell receptors exist only on the surface of T cells. By contrast, antibodies exist both as cell surface and soluble molecules and interact with intact antigen. Antibodies are the most diverse of all known proteins and any antigen presented to the immune system triggers the production of many different and specific antibodies.

Allergy is the bodies response in which certain components of the immune system react strongly to normally inoffensive foreign substances. Allergic disorders of organs such as lung, nasal mucosa, skin and the gastrointestinal tract are due to a spectrum of pathobiological events, which include vasodilation, increased vasopermeability, non-vascular smooth muscle contraction, leukocyte infiltration and local tissue destruction. The allergic event is known to be initiated by stereospecific interaction of allergen and IgE antibody on the surface of the tissue mast cells.

At the first instance, the silent process called sensization may begin when allergen enters the body for the first time, and the IgE antibodies are produced. As a result, IgE antibodies occupy IgE receptors on mast cells and basophils, ready to react promptly to the next encounter with allergen. Later exposures initiate more visible stages of allergy. Within seconds after allergen enters the body, it binds the IgE antibodies on mast cells. When it engages two IgE molecules and bridge them, it causes the IgE receptor (FcεRI) aggregation. Such aggregation activates the cell and starts a cascade of biochemical events (Figure 1.1), that directly and indirectly generate allergic symptoms. These biochemical events include 1) immoblisation of receptors, 2) phosphorylation of receptors, 3) activation of serine protease, 4)stimulation of lipid methylation, 5) stimulation of adenylate cyclase, 6) hydrolysis of phophatidylinositides, 7) increase in intracytoplasmic Ca^{2+} 8) activation of protein kinases and 9) activation of phosphatases [Lewis and Austen, 1981; Kinet, 1990].

Current therapy for allergic disease consists mostly of drugs aimed at symptomatic relief, which includes corticosteroids which have a broad spectrum anti-inflammatory effect. Many problems associated with corticosteroid treatment has been alleviated by localised administration of drugs, but there is a need for new cures that are more specific and efficient [Lichtenstein, 1993]. The formation of a complex between FcεRI and IgE molecule has been the target to develop novel therapeutics for allergy treatment [McDonnell et al., 1996]. Thus, potential drug design targets could be the blocking the FcεRI aggregation or interrupting the signal transduction.

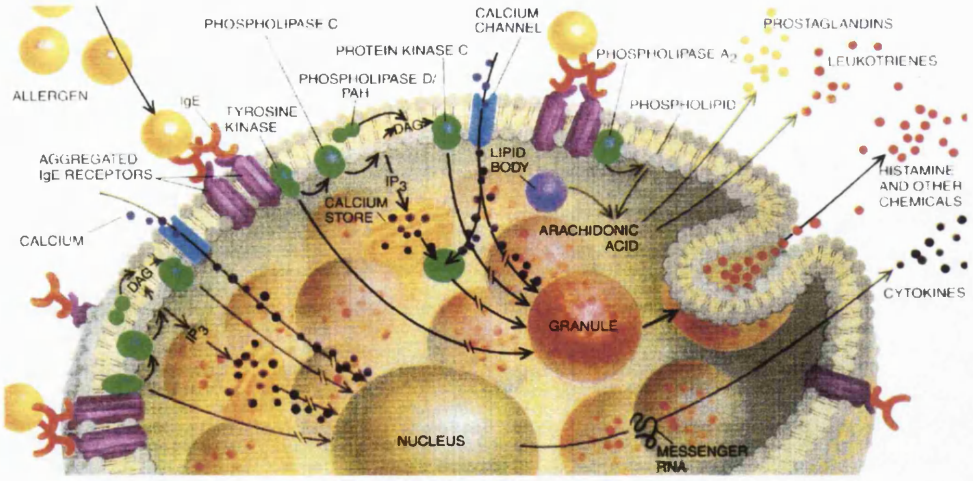

Figure 1.1 Activation of mast cells. The cascade of the biochemical events triggered by binding of a allergen to two IgE bound high affinity IgE receptors [Lichtestein, 1993].

1.2 High affinity IgE receptor

The high affinity IgE receptor (FcεRI) plays an important role in the allergy and inflammation processes. This receptor is polytopic (multimeric) receptor consisting of four subunits, one α, one β and γ-dimer connected by a disulfide bond ($\alpha\beta\gamma_2$) [Blank et al, 1989]. The proposed topography of the receptor is shown in Figure 1.2. It is a 7-helix integral membrane protein, with the α- and γ-chains containing one putative transmembrane (TM) helix and the β-subunit having four putative TM helices. The α-chain consists of two immunoglobulin C2 type domains (D1 and D2) and contains the IgE binding site [Sutton and Gould, 1993]. It is the interaction of IgE and FcεRIα and the subsequent cross-linking of the immunoglobulin by specific antigen, that activates numerous inflammatory cell types.

The β- and γ-chains play important roles in down stream signal transduction [Sutton and Gould, 1993; Beavan and Baumgartner, 1996]. Tyrosine phosphorylation of these subunits was pinpointed as an early biochemical event preceding the activation of protein kinase C and the rise of the intercellular calcium [Paolini et al., 1991]. It was found that the fusion proteins containing the Src homology 2 (SH2) domains of Syk and Lyn tyrosine kinases precipitated tyrosine-phosphorylated proteins from RBL-2H3 cell lysates. There was more binding of Syk SH2 to FcεRIγ than to FcεRIβ, whereas Lyn SH2 bound only to FcεRIβ. The SH2- mediated association of these two protein tyrosine kinases with FcεRI could play an important role in receptor signaling [Kihara and Sigaranian, 1994]. The immunoreceptor tyrosine-based activation motifs (ITAM), common to many receptors, were found to be interacting with SH2 domains [Labadia et al., 1997]. The motif detected in the cytoplasmic domain of the γ subunit ([D,E]-X2-Y-X2-L-X7-Y-X2-L) is known also

as a Reth motif [Reth, 1989]. The motif found twice in the cytoplasmic C-terminal tail of the β subunit was different: [RK]-X(2,3)-[DE]-X(2,3)-Y, than one detected in γ subunit.

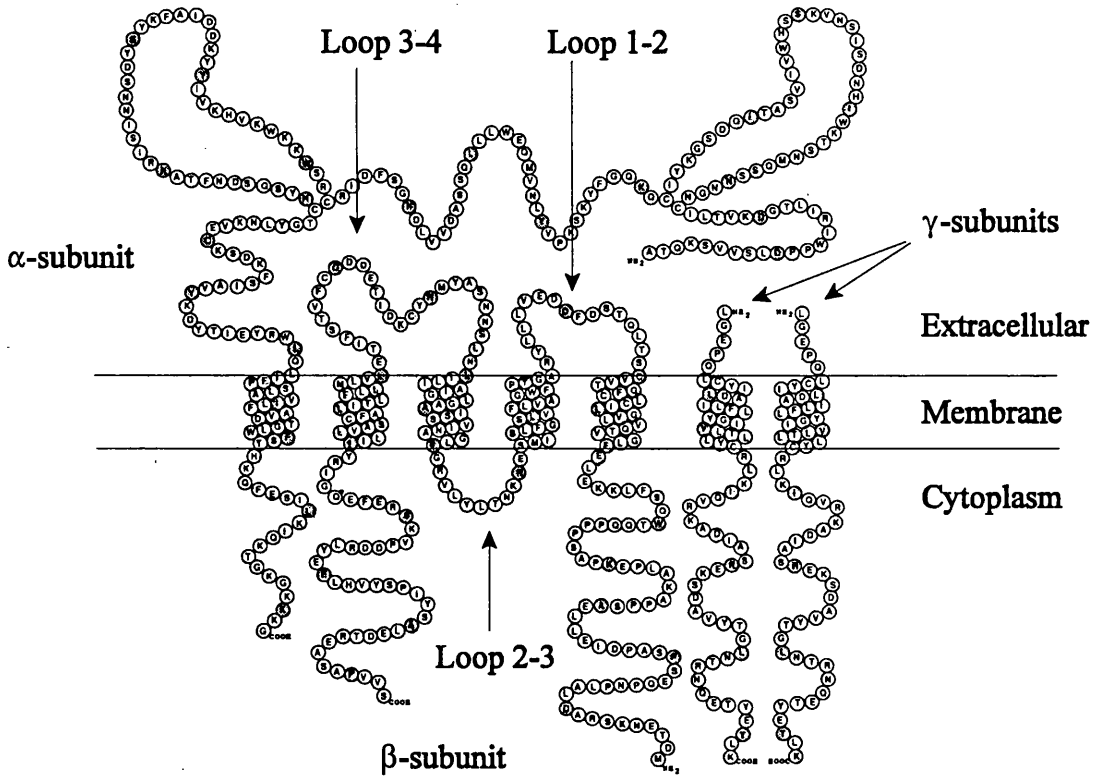

Figure 1.2 The proposed topology for the rat high affinity IgE receptor [Blank et al., 1989]

Tyrosine phosphorylation of β- and γ-subunits occurs in intact cells only for FcεRI that associate with detergent-resistant membrane domains, which are enriched in active Lyn. Furthermore, efficient in vitro tyrosine phosphorylation of FcεRI subunits occurs only for those associated with isolated domains. This association and in vitro phosphorylation are highly sensitive to low concentrations of detergent, suggesting that lipid-mediated

interactions with Lyn are important in FcεRI activation. Participation of membrane domains accounts for previously unexplained aspects of FcεRI-mediated signaling and may be relevant to signaling by other multimeric immune receptors [Field et al., 1997]. Earlier, it was shown that the interaction of α- and β- subunits of the high affinity IgE receptor can be stabilized by maintaining an appropriate (specific) phospholipids to detergent ratio during receptor purification [Rivnay, et al., 1982]. Such results demonstrated that membrane lipids preserve an interaction between two or more separate polypeptides. The stability and function of some membrane proteins strongly depend on the hydrophobic environment of the lipid bilayer or even on interactions with specific lipid components. The lipid bilayer has a crucial capacity for the structure/function relationship of the FcεRI, therefore it should be considered during studies.

The 3D structure of the FcεRI is unknown, due to difficulties in the isolation and purification of this multimeric receptor. Structural information for FcεRIα has so far been limited to modelling studies of the extracellular portion of based on homologous proteins of known structure [Padlan and Davies, 1986; Padlan and Helm, 1993; McDonnell et al., 1996], or the NMR studies of the extracellular FcεRI α-chain mimic peptides [McDonnell et al., 1997]. The structural information of the rest of the receptor was studied by Gibbons and co-workers; antibody studies [Gao et al., 1993, 1994]; the spectroscopic studies of the cytoplasmic part of FcεRIγ [Anderson et al., 1992; Anderson et al., 1994/95], spectroscopic studies of the cytoplasmic portion of the FcεRIα [Thomas et al., 1993; Zloh et al., 1997] and spectroscopic studies of the cytoplasmic C-terminal domain of the FcεRIβ [Zloh et al., 1994a; Zloh et al., 1994b]. Although some structural information has been obtained, the structure of FcεRI and mechanism of the signal transduction has yet to be precisely identified.

1.3 Membrane protein structure determination

Few membrane proteins have had their high resolution structure determined. The four porin structures [Weiss et al., 1991; Kreusch et al., 1994; Cowan et al., 1993] consist of a 16-stranded antiparallel β-barrel forming a cyclic or pseudocyclic structure. *Bacteriorhodopsin*, has been studied by electron diffraction of 2D crystals. The initial 7 α-helix bundle structure [Henderson and Unwin, 1975] was extended to 3.5 Å [Henderson et al., 1990]. It has been crystalized and diffraction studies performed [Schertler et al., 1993a], FT-IR and resonance Raman spectroscopy studies have been accomplished [Heberle et al., 1998], but the conformation of the connecting loops is still not experimentally determined in the BR protein. The structures of two photosynthetic reaction centre (PSRC) have been determined by X-ray crystallography from Rhodopseudomonas viridis [Deisenhofer et al., 1985] and Rhodobacter sphaerodies [Chang et al., 1986]. It has four subunits; transmembrane L and M subunits, a cytoplasmic H, and a cytochrome. The structure of the plant light harvesting complex (LHC) was solved by cryo- EM initially to 6.0 Å [Kühlbrandt and Wang, 1991] and now extended to 3.4 Å [Kühlbrandt et al., 1994]. More recently, the structure of the ryanodine receptor, the main intracellular calcium release channel, was determined using cryoelectron microscopy on the isolated receptor. Three-dimensional reconstruction shows the receptor to be composed of two main parts, a large square shaped cytoplasmic assembly and a smaller transmembrane assembly [Samso and Wagenknecht, 1998]. The other ion channel, KcsaA potassium channel, has been subject of electron [Li et al., 1998] and X-ray [Doyle et al., 1998] crystallography studies, which revealed that the protein is homotetramer, with two TM helices per monomer. The crystal structure of a mouse T-cell antigen receptor (TCR) Fv fragment complexed to the Fab

fragment of a specific anti-clonotypic antibody has been determined to 2.6 Å resolution [Housset et al., 1997].

The amount of experimental structural information for the membrane receptors is increasing daily, but the vast majority of the structures obtained are still based on molecular modelling. The whole family of the G-protein receptors are modelled based on the alpha-carbon template for the TM helices of the Rhodopsin family [Baldwin et al., 1997]. For example, a model of the melanocortin 1 receptor (MC1R) was created from data derived from multiple sequence analysis, a low-resolution EM-projection map of rhodopsin, and the approximate membrane thickness [Prusis et al., 1997].

A whole other class of membrane proteins studied by molecular modelling consists of ion-channels. It is believed that the amphipathic helix could be a key motif in the TM channels forming the pore. In the nicotinic receptor channel the amphipathic M2 helices delineate the pore, providing interaction sites for permeant cations and determining ionic selectivity [Bertrand, 1993; Unwin, 1993]. The helix supercoil was usually constructed such that the inner surface was lined by hydrophilic residues, and that the outer surface was lined by hydrophobic ones [Inouye, 1974]. The hydrophilic residues thus provide possible favourable interactions for permeant ions and/or water molecules, while the hydrophobic residues interact either with the hydrocarbon region of the lipid bilayer or with other protein TM segments. The modelling and simulation of nicotinic acetylcholine receptor is reviewed by Sansom et al., 1998. It was found that the voltage-gated K^+ channel was formed by an eight-stranded P-barrel and molecular dynamic simulations of the potential energy of a K^+ ion as translated along the model pore indicate that the two ionised Asp sidechains and the hydroxyl groups of the Tyr sidechains stabilise the partially desolvated ion as it passes through the narrowest region [Ranatunga et al., 1998]. Other ion-channels

were studied by molecular dynamics simulation by the same group, for example, a pore of voltage-gated sodium channels [Cosette et al, 1997], the channel-forming peptaibol alamethicin [Breed et al., 1997], Staphylococcal delta-toxin ion channels [Kerr et al., 1996]. These ion channel studies only modelled the pore, and suggesting that the truncated model could be used to explain the properties and/or mechanism of the protein.

The structures of membrane proteins with entirely α-helical transmembrane structure are consistent with the view that helix packing in integral membrane proteins is governed by the same interactions as those present in globular helix bundles [Rees et al., 1995]. The inter-helical distances observed in both BR and PSRC structures are consistent with that observed in globular proteins, with a mean distance of 9.9 Å in membrane proteins compared to 9.4 Å in globular proteins [Chothia et al., 1981].The crossing angles between adjacent helices are also consistent with those found in a survey of globular proteins [Reddy and Blundell, 1993] and for many helix pairs corresponds to CLASS "3-4" helix packing [Chothia et al., 1981] which has a calculated preferred crossing angle of +20°. In PSRC structures there is also a right α-handed four-helix bundle motif formed by TM helices [Presnell and Cohen, 1989]. Packing in LHC between TM helices A and B is CLASS "4-4" type [Chothia et al., 1981], the most frequently observed packing arrangement in globular proteins [Reddy and Blundell, 1993].

The two stage model of TM helix packing proposes that preformed, independently stable α-helices insert into the membrane, whereupon they pack with other TM helices without topological rearrangement [Popot and Engelman, 1990]. Thus, TM α-helices are autonomous folding units. Observational evidence for the model is summarised below: i) A hydrophobic α-helix is a stable entity in a membrane environment as all backbone hydrogen bonding groups are satisfied. ii) A number of proteins exist with a single TM

helix, for example, the influenza A virus M2 protein [Pinto et al., 1990]. Biochemical studies on the membrane protein (*Bacteriorhodopsin*) provide some evidence for the two stage model. Engelman and colleagues have conducted detailed investigations on the re-association of fragments of BR [eg. Khan and Engelman, 1992]. The synthetic peptides corresponding to helix A and helix B were incorporated into separate populations of vesicles. A proteolytic fragment corresponding to the other five helices (E-G) was also prepared in separate vesicles. Upon mixing of the three vesicle populations functional bR could be detected by retinal absorption and by X-ray diffraction of 2D crystals [Kahn and Engelman, 1992]. Similar studies with the E-G fragment and A-B fragment have been performed, again showing reformation of active BR [Popot and Engelman, 1990].

Biochemical data has also supported helix-helix association as being crucial to determining the structure of membrane proteins. For example, when the protein glycophorin A (which forms a TM helical dimer) is genetically fused to a soluble protein, the resulting chimaera also dimerises in SDS solutions. Mutagenesis of the glycophorin region of the chimaera demonstrated that the dimerisation is driven by hydrophobic contacts at the helix-helix interface [Lemmon et al., 1992].

The implications of the two-stage model in molecular modelling of TM helix bundles are that the simulation of packing preformed TM helices may be a reasonable approximation to the in vivo packing process and generates structures with helix packing characteristics similar to those seen in membrane protein structures.

1.3.1 Domains and subunits

The experimentally determined 3D-structure of only a few receptors are known, as a result of many problems related to the determination integral membrane protein structure. Alternative approaches to membrane protein structure determination are therefore required. One approach is to study individually soluble peptides that represent portions of the receptor primary structure. This approach will have merit to the extent that these domains maintain their native structure in the soluble peptides. The "module" concept proposed by Campbell and co-workers for large globular proteins with identified repeated sequences (modules) which correspond to single exons diverged from a primordial gene by exon shuffling and duplication [Baron et al., 1991]. A "domain" described by Schultz et al., 1979. has all of the observed features of a module except that it is not clearly associated with exon shuffling and duplication. Although less easy to identify than modules, domain structures can similarly be elucidated independently of the parent structure. This domain approach to structure determination of large proteins proposed by Campbell and coworkers [Baron et al., 1991] was used by others, for example, to study the 38 AA residue synthetic peptide with the sequence of the Titin N-terminus and revealed the presence α-helix structure [Musco et al., 1995]. The novel method of cutting the sequence of a large protein into small synthetic peptides with overlapping sequences was used to determine the secondary structure of vaccinia virus thymidine kinase, porcine adenylate kinase and yeast guanylate kinase [Behrends et al., 1996; Behrends et al., 1997].

The anisotropic environment of membrane receptors leads to into natural division in terms of environment. Thus each membrane protein can be classified into extracellular, transmembrane and cytoplasmic domains. Each environmental domain may then be further subdivided either on functional consideration or by criteria for a domain.

The fragments of BR were subjected to structural studies. The structure (in SDS micelles) of a synthetic peptide corresponding to residues 34-65 R (TM helix B) shows a proline-kinked α-helix for residues 42-60 [Lomize et al., 1992] The structure of the proteolytic fragment containing residues 163-231 was determined in chloroform/methanol [Barsukov et al., 1992]; two helices were identified from residues 168-191 and 198-227. The former of these corresponds to helix F of BR (residues 167-191 in native BR) and had a similar kink angle, whereas the latter corresponded to helix G (residues 203-225 in BR). The synthetic peptides of the connecting loops of the BR were studied by NMR [Yeagle et al., 1995; Yeagle et al., 1997; Yeagle et al., 1998].

When the concepts of modules and domains are applied to the FcεRI, some interesting features emerge. The α subunit of FcεRI is homologous to most Fcγ receptors [Kinet, 1990] and, like these, contains two homologous immunoglobulin related C2 domains. The extracellular portion of FcεRIα would be autonomous region on both modular and domain consideration. It was found that a β-hairpin region of the C-C' strands of the second extracellular domain plays an important role in the interaction with IgE [Sutton and Gould, 1993]. The extracellular portion of FcεRIα has so far been modelled based on homologous proteins of known structure [Padlan and Davies, 1986; Padlan and Helm, 1993; McDonnell et al., 1996], or the extracellular FcεRI α-chain mimic peptides have been studied by NMR [McDonnell et al., 1997]. The synthetic peptide with the sequence of the cytoplasmic C-terminal of FcεRIα was studied by CD and NMR, and revealed the presence of an α-helix moiety in the middle of the chain [Thomas et al., 1993; Zloh et al; 1997].

The conserved γ subunit together with the ζ chain of the T-cell receptor are thought to define a new gene family based on homology, location on the same chromosome, and

the fact that both are essential for the surface expression of their receptors [Kuster et al., 1990].The γ subunit forms a module and this module can be divided into cytoplasmic and transmembrane domains and extracellular part. The NMR structure of the cytoplasmic domain of γ-domain indicated that the linear chain had an α-helix near the C-terminal [Anderson et al., 1992; Anderson et al., 1994/5], revealing that the residues of the RETH (phosphorylation) motif should be on the same side of the helix and in the correct position to interact with SH2 protein as predicted by Reth, 1989. Anderson et al., 1992 have proposed a full structure for the monomeric γ-subunit.

The β subunit is homologus to Lys-44 CD-20 [Tedder et al., 1988], which also has four presumptive transmembrane domains and cytoplasmic N– and C-terminal tails. The rat β subunit consists of 243 residues and can be divided into domains on environmental grounds. Thus it has two cytoplasmic tails, four putative transmembrane α-helices, two extracellular connecting loops and a cytoplasmic connecting loop as proposed by Blank et al., 1989. (Figure 1.2). The β-subunit of rat FcεRI was the main subject of this work and it will be discussed in detail in later Chapters.

1.3.2 CD spectroscopy

The circular dichroism spectra are very sensitive to the secondary structure of polypeptides and proteins. The CD spectra between 260 and approximately 180 nm can be analyzed for the different secondary structural types: α-helix, parallel and antiparallel β-sheet, turn, and other. A number of review articles are available describing the technique and its application [Woody, 1995; Johnson, 1990]. Modern secondary structure determination by CD are reported to achieve accuracies of 0.97 for α-helices, 0.75 for β-sheet, 0.50 for turns, and 0.89 for other structure types [Manavalan & Johnson, 1987].

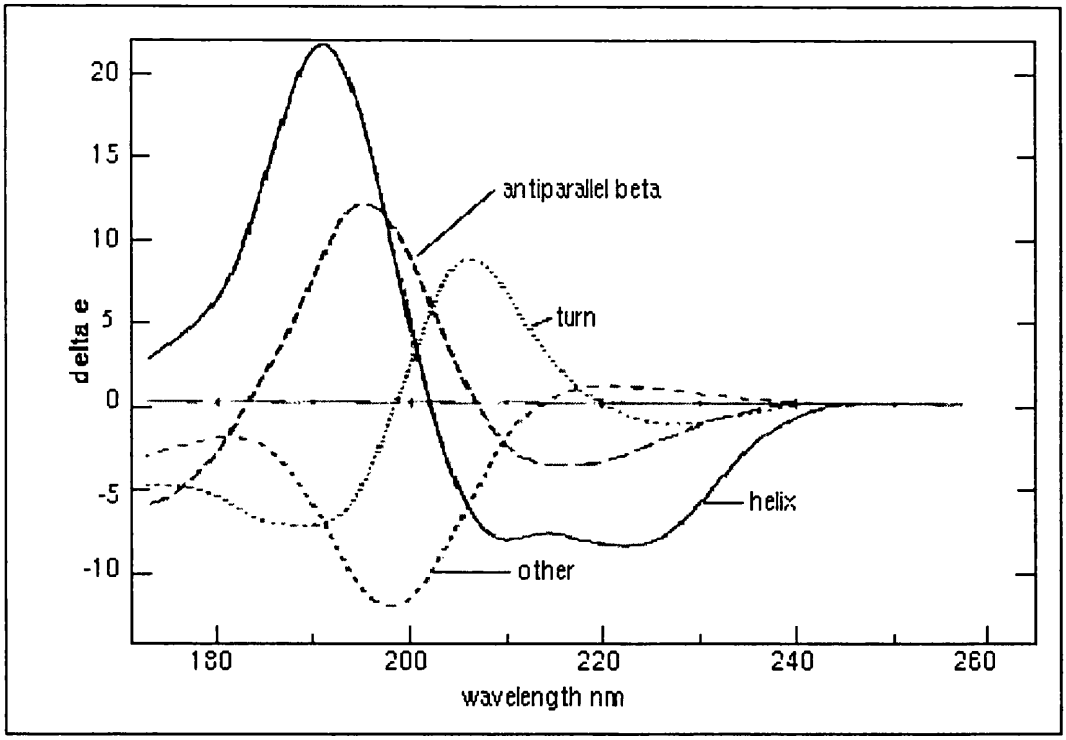

Figure 1.3 Circular dichroism spectra of "pure" secondary structures. Redrawn from Brahms & Brahms, 1980.

The simplest method of extracting secondary structure content from CD data is to assume that a spectrum is a linear combination of CD spectra of each contributing secondary structure type (e.g., "pure" α-helix, "pure" β-strand etc.) weighted by its abundance in the polypeptide conformation. The major drawback of this approach that there is no standard reference CD spectra for "pure" secondary structures. Synthetic homopolypeptides used to obtain reference spectra are in general, poor models for the secondary structures found in proteins. For example, the CD of an α-helix has been shown to be length dependent and no homopolypeptide system has been found that is a good example of the β-sheet structure found in proteins.

In response to these shortcomings, several methods have been developed which analyse the experimental CD spectra using a database of reference protein CD spectra containing known amounts of secondary structure [Provencher & Glöckner, 1981; Hennesey & Johnson, 1981; Manalavan & Johnson, 1987; Sreerama & Woody, 1994]. These methods are in general more accurate and reliable than the novel approach outlined above.

Two very important requirements for successful secondary structure analysis using these techniques deserves further comment. One is that the CD spectra need to be recorded from about 260 nm to at least 184nm (and preferable 178 or below; Johnson, 1990) and the other is that an accurate protein concentration (< 10% error) is essential. The assumptions and limitations of these techniques are discussed in detail by Manning, 1989.

Circular dichroism spectroscopy has been extensively applied to the structural characterization of peptides. The application of CD for conformational studies in peptides (like proteins) can be largely grouped into 1.) monitoring conformational changes (e.g., monomer-oligomer equlibria, substrate binding, denaturation, etc.) and 2.) estimation of secondary structural content (e.g., this peptide is 25% helical under these conditions). As already mentioned, CD is particularly well-suited to determine structural changes in both proteins and peptides. However, absolute structural content is more difficult and is prone to over-interpretation.

CD has been used in a variety studies on membrane proteins; some examples are cited below. For a membrane protein data set, the five-component spectra so obtained from by deconvolution consisted of two different types of α-helices (the α-helix in the soluble domain and the α(T)-helix, for the transmembrane α-helix), a β-pleated sheet, a class C-like spectrum related to β-turns, and a spectrum correlated with the unordered conformation.

The deconvoluted CD spectrum for the α(T)-helix was characterized by a positive red-shifted band in the range 195-200 nm (+95,000 deg cm^2/ mol), with the intensity of the negative band at 208 nm being slightly less negative than that of the 222 nm band (-50,000 and -60,000 deg cm^2/ mol, respectively) in comparison with the regular alpha-helix, with a positive band at 190 nm and two negative bands at 208 and 222 nm with magnitudes of +70,000, -30,000, and -30, 000 deg cm^2/ mol, respectively [Fasman, 1995]. The integral membrane protein diacylglycerol kinase (DGK) from Escherichia coli has been reversibly unfolded in a protein/detergent/mixed micelle system by varying the molar ratio of n-decyl beta-D-maltoside (DM) and sodium dodecyl sulfate (SDS) followed by CD and UV absorbance spectroscopy and assigning first unfolding phase to a denaturation event in a cytoplasmic domain and the second phase to denaturation of the membrane-embedded portion of the protein [Lau and Bowie, 1997]. CD can provide the information about state of aggregation of membrane proteins [Heyn, 1989].

1.3.3 NMR spectroscopy

Nuclear magnetic resonance (NMR) spectroscopy has proved itself a potentially powerful method for the determination of membrane protein three-dimensional structure.

Solid state NMR can be used to study an intact membrane protein by the determination of internuclear distances and orientations. The deconvolution of the NMR spectra is usually performed by using specifically isotopically labelled proteins in combination either with the orientation of the protein in the magnetic field, or with the sample rapidly rotating in the magnetic field (so-called magic angle spinning). These methods have been used to acquire structural information for membrane proteins [Wang et al., 1997; Grobner et al., 1998; Kumashiro et al., 1998; Williamson et al., 1998] and

membrane protein fragments [Bechinger et al., 1993; Ketchem et al., 1997; Rigby et al., 1998].

High resolution solution NMR spectroscopic methods have been used in this work, and therefore will be described in more detail. There are numerous texts that describe this methods and its applications [for example, Derome, 1987]

Each of the four most abundant elements in biological material (H, C, N, and O) have at least one naturally occurring isotope with non-zero nuclear spin and is in principle observable in an NMR experiment. The naturally occurring isotope of hydrogen, ^{1}H, is present at >99% abundance and forms the basis of the experiments described here. Other important NMR-active isotopes include ^{13}C and ^{15}N present at 1.1 and 0.4% natural abundance, respectively. The low natural abundance of these two isotopes makes their observation difficult on commonly isolated natural products. These two nuclei are however very extensively used for larger (>10 kD) proteins which can be isotopically enriched (to >95% if necessary) when cloned into over expression systems.

The spin angular momentum of nuclei with isotopes of overall non-zero spin will undergo a rotation motion called precession in the presence of an external magnetic field. The frequency of precession for each isotope is dependent on the strength of the external field and is unique for each isotope. For example, in a magnetic field of a given strength (e.g. 14.1 Tesla) all protons in a molecule will have characteristic resonance frequencies (chemical shifts) within a dozen or so parts per million (ppm) of a constant value (e.g., 600.13 MHz) characteristic of the particular nuclear type. These slight differences are due to the type of atom the proton is bound (e.g., C, N, O, or S), the local chemical environment and conformation of the molecule. Thus each proton should, in principle, be characterized by a unique chemical shift. In practice, this is never observed as some protons are found

to have degenerate chemical shifts. Other protons (e.g., some OH, SH, and NH3) are in rapid chemical exchange with the solvent and thus have chemical shifts indistinguishable from the solvent resonance. However, complete chemical shift assignments are often possible and are a prerequisite for structural studies using NMR parameters.

Structural information from NMR experiments come primarily from through-bond (scalar or J coupling) or through space (the nuclear Overhauser effect, NOE) magnetization transfer between pairs of protons. J couplings between pairs of protons separated by three or fewer covalent bonds can be measured. The value of a three-bond J coupling constant contains information about the intervening torsion angle, described by co called Karplus relationship:

$$^3J = A\cos(\theta) + B\cos^2(\theta) + C \qquad \text{Eq. 1.1}$$

where A, B, and C are empirically derived constants for each type of coupling constant (e.g., $3J_{\alpha HNH}$ or $3J_{\alpha H\beta H}$). Torsion angles cannot be unambiguously determined from a Karplus-type relationship since as many as four different torsion angle values correlate with a single coupling constant value. However, constraints on the dihedral angles ϕ are important structural parameters in the determination of protein three-dimensional structures by NMR.

The other major source of structural information comes from through space dipole-dipole coupling between two protons called the NOE. The intensity of an NOE is proportional to the inverse of the sixth power of the distance separating the two protons and is usually observed if two protons are separated by less than 5 Å. The use of the NOE intensities in the structural determination was pioneered by Gibbons and co-workers [Gibbons et al., 1975; Jones et al., 1978]. The NOE is a sensitive probe of short intramolecular distances. NOEs are categorized according to the location of the two protons

involved in the interaction. A network of these short inter-proton distances form the backbone of three-dimensional structure determination by 1D, 2D and 3D NMR.

A number of short distances are fairly unique to secondary structural elements. For example, α-helices are characterized by short distances between certain protons on sequentially neighboring residues (e.g., between backbone amide protons, d_{NN}, as well as between beta protons of residue i and the amide protons of residue i+1, $d_{\beta N}$). Helical conformations result in short distances between the alpha proton of residue i and the amide proton of residues i+3 and to a lesser extent i+4 and i+2. These i+2, i+3, and i+4 NOEs are collectively referred to as medium range NOEs while NOEs connecting residues separated by more than 5 residues are referred to as long range. Extended conformations (e.g., β-strands) on the other hand, are characterized by short sequential, $d_{\alpha N}$, distances. The formation of sheets also result in short distances between protons on adjacent strands (e.g., $d_{\alpha\alpha}$ and $d_{\alpha N}$).

The procedure for structure determination generally proceeds as follows: assign unequivocally all the molecule's resonances, measure the intensity of all the NOEs observed and calculate structures that match the experimental data.

Before a structure can be determined the pairs of protons responsible for each of the NOEs observed must be identified. The only way to do this is to assign every resonance in the molecule's spectrum. The strategy for assigning protein resonances known as sequential assignment was first developed by Gibbons and coworkers [Gibbons et al., 1975; Jones et al., 1978a, 1978b; Kuo et al., 1979; Ford et al., 1979], followed by Wuthrich and coworkers [Wutrich et al, 1979, 1982].

The NMR-based structures could be produced by Distance Geometry [Havel and Wuthrich, 1984, 1985] and/or Restrained Molecular Dynamics, as described below.

The quality of the NMR based protein structures depends on 1) the number of NOE distance constraints, 2) their assumed precision, 3) the method of structure calculation and 4) the size of the protein. The influence of these parameters was studied [Liu et al., 1992], and it was found that 1) global RMS decrease as the number of constraints increases up to 30% of of all potential constraints; 2) the accuracy of the average structure calculated by the Restrained Molecular Dynamics is greater than that structures obtained by purely geometric methods.

1.4 Molecular modelling

Molecular modelling is a discipline that contribute to the understanding of the molecular features, such as 3D conformations, molecular interactions, binding energies, etc., in a qualitative and sometimes quantitative way. It can be considered as a range of computerized techniques, based on theoretical chemistry methods and experimental data that can be used to analyze molecules and molecular systems, or even to predict molecular and biological properties. Some of the aspects of molecular modelling have been used in this work and they have been described briefly in this section.

1.4.1 Molecular mechanics

The potential energy surface of a macromolecule, described by a potential energy function comprises bonded terms (such as bond lengths, angles and dihedrals), non-bonded terms (such as van der Waals and electrostatic interactions) and restraint terms as shown in Eq.1.2.

$$E = E_{bond} + E_{angle} + E_{torsion} + E_{improp} + E_{VDW} + E_{elec} + E_{target} \quad \text{Eq. 1.2}$$

The covalent bond between two atoms is usually described by potential energy due to deformation of the bond lengths (E_{bond}):

$$E_{bond} = K_b(b - b_0)^2 \qquad \text{Eq. 1.3}$$

where K_b is the spring constant defining the strength of the interaction (comes from spectroscopic studies) and b_0 is the perfect bond distance for given two atoms (determined from X-ray crystallography).

Bending energy (E_{angle}) represents the deformation of bond angles,

$$E_{angle} = K_\theta(\theta - \theta_0)^2 \qquad \text{Eq. 1.4}$$

where K_θ is the strength of the bending motion and θ_0 represents the equilibrium bond angle. It was found that bond lengths and angles very similar in different structures, and that the folding of the macromolecules can be described by torsion angles. The energy changes involved in the rotation around a given bond ($E_{torsion}$) is usually small and tends to be periodic,

$$E_{torsion} = K_\varphi(1 + \cos(n\varphi - \delta)) \qquad \text{Eq. 1.5}$$

where K_φ is the force constant, n the periodicity and δ a reference angle at which the potential is maximum. It may be necessary to define improper torsion angles such as those involved in minimizing out-of-plane bending, for example keeping conjugate group planar, with each group having the energy term (E_{improp}) defined.

Between each two atoms, two nonbonded types of forces exist even for a neutral molecule: repulsion (due to electron cloud overlap) and attractive forces (due to induced dipole within an electron cloud). These could be represented by one van der Waals energy term (E_{VDW}), in which r^{-6} describes attractive interaction and r^{-12} represents repulsive forces, and depending on the depth (D) and position (r_0) of two atoms:

Eq. 1.6

$$E_{VDW}=4D[(\frac{r_0}{r_{ij}})^6+(\frac{r_0}{r_{ij}})^{12}$$

Electrostatic term (E_{elec}) describes the interaction between partial charges of atoms (formed due to electrostatic field around atom) by Coulomb's law,

Eq. 1.7

$$E_{elec}=\frac{q_i q_j}{4\pi\varepsilon_0\varepsilon r_{ij}}$$

E_{target} is an energy term to restrain the structure such that it satisfies experimental observations, for example this term is used to restrain specific inter-proton distances in accordance with those determined experimentally due to the Nuclear Overhauser Effect.

Molecular mechanics is based on energy minimisation, which employs the first derivative of the potential energy function to compute a new conformation. It is expected that the new conformation should have a lower energy that the previous one [Levitt, 1982]. Iteration of the process reduces the potential energy of the system until an energy minimum is reached. Hence, a cycle of energy minimisation represents a step in conformational space [McCammon and Harvey, 1987]. The problem with energy minimisation routines is that they become trapped in local minima, and there may be many energetically stable conformations of a protein or peptide, the one to which minimisation converges is unlikely to be the global minimum. The descent into local minima thus prevents efficient exploration of conformational space and other methods are used to overcome this problem. However, this method was used to model the 5-HT2 receptor [Kristiansen et al., 1993;Sytle et al., 1993] and human opoid receptors [Habibi-Nezhad et al., 1996].

1.4.2 Molecular dynamics

The basis of molecular dynamics is iteratively solving Newton's equations of motion for the macromolecule in order to obtain the atomic positions and velocities as a function of time. While energy minimisation is a convergent process (ie. a minimum in the potential energy surface is reached), molecular dynamics is non-convergent and thus explores the potential energy surface more efficiently [McCammon and Harvey, 1987]. Molecular dynamics relates the force, F_i, acting on the particle of mass, m_i, and acceleration a_i,

$$\overline{F_i}=m_i\overline{a_i} \qquad \text{Eq. 1.8}$$

The force can be calculated as the negative of the gradient using equation 1.9, if the interaction energy can be described by using the potential energy function (equation 1.1).

$$\overline{F_i}=-\frac{\delta E}{\delta \overline{r_i}} \qquad \text{Eq. 1.9}$$

In a molecular dynamics simulation, the evaluation of the of the atomic coordinates and velocities for each atom at a regular discrete time is performed. The solution of this problem is usually approximated by the Verlet algorithm [Verlet, 1967], or frequently for macromolecules, a constrained Verlet algorithm, known as SHAKE is used [van Gunsteren and Berendsen, 1977], in which the highest frequency motions are constrained.

Simulated annealing (SA) [Kirkpatrik et al., 1983] provides a method to overcome the local energy minimum problem. Through the heating of the molecular system and cooling it down, the search of the conformational space of a peptide or protein is much

more efficiently than energy minimisation. Simulated annealing, implemented via molecular dynamics using the Verlet algorithm for example [Verlet, 1967] has been incorporated into methods for the determination of protein structure both by X-ray crystallography and NMR spectroscopy, and in molecular modelling. For each application the E_{target} energy term (Equation 1.2) is being used to restrain the structure such that it satisfies experimental observations.

In all three applications conformational space is explored by high temperature molecular dynamics followed by the cooling of the system (the "simulated annealing") in such way that only energetically favourable structures are retained. In NMR structure determination SA/MD has been introduced as an alternative to distance geometric methods [Havel and Wüthrich, 1985] in order to generate structures suitable for refinement by molecular dynamics [Nilges et al., 1988a; Nilges et al., 1988b]. The SA/MD has been used to generate ensembles of models of proteins structures, or fragments thereof, for which secondary, but not tertiary structural information was available. The method has been used by Brünger and colleagues to predict the structure of the coiled-coil region of the yeast transcriptional activator, GCN4 [Nilges and Brünger, 1991; Nilges and Brünger, 1993] and the transmembrane dimerisation region of glycophorin A [Treutlein et al., 1992; Lemmon et al., 1994]. Subsequent determination of the GCN4 structure [O'Shea et al., 1991] revealed that the prediction was accurate [Nilges and Brünger, 1993]. The SA/MD protocol was also used to study the ion-channel pore forming and properties [Kerr et al., 1994; Kerr et al., 1996; Breed et al., 1997].

1.4.3 Protein docking

Specific recognition is the requirement for an unambigous biochemical function of proteins. The formation of enzyme complexes with substrate, antibody - antigen complexes, or folding of politopic proteins are examples of such a function. Modelling the interaction between molecules is a complex problem. Many forces are involved in the intermolecular association: hydrophobic, dispersion (van der Waals), hydrogen bonding and electrostatic (ion pairing). The major driving force appears to be hydrophobic interactions, but the specificity of the binding appears to be controlled by hydrogen bonding and electrostatic interactions [Fersht, 1984; Street et al., 1986]. Many different approaches were adopted in the the prediction of protein - protein complexes, commonly known as the protein docking, and some will be mentioned here. The DOCK software was developed as a rigid body docking [Kuntz et al., 1982] and evolved into a procedure which allowed the flexibility of the ligand [Knegtel et al., 1997]. FlexX software is an other attempt to dock a flexible ligand and protein using a pose clustering algorithm [Rarey et al., 1996]. The influence of the solvent was presented in the FTDOCK software [Jackson et al., 1998] and also combined with the genetic algorithm [Jones et al., 1995].

The GRAMM (the Global Range Molecular Matching) methodology used in this thesis is an empirical approach to smoothing the intermolecular energy function by changing the range of the atom-atom potentials [Katchalski-Katzir et al., 1992; Vakser, and Afalo, 1994; Vakser, 1995b]. The molecular pairs may be: two proteins, a protein and a smaller compound, two transmembrane (TM) helices, etc. It may be used for high-resolution molecules, for inaccurate structures (where only the gross structural features are known), in cases of large conformational changes. To predict the structure of a complex, it requires only the atomic coordinates of the two molecules. The algorithm performs an

exhaustive 6-dimensional search through the relative translations and rotations of the molecules. The technique permits the locating of the area of the global minimum of intermolecular energy for structures of different accuracy [Vakser, 1995b]. The quality of the prediction depends on the accuracy of the structures. Thus, the docking of high-resolution structures with small conformational changes yields an accurate prediction, while the docking of ultralow-resolution structures will give only the gross features of the complex [Vakser, 1995a; Vakser 1996].

1.5 Aim of the work

This chapter has introduced the key points about allergy processes, and the general importance of the high affinity IgE receptor. It has also discussed the structure elucidation of the membrane proteins. In the forthcoming chapters there are three main objectives:

a) Attempts will be made to provide the structural information for connecting loops of the β-subunit of rat FcεRI, and these are the subjects of Chapters 2. and 3.

b) The lipid - TM helix interaction and TM helix - TM helix packing in the transmembrane region of rat FcεRI will be subject of the Chapters 4., 5., and 6.

c) Using a combination of the obtained structural data from experiments and theoretical calculations, the plausible models of the β-subunit of rat FcεRI will be proposed in the Chapter 7.The knowledge obtained in this work could provide a basis for the rational design of further experiments, that could lead to computer aided drug design.

Chapter 2.

CONFORMATIONAL STUDIES OF THE CONNECTING LOOP 2-3 PEPTIDE OF THE β-SUBUNIT OF THE HIGH AFFINITY IgE RECEPTOR

2. CONFORMATIONAL STUDIES OF THE CONNECTING LOOP 2-3 PEPTIDE OF THE β-SUBUNIT OF THE HIGH AFFINITY IgE RECEPTOR

2.1 Background

The protein sequences of many membrane receptors and ion channels have been determined and, by utilizing a variety of prediction methods, putative models were proposed. They could posses seven α- helices of approximately 22 residues that span the membrane. These seven transmembrane helices divided such membrane proteins into a) extracellular and cytoplasmic domains and b) loop sequences that connect them. Crystallographic information for the multiple membrane spanning protein *Bacteriorhodopsin* confirmed such a basic form composed of bundles of α-helices that pack together [Henderson et al., 1990; Choi et al., 1992]. The bundle is embedded in the membrane with its long α-helix axes approximately normal to the plane of the membrane, and with an undefined structure for the extramembranous domains and loop sequences. A putative model could form a basis for understanding drug-receptor interaction [Sylte et al., 1993; Sylte et al., 1996; Kristiansen and Dahl, 1996] or voltage- and ligand-gated channels as sites for drug action, but a knowledge of the 3D structure of the receptor would greatly improve the study of drug-membrane protein interaction and drug design.

Advances in 3D structure determination and prediction of receptors have taken place, but there are still difficulties in obtaining high-resolution structural information on

whole receptors by techniques such as crystallography and solution NMR. Hence, alternative approaches are being developed: a) synthetic or genetic production of domains of receptors and their structural determination by crystallography and/or 2D/3D NMR [Anderson et al., 1993; Anderson et al., 1994/5; Barsukov et al., 1990; Padlan and Helm, 1992; Thomas et al, 1993; Yeagle et al., 1995; Yeagle et al, 1997; Zloh et al., 1994a; Zloh et al., 1994b; Zloh et al., 1995], b) combination of computational methods with some experimental facts [Zloh et al., 1995; Lemon et al., 1994; Adams et al., 1995] and c) computational models on their own [Sylte et al., 1993; Habibi-Nezhad et al., 1996].

The high affinity IgE receptor, Fc_eRI, possesses a tetrameric $\alpha\beta\gamma_2$ structure,[Blank et al., 1989]. The β-subunit is a polytopic protein with four hydrophobic membrane-spanning segments, whereas the individual α- and γ-subunits are bitopic proteins each containing one transmembrane domain. In the proposed model [Blank et al., 1989] the four transmembrane α- helices of the β-subunit were connected by three loop (connecting) sequences and there was no evidence for covalent interaction between different subunits.

Loop peptides prevent the diffusion of the helices away from each other [Kahn et al., 1992], and should favor interaction between helices connected by shorter loops. This natural division of the high affinity IgE receptor into domains led to the strategy of structure determination of synthesized peptides by CD, NMR-based molecular mechanics and dynamics studies. The β-subunit has been predicted to form a four helix bundle of the transmembrane α-helices and indicated an α-moiety structure within the loop peptides in TFE solution and in the presence of SDS micelles. This result rise to the model of the β-subunit with the motif TM helix - bend - loop helix - bend - TM helix occurring three times [Zloh et al., 1995] and to the suggestion that this motif might be common to 7-helix receptor. The cytoplasmic loop that connects transmembrane helices 2 and 3 of the β-

subunit of the high affinity IgE receptor is 11 residues long (Figure 1.2). In this chapter, an NMR study of the 11-residue loop peptide (loop 2-3) is presented and correlated with studies by circular dichroism and NMR based molecular modelling. The α-helix moiety was found in TFE solution which confirmed the proposal that α-helical loop peptides could connect transmembrane helices and form TM helix - turn - loop helix - turn - TM helix motif.

2.2 Material and Methods

The peptide loop 2-3, with the sequence ERKNTLYLVRG, was synthesized by Dr M. Danton and Dr I. Toth, School of Pharmacy, London.

2.2.1 Circular Dichroism

All CD spectra were recorded on a Jasco J600 and on Jasco J720 spectrometers at room temperature. Peptide samples were weighed out using a Sartorius balance (+/- 1 ug) and solvent added to give a peptide concentration of 0.4 mg/ml. All solvents were UV grade. pH measurements were made with a Ciba-Corning pH meter. Quartz QS cylindrical Helma cells with a path-lengths varying from 0.001 cm to 1 cm were used. The spectra were recorded over the wavelength range of 260 to 185 nm. The bandwidth was set to 0.2 nm and time constant to 4 s. Scan speed was 10 nm/min and step resolution 0.2 nm. Spectra were corrected for concentration, the solvent baseline subtracted and the $\Delta\epsilon$ values calculated. The plotted spectra were digitized by WinDig (Windows Digitizer) software (Lovy, 1996), taking the $\Delta\epsilon$ values at 1 nm in the 190 to 260 nm range. The obtained $\Delta\epsilon$ values were used to calculate the secondary structure by CDNN (Circular Dichroism Neural Network) software preforming CD spectra deconvolution [Böhm, 1997]. The result was expressed as a percentage of the five different secondary structures (α- helix, antiparallel and parallel β-sheet, turn and random coil), and normalized to 100 %.

2.2.2 NMR Spectroscopy

Peptide samples were weighed on the Sartorius analytical balance with a precision of +/- 0.1 mg, dissolved in D_2O, TFE-d2 and mixture of those two. The resulting solutions

were filtered through 0.2 μm Millipore aqueous/organic filters into 5mm Wilmad NMR tubes. The pH of aqueous samples was measured using a Ciba-Corning 120 pH meter with a Russell CMAWL/3.7/185 electrode. The pH adjustments were made if necessary using HCl, DCl, NaOH or NaOD to pH around 3.0. Aqueous samples were degassed using filtered N_2 and all samples sealed with parafilm.

The double distilled, deionized water was used, 99.96% D2O ampules were obtained from Fluorochem Ltd., UK and TFE-d3, solvent was obtained from GOSS Scientific Instruments Ltd., UK. TFE-d3 was converted to TFE-d2 by mixing it with two parts of water, standing for 30 minutes and then distilled. The peptide samples were measured using Gilson pipettes.

The 2 mM solutions of synthetic 11-residue loop peptide in the water-D_2O, TFE-d2 and water/TFE-d2 mixtures were used for the NMR experiments. NMR spectra were obtained with Brüker AM 500 MHz and AMX 600 MHz spectrometers at 298 K. 1D proton NMR spectra were obtained with 32K data points in the t_2 domain. All 2D NMR DQF COSY [Rance et al., 1983], TOCSY [Bax and Davis, 1985] and NOESY [Jeener et al., 1979; Kumar et al., 1980] spectra had 512 increments in t_1 with 2048 data points in t_2 domain. TOCSY spectra were recorded with a spin-lock mixing time of 55 ms, and mixing times of 80, 150, 300 and 500 ms were used in NOESY experiments. All 2D spectra were accumulated in a phase sensitive manner using time-proportional phase incrementation for quadrature detection in F_1. Felix 2.3 software [Biosym Inc., USA] was used to process NMR spectra. Chemical shifts were referenced to internal TSP and TFE accordingly. Sequence-specific assignments of the ^1H NMR spectra were obtained using standard approaches and the results are listed in Tables 2.2, 2.3 and 2.4.

2.2.3 Structure Calculations

The three dimensional structures of the peptide in different solvents were determined using intraresidual and sequential NOEs. NMR-based molecular modelling was carried out by XPLOR 3.1 program [Brunger et al., 1987; Brunger, 1993], using simulated annealing protocols with constraints derived from 2D NOESY and ROESY experiments. NOE intensities were characterized as strong, medium and weak and translated in the corresponding upper limits distance range constraints of 2.5, 3.5 and 5.0 Å, respectively. A correction factor of 0.5 Å for the use of pseudoatoms was added to interproton distance restraints involving methyl groups to account for the apparent higher intensity of the peaks. Lower bounds between nonbonded atoms were set to the sum of their van der Waals radii (about 1.8 Å). Energy refinement calculations (restrained minimizations and dynamics) were carried out on 20 for water and water-TFE, and on 50 structures for TFE.

2.3 Results and Discussion

2.3.1 Circular dichroism spectroscopy of the interconnecting loop peptide (loop 2-3).

Circular dichroism and perturbation CD can reveal the presence of individual conformational moieties and regular conformations and give information about the conformational equilibria that exists between them [Anderson et al., 1992; Anderson et al., 1994/5, Thomas et al., 1993; Siligardi et al., 1991; Siligardi et al.,1994]. The CD spectra of the loop 2-3 peptide was recorded under a variety of conditions in order to ascertain the range of conformations available to this cytoplasmic loop domain. The water-TFE titration of the 11- residue peptide (Figure 2.1) contains two isosbestic points corresponding to an equilibrium between three conformational states I (H_2O), II (between 40-80% TFE) and III (between 95-100% TFE). The transitions (T_s) between these states was shown to be cooperative (equivalent of unfolding or melting) by Figure 2.2. The existence of those cooperative transitions, albeit with broad T_s behaviour supported conclusion from the existence of the isobestic points in Figure 2.1. A conformational equilibrium between different state of moieties existed and that different moieties were stabilized/destabilized according to solvent composition. Further information concerning the nature of conformational states I, II and III was deduced by deconvolution of the actual CD spectra using CDNN software (Table 2.1).

State III contained α-helix which was destabilized in states I and II. The conformational interpretation of state I CD spectra is still controversial, but a combination of FTIR, IR-CD, perturbation CD and CD spectral stimulation has confirmed earlier proposals that it is a summation of a limited number of regular conformations, a major portion of which are turn conformations and left-handed extended helices (LHE) [Drake et

al., 1988]. There are still examples where this peptide CD spectrum is interpreted as representative of "random coil" or "disordered structures". Woody (1991) has summarized these data and arguments and, partly because of theory, but also because of the existence of cooperative transitions and isosbestic points, he has favoured the LHE helix (or polyproline II) proposal.

The CD spectra of the loop peptide 2-3 in the presence of SDS micelles was presented in Figure 2.3. Addition of SDS at concentrations above its CMC increased the α-helical content in H_2O, and concomitantly reduced the content of the extended (LHE) conformational moiety (Table 2.1). The presence of the SDS micelles induced the conformational change from state I to the conformation similar to the state III.

These CD studies of the cytoplasmic 11- residue peptide in TFE, indicated a conformational equilibrium in which a one component or moiety was an α-helix structure. That was expected since TFE promotes α-helix secondary structure [Kemmnik and Creighton, 1995; Shiraki et al, 1995]. The addition of SDS at concentrations above critical micellar concentration, increased the α-helical content in H_2O. This indicated that this peptide could adopt a defined conformation dependent upon solvent polarity, and that it could be a suitable subject for NMR analysis.

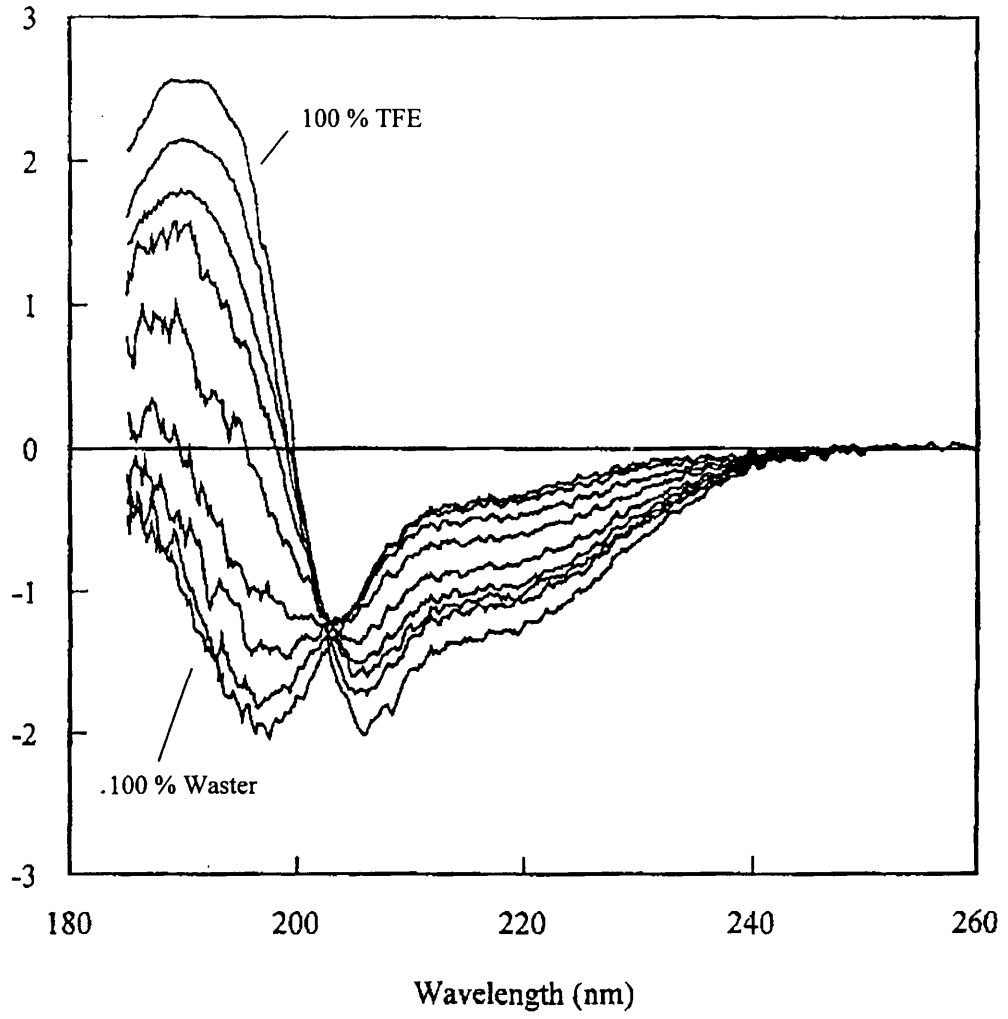

Figure 2.1 The electronic circular dichroism spectra for loop 2-3 of the β-subunit of the high affinity IgE receptor at different TFE/water compositions during water-trifluoroethanol (TFE) titration (c = 0.4 mg/ml; 0.02cm quartz cell; step resolution = 0.2 nm; ns = 1). The following solvent compositions were used: 0 % TFE - 100 % water; 7.5 % TFE - 92.5 % water; 15 % TFE - 85 % water; 20% TFE - 80 % water; 30% TFE - 70 % water; 50% TFE - 50 % water; 75% TFE - 25 % water; 90% TFE - 10 % water and 100% TFE - 0 % water.

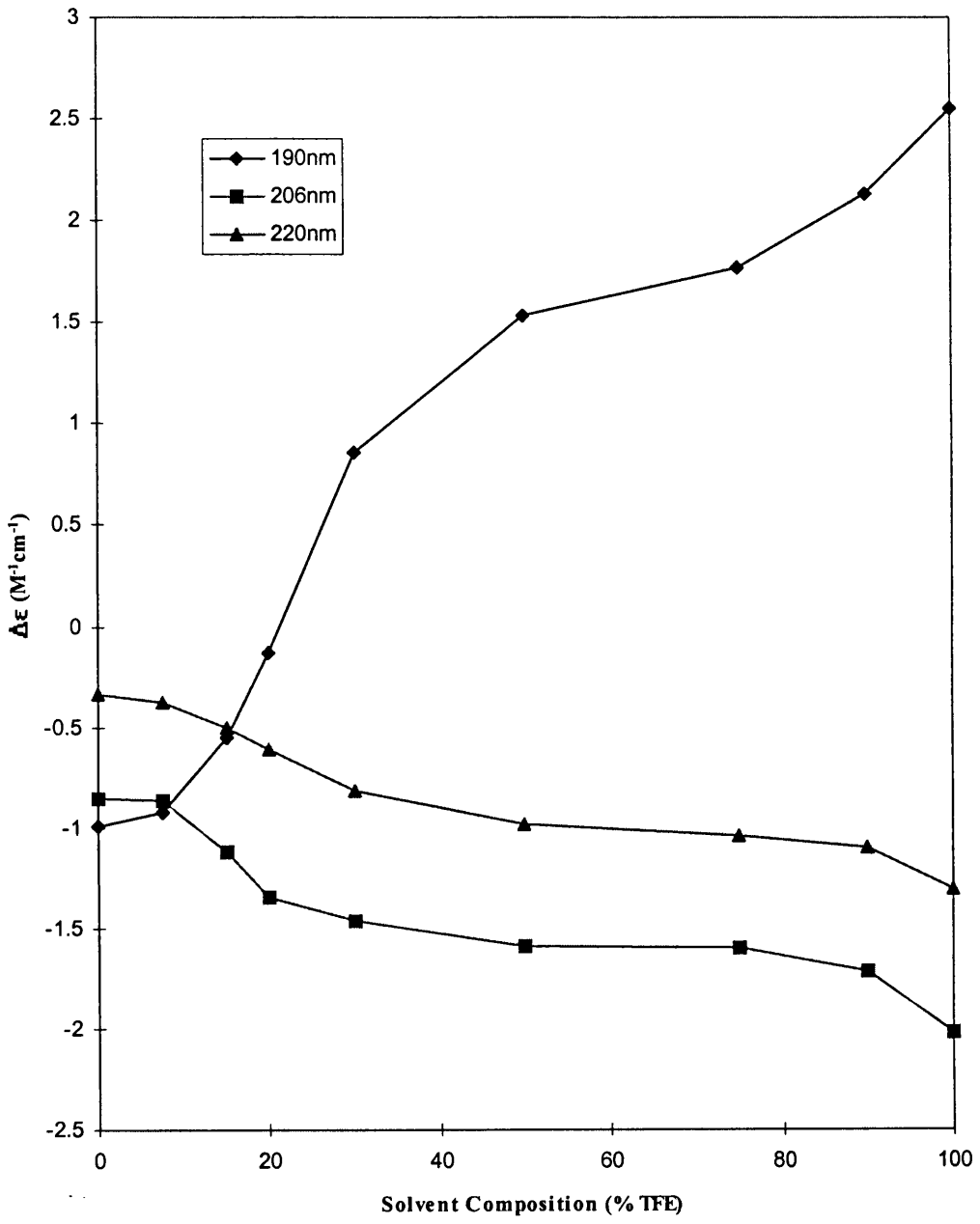

Figure 2.2 Changes in Δε observed at 190, 206 and 220 nm in the CD spectra of loop 2-3 as the solvent composition was altered during TFE/water titration.

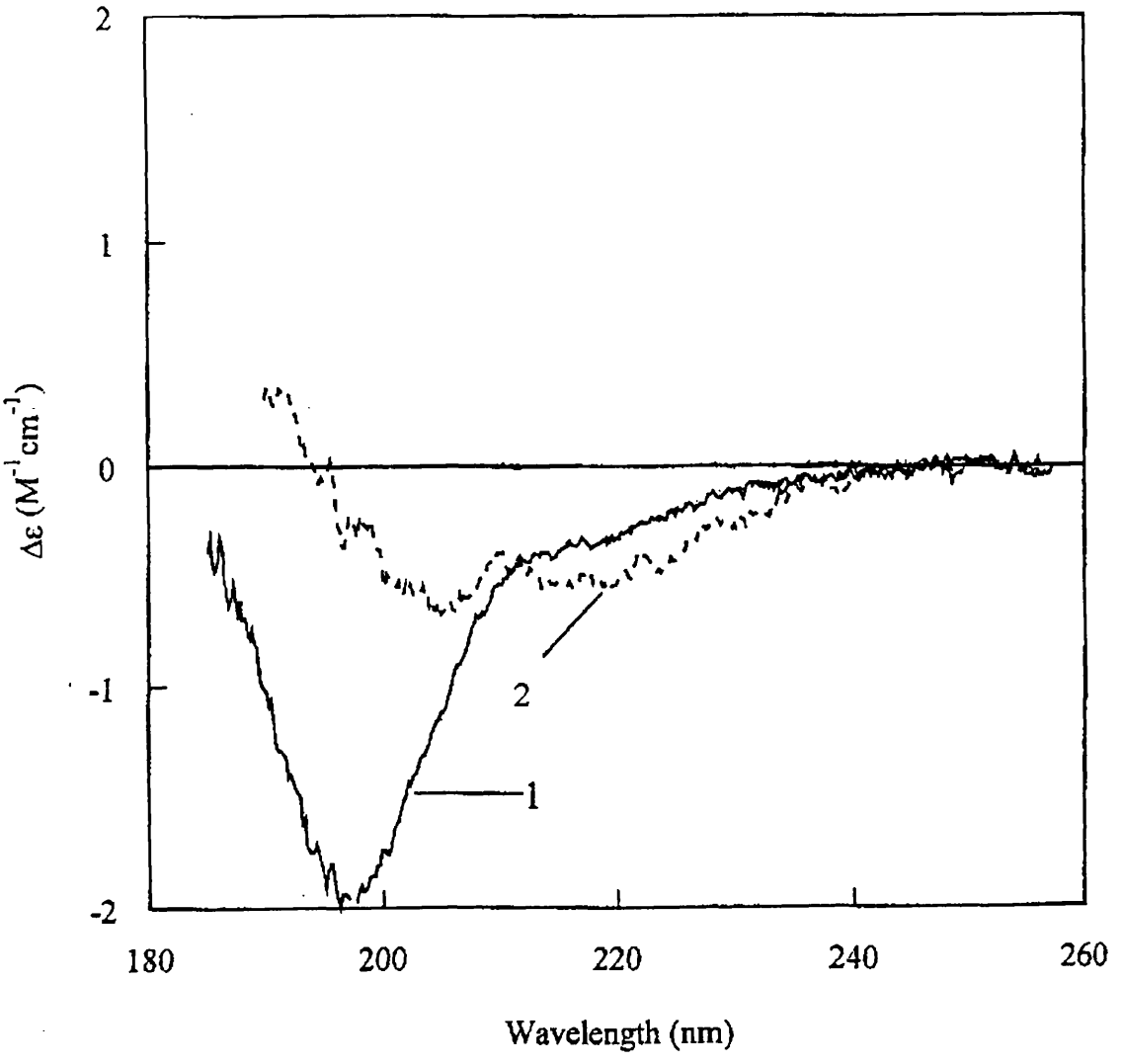

Figure 2.3 Electronic CD spectra of loop 2-3 in (1) water and (2) water + supramicellar SDS concentration (20 mM SDS final concentration; c = 0.4 mg/ml; 0.02 cm quartz cell; step resolution = 0.2 nm; ns = 1).

Table 2.1 The calculated secondary structure of the loop peptide that connects TM helices 2 and 3 of the β-subunit of the high affinity IgE receptor based on the CD spectra of the solvent titration from the pure water to pure TFE solution and in the presence of SDS micelles.

	α- helix	Antiparallel	Parallel	β-turn	Random
100%H_2O 0% TFE	10.1	36.7	9.1	15.6	27.91
90% H_2O 10% TFE	10.9	36	9.2	15.7	28.2
85% H_2O 15% TFE	11.5	34.7	9.2	15.8	28.8
80% H_2O 20% TFE	12.5	33	9.3	15.8	29.4
70% H_2O 30% TFE	14.3	29.7	9.3	16.3	30.4
50% H_2O 50% TFE	16	27	9.4	16.6	31
25% H_2O 75% TFE	17	25.4	9.4	16.7	31.5
10% H_2O 90% TFE	18.2	23.8	9.4	16.9	31.7
0% H_2O 100% TFE	20	21.7	9.3	17.1	31.9
H_2O + SDS micelles	13.5	30.4	9.3	15.7	31

Please note: the obtained results by CDNN software were normalized to 100%.

2.3.2 NMR Spectroscopy of loop 2-3

The 1D and various 2D NMR spectra were obtained for the loop 2-3 peptide dissolved in 90 % H_2O/ 10 % D_2O, TFE-d2 and 40 %H2O/ 60 % TFE-d2 media. These solvent compositions corresponded to the solvent mixtures in which peptide adopted three different conformational states of the loop 2-3 as found by CD analysis. NMR structural studies of the loop 2-3 in these solvent mixtures should shed more detailed light on the conformational space that the loop 2-3 peptide could occupy.

2.3.2.1 NMR spectra of loop 2-3 in TFE

The expansions of the 1D proton NMR spectrum of the loop 2-3 is shown in Figure 2.4. The two types of NH peaks with different intensities were observed, and this could imply the presence of impurity in the sample, but evidence that the lower and high intensity peaks corresponded to different conformations of the loop 2-3 (major and minor components). The ratio between area under peaks for these two components indicated the presence of less than 10 % of the minor component.

The eight residues were detected in minor component. The minor component was easily detected in the amide region of the 1D spectrum. In the α-proton region of the 1D spectrum the peaks of three residues in minor component could be observed. For the rest of the side chains only the two CH_3 groups were observed in the minor component.

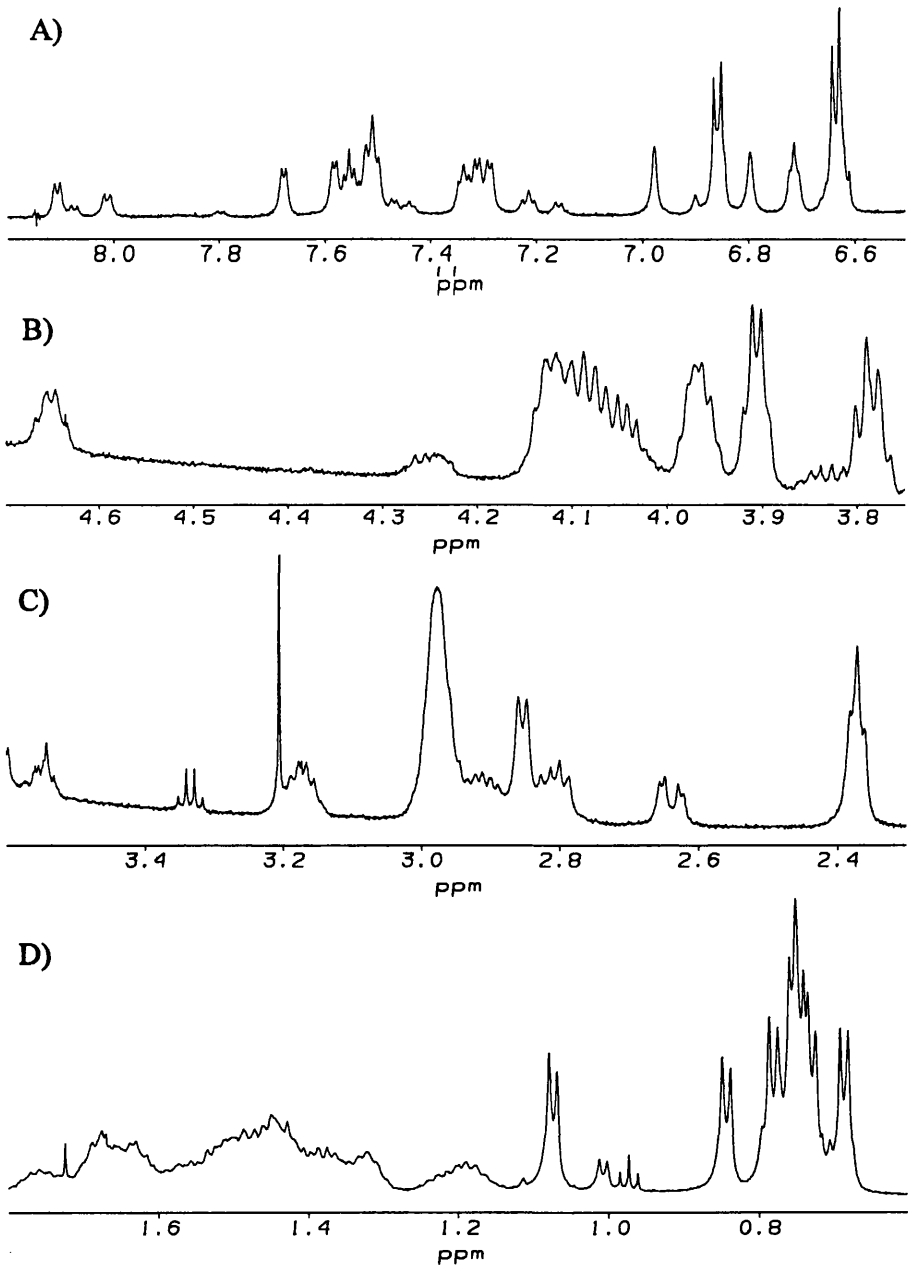

Figure 2.4 The expansions of the 1D proton NMR spectrum of the loop 2-3 of the β subunit of high affinity IgE receptor in TFE-d2; T= 298K, c=2 mM. A) amide and aromatic region, B) α proton region, C) and D) show the rest of the spectrum.

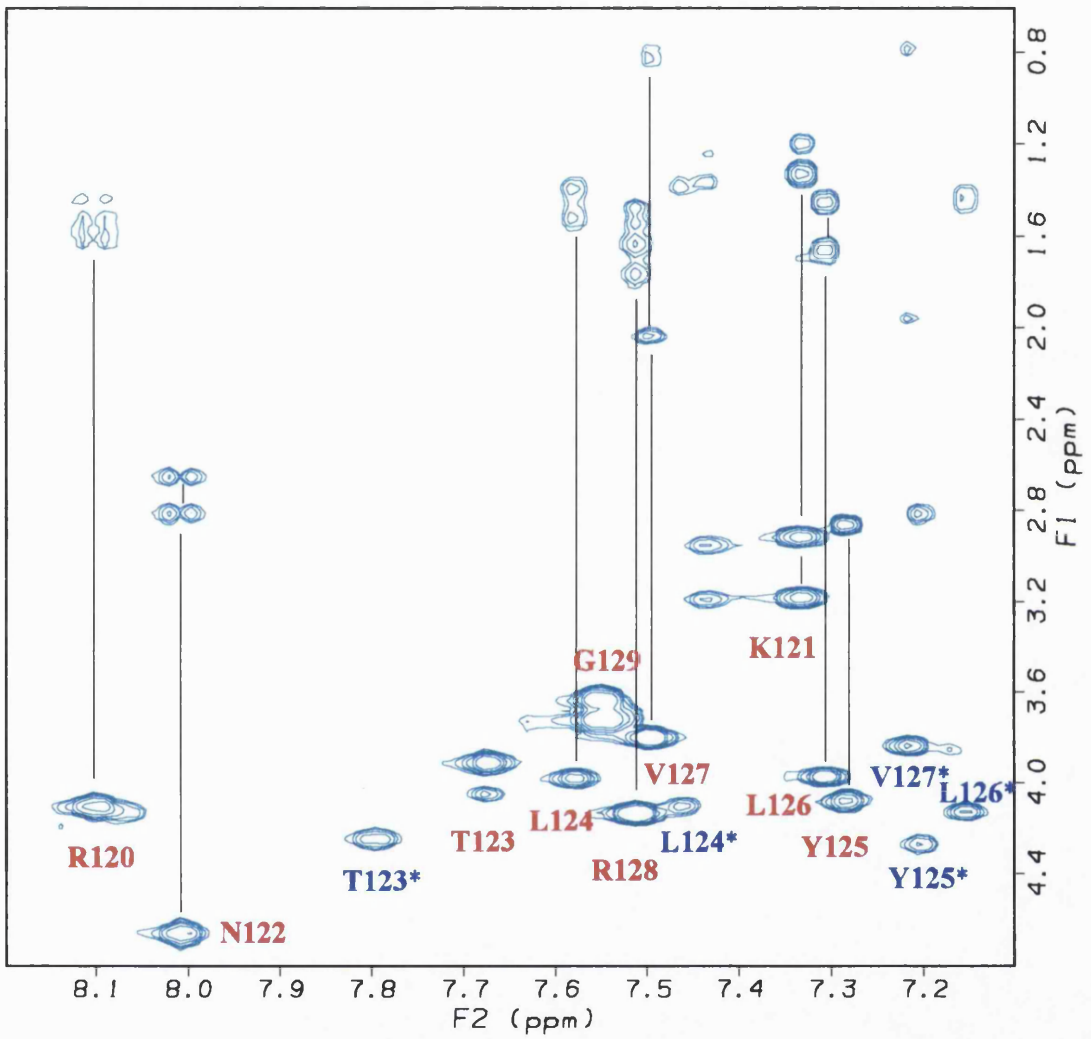

Figure 2.5 The NH/sidechain region of a 600 MHz TOCSY spectrum (τ_m = 55ms) used to assign the amino acid spin systems of 2 mM loop 2-3 of the β-subunit of the high affinity IgE receptor in TFE-d2 at 298K.

A)

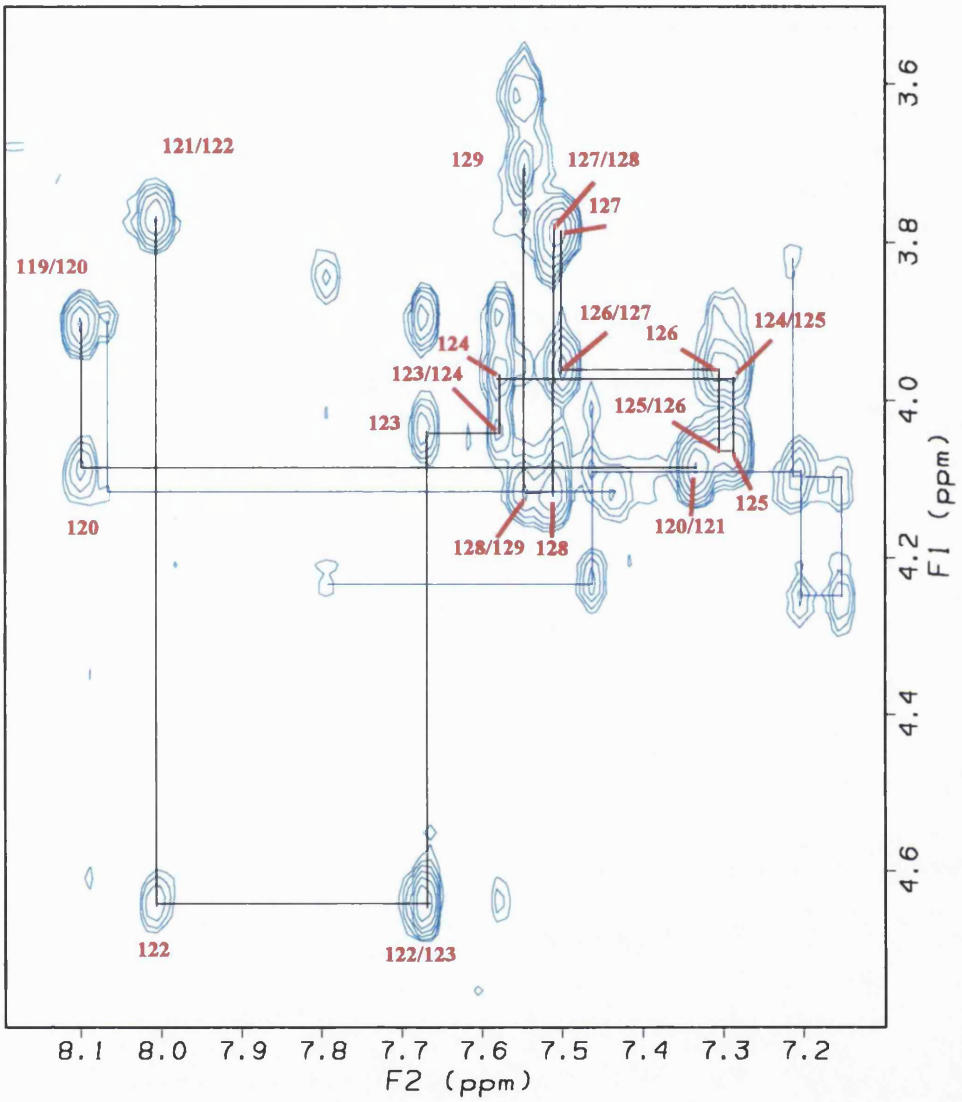
121/122
129
127/128
127
119/120
126/127
126
124/125
124
123/124
123
125/126
125
120
120/121
128/129
128
122
122/123
8.1
8.0
7.9
7.8
7.7
7.6
7.5
7.4
7.3
7.2
F2 (ppm)
3.6
3.8
4.0
4.2
4.4
4.6
F1 (ppm)

B)

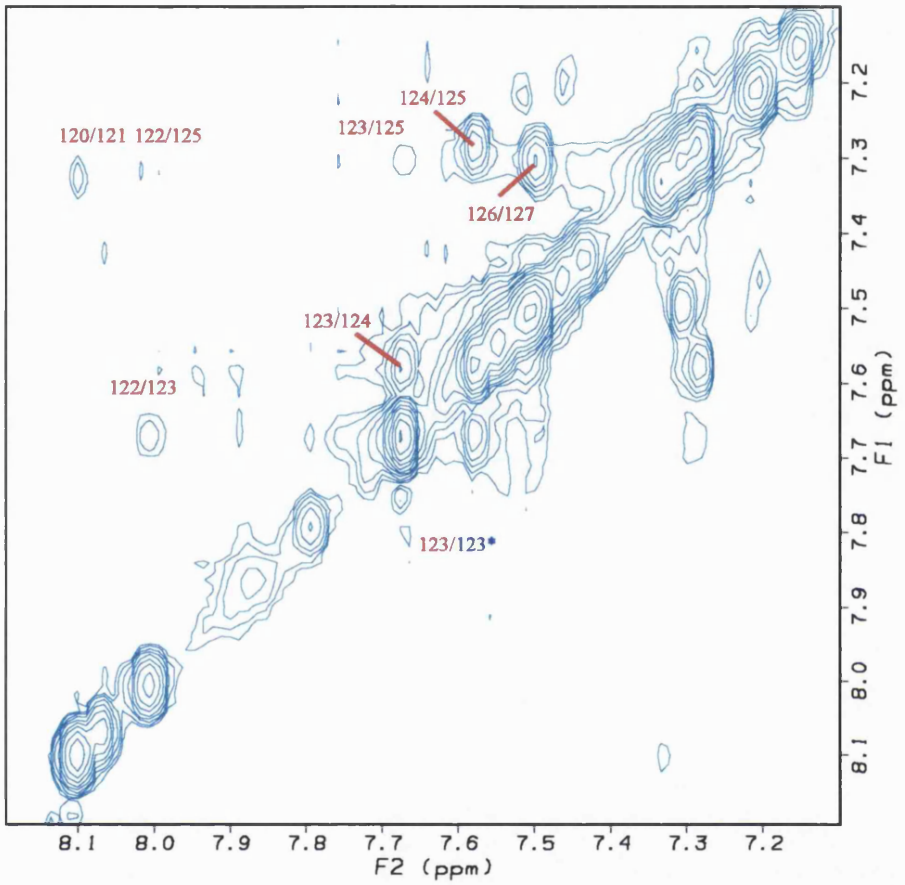

Figure 2.6 The finger print (NH/α proton) A) and NH/NH B) region of a 600 MHz NOESY spectrum (τ_m = 300ms) of 2 mM loop 2-3 of the β-subunit of the high affinity IgE receptor in TFE-d2 at 298 K.

Table 2.2 Assignment of spin systems of the 600 MHz ^{1}H NMR spectra of the loop 2-3 major component in TFE at 298K.

Residue	NH	αH	βH	γH	δH	Other	$^3J_{NH}$ (Hz)
E119		3.9	2.36	2			
R120	8.1	4.1	1.58	1.47	2.97	6.90;5.80	5.5
K121	7.33	3.76	1.67	1.18	1.31	3.17;2.90	6.6
N122	8.01	4.64	2.81;2.63	6.79;5.70			6.1
T123	7.67	4.03	3.9	1.07			5.5
L124	7.58	3.97	1.48	1.37	0.68		5
Y125	7.28	4.07	2.84;2.78		6.84	6.63	5.5
L126	7.3	3.97	1.63	1.43	0.73		5.5
V127	7.5	3.82	2	0.84;0.75			7.7
R128	7.51	4.14	1.75;1.60	1.45	2.97	6.97;5.84	6.6
G129	7.55	3.73	3.62				

The major component corresponded to the conformational state III described in the section 2.3.1. The spin system assignment of individual residues of the ^{1}H NMR spectra in TFE of the loop 2-3 was achieved by DQF COSY and TOCSY spectra (Figure 2.5) and the sequential assignments using the fingerprint regions of TOCSY and NOESY spectra (Figure 2.6) and the walk along backbone strategy [Wutrich, 1984]. The sequence of the peptide was ERKNTLYLVRG. In the fingerprint region of the TOCSY spectra, 15 NH to αH atoms on crosspeaks were detected (Figure 2.5.) indicating the coexistence of the two stable conformations (components) in equilibrium in the TFE solution (second component designated by *). The full assignment of the major component in the NMR spectra of the

loop 2-3 is presented in the Table 2.2 (named state III according to the CD analysis) with the partial assignment of the minor component of the loop 2-3 in Table 2.3. Some of the peaks of the minor component were in the noise level and could not be detected. Some residues for the two components had different NH and αH chemical shifts, with the biggest difference detected in the middle of the peptide. The chemical shift difference for the NH peaks of the N122 residue in two components were 0.55 ppm. A similar phenomena was reported for the dimerization of the interleukin-8-8, when the different chemical shifts were observed for the same residue in the monomeric and dimeric form of the protein [Clubb, et al., 1994]. The presence of the loop 2-3 dimers in the sample could therefore be assumed.

The major component, as predicted by CD, was identified as an α-helix by specific cross-peaks appearing in the NOESY spectrum (Figure 2.6C). In the NH to NH region of the NOESY spectrum, cross-peaks characteristic for an α-helix were identified for pairs of residues N122:T123, N122: L126, L124:Y125, T123:L126, etc.

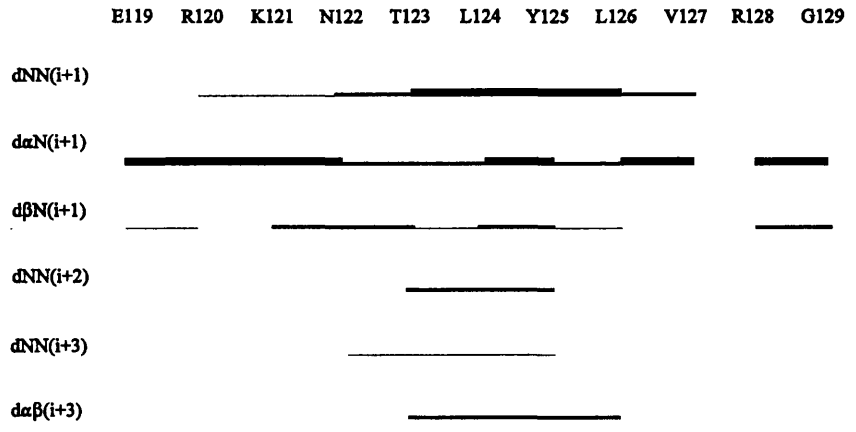

Figure 2.6C Summary of sequential and medium range NOE connectivities observed for the loop 2-3 in TFE-d2. The intensities of NOEs are categorised as strong, medium and weak and are represented by the thickness of the lines.

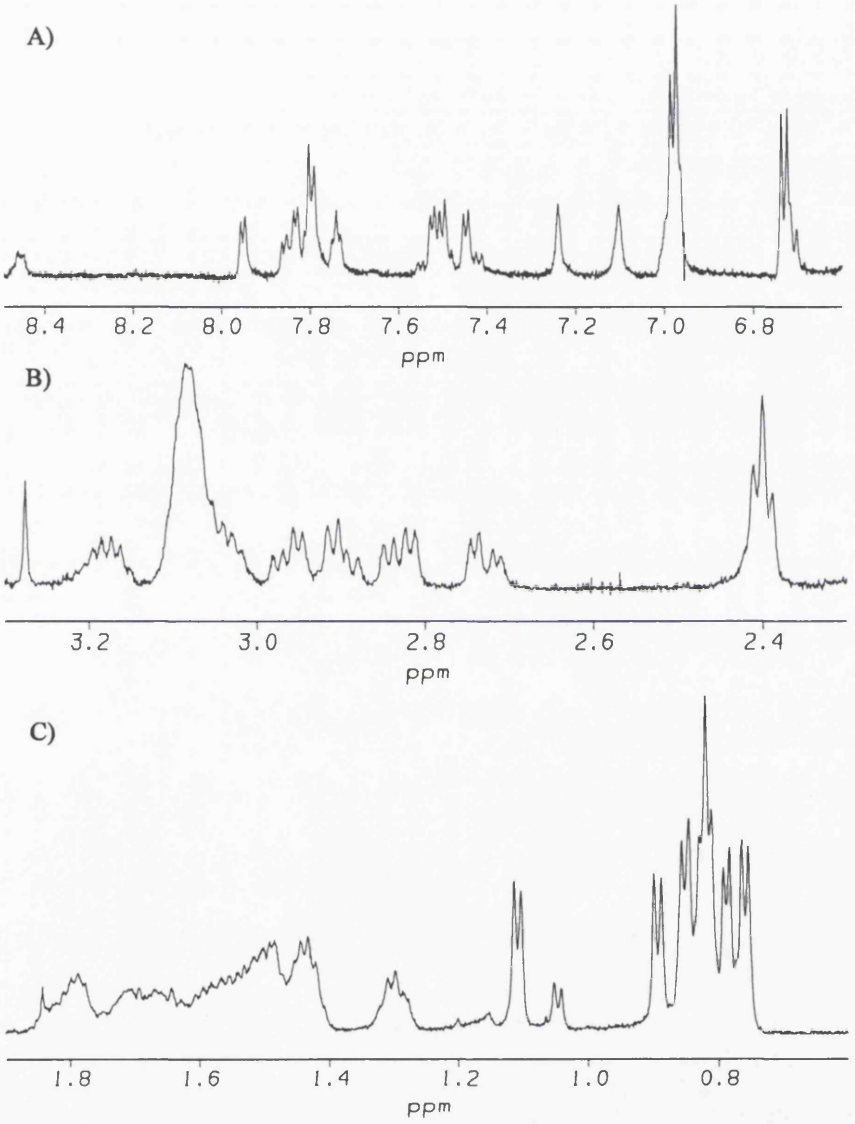

Figure 2.7 The expansions of 1D proton NMR spectrum of the loop 2-3 of the β-subunit of the high affinity IgE receptor in H_2O/TFE-d2 (4:6); T= 298K, c=2 mM. A) amide and aromatic region, B) β proton region and C) shows the rest of the spectrum.

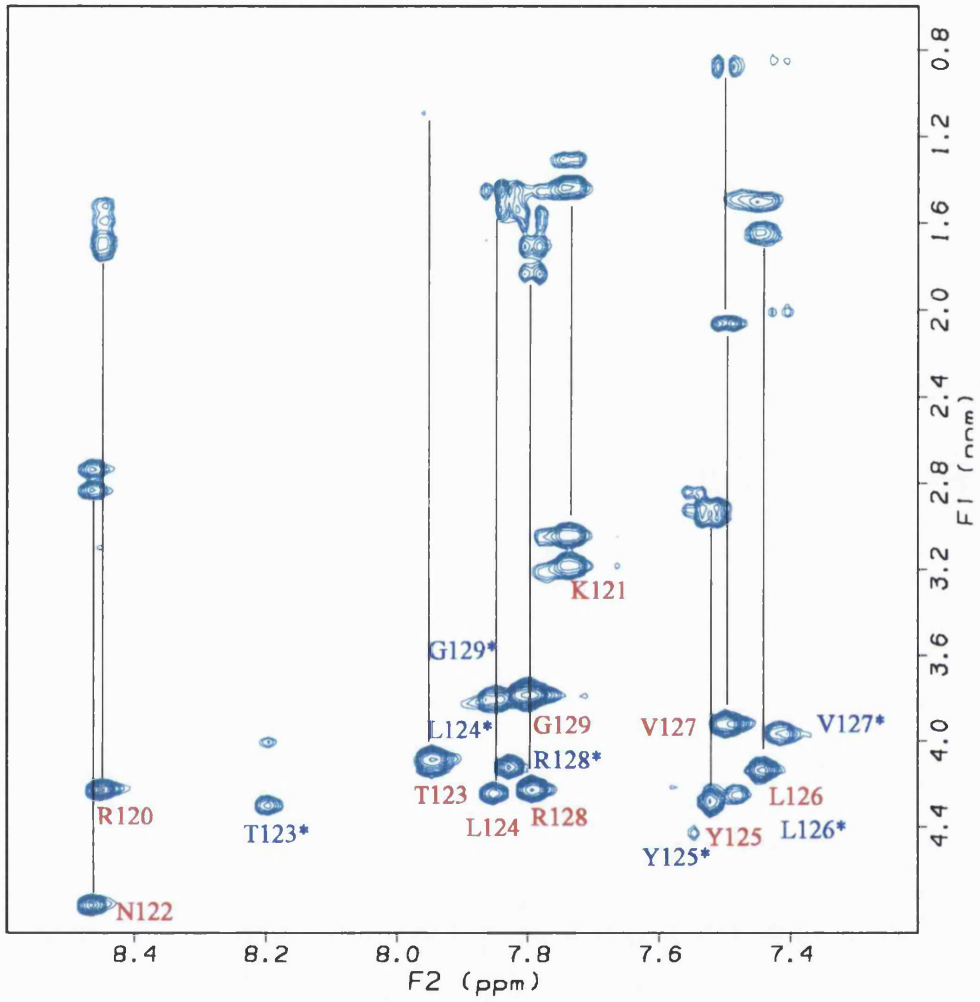

Figure 2.8 The NH/sidechain region of the of a 600 MHz TOCSY spectrum (τ_m = 55ms) used to assign the amino acid spin systems of 2 mM loop 2-3 of the β-subunit of the high affinity IgE receptor in H_2O/TFE-d2 (4:6) at 298K.

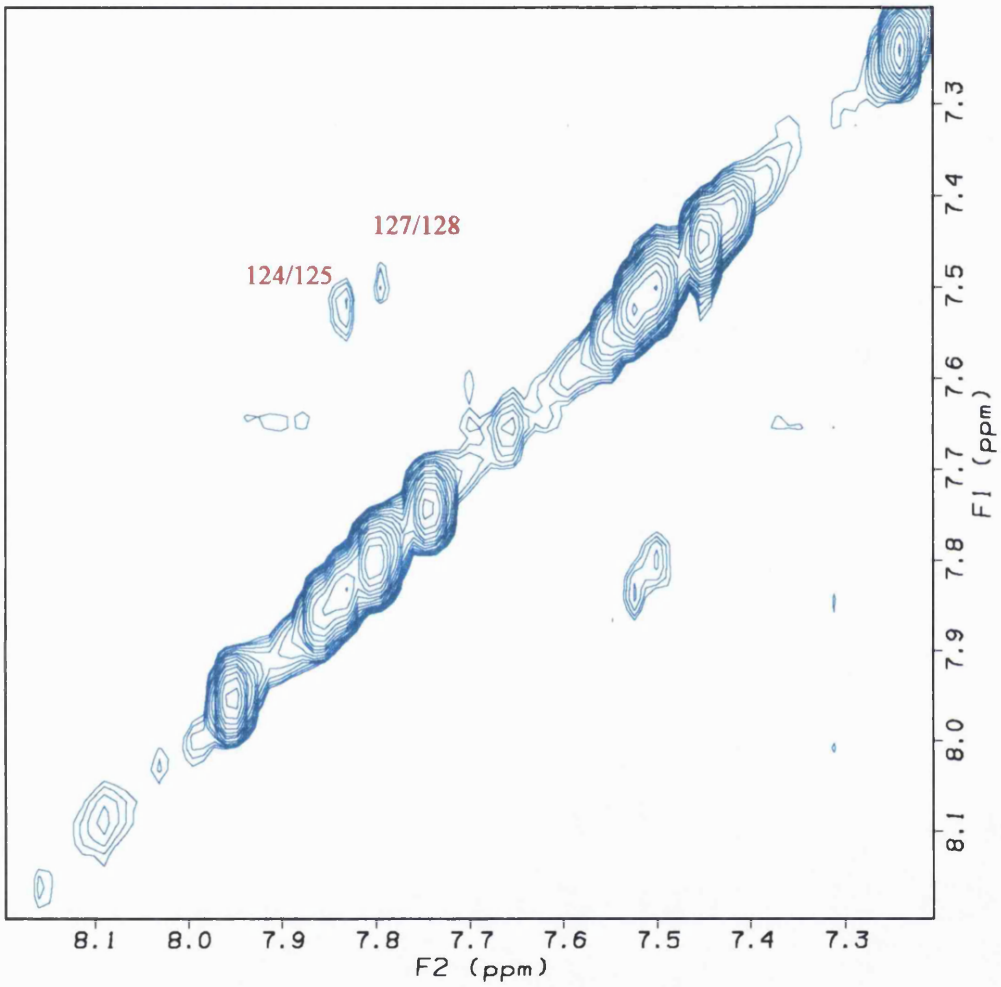

Figure 2.9 The NH/NH region of the of a 600 MHz NOESY spectrum (τ_m = 300ms) of 2 mM loop 2-3 of the β-subunit of the high affinity IgE receptor in H_2O/TFE-d2 (4:6) at 298 K.

Table 2.3: Assignment of spin systems of the ^{1}H NMR spectra of the minor component of the loop 2-3 in TFE at 298K.

Residue	NH	αH	βH	γH	Hδ
E119					
R120	8.06	4.14			
K121	7.43			1.25	3.21;2.96
N122	7.46				
T123	7.81	4.25	4.01	1	
L124	7.45	4.11	1.47	1.47	1.39
Y125	7.19	3.85	2.82		
L126	7.14	4.14	1.47	1.42	
V127	7.21	3.84	1.97	0.81	
R128					
G128					

2.3.2.2 NMR spectra of loop 2-3 in 40 % H2O / 60 % TFE-d2

The loop 2-3 peptide was studied by NMR when dissolved in 40 % H2O / 60 % TFE-d2. This solvent mixture corresponded to the environment in which loop 2-3 adopted conformational state II according to the CD analysis. The expansions of the 1D NMR spectrum of the loop 2-3 are shown in Figure 2.7. All NH protons were grouped into three regions and they did not overlap (Figure 2.7A). The other component, described in the previous section, was also detected in this solvent system, but the chemical shifts of the NH protons of the minor component were similar to the values of the major component. In the

region of the methyl groups of the NMR spectra (Figure 2.7C) only the CH_3 of the Thr123 for the different components could be observed.

The assignment of the NMR spectra of the loop 2-3 in the this 40 %H_2O/ 60% TFE-d2 solvent mixture was performed in the similar manner as described in the 2.3.2.1 section. There was a problem in assign the peaks belonging to the amide protons of arginine and lysine. The spin system assignment is shown in the TOCSY spectrum (Figure 2.8). The assignment is presented in Table 2.4.

The number of the NOE peaks in the NOESY spectrum of the loop 2-3 in the solvent mixture is smaller compared to the NOESY spectrum of the peptide in pure TFE. The state II was less folded and probably more flexible than the conformational state III. In the NH to NH region of the NOESY spectrum (Figure 2.9) only two NOE peaks were detected, L124:Y125 and V127:R128. This was in agreement with results from solvent titration followed by CD, that state II was an extended structure, less folded conformation than state III when loop 2-3 was dissolved in pure TFE.

2.3.2.3 NMR spectra of loop 2-3 in 90 % H_2O / 10 % D_2O

Loop 2-3 was studied by NMR spectroscopy in 90 % H_2O / 10 % D_2O. Expansions of the 1D proton NMR spectrum are shown in Figure 2.10. The peaks of amide proton region were well resolved (Figure 2.10A), while peaks of 5 αH overlapped in the 4.15 to 4.31 ppm region.

Table 2.4. Assignment of spin systems of the ^{1}H NMR spectra of loop 2-3 in H_2O/TFE-d2 (4:6) at 298K.

Residue	NH	αH	βH	γH	δH	Other	$^3J_{NH}$ (Hz)
E119		4	2.40;2.10				
R120	8.5	4.22	1.68	1.51	3.09		
K121	7.8	3.67	1.77	1.3	1.42	3.19;3,09	5.9
N122	8.5	4.77	2.83;2.74				
T123	7.9	4.12	4.08	1.08			5.9
L124	7.8	4.12	1.53	1.44	0.8		5.3
Y125	7.5	4.28	2.99;2.90		6.98;6.74		5.9
L126	7.4	4.14	1.62	1.5	0.76		6.5
V127	7.5	3.93	2.1	0.87;0.82			6.5
R128	7.8	4.22	1.80;1.69	1.52	3.09		7.1
G129	7.8	3.8					

The spin system and sequential assignments were achieved using 2D proton TOCSY and NOESY NMR spectra (not shown) and the results of are shown in Table 2.5. The small number of NOE peaks in the NOESY spectrum was consistent with the conclusions based on the CD experiments, that loop 2-3 was in extended form when dissolved in water (called conformational state I).

Again there were NH peaks indicated the presence of the minor component, but in this case it was not possible to do assignments for this conformation, because there were not enough peaks in the 2D NOESY. The chemical shift values of the NH and αH of the loop 2-3 in this set experiments could be compared to the corresponding values of the

chemical shifts for the peptide in the random coil structure. One of the methods for such comparison was using the chemical shift index (CSI) as described by Wishart et al., 1992. The prediction of the secondary structure of the protein was based on the comparison of the αH chemical shift of the peptide with values from the peptide possessing random coil structure (CSI = δ_s - δ_{rc}). The negative values of CSI were normalized to -1, and positive values were normalized to +1. The stretch of four residues with positive CSI were assigned to a β-sheet structure, while stretch of four or more residues with negative CIS were assigned as an α- helix. This method could be applied only to proteins dissolved in water and it could not be applied to other solvents or solvent mixtures. The chemical shift index plot for the loop 2-3 in water is shown in the Figure 2.11. There was no stretch long enough to indicate either α- helix or β-sheet. The chemical shift values of NH and αH were also compared to the random coil values of Wutrich, 1986, and these values are shown in the Figure 2.12. The residual chemical shift was obtained by subtracting random coil chemical shift values from the experimental shifts. The chemical shift values differed from random coil values for both type of atoms. The NH protons were more sensitive to the environment, with positive NH residual chemical shifts for the charged terminal residues and negative NH residual chemical shifts for the hydrophobic part of the peptide. The αH residual chemical shifts were close to zero for most part of the peptide (except for the N-terminal part). Chemical shift analysis for the NH and αH supported the conclusion from the CD studies, that the peptide did not adopt the random coil structure. However that whole structure of the peptide was a limited number of regular conformations, a major portion of which were turn conformations and left-handed extended helices (LHE) [Drake et al., 1988]. The coupling constants indicated the averaging between multiple conformation because of a flexible backbone (Table 2.5).

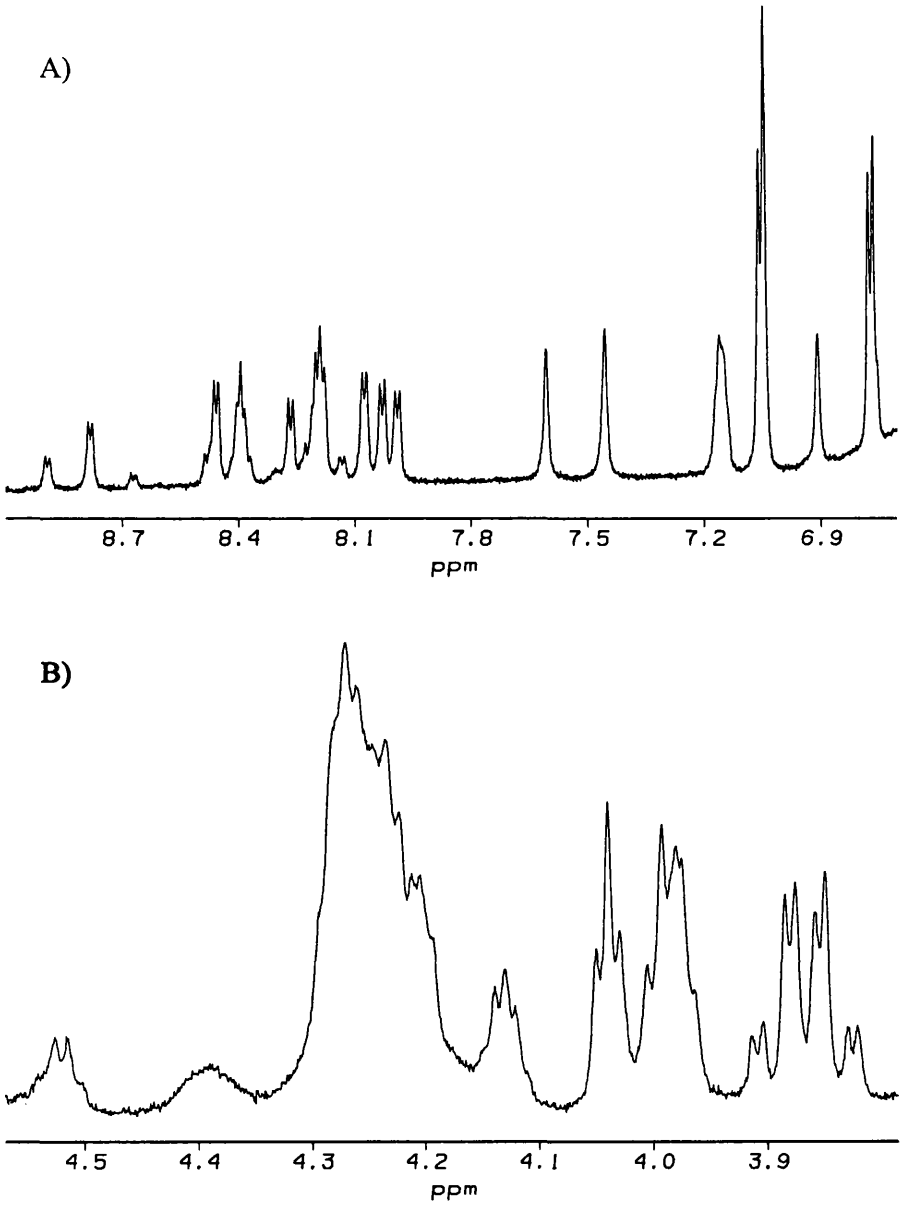

Figure 2.10 The expansions of 1D proton NMR spectrum of the loop 2-3 of β-subunit of high affinity IgE receptor in H_2O/D_2O (9:1); T= 298K, c=2 mM. A) amide and aromatic region and B) alpha proton region.

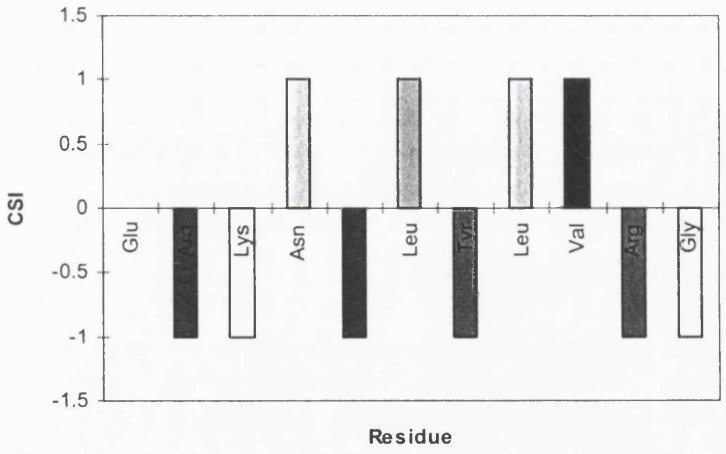

Figure 2.11 Chemical shift index (CSI) plot of αH for the loop 2-3 dissolved in aqueous solution (H_2O/D_2O - 9:1).

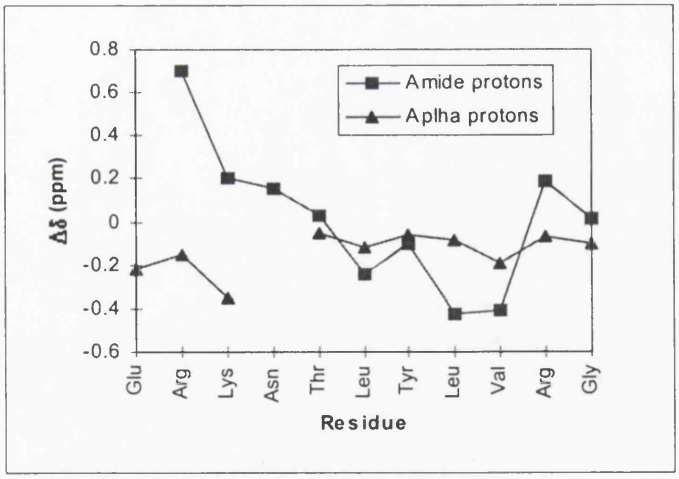

Figure 2.12 Residual chemical shift plot of NH and αH protons for the loop 2-3 dissolved in water (H_2O/D_2O - 9:1).

Table 2.5 Assignment of spin systems of the ^{1}H NMR spectra of loop 2-3 in H_2O/D_2O (9:1) at 298K (nd - not detected).

residue	NH	αH	βH	γ	δ	Other	$^3J_{NH}$ (Hz)
E119		4.07	2.37;2.10				-
R120	8.97	4.23	1.72	1.60;1.54	3.15		-
K121	8.21	4.01	1.83	1.31	1.48	3.15	6.6
N122	8.9	nd	2.86;2.76				6.6
T123	8.27	4.19	4.12	1.05			6.6
L124	8.18	4.26	1.46	1.33	0.8		6.6
Y125	8.08	4.54	3.00;2.85	7.06	6.78		6.6
L126	7.99	4.29	1.5	1.42	0.77		6.6
V127	8.03	3.99	1.97	0.87			6.6
R128	8.46	4.31	1.82;1.75	1.58	3.21		7.6
G129	8.4	3.89					-

2.3.2.4 Comparison of 1D NMR spectra of the loop 2-3 in different solvent systems

The solvent titration from water to TFE of loop 2-3 followed by CD indicated the conformational change with two cooperative transitions (Figure 2.2) between three different conformational states. Those three conformational states were studied by NMR and it was observed that the NMR spectra were different. The chemical shifts versus residue number were presented for the NH and αH (Figures 2.13A and 2.13B, respectively).

A)

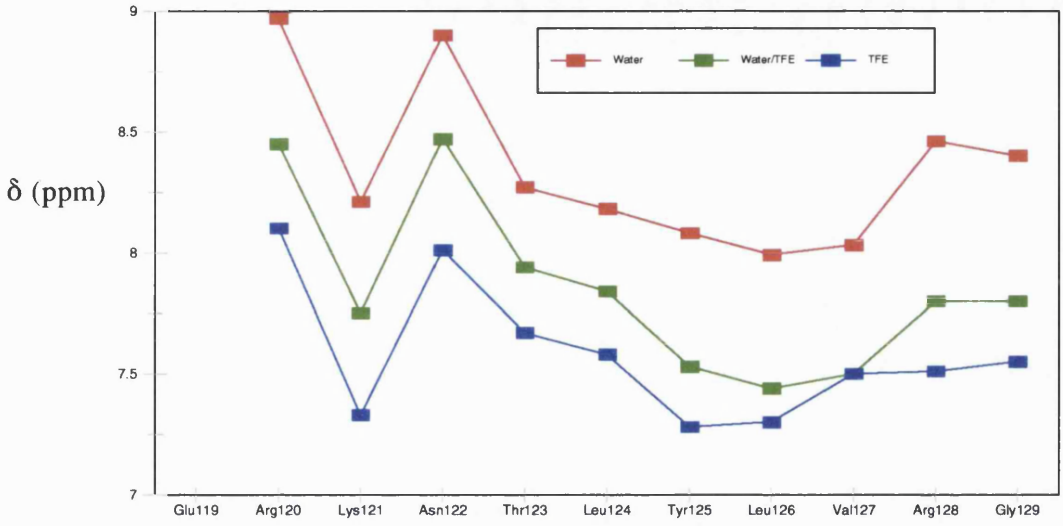

B)

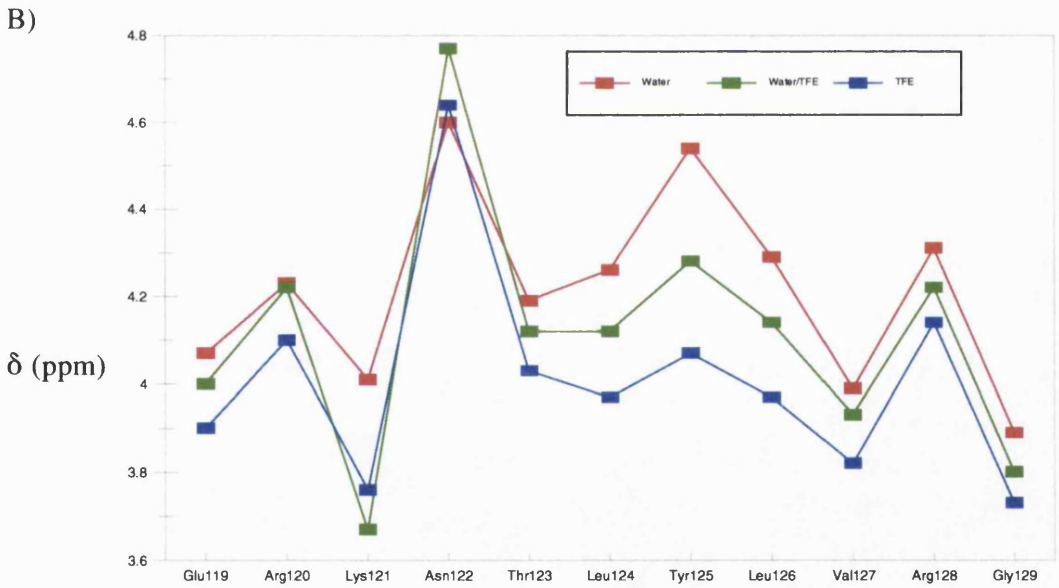

Figure 2.13. Observed chemical shifts vs sequence A) NH and B) αH for loop 2-3 of the β-subunit of high affinity IgE receptor in three different solvents; water, water/TFE (4:6) and TFE.

The NH protons were sensitive to environmental perturbation, although the change was not uniform along the sequence. In the highly polar environment, pure H_2O/D_2O, the NH protons were deshielded, and by adding up to 60% of less polar TFE, the chemical shifts of all NH protons moved upfield (Figure 2.13A). The largest change was observed for the NH protons of the residues Tyr125, Leu126 and Val127, indicated the most dramatic change of the conformation in that part of the backbone. Further titration was followed by the change in the chemical shift of the amide protons for the whole polypeptide chain, due to solvent polarity change and alternating the exposure of the amide protons. The chemical shift of the alpha protons can be used to evaluate the secondary structure (conformation) of peptides (Wishart et al., 1992.), but during the solvent titration the chemical shifts were also altered due to solvent polarity change. The fact that the chemical shift of the alpha protons did not change uniformly along the chain (Figure 2.13B) indicated that the polarity of the solvent was not only reason for the change in chemical shift. The alpha proton chemical shifts of the C-terminus end experienced small but uniform change. The alpha proton chemical shift of K121 changed only during the first addition of TFE, and a significant change was observed in the middle part of the chain. The largest change was noticed for the alpha proton of the Y125. These were the basis for the conclusion that largest conformational for change was in the middle of the chain. This was consistent with deductions from other experiments. The different CD spectra of the loop 2-3 in water and TFE could be explained by the conformational transition in the middle part of the peptide.

2.4 NMR Based Molecular Modelling

All NMR based molecular modelling was performed with X-PLOR 3.1 modelling software.

2.4.1 Loop 2-3 in 90 % H_2O / 10 % D_2O - Conformational State I

NOE-derived distance constraints and $3J_{NH\alpha H}$ coupling constants were input as restraints in the X-PLOR 3.1 program. The structural information from the NOESY spectrum consisted of the 46 distance constraints (28 intraresidual; 15 sequential and 3 medium range constraints). The distribution of the constraints through the 11-residue sequence is presented in Figure 2.14. Medium range constrains were between three or four residues apart. The low number of the constraints could be explained in two ways; the peptide could be linear or the peptide was flexible.

First, the RANDOM.INP protocol (a simulated annealing protocol for NMR structure determination) was used (Nilges et al., 1988a; Nilges et al., 1988b) instead of the Distance Geometry protocol. The starting structure for RANDOM.INP protocol was completely arbitrary. The 20 resulting structures were regularized by the Distance Geometry Simulating Annealing (DGSA.INP) protocol. The calculated structures were refined further by REFINE.INP protocol, as described in the X-PLOR manual. The 10 lowest energy structures were superimposed as in Figure 2.15

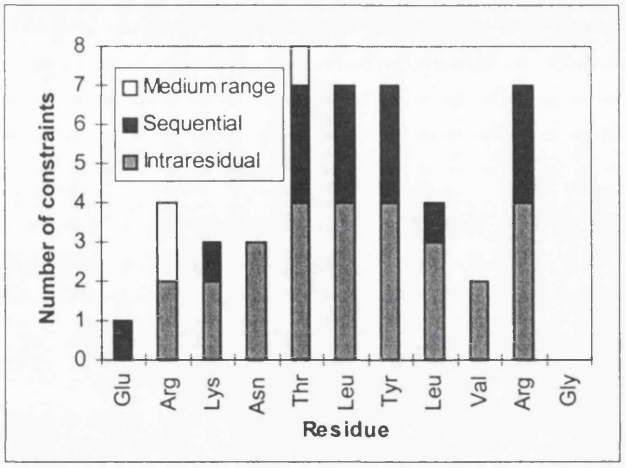

Figure 2.14 The number of the intraresidual, sequential, and medium range distance constraints versus sequence of the loop 2-3 in 90 % H_2O / 10 % D_2O.

In determining the three-dimensional structure of a peptide when it is unfolded the NMR spectrum represents an average over an ensemble of molecular conformations, which may interconvert rapidly relative to the chemical shift time scale [Wutrich, 1986]. The observed chemical shifts were a population-weighted averages of the shifts in the individual conformations. The spin-spin couplings are also population - weighted averages calculated using a Karplus type dependence on the dihedral angles. In the three-dimensional structure determination, the NOE intensities are averaged, where $1/r^6_{ij}$, where r_{ij} defines the distance between two protons again averaged over individual conformations.

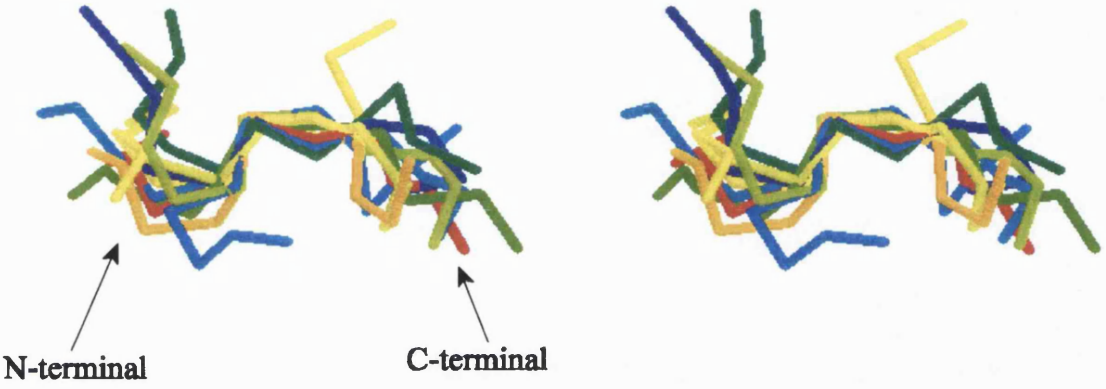

Figure 2.15 Stereoview of the overlap of the Cα positions of the ten lowest energy structures obtained from the NMR data for the loop 2-3 in 90% H_2O / 10 % D_2O. The structures are aligned to give a best fit for residues 5-8 to the first structure. The average RMS deviation for these Cα atoms is 0.62.

Deviation of ^1H chemical shifts from the random coil values indicated the presence of a non-random structure in the loop 2-3 peptide. The NOE distance constraints were collected and the structures calculated. The input data could not be satisfied by a single, well-defined structure, but the result was a set of structures, that indicated a flexible backbone. The common features were observed for the sets of the four residues(E119 to N122; N122-Y125 and L126-G129), with RMS in the range from 0.6 to 0.9 Å. The best fit was for the peptide stretch from Asn122 to Tyr125 with RMS 0.625 Å (Figure 2.15). The Ramachandran plot for the lowest energy structure (Figure 2.16) confirmed the

conclusion obtained by calculating CIS, that the peptide was not in a random coil conformation, but that residues of it occupied "structured" conformational space. Those residues were not forming stretches long enough to satisfy the criteria for folded structures, and this confirmed the conclusion made from the CD spectra of the loop 2-3 in the conformational state I.

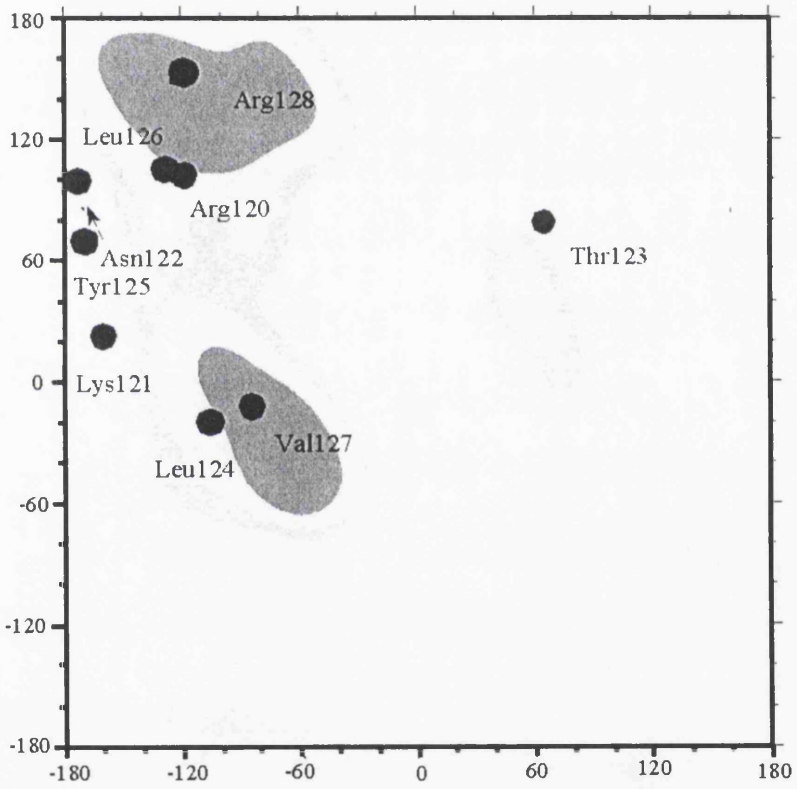

Figure 2.16 The Ramachandran ϕ,ψ plot for the lowest energy NMR based structure of the loop 2-3 peptide in 90 % H_2O / 10 % D_2O.

2.4.2 Loop 2-3 in 40 % H2O / 60 % TFE-d2 - Conformational State II

The simulated annealing calculations with random starting structures, using the program X-PLOR, as described in the 2.4.1 section, were used to generate conformations consistent with 60 NMR derived distance constraints and 7 dihedral constraints. Interproton distances were derived from the cross-peak intensities in the NOESY spectra (expansion shown in the Figure 2.9). The distribution of the constraints through the sequence was presented in the Figure 2.17.

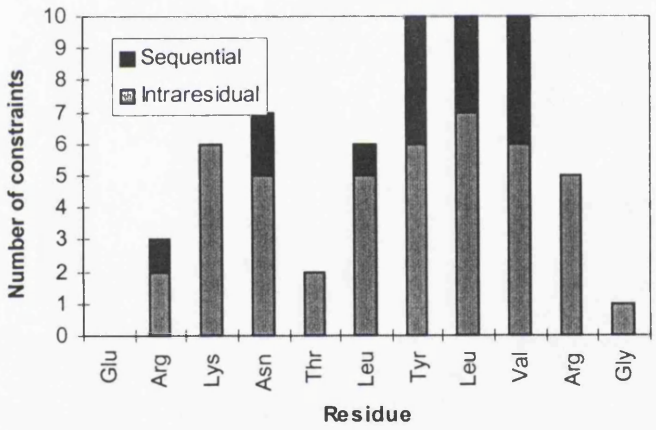

Figure 2.17 The number of the intraresidue and sequential distance constraints versus sequence of the loop 2-3 in 40 % H2O / 60 % TFE-d2.

Fifty structures generated, but only the ten of the lowest energy were analysed. All satisfied the NOE distance constraints (Figure 2.18). Superposition of these ten structures

with respect of the backbone atoms gives an RMSD of 2.23 Å. This RMSD was quite high indicating a very flexible structure. However, a separate superposition of alpha protons of residues E119 to N122, T123 to L126 and L126 to G129 gave significantly smaller RMSD values of 0.76, 0.34 and 0.86 Å, respectively. This implied the flexible links (or undefined links) between three more precisely defined regions. Multiple conformations are likely to be populated by this peptide in this solvent system, but a single conformation could be a good representation for a reasonable average structure. The lowest energy structure was shown in Figure 2.19, and it could be assigned as a representative structure for the conformational state II that was observed during solvent titration followed by CD.

2.4.3 Loop 2-3 in TFE - Conformational State III

The structural information from NOESY spectra (175 distance constraints) and coupling constants (9 torsional angle constraints) for the major component were used to calculate the model of the 11-residue peptide loop 2-3 of the high affinity IgE receptor by using the program X-PLOR, as described in the 2.4.1 section.

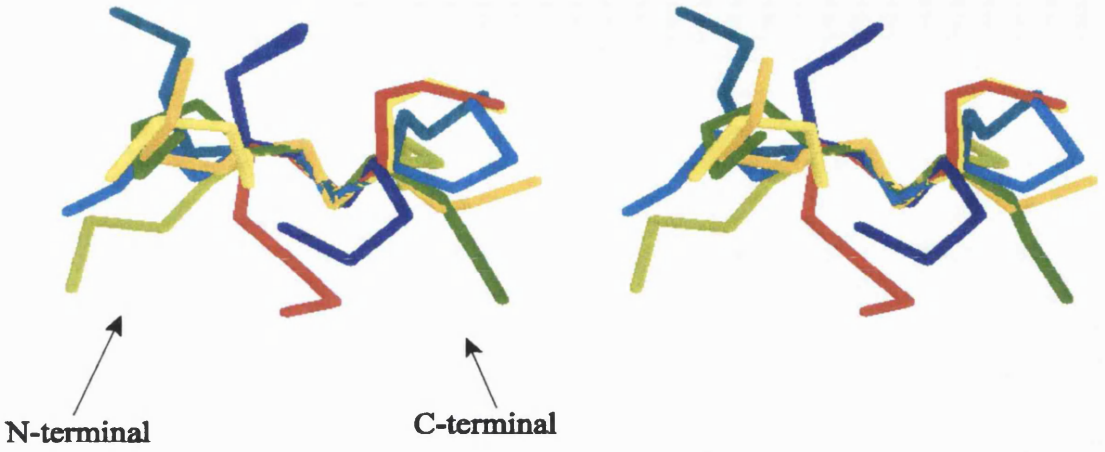

Figure 2.18 Stereoview of the overlap Cα positions of the ten lowest energy structures obtained from the NMR data for the loop 2-3 in 40 % H2O / 60 % TFE-d2. The structures are aligned to give a best fit for residues 5-8 to the first structure. The average RMS deviation for these Cα atoms is 0.34.

The other minor component was not modelled since only a insufficient number of NOE constraints were observed. An alternative explanation could be that the minor component was an aggregated loop 2-3 peptide. The loop2-3 peptide had the tendency to aggregate, even in low concentration samples for the CD experiments. The β-sheet aggregation was particularly observed in the presence of the submicellar concentration of SDS (results not shown). It could not be avoided, since the lowering of the sample concentration would lead to low quality NMR spectra. However, the presence of the second, minor component did not affect the three-dimensional studies of the loop 2-3 by NMR.

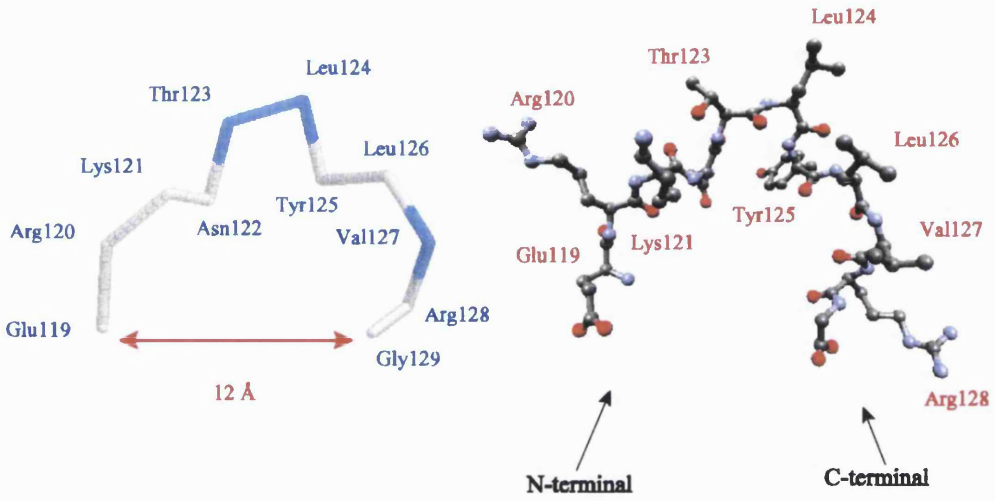

Figure 2.19 Lowest energy NMR based structure of the loop 2-3 of the β subunit of the FcεRI in 40 % H2O / 60 % TFE-d2; A) Cα chain and B) whole molecule.

The distribution of the constraints throughout the sequence is presented in Figure 2.20.

Fifty model structures were generated and analysed with NMRCLUST software [Kelley et al, 1996]. NMR based modelling therefore resulted in three clusters of models each cluster having different conformations. However, neither cluster of the conformations fully satisfied the distance constraints and each of the structure clusters violated to some extent different distance constraints.

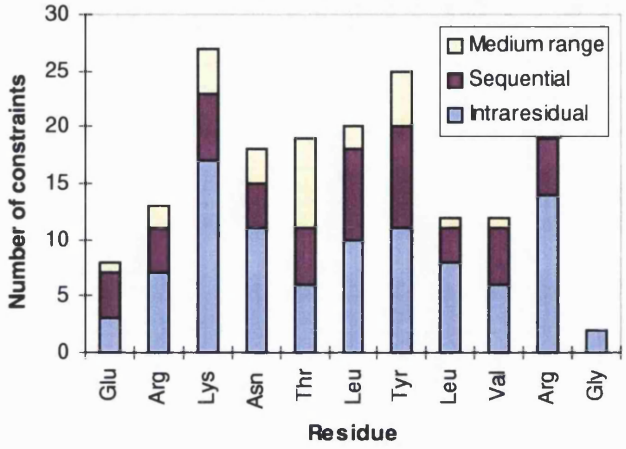

Figure 2.20 The number of the intraresidue, sequential, and medium range distance constraints versus sequence of the loop 2-3 in TFE-d2.

The seven structures of the loop 2-3 peptide in TFE within the first cluster contained an α- helical structure (Figure 2.21) and thus confirmed the results of the CD study. The RMSD for the alpha protons was 1.21 Å for the whole chain and 0.27 Å for the alpha protons of the α- helical moiety. This indicated that the peptide was flexible, especially at the N-terminal end of the chain. Still, it provided useful information about the structures that this peptide could adopt. These calculated structures of the 11-residue loop 2-3 peptide were in good agreement with the structure of the sequence that connects two TM helices in the model of the α- subunit of high affinity IgE receptor [Zloh et al., 1995]. The distances between C- and N-terminus of the NMR based calculated structures of the 11-residue bridge peptide were also in the range of 9 to 17 Å, which corresponded to the distance between the C-terminus of the TM helix 2 and the N-terminus of the TM helix 3 of the β-subunit packed into a four helix bundle.

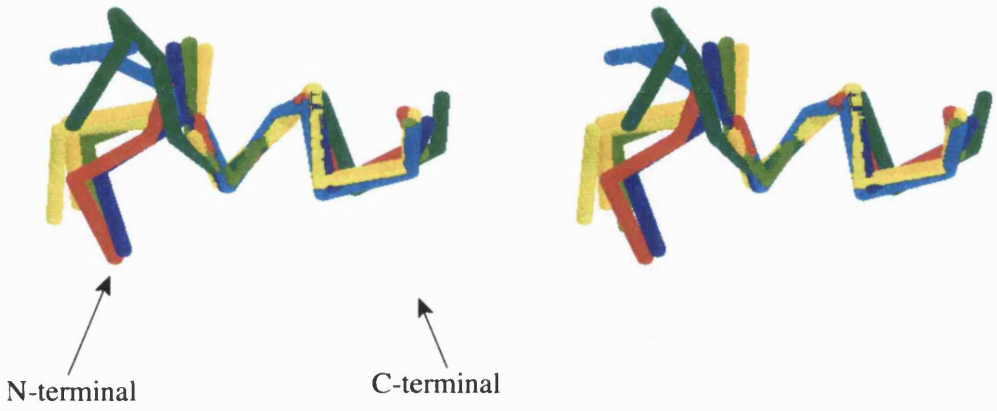

Figure 2.21 Figure 2.18 Stereoview of the overlap Cα positions of the seven structures from the first cluster obtained from the NMR data for the loop 2-3 in TFE-d2. The structures were aligned to give a best fit for residues 5-8 to the first structure. The average RMS deviation for these Cα atoms is 0.27 Å.

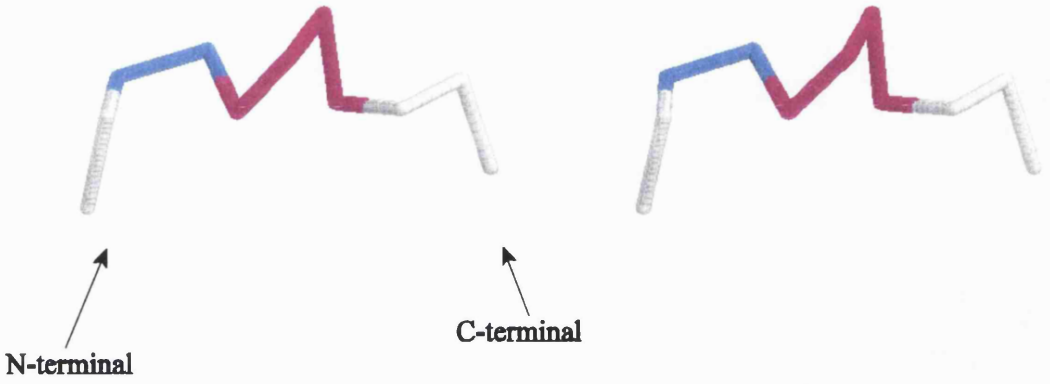

Figure 2.22 Lowest energy NMR based structure for the loop 2-3 of the β subunit of the FcεRI in TFE-d2.

Ten folded structures of the second cluster of conformations were shown in the Figure 2.22. The RMSD for the alpha protons of the whole chain was 1.90 Å. Again, separate superposition of residues E119 to N122, T123 to L126 and L126 to G129 gave significantly smaller RMSD values of 0.59, 0.26 and 0.1 Å, respectively. The overlap of the structures was satisfactory even in the wider range of residues, from T123 to R128. This again implied a flexible link between two more precisely defined regions, similar to the situation when the loop 2-3 peptide was dissolved in the 40% H_2O/ 60% TFE. The 3_{10} -helix features were detected for this second cluster of the NMR based models.

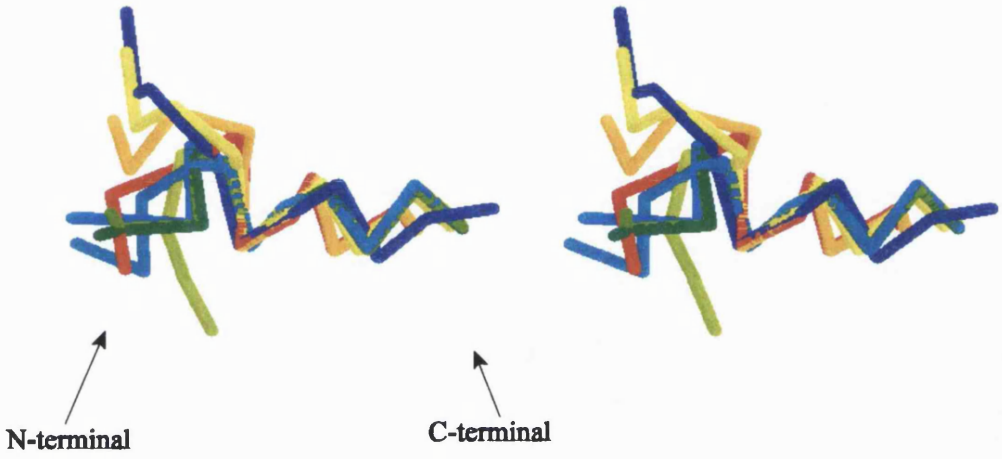

Figure 2.23 Stereoview of the overlap Cα positions of the ten structures from the second cluster obtained from the NMR data for the loop 2-3 in TFE-d2. The structures are aligned to give the best fit for residues 5-8 to the first structure. The average RMS deviation for these Cα atoms is 0.26 Å.

Ten structures of the third set of conformations are shown in Figure 2.23. The RMSD for the alpha protons of the whole chain was 1.00 Å. Again, separate superposition of residues E119 to N122, T123 to L126 and L126 to G129 gave significantly smaller RMSD values of 0.46, 0.12 and 0.57 Å, respectively. This again implied flexible links (or undefined links) between three more precisely defined regions, like the conformational state II, when the loop 2-3 peptide was dissolved in the 40% H_2O/ 60% TFE.

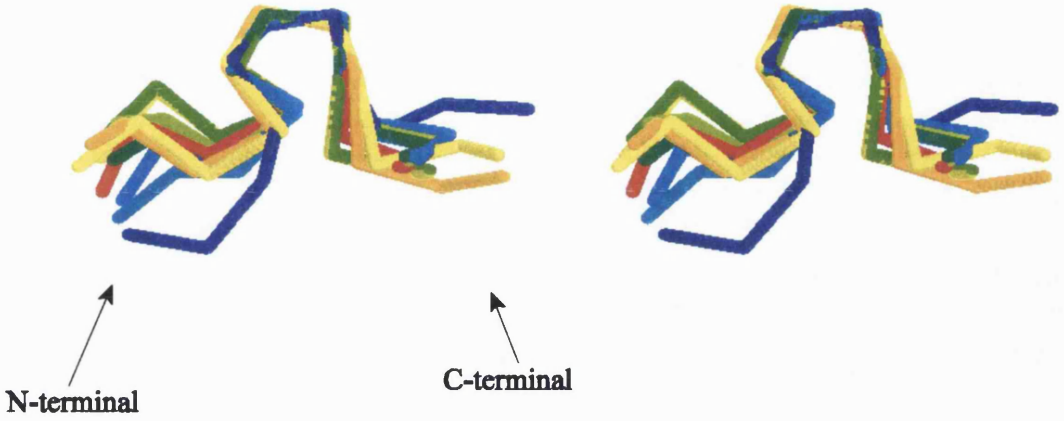

Figure 2.24 Stereoview of the overlap Cα positions of the ten structures from the third cluster obtained from the NMR data for the loop 2-3 in TFE-d2. The structures were aligned to give the best fit for residues 5-8 to the first structure. The average RMS deviation for these Cα atoms is 0.12 Å.

The presence of the three different structures in solution could explain the high number of distance constraints for a such small peptide, which was about 16 constraints per residue, and would produce a well defined folded structure. Instead, flexible structures were observed, confirming the presence of the multiple conformations of the loop 2-3 in pure TFE.

2.4 Summary

The cooperative conformational transitions between distinct conformational states (folding) of the loop 2-3 peptide were observed by CD during solvent titration from water to TFE. Isodichroic points in solvent perturbation CD in combination with graph of $\Delta\epsilon$ versus solvent composition at three wavelengths revealed cooperative conformational transitions at two values of T_s. That was interpreted to mean that stable and different conformations existed at each solvent composition, namely state I (0 % to 15 % TFE), state II (40 % TFE to 75 % TFE) and conformational state III (95 % TFE to 100 % TFE). CD spectra deconvolution indicated that an α-helical content increased during solvent titration from 0 % TFE to 100 % TFE. The presence of the α-helical moiety in water + SDS micelles was detected.

The 1D and 2D NMR spectra were used to examine state I, state II and state III. The NMR-based molecular modelling confirmed the conclusion from the CD experiments. As described in section 2.4.1, conformational state I in water was flexible, consisting of interconverting structures. During solvent titration, the largest change in the structure was observed in the central residues of the polypeptide chain. In the first instance the turn structure was observed for those residues in the conformational state II of the loop 2-3. The titration curve in the CD experiment (Figure 2.2) implied that the folding process might not be finished when loop 2-3 was dissolved in the 100 % TFE. This was confirmed by the three sets of different calculated structures for the state III. The α-helix, 3_{10}-helix and turn structures were detected in the middle of the peptide for these three conformations. The each of these conformations of the state III had flexible ends of the loop 2-3 peptide

The elucidation of the structure of the loop 2-3 peptide could shed some light on the problem of conformation of the receptors. This sequence could be considered as part of the large family of the membrane protein domains that requires better understanding.

Even for the well studied 7 helix membrane protein, *Bacteriorhodopsin*, the structure of the connecting loops was not revealed. The experimental approach used in this chapter was also used by some other groups to determine the conformation of the connecting loops of bovine rhodopsin (Yeagle et al., 1995; Yeagle et al., 1997). Two conformational motifs were found in three cytoplasmic loops of bovine rhodopsin. The first motif was the β-turn in the middle of the first two cytoplasmic loops (Yeagle et al., 1997). The second motif was found in the third connecting loop. It was first reported as a α-helix in the middle of the loop (Yeagle et al., 1995), but further refinement led to the conclusion that this loop helix was extension TM helix well above the membrane (Yeagle et al., 1997).

The structure of the loop 2-3 peptide was studied in the absence of the rest of high affinity IgE receptor (sequence of the loop 2-3 connects TM helices 2 and 3 in the receptor) and in the absence of the membrane. The common difficulty in cases like this is that any particular conformation is adopted in only a small fraction of molecules at any time. A useful technique to magnify these tendencies is to use other solvents, like TFE. This enhances the helicity of the peptide segments, but apparently only if the residues have an intrinsic propensity to adopt that conformation [Nelson and Kallenbach, 1989; Lehrmann et al., 1990; Storrs et al., Sonnichensen et al., 1992; Jasanoff and Fersht, 1994; Shiraki et al., 1995; Kemmink and Creighton, 1995]. Thus, the most suitable system for studying the conformation of the free loop 2-3 was pure TFE. This solvent provided the

most folded conformation that could be representative for the structure of the sequence in the receptor's final conformation.

The NMR studies of the 11-residue loop 2-3 peptide of high affinity IgE receptor confirmed the presence of three coexisting folded conformations in TFE, one of which was α- helical in structure. Since the helical structure was also indicated by CD in the solution containing the SDS micelles (simulating the lipid membrane), this connecting peptide could adopt an α- helical secondary structure in the intact receptor (a folding of the loop 2-3 into other types of structure could be also possible). This found structure for the loop 2-3 peptide was similar to the reported helical motif of the BR connecting loop by [Yeagle at al, 1995].The middle part of the loop 2-3 peptide was incorporated in the defined structure in the absence of the TM helices and in the absence of the membrane. The portions of the peptide that was flexible (which links between the parts with defined structure) will take on structure when covalently connected to the TM helices 2 and 3 of the β-subunit of IgE receptor. The TM helices connected by a such loop are represented topographicaly in Figure 2.25 , and a such motif "TM helix - bend - loop helix - bend - TM helix" could appear in other integral membrane protein.

The question could be asked about the structure formation of the loops that connect the transmembrane helices of integral membrane proteins. One hypothesis suggests that loop formation is driven by packing and location of the transmembrane helices, which in turn force the loop conformation. Another hypothesis suggests initially that a substructure forms with two transmembrane helices connected by a loop, which is then inserted into the membrane (Engelman et al., 1981). The former hypothesis implies that the conformation of the loop is primarily determined by the folding of the ensemble of transmembrane

helices, and the latter hypothesis implies that the amino acid sequence of the loop itself should direct the conformation of the loop. The structural information obtained here is more consistent with the former hypothesis. The structure of the loop 2-3 was flexible in the absence of a transmembrane helices and the membrane and the rest of the protein, and depended on the solvent used.

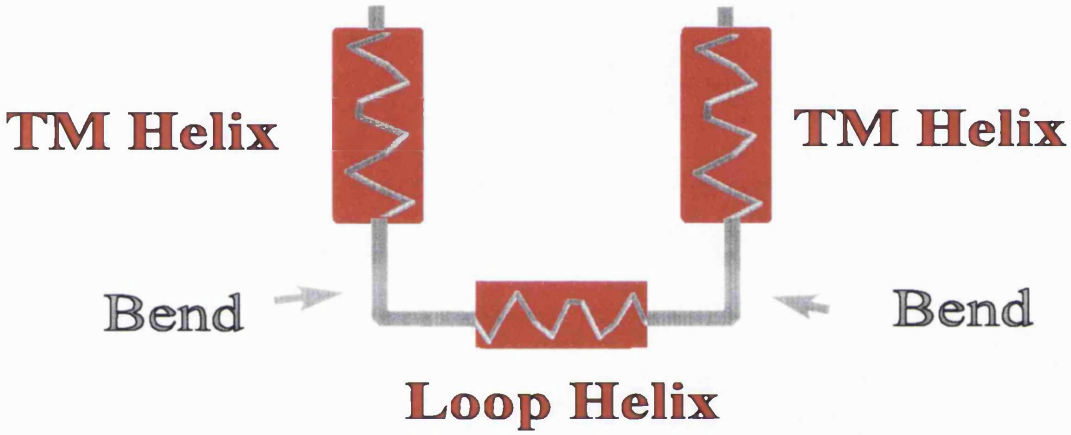

Figure 2.25. Conformational motif in the high affinity IgE receptor.

Despite the limiting factors of this approach, the obtained information could be an important conceptual tool. To summarize, the CD, NMR and molecular modelling studies predicted the possibility of forming TM helix -bend - loop helix - bend - TM helix motif in the β-subunit of high affinity IgE receptor.

Chapter 3.

CONFORMATIONAL STUDIES OF THE CONNECTING LOOP 1-2 PEPTIDE OF THE β-SUBUNIT OF THE HIGH AFFINITY IgE RECEPTOR

3. CONFORMATIONAL STUDIES OF THE CONNECTING LOOP 1-2 PEPTIDE OF THE β-SUBUNIT OF THE HIGH AFFINITY IGE RECEPTOR

3.1 Background

The natural division of the high affinity IgE receptor into domains led to a strategy of cutting it into smaller peptide domains or structural units and to determine the structure of peptides, corresponding to these regions, by CD or NMR and molecular mechanics and dynamics studies. The anisotropic environment of membrane receptors leads to their natural division in terms of domains. Thus, each membrane receptor can be classified into extracellular, transmembrane and cytoplasmic domains. Using this approach, several domains of the high affinity IgE receptor have already been experimentally and theoretically studied (Anderson et al., 1992; Anderson et al., 1995; Beavil, *et. al,* 1993; Padlan & Helm, 1992; Zloh et al., 1994a; Zloh et al., 1994b; Zloh et al., 1995).

In this chapter, the 17-residue peptide containing the sequence (S81-T82-L83-Q84-T85-S86-D87-F88-D89-D90-E91-V92-L93-L94-L95-Y96-R97) of the first extracellular loop of the β subunit (designated as loop 1-2, see Figure 1.2) of FcεRI was synthesized and its structure in different solvents investigated by NMR based conformational calculations. Our aim was to give structural information which could contribute significantly to an understanding of the structure of the surface of the IgE-receptor. A better understanding of the topology of the receptor is crucial not only to comprehend the mechanism of the release

of allergic mediators but also for improving drug design targets related to inflammation. The α-helical conformation for the loop 1-2 peptide was proposed from CD experiments in water solution and in the presence of the SDS micelles (Zloh et al., 1995). The presence of an ordered structure for loop 1-2 peptide in solution suggested, therefore, that the loop connecting hydrophobic helices of a multi-spanning membrane protein could be a determinant of integral membrane protein folding. The hydrophobic effect and the packing of the helices within the membrane could be one of the driving forces which determines most of the folding, but the connecting loops could have in their primary sequences the information necessary to form an independent, well-defined structure, which could then define a helical hairpin and lead to an insertion of a largely prefolded section of the protein into the membrane during the biosynthesis. This is a further reason why the role of the connecting loops deserves more attention.

This strategy offers support for an alternate approach to membrane protein structure determination, in which the extramembraneous domain structures of the integral membrane protein can be solved and the resulting conformations docked with the helices of the transmembrane domain.

3.2 Material and Methods

The peptide loop 1-2 was provided by Dr M. Dalton and Dr I. Toth, School of Pharmacy, University of London.

3.2.1 CD Spectroscopy

The CD spectra were recorded on a Jasco J720 spectrometer at room temperature. Peptide samples were weighed out using a Sartorius balance (+/- 1 ug) and solvent added to give a peptide concentration of 0.2 mg/ml. pH measurements were made with a Ciba-Corning pH meter. Quartz QS cylindrical Helma cells with a path-lengths varying from 0.001 cm to 1 cm were used. The spectra were recorded over the wavelength range of 260 to 185 nm. The bandwidth was set to 0.2 nm and time constant to 4 s. Scan speed was 10 nm/min and step resolution 0.2 nm. The solvent baseline subtracted and the $\Delta\epsilon$ values calculated. The plotted spectra were digitized by WinDig (Windows Digitizer) software (Lovy, 1996), taking the $\Delta\epsilon$ values at 1 nm in the 190 to 260 nm range. The obtained $\Delta\epsilon$ values were used to calculate the secondary structure by CDNN (Circular Dichroism Neural Network) software preforming CD spectra deconvolution [Böhm, 1997]. The result was expressed as a percentage of the five different secondary structures (α-helix, antiparallel and parallel β-sheet, turn and random coil), and at end the result was normalized to 100 %.

3.2.2 NMR Spectroscopy

The 2 mM solution of synthetic 17-residue peptide in the methanol-d3 (99% atom D, GOSS Scientific Instruments limited, UK) and DMSO-d6 (99.9 % atom D, Aldrich Chem. Co., USA) were used for NMR experiments. NMR spectra were obtained with a

Brüker AM 500 MHz and AMX 600 MHz spectrometers at 298 K. 1D proton NMR spectra were obtained with 32K data points in the t2 domain, all 2D NMR DQF COSY (Rance et al., 1983), TOCSY (Bax and Davis, 1985) and NOESY (Jeener et al., 1979; Kumar et al., 1980) spectra had 512 increments in t1 with 2048 data points in t2 domain. TOCSY spectra were recorded with a spin-lock mixing time of 60 ms, and mixing times of 300 and 500 ms were used in NOESY experiments. All 2D spectra were accumulated in a phase sensitive manner using time-proportional phase incrementation for quadrature detection in F_1. Felix 2.3 software (Biosym Inc.,) was used to process NMR spectra. Chemical shifts were referenced to internal methanol and DMSO, accordingly. Sequence-specific assignments of the ^{1}H NMR spectra were obtained using standard approaches and the results are listed in Tables 3.2 and 3.3.

3.2.3 NMR Based Molecular Modelling

. The three dimensional structures of the peptide in different solvents were determined by using intraresidual and sequential NOEs. NMR-based molecular modelling was carried out by XPLOR 3.1 program (Brunger et al., 1987), using simulated annealing protocols with ambiguous constraints (Nilges, 1995), using 165 intraresidual, 9 sequential, 8 medium range, and 36 ambiguous distance constraints for the peptide in the methanol and 59 intraresidual, 34 sequential, 9 medium range, and 72 ambiguous distance constraints for the peptide in the DMSO derived from 2D NOESY and ROESY experiments. NOEs intensities were characterized as strong, medium and weak and translated in the corresponding upper bounds distance range constraints of 2.5, 3.5 and 5.0 Å, respectively. A correction factor of 0.5 Å for the use of pseudoatoms was added to interproton distance restraints involving methyl groups to account for the apparent higher intensity of the peaks

[Wüthrich et al., 1986]. Lower bounds between nonbonded atoms were set to the sum of their van der Waals radii (about 1.8 Å). Energy refinement calculations (restrained minimizations and dynamics) were carried out on 20 structures for both solvents. The average structures were obtained from the ten lowest energy structures.

3.3 Results and Discussion

3.3.1 Electronic Circular Dichroism Studies on Loop 1-2

The relatively low solubility of the loop peptide 1-2 in H_2O and TFE made their complete study by perturbation CD difficult to perform. UV CD spectra of the peptide in water and peptide in water and in presence of SDS micelles were obtained. In the case of the aqueous solution (Figure 3.1), the shape of the CD curve indicated the presence of an α-helical moiety. A positive band occurred around 190 nm, and one negative band at 220 nm with a shoulder at 205 nm. The appearance of these three peaks probably indicated the presence of α-helix in the peptide, but the ratio of maximum and minimum values of the positive and negative bands was around 1:1, which was not characteristic for the pure α-helix structure; but indicated the presence of the other types of secondary structures, like antiparallel and parallel β-sheet, different types of turn moieties and/or random coil structure. The UV CD spectra of the loop peptide 1-2 changed significantly upon addition of SDS above the CMC concentration (Figure 3.2). The positive band at 190 nm increased in intensity, and two separated negative bands were observed at 205 and 221 nm, with a shape of the CD spectrum similar to the shape of the CD spectra of the protein with high α-helix content. The intensity ratio of the positive to negative extremes was around 1.6, higher than

the corresponding ratio when loop 1-2 peptide was dissolved only in water. This indicated the conformational change, actually, extending the stretch of the α-helix structure.

The secondary structure calculations based on the CD spectra were performed using CDNN software (as described in the methods 3.2.1) and the results were presented in the Table 3.1. The helical component was calculated to be 15.2 % when loop 1-2 peptide was dissolved in water, while the β-sheet content (antiparallel + parallel) was 36.3 %, turn structure was estimated to be 16.2 %. The CDNN software was optimized for the calculation of the secondary structure of proteins. The calculated percentage of the secondary structure of small peptides could be considered as a rough indication and it could be used to follow the conformational behavior of the peptides in different environments.

Table 3.1. The percentage of the secondary structure of the loop 1-2 of the β-subunit of high affinity IgE receptor calculated by CDNN program from far UV CD spectra of the peptide in water and in presence of the SDS micelles (T=298 K, pH=3.08, supernatant concentration, above CMC concentration of SDS micelles)

Secondary structure	Peptide in water	Peptide in water + SDS
% α-helix	15.2	18.7
% antiparallel β	26.7	22.4
% parallel β	9.6	9.5
% β-turn	16.2	16.9
% random coil	32.3	32.5

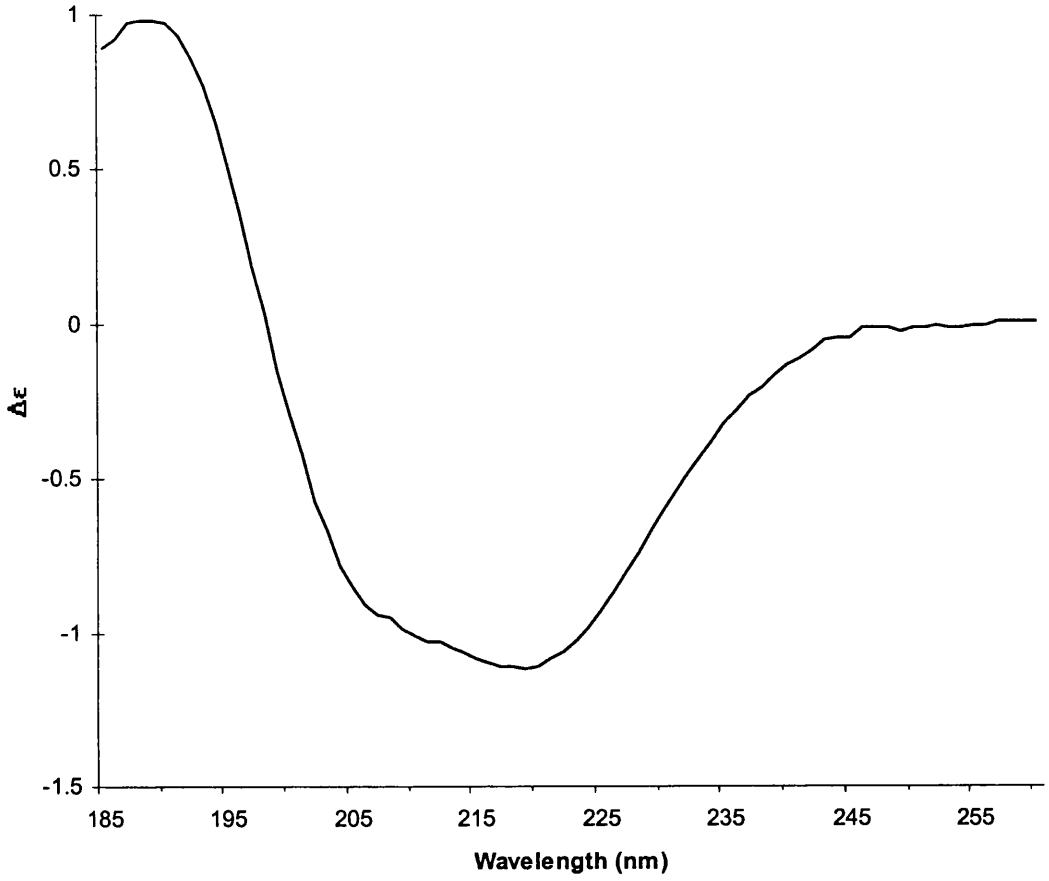

Figure 3.1 The circular dichroism spectrum of the 17-residue loop 1-2 peptide of the β-subunit of the high affinity IgE receptor: c = 0.2mg/ml; 0.02 cm cell; pH = 3.08; T = 298 K.

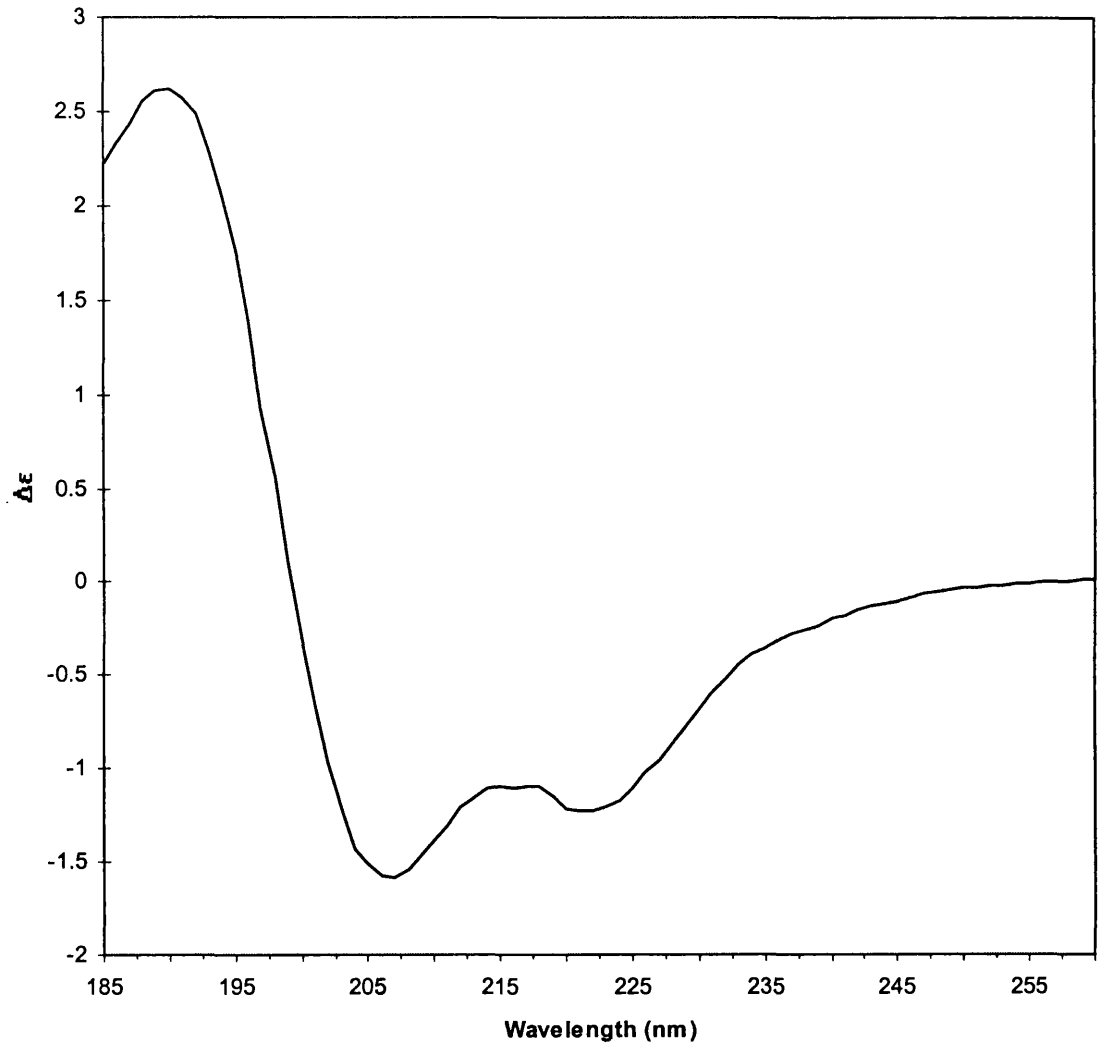

Figure 3.2 The circular dichroism spectra for 17-residue loop 1-2 peptide of the β-subunit of the high affiity IgE receptor in water + SDS micelles, supernatant concentration in water after spinning; 0.02 cm cell; pH = 3.08; T= 298 K, above CMC concentration of SDS micelles.

In the case of the loop 1-2, the calculated results confirmed the conclusion based on the shape of the CD spectrum that α-helical moiety could be present in the structure. The calculated secondary structure of the loop 1-2 in the presence of SDS micelles indicated an increase in the α-helical content and a decrease the content of the β-sheet structure. This conformational change was responsible for the increasing of the intensity of the positive band at 190 nm and the appearance of the two negative bands at 205 and 221 nm. Such behavior, refolding of the β-sheet structure into α-helix structure, is known for other small peptides [van Stosch, et al., 1995] during solvent titration from water to TFE. Many consider that the presence of SDS micelles emulates the presence of the lipid bilayer and it thus had a helix-promoting effect on the loop 1-2.

3.3.2 NMR Studies of the Loop 1-2

Due to the low solubility of the loop 1-2 peptide, it was not possible to do NMR experiments in the same conditions as for the CD studies. In order to investigate the conformational space that this fragment loop 1-2 could occupy, two different solvents were used to study the free peptide in solution. The NMR spectra of a 2 mM solution of the loop 1-2 peptide were obtained in two solvents, methanol-d_3 and DMSO-d_6, since the peptide had low solubility in water and other solvents (like TFE).

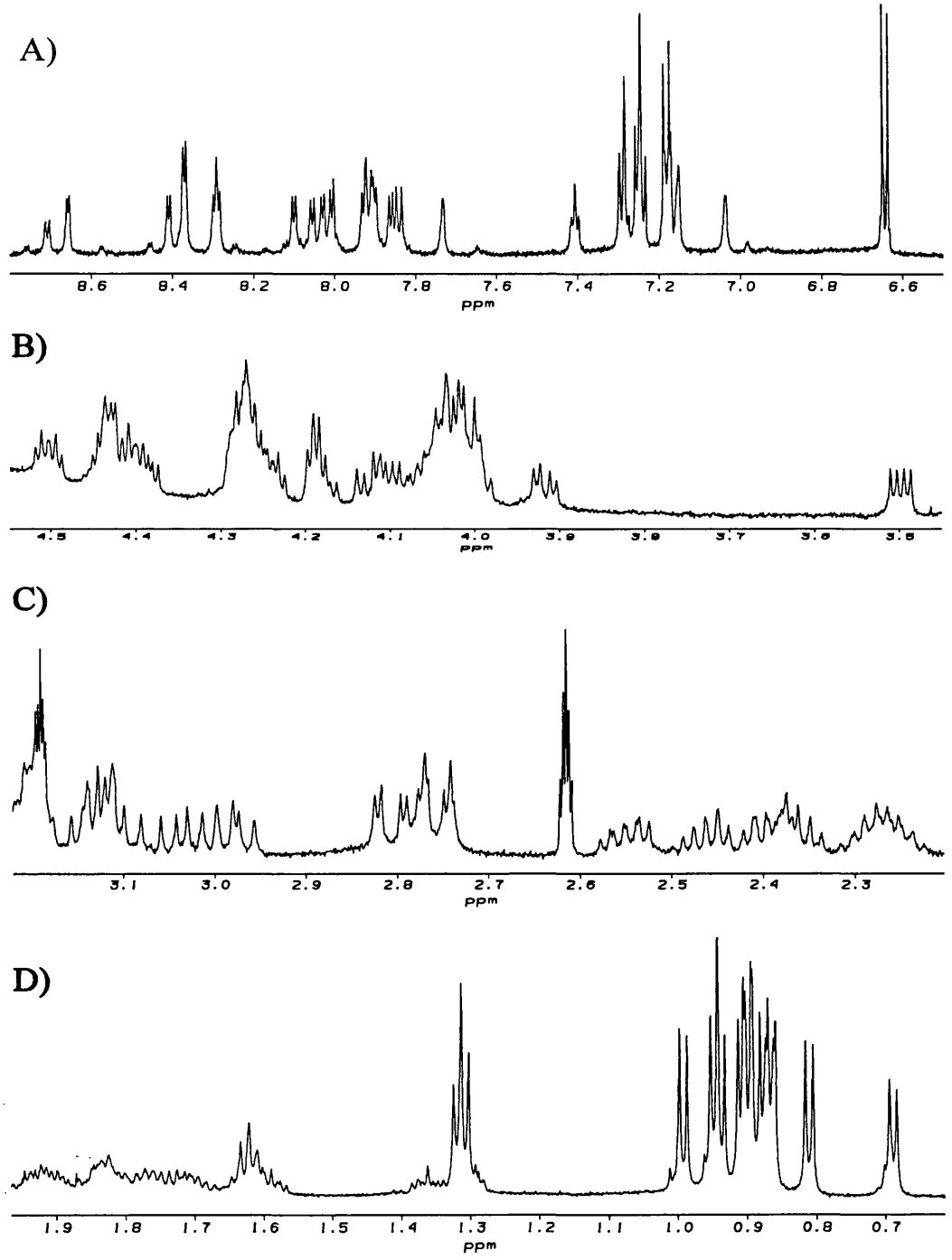

Figure 3.3 The expansions of 1D proton NMR spectrum of the loop 1-2 of β-subunit of high affinity IgE receptor in methanol-d3; T= 298K, c=2 mM. A) amide and aromatic region, B) Hα region, C) and D) rest of the spectrum.

Table 3.2 Assignment of spin systems of the ^{1}H NMR spectra of loop 1-2 of β-subunit of high affinity IgE receptor in methanol at 298K at 600 MHz.

Residue	NH	αH	βH	Other	$^3J_{NH}$ (Hz)
S81		4.19	4.12, 4.01		
T82	8.71	4.43	4.19	1.33	6
L83	8.37	4.18	1.73, 1.72	1.62	4.6
				0.99, 0.95	
Q84	8.05	4.1	2.25, 2.05	2.46, 2.36	5.2
				7.74, 7.04	
T85	7.86	4.25	4.03	1.3	5.8
S86	8.29	4.24	4.01, 3.92		5.4
D87	8.37	4.5	3.03, 2.81		4.6
F88	8.29	4.27	3.26, 3.21	7.29, 7.16	4.9
				7.25	
D89	8.66	4.28	3.11, 2.77		3.6
D90	8.41	4.41	3.13, 2.76		4.3
E91	8.1	4	2.28, 2.08	2.55, 2.38	5.1
V92	8.04	3.5	2.07	0.87, 0.69	4.8
L93	7.89	4.05	1.92, 1.84	1.62	6
				0.99, 0.94	
L94	7.93	4.03	1.89, 1.85	1.6	4.4
				0.90, 0.90	
L95	8.01	4.04	1.82, 1.76	1.36	5.2
				0.85, 0.81	
Y96	7.91	4.39	3.13, 2.98	7.18, 6.64	7.9
R97	7.84	4.27	2.00, 1.93	1.78, 1.70	7.8
				3.20, 7.41;	
				7.25	

3.3.2.1 NMR Studies of the Loop 1-2 in methanol

The expansions of the 1D proton NMR spectrum of the loop 1-2 peptide is methanol shown in the Figure 3.3. The amide region of the spectrum (Figure 3.3A) had well-dispersed chemical shifts of amide protons, with some overlapping peaks, for example two peaks overlapped at positions 8.37 ppm and 8.27 ppm, and there was an overlap of three peaks in the region between 7.91 and 7.93 The $^{3}J_{NH\alpha}$ coupling constants were in the range 3.6 to 7.9 Hz range. The amide peak of the first residue S81 was not detected. The presence of the low concentration component was detected, that could not be assigned. It did not affect three-dimensional studies of the loop 1-2 by NMR.

In the aromatic region of the 1D spectra of the loop 1-2 in methanol, the singlets (at 7.04 and 7.74 ppm), two doublets (6.64 and 7.18 ppm), one triplet (7.41 ppm) and three multiplet peaks (7.16, 7.25 and 7.29ppm) were detected (Figure 3.3B). Those peaks originated from the aromatic residues (F^{88} and Y^{96}) and other residues containing the amide protons in the side chain (Q^{84} and R^{97}). The region of the α protons in the 1D spectrum had some residual water peak (Figure 3.3C), that disabled the correct integration. The peaks in that region were overlapping, but all Hα were found, and their assignment was achieved through 2D NMR spectra. The double doublet at 3.92 ppm was detected with 4.45, 6.92 and 4.74 Hz separation between peaks. At 3.50 ppm the quartet was detected, and 5.05 Hz separation in between the maxima of the peak. The three quartet peaks of the β protons were clearly resolved at positions: 3.03 ppm (with 9.85, 7.3 and 9.6 Hz separation), 2.98 ppm (10.59, 3.77 and 10.37 Hz separation) and 2.81 ppm (4.14, 12.67 and 4.18 Hz separation). The peaks in the rest of the spectrum were overlapping, with only three doublets of the CH_3 groups of the leucine and valine residues resolved from others at positions 0.99 ppm (6.41 Hz), 0.81 ppm (7.25 Hz) and 0.69 ppm (6.45 Hz).

The spin system identification of the loop 1-2 in the methanol was achieved using TOCSY spectra, which showed both direct and multiple-relayed correlation. The NH to sidechain region of the TOCSY spectrum of the loop 1-2 peptide in methanol is shown in Figure 3.4. The two threonine residues assignments (T82 and T85) were straightforward and unambiguous, even the two α protons had similar chemical shifts. The crosspeaks from NH to α, β protons were easily identified and distinguished in the amide region of the spectrum. The first threonine residue , T82 had crosspeaks at 8.71; 4.43 and confirmed by a strong crosspeak between the NH to CH_3 γ-protons (8.71;1.33), and crosspeak between α- and β-proton (4.43;4.15). The crosspeak at 8.71; 4.15 ppm was not found.

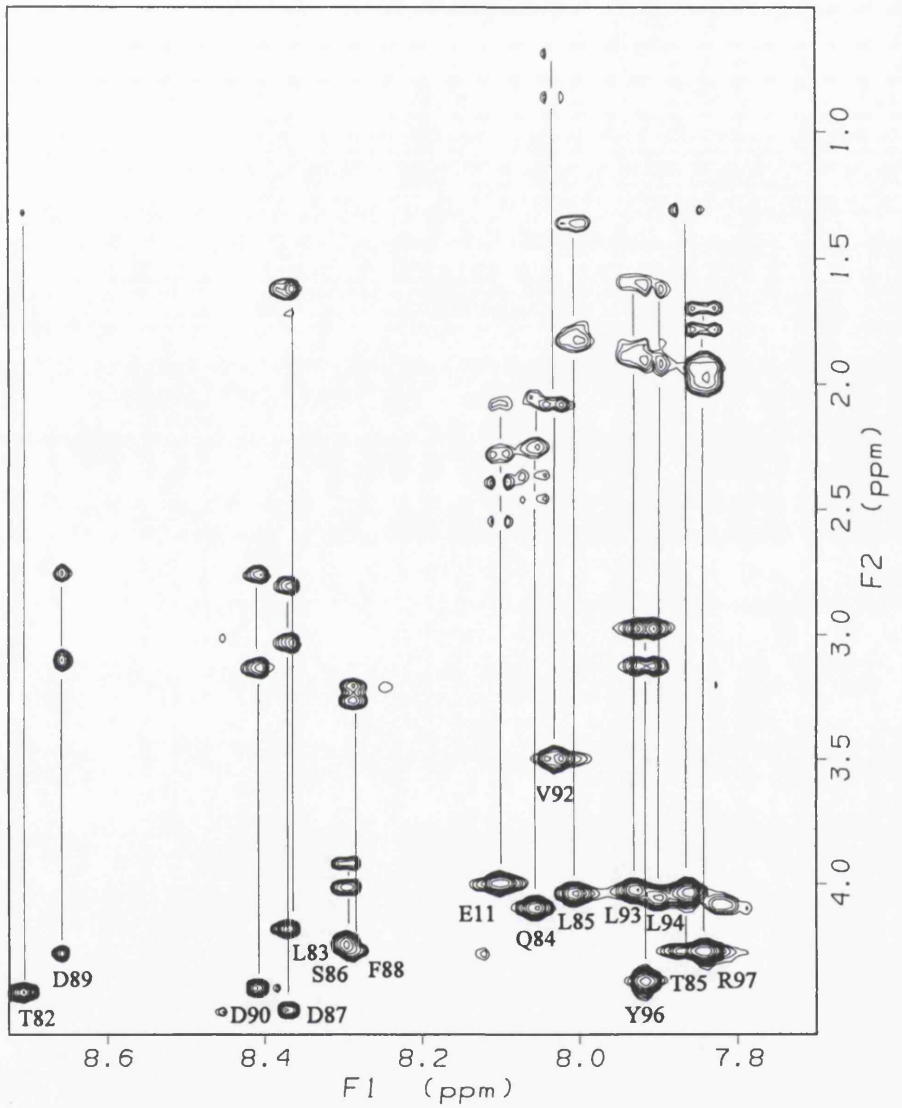

Figure 3.4 The NH/sidechain region of the of a 600 MHz TOCSY spectrum (τ_m = 60ms) used to assign the amino acid spin systems of 2 mM loop 1-2 of the β-subunit of high affinity IgE receptor in methanol-d3 at 298K.

The spin system assignment of the threonine residue, T85, was fully confirmed by α- to β-protons (4.44;4.03 ppm) and α- to γ- (4.44; 1.30 ppm) crosspeaks. The only valine residue was identified by crosspeaks between NH and β, γ protons. The anomalous chemical shift of the α proton of valine residue at 3.50 was connected to the 8.04 ppm peak in the amide proton region of the 2D TOCSY spectrum. Further connections were observed for other protons in the valine residue. Aromatic residues were identified through correlation of the ring protons to the backbone protons in the NOESY spectrum. The three aspartic acid residues were grouped in the TOCSY spectrum without overlapping, and they have been assigned by crosspeaks from the NH to β protons, and crosspeaks from α to β protons. The assignment of the four leucine residues was straightforward, with some difficulties in resolving the crosspeaks from γ to δ protons due to overlapping. The long chain of the basic residue, R97 was easily distinguished owing to its characteristic TOCSY crosspeaks from NεH or CεH to α proton, and reverse transfer pathway from NH to NεH and CεH. All the crosspeaks from the remaining residues were present in the TOCSY spectrum, and assignment to individual residues was only achieved at the later sequence-specific stage.

The sequential assignment was not straightforward, since there was overlap present in the α-proton chemical shifts in the NOESY spectrum (Figure 3.5). The crosspeaks between α-proton of F88 and NH proton of D89 were not observed since the chemical shifts of their α-proton were in the very narrow range (from 4.27 to 4.28 ppm) and it was not possible to distinguish the sequential from the intraresidue peak. Small dispersion of chemical shifts of the L93, L94 and L95 led to difficulty to differentiate crosspeaks in the 2D region 7.9-8.0; 4.5-4.0 of the 2D NOESY spectrum. In the rest of the spectrum the

assignment of the peaks was difficult because of small dispersion of the α-proton chemical shifts.

3.3.2.2 NMR Studies of the loop 1-2 in DMSO

The 1D NMR spectrum of the loop 1-2 in DMSO is shown in Figure 3.6. The amide region of the spectrum was divided into two different areas (Figure 3.6A), downfield (between 8.5 and 7.9 ppm) with well separated peaks, and upfield (between 7.9 and 7.6 ppm) where peaks overlapped. The amide proton of the first residue, S81 was located as a broad singlet (that singlet had a crosspeak to other singlet at 9.15 ppm). The detected $^{3}J_{NH\alpha}$ coupling constants for the NH peaks were in the range of 6.9 to 8.3 Hz (Table 3.3). In the aromatic region, two singlets (at 7.09 and 6.78 ppm), two doublets (at 6.98 and 6.59 ppm) and triplet (at 7.46 ppm) were resolved, and rest of the peaks belonging to aromatic and side chain amide protons were located in the 7.26 to 7.12 ppm range. The peaks of the α protons were located between 4.6 and 3.9 ppm, and they overlapped.

The residual water peak was located at 3.35 ppm, and it did not overlap with peaks of the peptide. The peaks of the CH_3 groups were grouped in the 0.9 and 0.70 ppm, except the two CH_3 group peaks which originated from threonine residues.

The assignment of the spin systems of the loop 1-2 peptide in DMSO was carried out in a similar manner to the assignments of the peptide NMR spectra in methanol (Figure 3.7).

A)

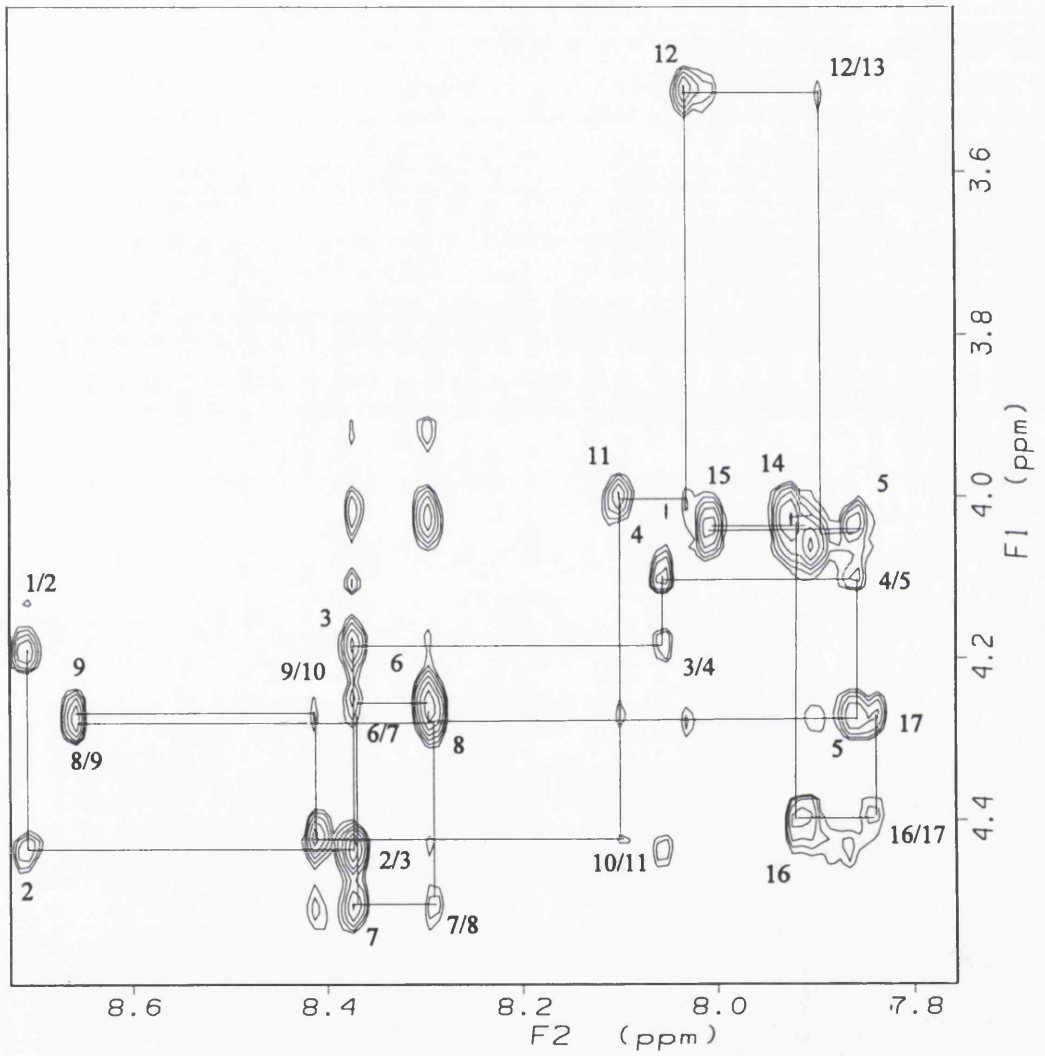
12
12/13
11
15
14
5
4
4/5
1/2
3
3/4
9
9/10
6
6/7
8
8/9
17
5
16/17
2/3
10/11
16
2
7
7/8
8.6
8.4
8.2
8.0
7.8
F2 (ppm)
3.6
3.8
4.0
4.2
4.4
F1 (ppm)

B)

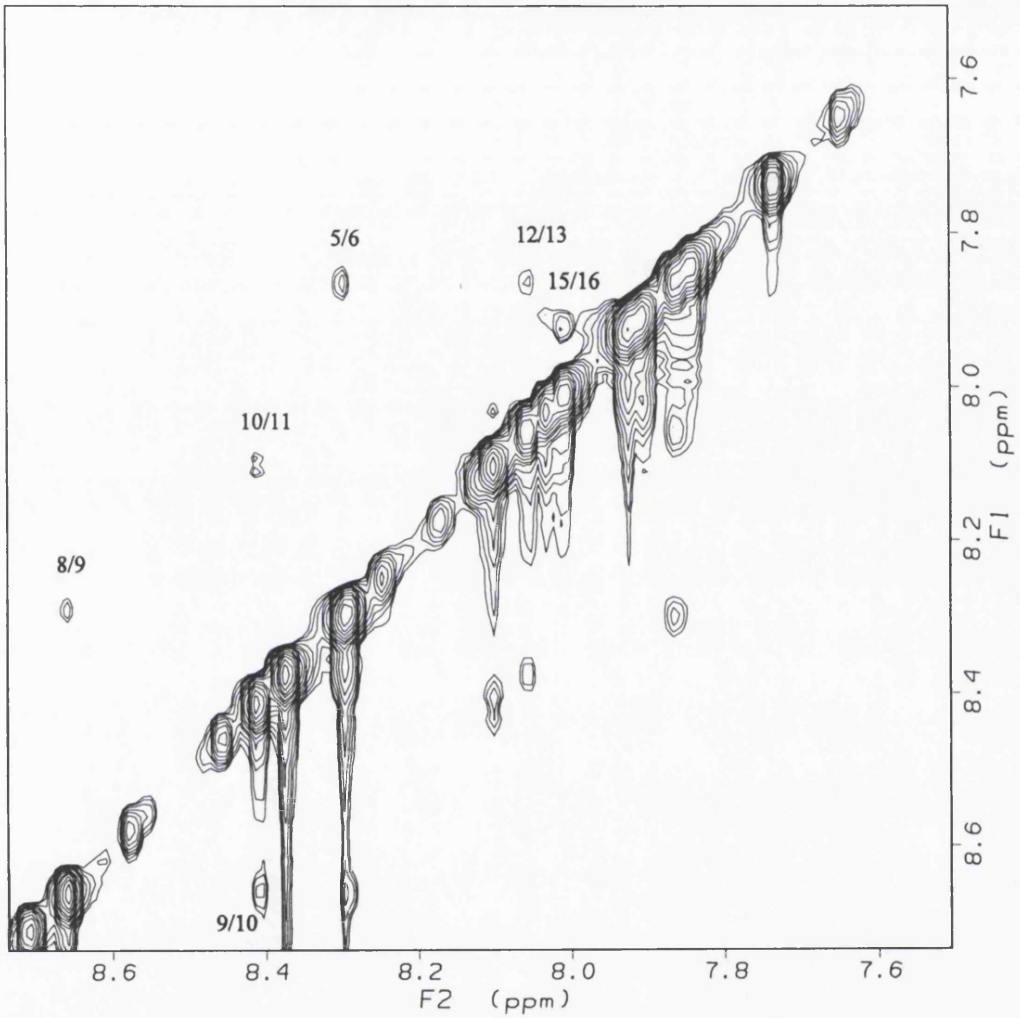

Figure 3.5 The finger print (NH/Hα) A) and NH/NH B) region of the of a 600 MHz NOESY spectrum (τ_m = 300ms) of 2 mM loop 1-2 of the β-subunit of high affinity IgE receptor in methanol-d3 at 298 K.

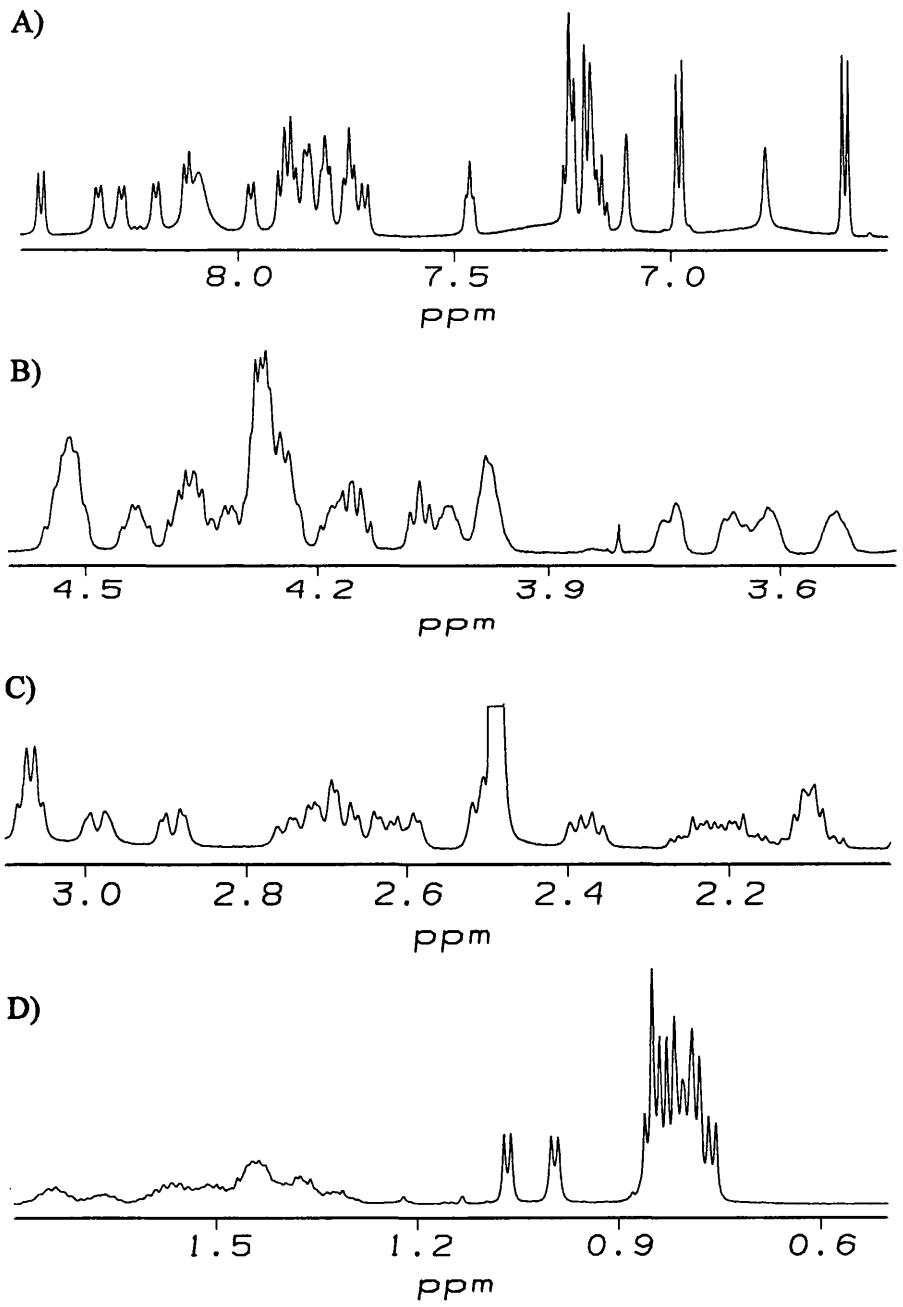

Figure 3.6 The expansions of 1D proton NMR spectrum of the loop 1-2 of β-subunit of high affinity IgE receptor in DMSO-d6; T= 298K, c=2 mM. A) amide and aromatic region, B) alpha proton region and C) rest of the spectrum.

Table 3.3 Assignment of spin systems of the ^{1}H NMR spectra of loop 1-2 of the β-subunit of high affinity IgE receptor in DMSO at 298K.

Residue	NH	αH	βH	Other	$^3J_{NH\alpha}$(Hz)
S81	8.09	3.98	3.74, 3.66		
T82	8.46	4.28	4.05	1.07	7.4
L83	7.9	4.32	1.6	1.45, 0.86	
Q84	8.12	4.28	1.88, 1.73	2.1	7.3
				7.22, 6.79	8.3
T85	7.71	4.27	3.98	0.99	
S86	7.84	4.36	3.62, 3.53		
D87	8.27	4.52	2.60, 2.37		
F88	7.84	4.43	2.98, 2.74	7.22, 7.18	
				7.2	
D89	8.32	4.54	2.73, 2.51		6.9
D90	8.19	4.52	2.68, 2.51		7.3
E91	7.81	4.24	1.86, 1.74	2.21	
V92	7.75	4.07	1.92	0.83	
L93	7.97	4.27	1.55	1.40, 0.83	
L94	7.87	4.25	1.56	1.37, 0.77	7.5
L95	7.8	4.18	1.51	1.34	
				0.83, 0.76	
Y97	7.74	4.38	2.89, 2.69	6.98, 6.59	
R98	7.88	4.15	1.67	1.44, 3.10	
				7.48, 7.09	

The sequential assignment was not straightforward, because there was an overlap between crosspeaks in the amide to Hα region of the NOESY spectrum, since there are a number of residues with similar chemical shifts in both NH and α protons (Figure 3.8).

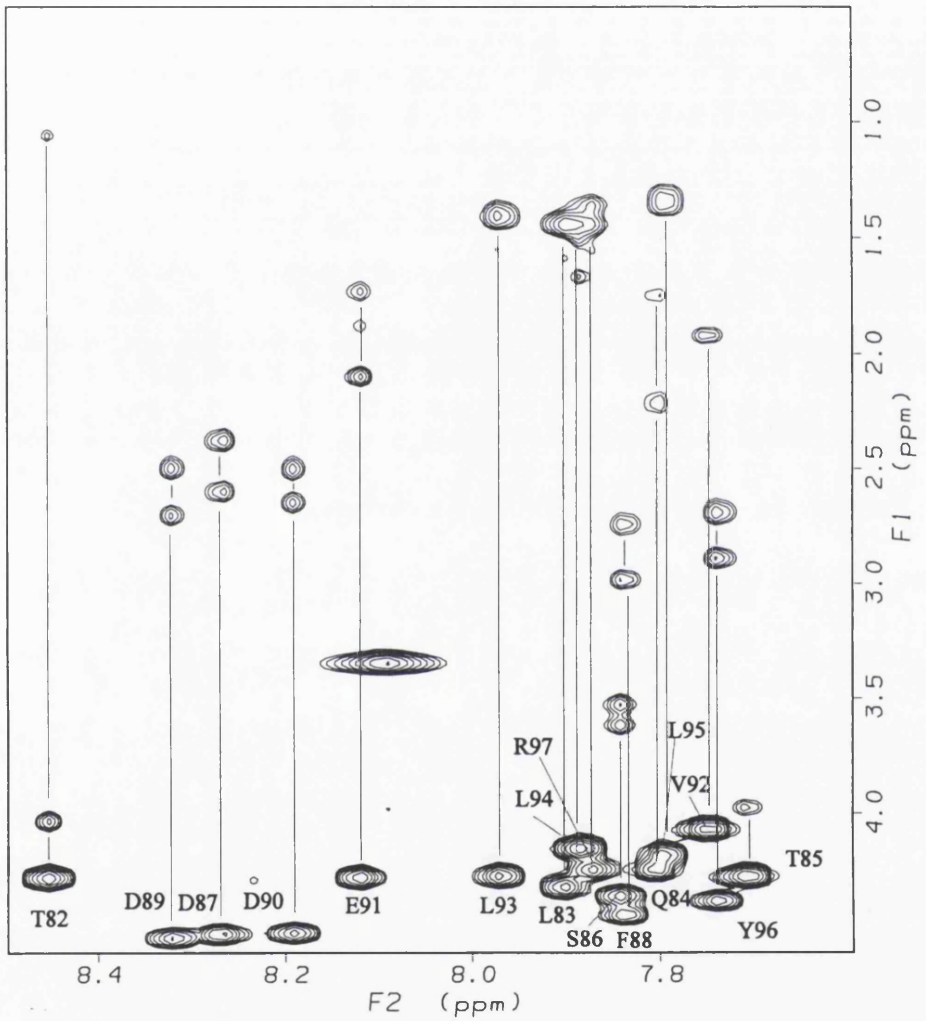

Figure 3.7 The NH/sidechain region of the of a 600 MHz TOCSY spectrum (τ_m = 60ms) used to assign the amino acid spin systems of 2 mM loop 1-2 of the β-subunit of high affinity IgE receptor in DMSO-d6 at 298K.

A)

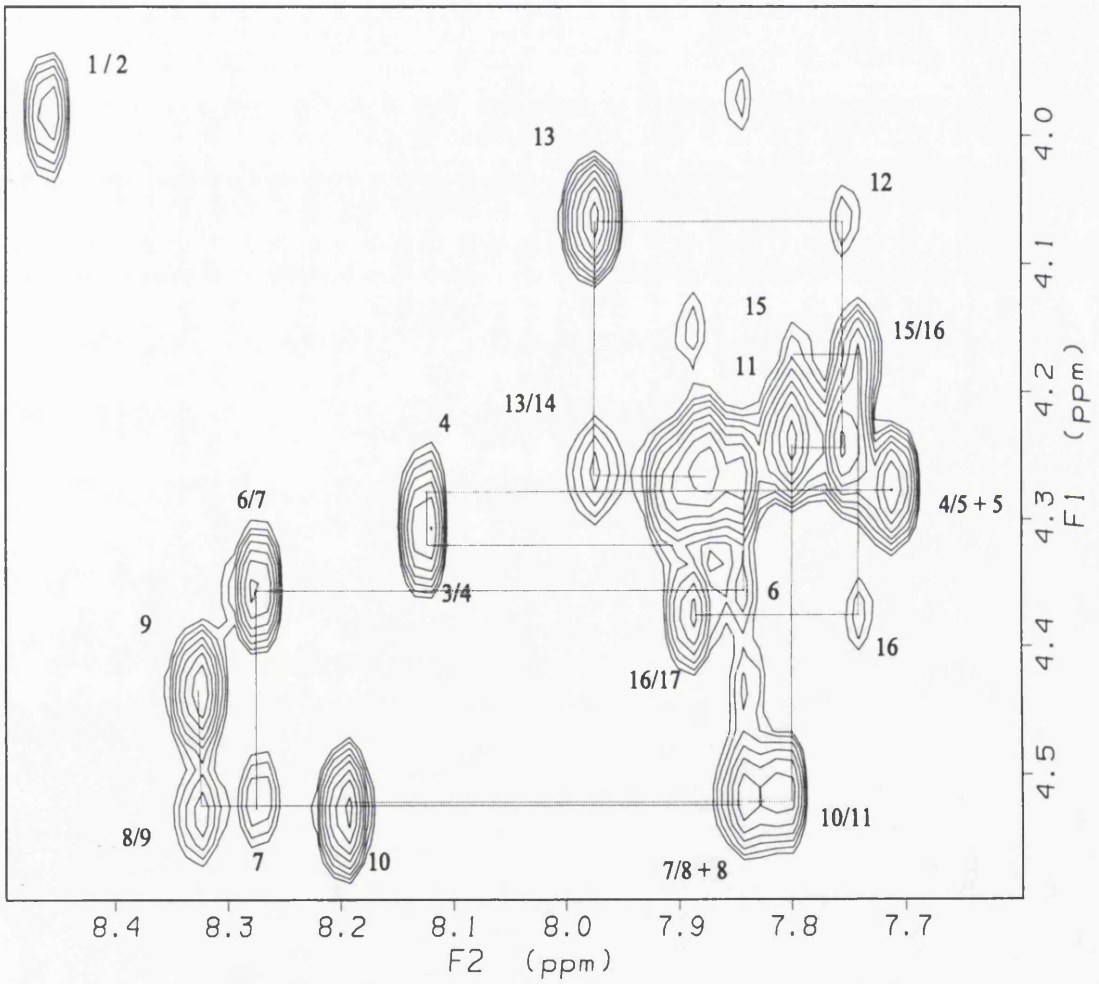
1 / 2
13
12
15
15/16
11
13/14
4
4/5 + 5
6/7
3/4
6
9
16
16/17
8/9
7
10
10/11
7/8 + 8
8.4
8.3
8.2
8.1
8.0
7.9
7.8
7.7
F2 (ppm)
4.0
4.1
4.2
4.3
4.4
4.5
F1 (ppm)

B)

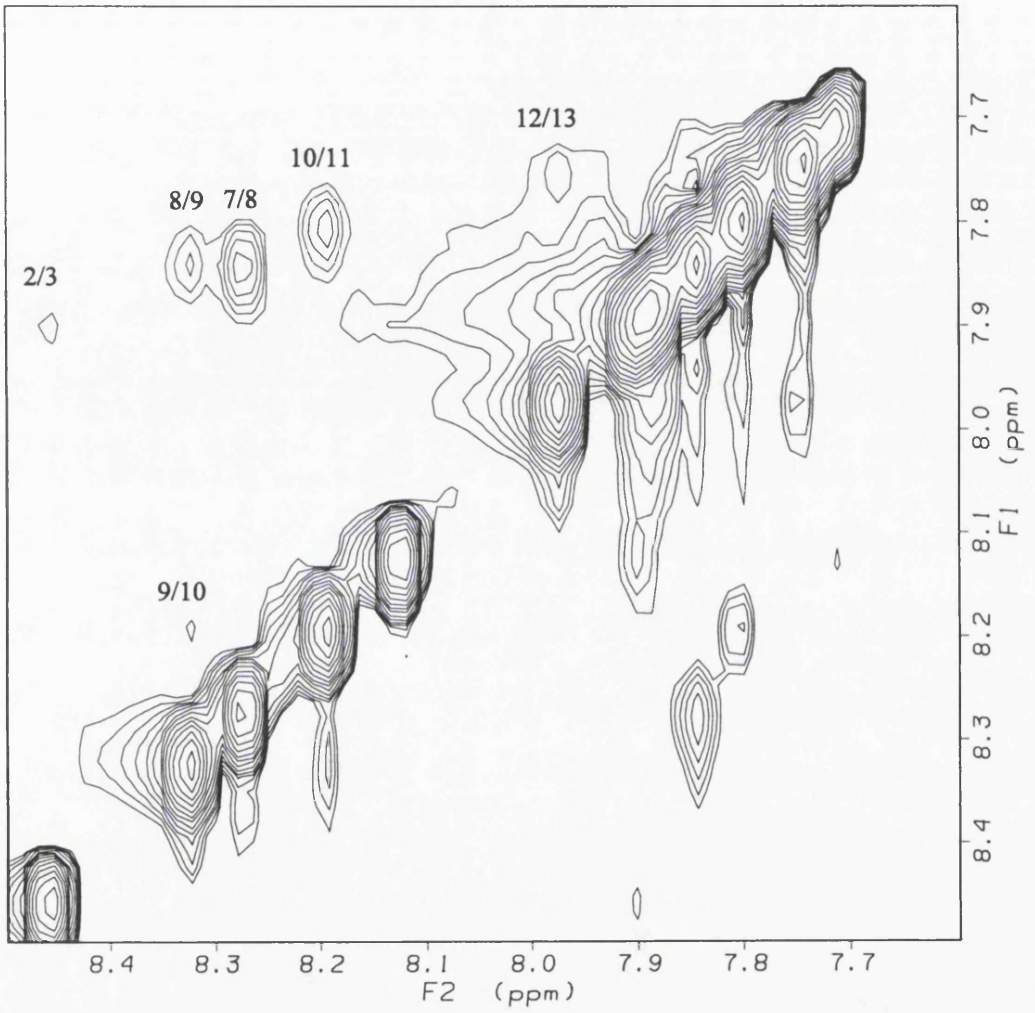

Figure 3.8 The finger print (NH/αH) A) and NH/NH B) region of the of a 600 MHz NOESY spectrum (τ_m = 300ms) used for sequential assignment of 2 mM loop 1-2 of the β-subunit of high affinity IgE receptor in DMSO-d6 at 298K.

Further information about the conformations of the peptide in solution can be extracted from measurements of coupling constants. Three-bond HN-αH coupling constants ($^3J_{NH\alpha}$) coupling constants were measured from 1D spectra and were related to backbone conformation (ϕ torsion angles) (Stern et al., 1968; Redfield et al., 1990). The results, also listed in Tables 3.2 and 3.3, showed that for the peptide in methanol such J-values were consistent with the presence of an ordered structure in the central region of the peptide. In particular the $^3J_{NH\alpha}$ values for the terminal residues of the peptide in methanol solution were slightly larger than would be expected from a standard α-helical conformation while those in the central region were less than 6 Hz. It was possible to measure the coupling constants only for 6 out of 17 residues for the peptide in DMSO solution and those values were larger than the corresponding values for the peptide in methanol.

3.3.3 NMR Based Structure Calculations of the Loop 1-2.

The structural information from NOESY spectra in methanol (218 distance constraints - 165 intraresidual, 9 sequential, 8 medium range, and 36 ambiguous) and coupling constants (17 torsional angle constraints) for the loop 1-2 peptide conformation were used to calculate the model of the structure of the 17-residue bridge peptide of the high affinity IgE receptor. The presence of NOE crosspeaks that could not be assigned without some knowledge of the real structure led us to the use of the ambiguous constraints. The restraints had been listed directly in terms of the proton chemical shift assignment and the NOE peak table without having assigned NOE crosspeaks to proton pairs (Nilges, 1995).

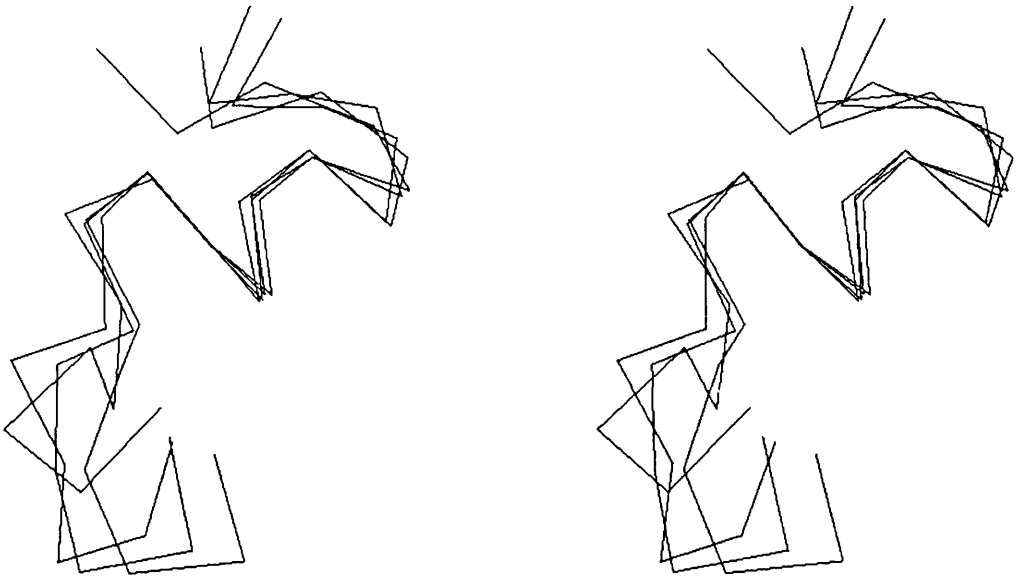

Figure 3.9 Stereoview of the overlap of the C_α positions of the four best structures obtained from the NMR data for the loop 1-2 in methanol. The structures were aligned to give a best fit for residues 6-10 to the mean structure. The average RMS deviation for these C_α atoms is 0.46.

A stereoview of the overlap of the best five structures obtained after minimization for the peptide in methanol is showed in Figure 3.9. The 174 distance constraints (59 intraresidual, 34 sequential, 9 medium range, and 72 ambiguous) were used for the NMR-based structure calculation for the loop 1-2 in the DMSO.

3.3.4 Overall Structures of the Loop 1-2 in Different Solvents.

The lowest energy structures identified the location of the helical moiety in the middle of the peptide chain, between residues S86 and E91. The RMSD values were 3.36 Å and 0.46 Å for the backbone atoms of the whole chain and of the α-helical moiety, respectively. This indicated that peptide was flexible, especially at the ends of the chain. The lowest energy structures, calculated based on the constraints derived from NMR spectra in DMSO solution indicate a more flexible chain with the RMSD value for the backbone atoms of the whole chain of 3.28 Å, It contained an folded conformation in the middle of the chain. The RMSD value for the backbone atoms of the residues between Ser86 and Asp90 was 0.86. The disorder in the end of the molecule in both the solvents was in agreement with the absence of the long range NOE distance constraints. In both solvents there was no evidence of the presence of different conformations of the loop in equilibrium between each other. This is consistent with either a single conformation or a dominant conformation that is rapidly interconverting with other minor structures. The average structure of loop 1-2 in methanol appeared in Figure 3.10A and it was compared with the average structure for the peptide in DMSO in Figure 3.10B.

Both the structures in Figure 3.10 of the loop 1-2 peptide exhibited some remarkable features. One is that most of the structure was reasonably well ordered, even though the peptide was relatively small. In the calculated structure in methanol the hydrogen bonds were detected along the helix between the C=O of S86 and the NH of D90 and between the C=O of D87 and the NH of E91. The calculated structure in DMSO the resembled a distorted helix, with the hydrogen bonds detected between the C=O of S86 and the NH of E91 and between the C=O of D87 and the NH of D90. Moreover, the amino terminal and the carboxyl terminal of the peptide are located close to each other (about 4.3

Å), thus completing the loop and positioning these termini appropriately for connection with adjacent transmembrane helices as would be expected to occur in the intact high affinity IgE receptor. The putative first two transmembrane helices do not extend beyond the hydrophobic region on the extracellular face because neither side of the peptide shows an α-helical structure.

Figure 3.11 shows a stereoview of the superimposition of the same region among the residues S86 and E91 of the loop 1-2 peptide in two different solvents. As can be seen the structural organisation of the peptide is the same in that region and there is not a large difference between the two structures that can be considered both helical.

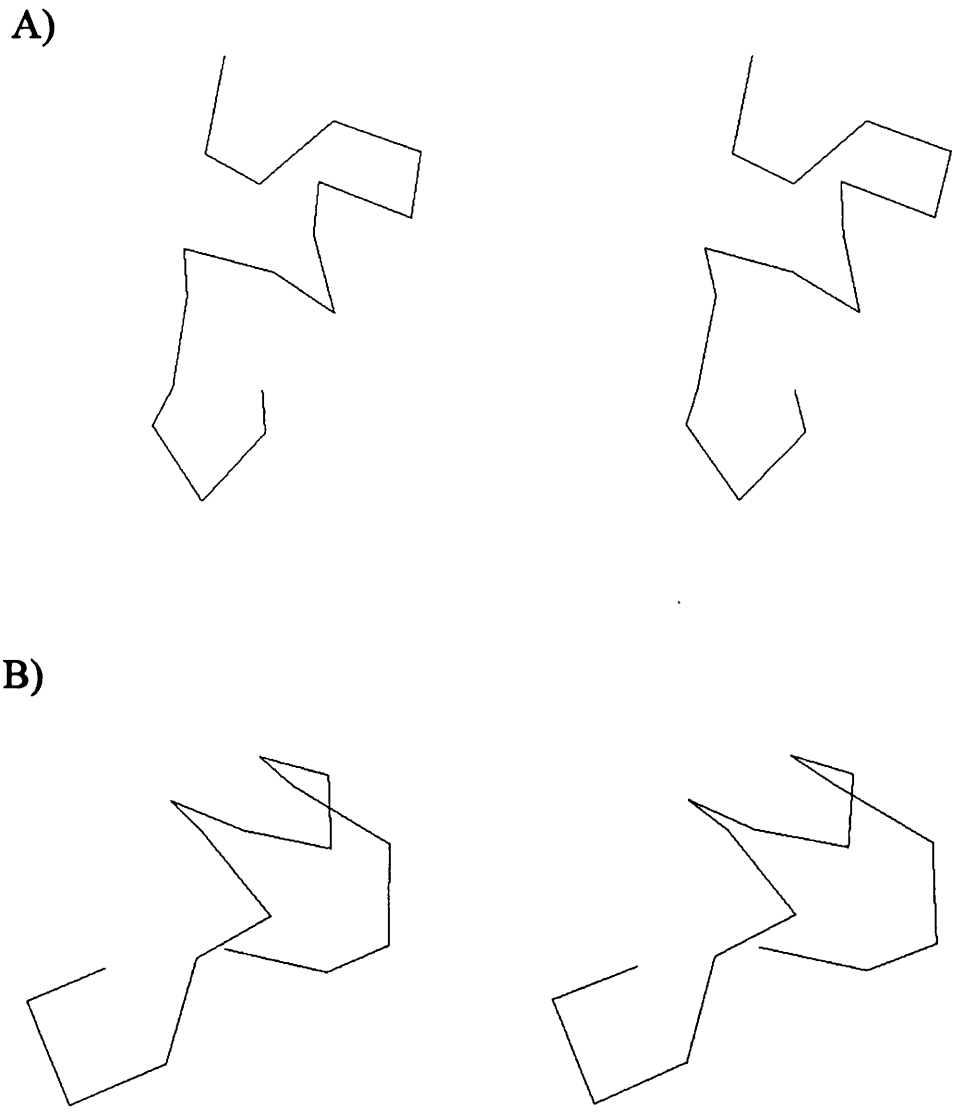

Figure 3.10 Averaged NMR based structure for the first extracellular loop of the β subunit of the FcεRI in methanol (A) and DMSO (B).

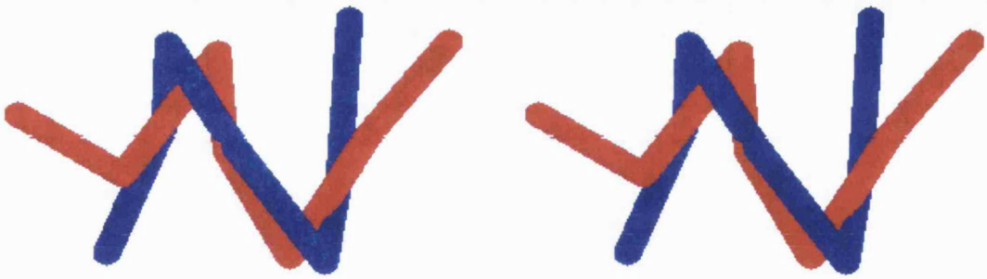

Figure 3.11 Overlap of the residues T85-E91 of the mean structures of the loop 1-2 in methanol (red) and DMSO (blue). Only C_α atoms were used in the superimposition

3.4 Summary

These NMR based calculated structures of the 17-residue connecting peptide were in good agreement with the structure of the connecting loop between two transmembrane helices in the proposed model for the β subunit of high affinity IgE receptor (Zloh et al., 1995).

Moreover, the CD spectra of the loop 1-2 were recorded under different conditions. The relatively low solubility of bridge peptide loop 1-2 in H_2O and TFE made their complete study by both CD and NMR in these solvents difficult to perform. The aqueous solution spectra of loop 1-2 indicated a conformational equilibrium in which one component or moiety was an α-helix structure. The addition of SDS at concentrations above critical micellar concentration increased the α-helical content in water. This bridge peptide was also subjected to Chou-Fasman and related algorithm, which were consistent with their central residues having α-helical characteristics (Zloh et al., 1995). The terminal

portions of loop 1-2 which were less structured will fold when covalently connected to the first two transmembrane helices of the receptor. The orientation of the transmembrane helices and the presence of the helical region in the middle of the loop on the surface of the cell, outside the membrane, may thus influence the ability of the extracellular loop, and in particular, to interact with the extracellular tail of the α-subunit of the IgE receptor.

The primary sequence of the loop of this integral membrane protein contains the information content to make the requisite turn, without the influence of the transmembrane helices to which the turn are connected. But both the turn and the helix-helix interactions may be important (Rees et al., 1989; von Heijne, 1992). The observation of the structure in the loop may shed some light on the problem of the insertion of membrane proteins into membranes during the biosynthesis. One question that has arisen concerns the formation of the loops that connect the transmembrane helices of integral membrane proteins. One hypothesis suggests that loop formation is driven by packing and transmembrane location of the transmembrane helices, which in turn force the loop conformation. Another hypothesis suggested initially that a substructure forms with two transmembrane helices connected by a loop, which then inserted into the membrane (Engelman et al., 1981). The former hypothesis implies that the conformation of the loop is primarily determined by the folding of the ensemble of transmembrane helices, and the latter hypothesis implies that the amino acid sequence of the loop itself should direct the conformation of the loop. The structural information obtained here was more consistent with the latter hypothesis than the former. Much of the sequence of the loop 1-2 is incorporated in a defined structure in the absence of a transmembrane helices and in the absence of the membrane and the rest of the protein.

The α-helical moiety found in the middle of the loop 1-2 peptide could suggest the appearance of the "TM helix - bend - loop helix - bend - TM helix" motif, as discussed in summary of Chapter 2 for the loop 2-3 (Figure 2.25). This pattern occurred twice for the β-subunit of FcεRI, implying that this motif could be common for the TM helix connecting loops in membrane proteins, such as ion-channels and receptors.

Chapter 4

INTERACTION OF TRANSMEMBRANE HELICES WITH DODECANE: MAPPING OF HYDROPHOBIC SURFACES BY MOLECULAR MODELLING

4. INTERACTION OF TRANSMEMBRANE HELICES WITH DODECANE: MAPPING OF HYDROPHOBIC SURFACES BY MOLECULAR MODELLING

4.1 Background

Molecular modelling has often helped to clarify important aspects related to receptor structure. Many of the theoretically determined 3-D structures of membrane proteins were derived from studies based upon the comparison with the conformation of *Bacteriorhodopsin* and/or models which relied on homology with the family of G-protein coupled receptors (GPCRs) [Elling et al.,1995; Herzyk and Hubbard, 1995; van Rhee, et al., 1995, Habibi-Nezhad et al., 1996]. However, there are whole classes of membrane proteins, which are not homologous to these two latter proteins, consisting of several polypeptide chains with higher degrees of structural complexity, which represent a difficult problem that can be better solved using molecular modelling in combination, preferably, with experimental and other data. Although the TM helices are all hydrophobic, these are selected to be involved in helix - helix interactions to form higher order structures, such as coiled coils and helix bundles. Finally, after folding, TM helices must specifically interact with membrane lipids, usually their fatty acid and related components.

The integration of the transmembrane proteins into the lipid bilayer is one of the crucial prerequisites for the correct functioning of the protein. In studies regarding integral membrane proteins the role of phospholipids composing the bilayer should be taken into

account as stated. The integration of a transmembrane protein in the lipid bilayer depends strongly on the interactions that the macromolecule establishes with the membrane lipids. Several studies were performed in order to obtain information on the possible matching of the lipid chain configuration and packing of lipid elements to and around the hydrophobic surface of protein and helices. Molecular modelling was used to study the packing of the proteins in the lipid environment [Wallace and Janes, 1991; Wang and Pallman, 1991; Xing and Scot, 1992;]. The features of the ordered lipid chains in the crystals were studied by X-ray crystallography [Baldwin et al, 1988]. The information about interactions in lipid-protein systems as followed by NMR, ESR and other methods could be found in reviews [Cserhati and Szogyi, 1991; Cserhati and Szogyi, 1992; Cserhati and Szogyi, 1993; Marsh, 1993].

The subject of this work was another aspect of the lipid - helices interaction. Inside the membrane, both the relative helix-helix and helix-lipid interactions define the helix arrangement in the folded macromolecule but also the surfaces exposed to lipids. Lipid-protein interactions may be therefore used as one of the constraints for modelling the structure of membrane proteins integrated into lipid bilayer. For instance, using hydrophobic moments Taylor et al., 1994 correctly predicted the lipid-exposed faces of the TM helices of Rhodopsin and also successfully predicted the helix packing in agreement with the crystal structure. There have been other attempts to predict lipid facing sides of helices and model receptors using hydrophobic moments [Green, 1991; Habibi-Nezhad, et al, 1996; Kristiansen et al., 1993; Kristiansen and Dahl, 1996; Sytle et al., 1993; Sytle et al., 1996].

In this and next chapters, the complementary de-novo, yet simple, approach was used to predict the orientation of the TM helices in the 7-helix bundles of the high affinity

IgE receptor (FcεRI). A lipid molecule can interact with a peptide in many different ways [Cserhati and Szogyi, 1991; Cserhati and Szogyi, 1992; Cserhati and Szogyi, 1993; Marsh, 1993]. Hydrophilic, hydrophobic or mixed interactions can be established between the polar head groups or the apolar fatty acid side chains of a phospholipid and the amino acidic residues of a protein or a peptide. The strong association of phospholipids with the various proteins or peptides changes the structure of the interacting molecules and thus their biological activity.

Formally, a phospholipid molecule can be considered as divided into five different moieties: a polar head, a negatively charged phosphate group, the glycerol residue, saturated and unsaturated fatty acid chains bound to it (Figure 4.1).

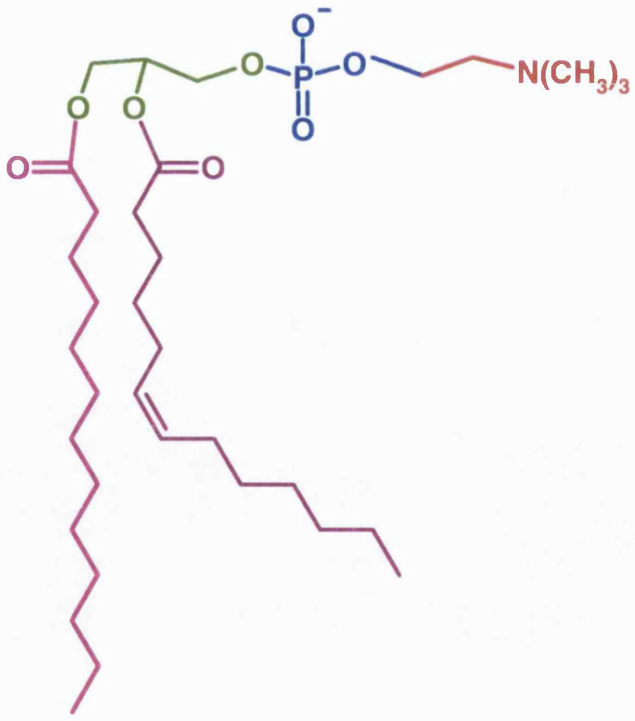

Figure 4.1 Schematic representation of five different moieties of the phospholipid (PC).

positions were then chosen, with a separation of 5Å between the helix and dodecane, and

Each component or structural moiety of the lipid can play a different role when interacting with a macromolecule. A negatively charged phosphate group, for example, or a charged polar head (like the polar head of the phosphatidylethanolamine or phosphatidylcholine) can exhibit coulombic or hydrogen-bonding interactions with the polar moieties at the ends of a transmembrane helix or with the peptide loops connecting two TM consecutive helices. Similarly, within the membrane, hydrophobic interaction usually leads and helps drive the folding and the packaging of the helices and of the entire protein.

At the interface between the membrane and the aqueous environment hydrogen bonds, for example, between the glycerol residue and the amino acid side chains and backbone of the macromolecule can reinforce and stabilise the structure.

For this purpose we analysed firstly via molecular modelling and dynamics, the possible interaction of the six different TM helices of the FcεRI [proposed by Blank et al, 1987] with the apolar moieties of a phospholipid molecule. Thus hydrophobic interaction between the saturated fatty acid chain of the phospholipid and the different TM helices of were studied by molecular modelling.

The mapping of the helix surface hydrophobicity has relative manner, by comparison interaction energies. The initial assumption was that lipid fatty acid chains would interact with certain surfaces more and therefore produce low energy complexes between lipid and TM helix. In the first instance, for simplicity, the TM helix was replaced by a fully symmetric poly-alanine α-helix to provide the basis for more complex helices from integral membrane proteins and the dodecane molecule was used to mimic the hydrocarbon chain of the saturated fatty acid. The poly-alanine and dodecane were always longitudinally oriented with a long axes parallel to each other. The eight rotational

positions were then chosen, with a separation of 5Å between the helix and dodecane, and with the dodecane rotating around middle part of the helix (Figure 4.2) giving the positions at 0°, 45°, 90°, 135°, 180°, 225°, 270° and 315°.

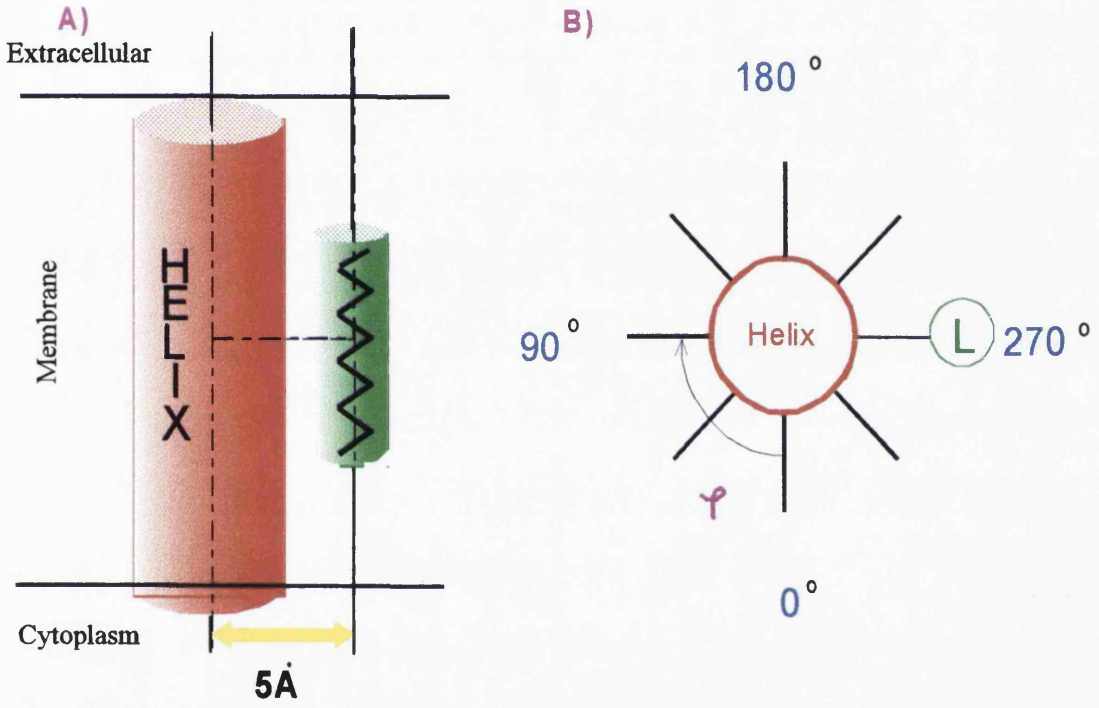

Figure 4.2 The schematic representation of the study of TM helix (red) and dodecane (green) hydrophobic interaction , A) sideview and B) view above the membrane.

4.2 Methods

The interaction energies between the *Bacteriorhodopsin* helices, FcεRI helices, and poly-ALA helix and dodecane were calculated by X-PLOR (Brunger, et al., 1987) using the CHARMM 22x parameter set, and dielectric constant of 1.0. The ideal α-helix geometry was chosen as a starting structure for TM helices. Helical backbone geometry was explicitly maintained during simulations through imposition of a one-sided distance restraint with an upper boundary of 3.2A between I oxygens and I+4 nitrogens along the length of the helix. The fully extended forms of dodecane was again used as a starting geometry. The helix and ligand were always oriented with their long axes parallel to each other. The eight rotational positions were considered (figure 4.2) , with a separation of 5Å between axes of the the helix and dodecane. Energy minimization consisting of 2000 steps of Powell minimization steps was used.

In the second procedure, the modified simulated annealing protocol [Adams et al, 1994] was also used, namely, 1) a 2ps molecular dynamics heating stage at 600K with a timestep of 1fs, 2) a 2ps constant temperature molecular dynamics simulation at 300k with timestep of 2fs. and 3) 1000 steps of Powell energy minimisation. The α-helical hydrogen bond restraints were maintained active during the simulation stages, but no other restraints were applied during the constant temperature simulation and energy minimisation stages.

The interaction energies between the dodecane and the helices were calculated relative to those when the two molecules were far apart: ΔE=E(close)-E(far). Thus, negative values of interaction energies corresponded to stabilization. The 360° position is equivalent to 0° position in all graphs and tables.

Table 4.1 The amino acid colour scheme used by RasMol software[Sayle, 1995].

Residues	Colour
Asp, Glu	bright red
Lys, Arg	blue
Cys, Met	yellow
Ser, Thr	orange
Phe, Tyr	mid blue
Asn, Gln	cyan
Gly	light grey
Leu, Val, Ile	green
Ala	dark grey
Trp	pink
His	pale blue
Pro	flesh

Several molecular graphics programs were used for the analyzing the complexes and creating the pictures: RasMol and RasWin Versions 2.6b [Sayle, 1995], WebLab Viewer Version 2.01 [Molecular Simulations Inc., 1997], MolMol Version 2.51 [Billeter and Xia, 1997]. Besides the CPK colour scheme, the RasMol colour scheme was used for the amino acid residues presentation (Table 4.1). Dodecane is always presented as a "stick model" coloured green. The helix atoms within a distance of 4 Å from dodecane were depicted as CPK model in the figures of dodecane-helix complexes. The rest of the helix was shown in the "wireframe" presentation. The orientation of the TM helices of the FcεRI was always consistent with the orientation as it was shown in the Figure 1.2, namely, the TM helices of the α- and γ-subunit had their N -terminal ends at the top of the page, like 2^{nd} and 4^{th} helices of β-subunit, while 1^{st} and 3^{rd} helices of the β-subunit had their C-terminal ends on the top of the page.

4.3 Results

4.3.1 Interaction of poly-alanine with dodecane

The ideal α-helix geometry of the poly-alanine molecule, mimicking the transmembrane helix, was used to study the hydrophobic interaction with lipids and hence to map the surface. For simplicity the fully symmetric hydrophobic dodecane molecule was chosen as a ligand instead of a phospholipid, since it has no polar groups, and only van der Waals interaction would be encountered. Dodecane is also an anaesthetic and studies could provide a basis for understanding its effect on anaesthetic receptors and ion channels. The poly-alanine helix has uniformly distributed nonpolar CH_3 groups, shielding the polar groups of the backbone, and therefore the essentially same interaction energies were expected for all eight rotational positions. Figure 4.3 shows the interaction energies between the poly-alanine helix and dodecane calculated by the X-PLOR minimization protocol. The poly - Ala - dodecane behaved as predicted. All interaction energies were negative (-11.9±1.8 kcal/mol), indicating the favourable interaction between dodecane with poly-ALA helix. Two shallow maxima and two minima, with 3.6 kcal/mol difference between highest and lowest interaction energies resulted. This difference between highest and lowest interaction energies was the result of the different packing due to rotational symmetry of the poly-alanine helix, so it could be considered as a lower limit above which interaction energies becomes significant. Also, this energy is similar to the energy barrier of the rotation around C - C single bond in ethane (2.9 kcal/mol).

The most stable complex between poly-alanine and dodecane (interaction energy -13.7 kcal/mol) resulted from the minimization protocol was presented in the Figure 4.4A. The packing was maximum so hydrophobic interaction between alanine CH_3 groups and dodecane CH_2 group was maximized. The simulation protocol was also used and the energy

of the most stable complex (Figure 4.4B) was -13.2 kcal/mol. The hydrophobic interaction was maximized in this case, but the dodecane migrated in an uncontrolled fashion and this was not suitable for mapping of the surface. For the hydrophobicity mapping of the TM helices, the minimization protocol was therefore used through the rest of the thesis.

The comparison between highest and lowest energy positions was the most important feature of this experiment. The difference of interaction energies between the highest and lowest energy positions bigger than 3.6 kcal/mol will be considered as significant.

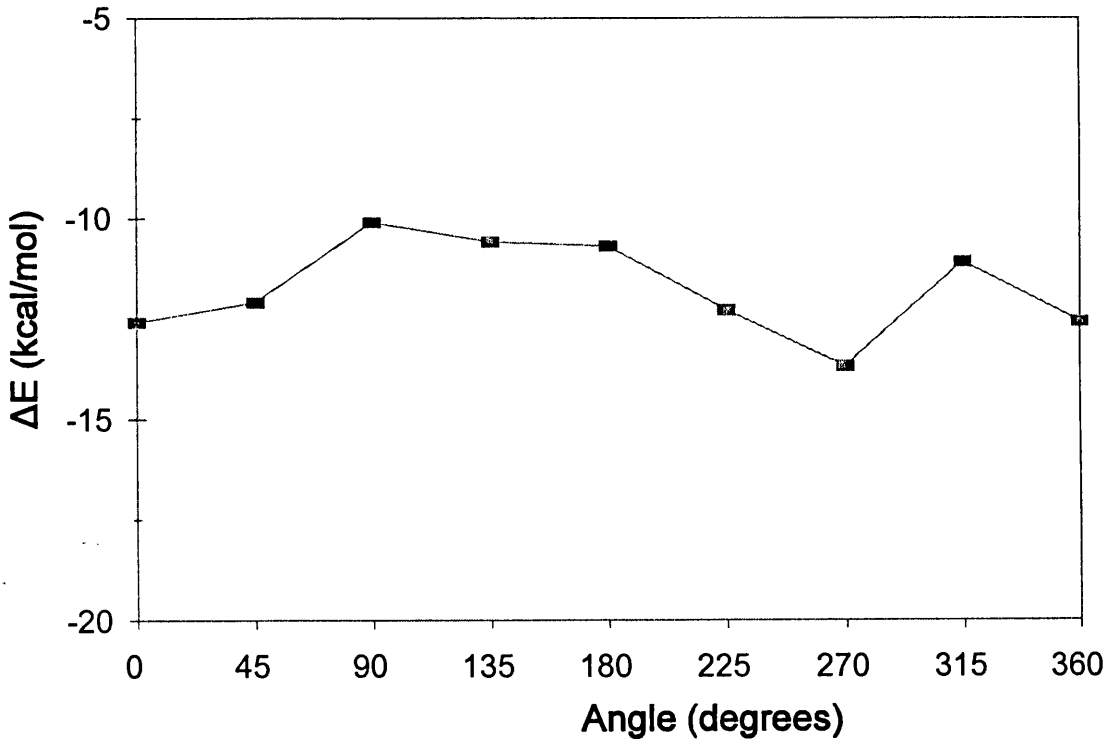

Figure 4.3 The interaction energy between Poly-alanine and Dodecane as a function of the rotation of dodecane around helical axis as described in methods.

These data/conclusions encouraged the study of more complex helices and lipids with same way, but particularly to apply this method to a known model system, where both the helix - helix and lipid - helix interfaces have been structurally defined by crystallography. *Bacteriorhodopsin* was chosen as the model system and the FcεRI as a structurally unknown example of a 7 helix integral membrane protein.

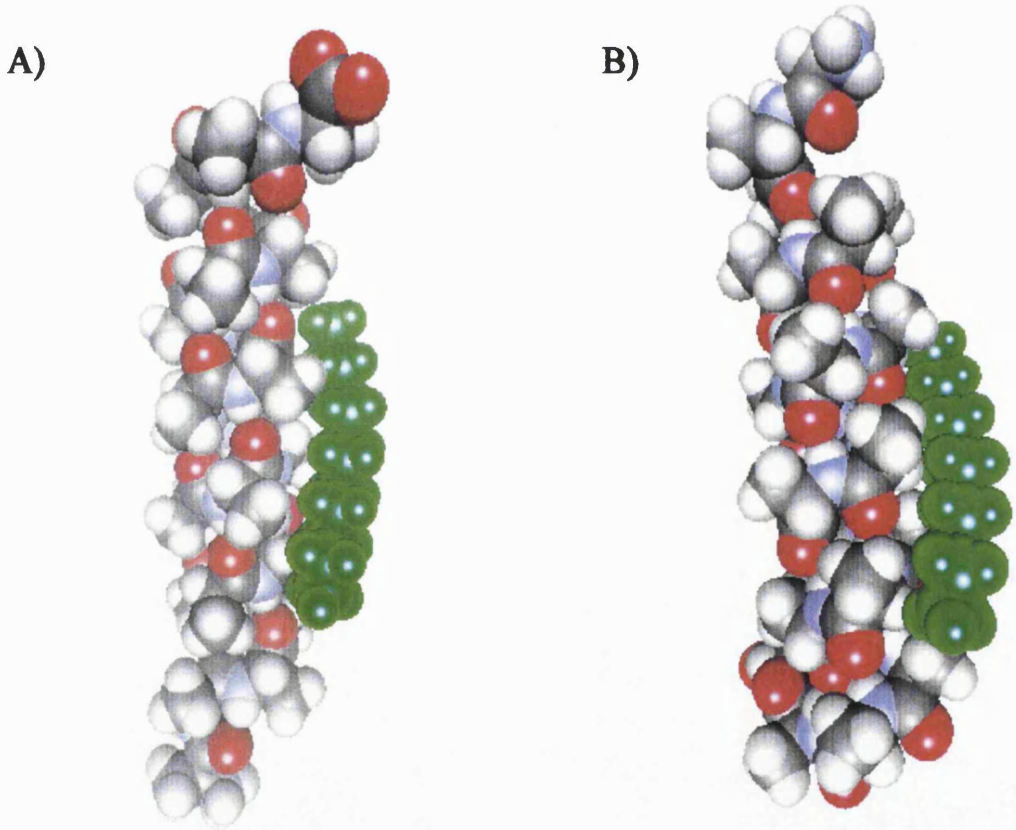

Figure 4.4 The most stable complexes between poly-alanine helix and dodecane as a result from A) minimization and B) simulation protocol.

4.3.2 Interaction of the transmembrane helices of *Bacteriorhodopsin* with dodecane

The *Bacteriorhodopsin* (BR) is a light-driven pump, that is found in the membrane of *Halobacterium halobium*. Its structure was determined by high resolution crystal structural analysis [Henderson et al., 1990]. BR is a 7-helix membrane protein and the helix bundle is presented in Figure 4.5A. The TM helices were between 20 to 25 residues long and were arranged in the two layers that were packed together; the layers contained either three or four α-helices. The *Bacteriorhodopsin* is specific, since it binds retinol molecule in the bundle cavity. The purple colour is produced by the chromophore retinal. The *Bacteriorhodopsin* does not belong to G-protein linked family of receptors. A map of the structure was obtained by electron microscopy and diffraction [Henderson et al., 1990], with the resolution of 3.5 Å in the plane of the membrane and lower resolution perpendicular to the membrane. The map had a strong density for seven α-helices, and bulky aromatic side chains of phenylalanine, tyrosine and tryptophan were used as guide points for the building of a complete atomic model of the 7 TM helices. The retinal molecule was surrounded by 21 amino acids contributed by five helices and bound to Lys216 through a protonated Schiff base. Retinol is amphiphatic, with long a hydrophobic chain, so the TM helices were expected to be hydrophobic in the 7 - helix bundle cavity.

The outer surface of the *Bacteriorhodopsin* is very lipophylic, the three lipid molecules have to be between two bundles in order for crystals to be formed [Popot et al, 1994]. The sideview of the surface of the *Bacteriorhodopsin* molecule was presented in Figures 4.5B and 4.5C. The polar residues were coloured in red (negative charge) and blue (positive charge), and more intense colour indicated the more polar nature of the surface. The side of the helix bundle has low intensity red and blue colours, since most of the

surface residues were hydrophobic (nonpolar). The helix ends had more intense colours, since the charge residues were located there in a function of a TM helix breakers.

The analysis of the TM helix contacts in the *Bacteriorhodopsin* 7 helix bundle was performed through calculating the distance between atoms in different helices. The cutoff distance of 4.5Å between two atoms in different helices was used, which was a more restrictive limit compared to the cutoff distance defined by Chou, et al., 1992, namely, $(2\text{-}2^{1/6})(r_i+r_j)$, where the r_i+r_j notified the sum of van der Waals radii of two atoms, i and j. The residues not involved in contacts between TM helices were examined for their orientation, to determine exposure to the lipid bilayer. That determined the lipid facing side of the helices. The sideview of the surface of the *Bacteriorhodopsin* molecule was presented in Figures 4.5B and 4.5C, while the helical wheel presentation is shown in Figure 4.5D.

The ideal α-helix geometry of the TM helices of the BR, mimicking the transmembrane helices, were used to study the hydrophobic interaction with lipids and hence to map the surface. Again, for simplicity the fully symmetric hydrophobic dodecane molecule was chosen as a ligand instead of a phospholipid, since it has no polar groups, and only van der Waals interaction would be encountered. Table 4.2 shows the interaction energies between the TM helices and dodecane calculated by the X-PLOR minimization protocol and these will be discussed in the Section 4.3.2

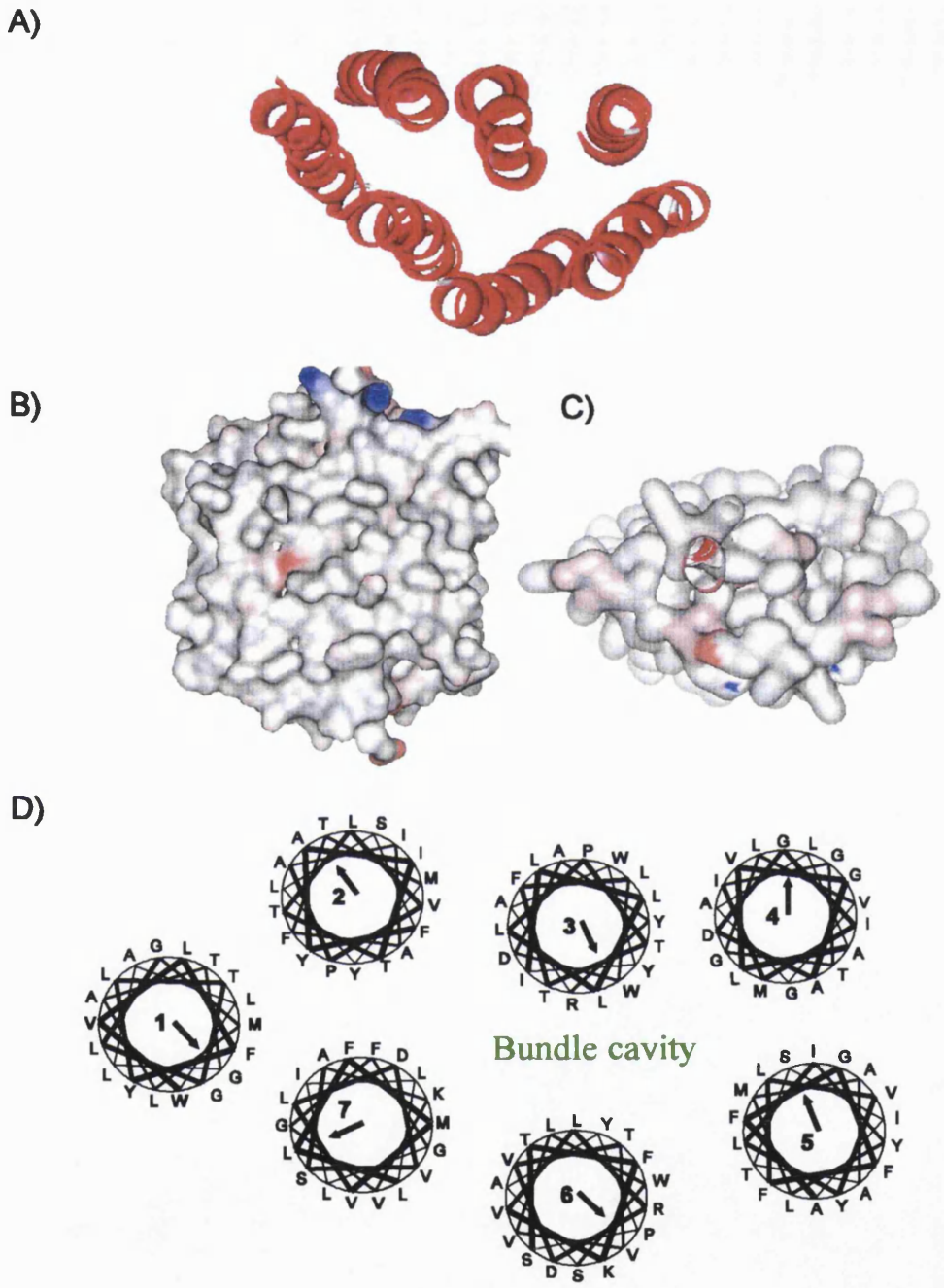

Figure 4.5 7 helix bundle of *Bacteriorhodopsin*; A) backbone, B) sideview and C) above the membrane view of the surface and D) helical wheel presentation with hydrophobic moments.

Table 4.2 The interaction energies between TM helices of *Bacteriorhodopsin* and dodecane in eight rotational positions around each TM helix calculated by minimization protocol as described in Section 4.2.

Angle(°)	Energy (kcal/mol)						
	BR - I	BR - 2	BR - 3	BR - 4	BR - 5	BR - 6	BR - 7
0	-6.4	-10.5	-19.0	-7.0	-13.1	-15.6	-12.1
45	-6.8	-11.2	-9.6	-13.5	-15.4	-15.6	-16.9
90	-10.4	-14.0	-15.0	-13.9	-10.2	-7.0	-12.1
135	-11.5	-12.7	-13.8	-13.8	-8.3	-14.6	-13.8
180	-10.2	-18.1	-16.8	-13.8	-9.3	-11.0	-7.5
225	-11.1	-12.3	-10.8	-10.2	-10.5	-12.9	-19.5
270	-17.5	-8.2	-18.5	-14.3	-15.7	-10.8	-15.2
315	-17.3	-13.9	-13.3	-18.0	-10.1	-14.3	-12.1
360	-6.4	-10.5	-19.0	-7.0	-13.1	-15.6	-12.1

4.3.2.1 The TM helix 1 of *Bacteriorhodopsin:*

The helical net plot of TM helix 1 (E^{9}WIWLALGTALMGLGTLYFLVKGM^{32}) adopted from *Bacteriorhodopsin* crystal structure [Henderson et al., 1990] is presented in Figure 4.6A. The helix axis is depicted longitudinally (≈30 Å) and the x-axis represents 0-360° around helix. In accordance with crystal structure, amino acid residues E9, W10, W12, L13, A14, G16, T17, M20, G21, T24, Y26, F27, L28, K30, and G31 on the 0-180° helix surface (depicted as red circles) interact with other helices (2 and 7). By corollary and diagram (Figure 4.5C) amino acid residues amino acid residues I11, W12, L15, G16, L19, M20, G21, L22, G23, T24, Y26 and F27 on the 180-360° helix surface (depicted as a full or half green circles) are involved in helix 1 with fatty acid chains of the lipid bilayer. (The residues presented as a half red - half green circles are exposed to the lipid bilayer and also interact with other TM helices.) These two complementary TM helix 1 surfaces spread through the two leaflets of the bilayer.

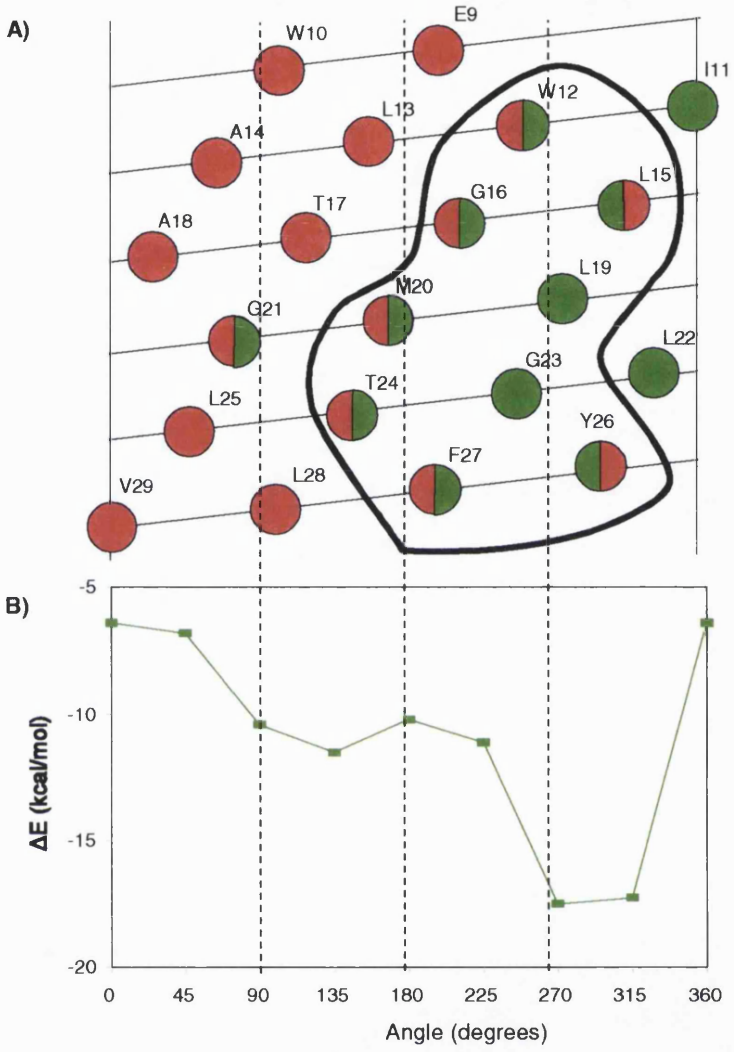

Figure 4.6 The hydrophobic surface mapping of the transmembrane helix 1 of the *Bacteriorhodopsin* A) The helical net plot outlines the amino acid residues in the contact with other TM helices (depicted as red circles), amino acid residues exposed to lipid bilayer (depicted as green circles), while half red - half green circles represent residues exposed to the lipid bilayer and in contact with other TM helices in the crystal structure. Solid lines encircled the residues in the contact with dodecane in the most stable complexes determined by calculation. B) The interaction energy between the TM helix 1 of the *Bacteriorhodopsin* and dodecane as a function of the rotation of dodecane around helical axis as described in methods.

The ideal α-helix geometry of TM helix 1 of BR was used in the computational procedure described in the 3.2 section of this chapter. The hydrophobic probe and anaesthetic molecule, dodecane was rotated around the TM helix 1. The resulting interaction energy between TM helix and dodecane was plotted against rotational angle in order to map the relative hydrophobicity of TM helix 1 surface (Figure 4.6B). The least hydrophobic surface of the helix, according to these calculations, was 0° to 180° which corresponded to the surface in the BR that interacted with other helices (Figure 4.6A).

The most hydrophobic surface (the lowest interaction energy complex with -17.5 kcal/mol interaction energy), as calculated, was between 225° and 270° rotational positions which corresponded to the same surface on the BR which crystallography showed to be lipid interaction surface. The solid line endorse the surface on TM helix 1 of BR that interacted with dodecane in most stable complex. This surface substantially agreed with lipid interacting surface of TM helix 1 in crystal structure. The corollary indicates that this approach should give realistic result the when applied to other TM helices of BR, but more interestingly to unknown receptor helix surfaces of the FcεRI.

4.3.2.2 The TM helix 2 of *Bacteriorhodopsin*

(D^{38}AKKFYAITTLVPAIAFTMYLSMLL^{62})*:* The helical net plot of the TM helix 2 of BR is shown in Figure 4.7A. The helix axis is again depicted longitudinally (≈30 Å) and the x-axis represents 0° to 360° around helix. The residues K40, K41, A44, I45, I52, T55, and S59 of the TM helix 2 did not interact with neighbouring TM helices in the crystal structure (depicted as a full green circles). The surface defined by those residues was probably interacting with membrane lipids. Some of the residues (T47, V49 and M56) were involved in the helix - helix interaction and partially exposed to the lipid bilayer (green -

red circles in Figure 4.7A), while the residues Y43, T46, P50, A53, F54, Y57, L58 and M60 (depicted as red circles) were fully buried in the helix bundle .

The calculated interaction energy between TM helix 2 (with ideal α-helix geometry) and dodecane in eight rotational positions is shown in Figure 4.7B. Most of the interaction energies were falling in the range that corresponded to the interaction energies between dodecane and poly - Ala, except complexes formed at 180° and 270° rotational positions. The most stable complex between TM helix 2 and dodecane (at 180° rotational angle) had interaction energy of -18.1 kcal/mol and it involved residues encircled by solid line in Figure 4.7A, namely, A44, I45, L48, I52, T55, M56 and S59. Some of these residues were involved in the contacts with other TM helices, but most of them were exposed to the lipid bilayer. The good prediction of the lipid facing side of the TM helix 2 of *Bacteriorhodosin* by using molecular modelling substantiated further the conclusion from 4.3.2.1.

4.3.2.3 The TM helix 3 of *Bacteriorhodopsin*

The helical net plot of the TM helix 3 of BR (E^{74}QDPIYWARYADWLFTTPLLLLDLALL^{100}) is shown in Figure 4.8A. According the crystal structure, all residues of TM helix 3 were in contact with other helices, but few residues were exposed to the lipids (P77, W80, A81, L87, F88, P91 and L92). The surface of this helix exposed to the lipid bilayer was small.

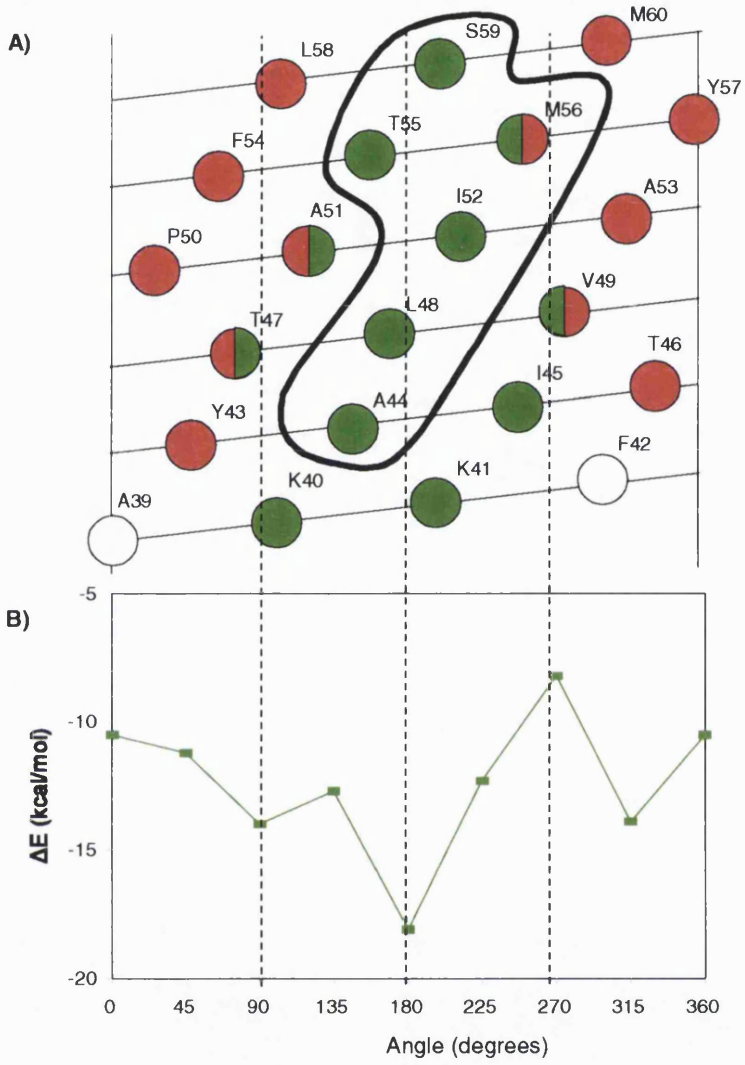

Figure 4.7 The hydrophobic surface mapping of the transmembrane helix 2 of the *Bacteriorhodopsin* A) The helical net plot outlines the amino acid residues in the contact with other TM helices (depicted as red circles), amino acid residues exposed to lipid bilayer (depicted as green circles), while half red - half green circles represent residues exposed to the lipid bilayer and in contact with other TM helices in the crystal structure. Solid lines encircled the residues in the contact with dodecane in the most stable complexes determined by calculation. B) The interaction energy between the TM helix 2 of the *Bacteriorhodopsin* and dodecane as a function of the rotation of dodecane around helical axis as described in methods.

The calculated interaction energy between TM helix 3 and dodecane is shown in Figure 4.8B. All positions of dodecane around helix produced stable complexes, with interaction energies in the range of -9.8 to -19 kcal/mol. The most stable complex between dodecane and TM helix 3 involved the W80, A81, Y83, A84, L87, F88, P91, and L92 (the interaction energy was -19 kcal/mol at 0° rotational angle). Solid line in Figure 4.9 encircles the residues that were in contact with dodecane in most stable/ hydrophobic complex. The similar interaction were observed for the complex at 270° rotational angle. Most of the residues in most stable complex were exposed to the lipid side, except Y83 and A84 (this residue is buried inside of the helix bundle). The prediction of surface of 270° to 360° as the lipid facing interface of the TM helix 3 was in an excellent agreement with crystallography data. The other lowest energy complex was observed at 180° rotational position with the interaction energy of -16.8 kcal/mol. It involved residues A81, R82, A84, D85, F88, T89, L92, and D96 in the interaction with dodecane. Despite the favourable interaction and some correctly predicted residues, this result did not predict the correct lipid facing side. For the TM helix 3 of BR, most stable complex represents the better prediction of the lipid facing side. The correct prediction of the lipid facing side was amazing, since the lipid exposed surface of helix is very small in the crystal structure.

4.3.2.4 The TM helix 4 of *Bacteriorhodopsin:*

The sequence of the TM helix 4 is G^{106}TILALVGADGIMIGTGLVGAL^{127} and the helical net plot is shown in Figure 4.9A. The residues in the contact with other helices in the crystal structure are T107, I108, A110, L111, A114, D115, I117, M118, T121,G122, L123, V124, G125, A126 and L127 (depicted as a red circles). The residues of the TM helix 4 fully or partially exposed to the lipid bilayer were G106, L109, L111, V112,G113,

G116, I117, I119, G120, L123, V124, and L127 (depicted as a green or half green - half red circles).

The calculated interaction energy between TM helix 4 of BR and dodecane in eight different positions is shown in Figure 4.9B. Three regions of interactions energies could be distinguished. The high energy complex was formed at 0° rotational position with interaction energy of -7 kcal/mol. The surface of the TM helix 4 involved in the forming of this complex should be part of the helix interface. The region of the 45° to 180° had averagely interaction energy of around -14 kcal/mol, which indicated the favourable interaction with dodecane. The mapping of the helix surface hydrophobicity has relative manner, by comparison interaction energies. The initial assumption was that lipid will interact with certain surfaces more and therefore produce low energy complexes with dodecane. The lowest energy complex was formed for the 315° rotational position with interaction energy of -18 kcal.mol. This complex had most favourable interaction with dodecane compared with complexes in other position. Therefore, it can be concluded that surface involved in this interaction should be lipid facing side in the helix bundle. The dodecane interacted with L109, V112, G113, G116, I119, G120, L123, and V124 residues The solid line in Figure 4.9 encircles the predicted lipid facing surface of the TM helix 4 of BR. The predicted lipid facing side was in excellent agreement with experimental structure of *Bacteriorhodopsin*.

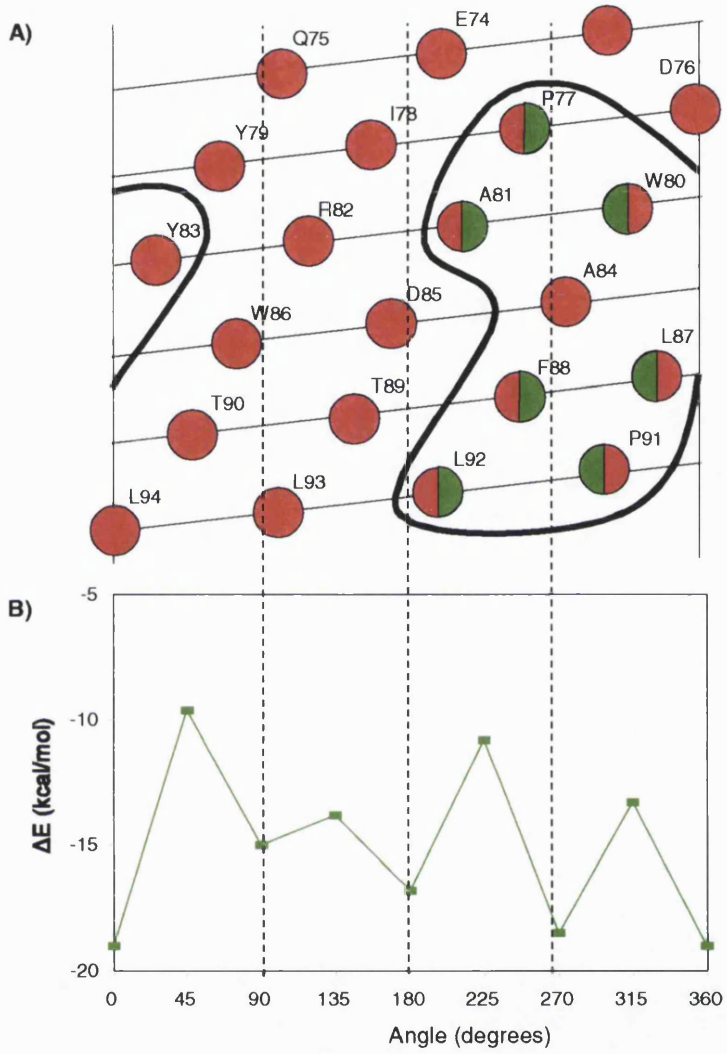

Figure 4.8 The hydrophobic surface mapping of the transmembrane helix 3 of the *Bacteriorhodopsin* A) The helical net plot outlines the amino acid residues in the contact with other TM helices (depicted as red circles), amino acid residues exposed to lipid bilayer (depicted as green circles), while half red - half green circles represent residues exposed to the lipid bilayer and in contact with other TM helices in the crystal structure. Solid lines encircled the residues in the contact with dodecane in the most stable complexes determined by calculation. B) The interaction energy between the TM helix 3 of the *Bacteriorhodopsin* and dodecane as a function of the rotation of dodecane around helical axis as described in methods.

4.3.2.5 The TM helix 5 of *Bacteriorhodopsin*

The helical net plot of the TM helix (W^{137}WAISTAAMLYILYVLFFGFT^{157}) is shown in Figure 4.10A. The residues of the TM helix 5 exposed to the lipid bilayer were depicted as a full and half green circles, namely, W137, A139, I140, T142, A143, L146, Y147, Y150, V151, F153 and G155.

The calculated interaction energy between helix and dodecane in eight rotational positions is shown in Figure 4.10B. The two low energy complexes were detected, at 45° and 270° positions, with similar energies -15.4 and -15.7 kcal/mol, respectively. The most stable TM helix dodecane complex involved the I140, A144, Y147, I148, V151, and L152 residues (the interaction energy was -15.7 kcal/mol). This complex was partially exposed, and partially buried into the centre of the helix bundle. The other stable complex was formed when it interacted with residues A139, T142, A143, L146, Y147, Y150, and F153 of TM helix 5 (the interaction energy was -15.4 kcal/mol at 45° rotational position). This time, the less stable complex was better prediction of the correct lipid facing side.

4.3.2.6 The TM helix 6 of *Bacteriorhodopsin:*

The helical net plot of the TM helix (E^{166}VASTFKVLRNVTVVLWSAYPVVWLI^{191}) is shown in Figure 4.11A. Again, the surface of this helix exposed to the lipids in the experimentally determined structure was small. This helix had residues E166, V167, S169, K172, V173, N176, V177, V180, S183, A184 and V187 to the lipids of the bilayer. This was an unusual helix, it had some charged and polar groups exposed to the lipids.

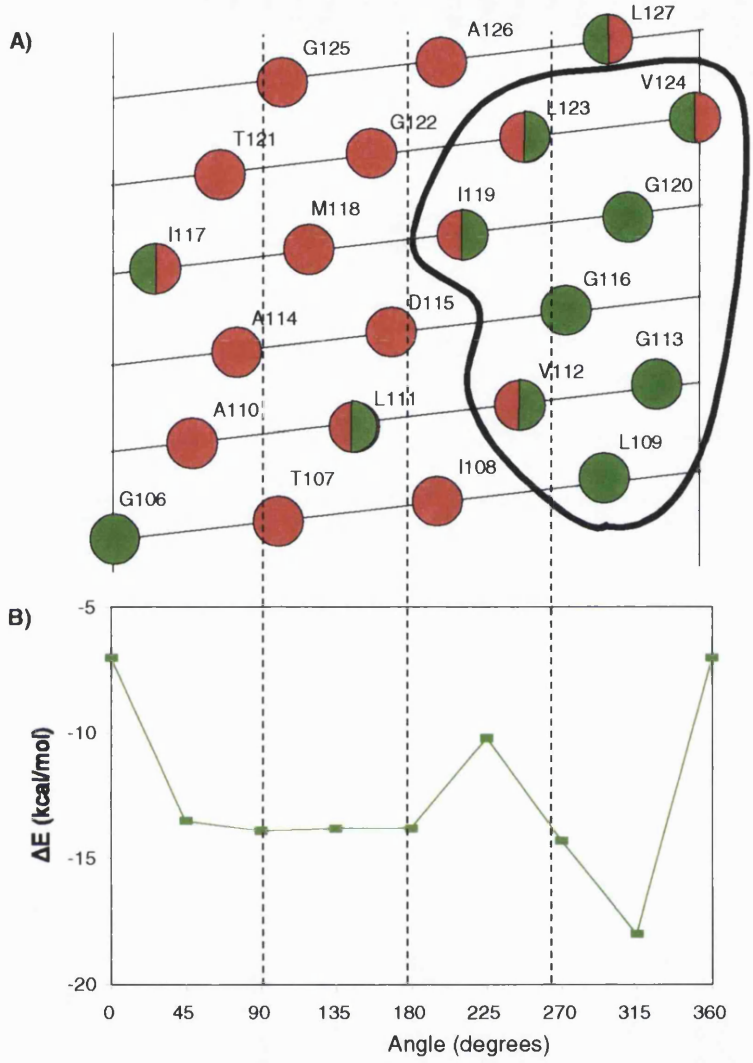

Figure 4.9 The hydrophobic surface mapping of the transmembrane helix 4 of the *Bacteriorhodopsin* A) The helical net plot outlines the amino acid residues in the contact with other TM helices (depicted as red circles), amino acid residues exposed to lipid bilayer (depicted as green circles), while half red - half green circles represent residues exposed to the lipid bilayer and in contact with other TM helices in the crystal structure. Solid lines encircled the residues in the contact with dodecane in the most stable complexes determined by calculation. B) The interaction energy between the TM helix 4 of the *Bacteriorhodopsin* and dodecane as a function of the rotation of dodecane around helical axis as described in methods.

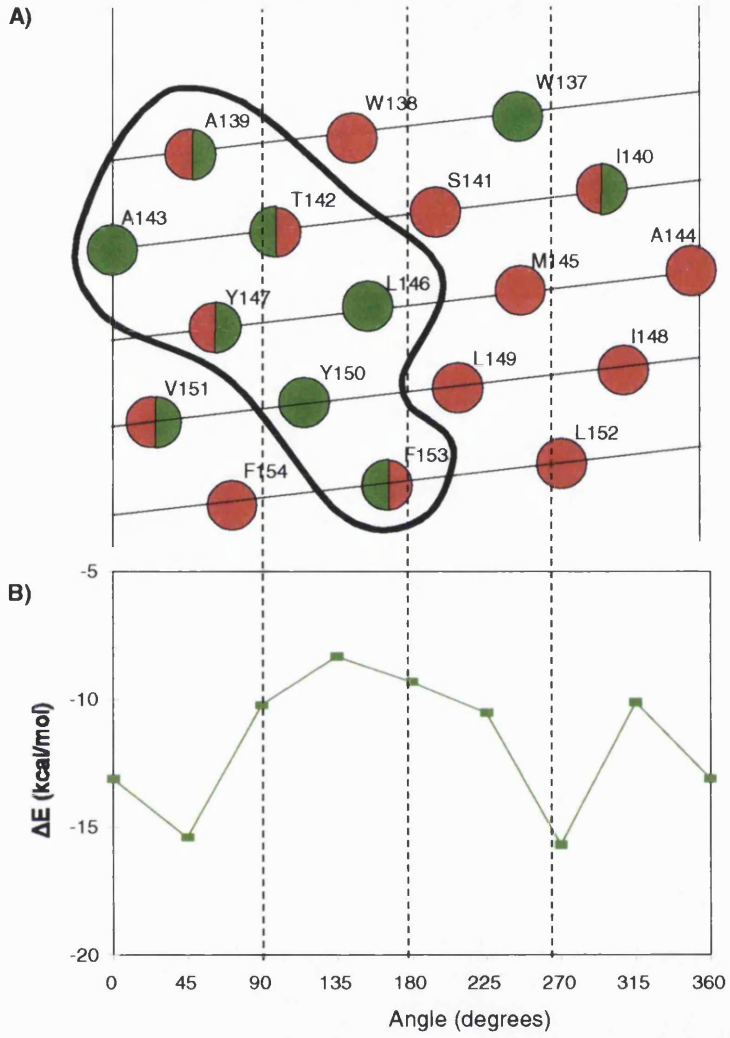

Figure 4.10 The hydrophobic surface mapping of the transmembrane helix 5 of the *Bacteriorhodopsin* A) The helical net plot outlines the amino acid residues in the contact with other TM helices (depicted as red circles), amino acid residues exposed to lipid bilayer (depicted as green circles), while half red - half green circles represent residues exposed to the lipid bilayer and in contact with other TM helices in the crystal structure. Solid lines encircled the residues in the contact with dodecane in the most stable complexes determined by calculation. B) The interaction energy between the TM helix 5 of the *Bacteriorhodopsin* and dodecane as a function of the rotation of dodecane around helical axis as described in methods.

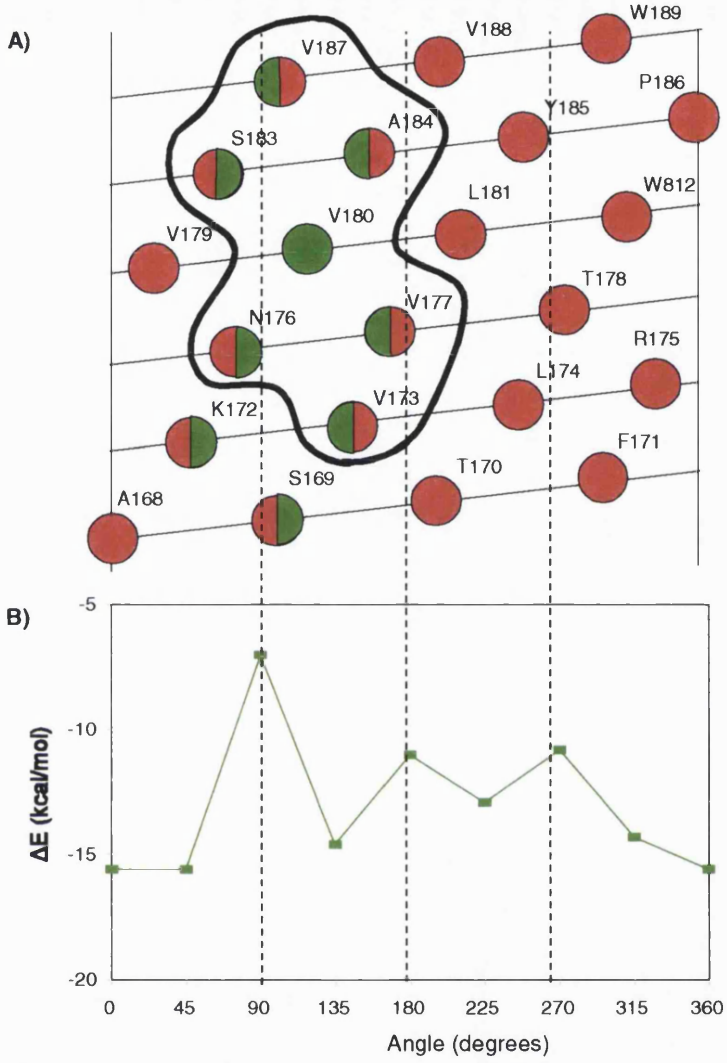

Figure 4.11. The hydrophobic surface mapping of the transmembrane helix 6 of the *Bacteriorhodopsin* A) The helical net plot outlines the amino acid residues in the contact with other TM helices (depicted as red circles), amino acid residues exposed to lipid bilayer (depicted as green circles), while half red - half green circles represent residues exposed to the lipid bilayer and in contact with other TM helices in the crystal structure. Solid lines encircled the residues in the contact with dodecane in the most stable complexes determined by calculation. B) The interaction energy between the TM helix 6 of the *Bacteriorhodopsin* and dodecane as a function of the rotation of dodecane around helical axis as described in methods.

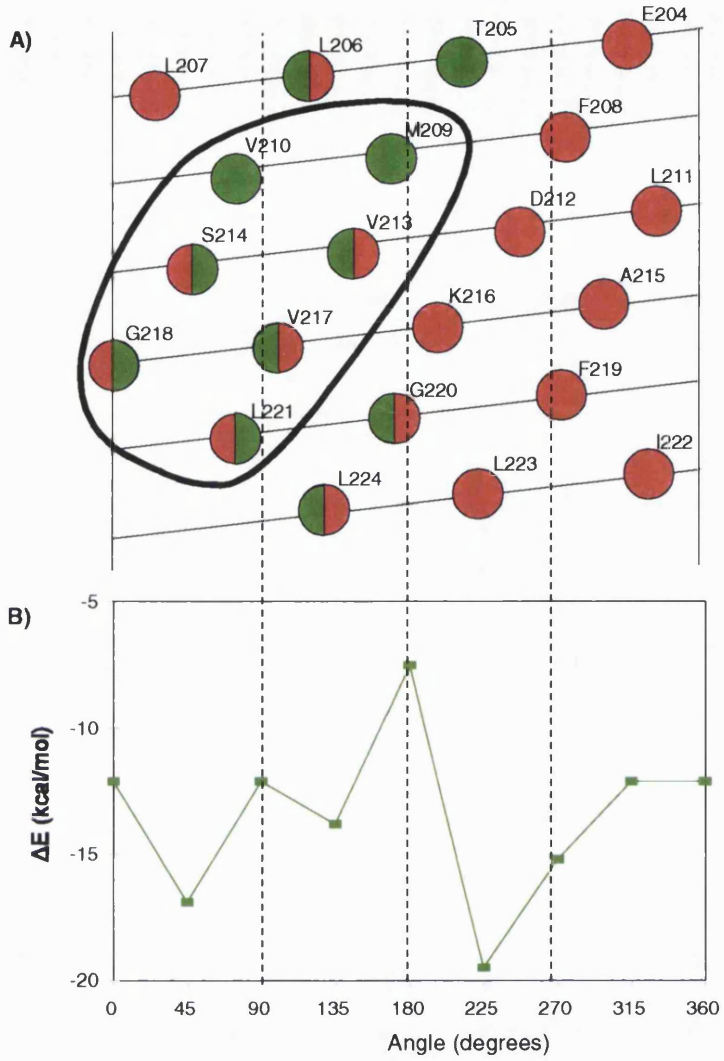

Figure 4.12 The hydrophobic surface mapping of the transmembrane helix 7 of the *Bacteriorhodopsin* A) The helical net plot outlines the amino acid residues in the contact with other TM helices (depicted as red circles), amino acid residues exposed to lipid bilayer (depicted as green circles), while half red - half green circles represent residues exposed to the lipid bilayer and in contact with other TM helices in the crystal structure. Solid lines encircled the residues in the contact with dodecane in the most stable complexes determined by calculation. B) The interaction energy between the TM helix 7 of the *Bacteriorhodopsin* and dodecane as a function of the rotation of dodecane around helical axis as described in methods.

The calculated interaction energy between helix and dodecane in eight rotational positions is shown in Figure 4.11B. The behaviour was complicated, and among all positions, two were presented. The dodecane complex I at 0° involved F171, L174, R175, T178, W182, and Y185 residues (the interaction energy was -15.6 kcal/mol at). The dodecane complex II at 125° involved residues: V173, N176, V177, V180, L181, A184, and V187 residues (the interaction energy was -14.6 kcal/mol).The solid line denotes the residues of the complex II in the Figure 4.11A. The less stable complex II better represents the lipid exposed side of the TM helix 6. In this case the prediction was not so clear as in previous cases. It could be said that some surfaces could be excluded as a lipid facing sides, namely, rotational positions at 90° and from 180° to 270°. Even in such case, the additional information was obtained to aid a molecular modelling of the membrane helix bundle.

4.3.2.7 The TM helix 7 of *Bacteriorhodopsin:*

The helical net plot of the TM helix 7 of BR is presented in Figure 4.12A. (N^{202}IETLLFMVLDVSAKVGFGLILLR^{225}). The lipid exposed residues of TM helix 7 were I203, L206, L207, M209, V210, V213, S214, V217, G218, L221, I222 and L224 in the crystal structure (depicted as green circles). Other residues were buried in the helix bundle (depicted as red circles).

The calculated interaction energy between helix and dodecane in eight rotational positions is shown in Figure 4.12B. Most stable complex was formed at 225° when dodecane interacted with residues F208, L211, D212, A215, K216, F219, G220, and L223, and it was a bad prediction of the lipid facing side. The residues involved in the forming this complex were involved in the helix - helix interaction and buried in the bundle. Other complex, at 45° involved residues M209, V210, V213, S214, V217, G218, and L220, and

predicted the correct lipid facing side of the TM helix 7. Again, the difference in the interaction energy of two complexes was 2.9 kcal/mol, and it was in the range of computation error determined by studying of the poly-alanine complex. Therefore, they were equivalent and both could be considered as a lipid facing side. Since one complex is a bad prediction of the lipid facing side, only helix - helix exposed surface could be proposed, and in this case position at 180° should be considered to be oriented towards helix bundle interior.

4.3.3 Interaction of transmembrane helices of FcεRI with dodecane

4.3.3.1 The TM helix of α-subunit:

In the FcεRI, the α-subunit contains single TM helix, designated as TM helix α, (L^{205}IFPSLAVILFAVDTGLWF^{223}), which is presented in Figure 4.13A. It interacted with the dodecane with two sides of preferable interaction (at the 135° and 270° rotational positions), and the two sides with less favourable interaction (at the 0° and 180° rotational positions) (Figure 4.13B). The differences in the interaction energies were above the threshold defined earlier in the Section 4.3.1, implying the presence of the dodecane/lipid favourable surfaces. The most stable complex was formed at the 270° rotational position with interaction energy of the -15 kcal/mol and the residues F207, L210 A211, L214, F215, D218 and W222 were involved in the forming of the complex (Figure 4.14C). The complex at 90° rotational position involved the residues S209, V212, I213, A216, T219 and G220 constituted contact surface with dodecane (Figure 4.14D). The complex at the 90° was less stable than complex at 270° with interaction energy of -13.2 kcal/mol. The residues of these interaction sites were mostly hydrophobic with contributions of some polar residues. Surprisingly, the least stable complex at 0° involved only the hydrophobic

residues, L210, I213, L214, V217 and L221 (Figure 4.14A). All these latter residues were large branched and dodecane could not pack well around them. The dodecane could not also pack well in the other least stable complex at 180° (Figure 4.15B), and so it interacted with a small number of the atoms of V212, A216, T219 and G220.

However, the mapping of the helix hydrophobicity predicted two lipid favourable surfaces, which were described earlier and they were depicted in the helical net plot (Figure 4.13A) as a blue (270° rotational position) and yellow (90° rotational position) circles. It was not possible to determine which one is correct prediction without additional information, and that will subject of the next Chapters.

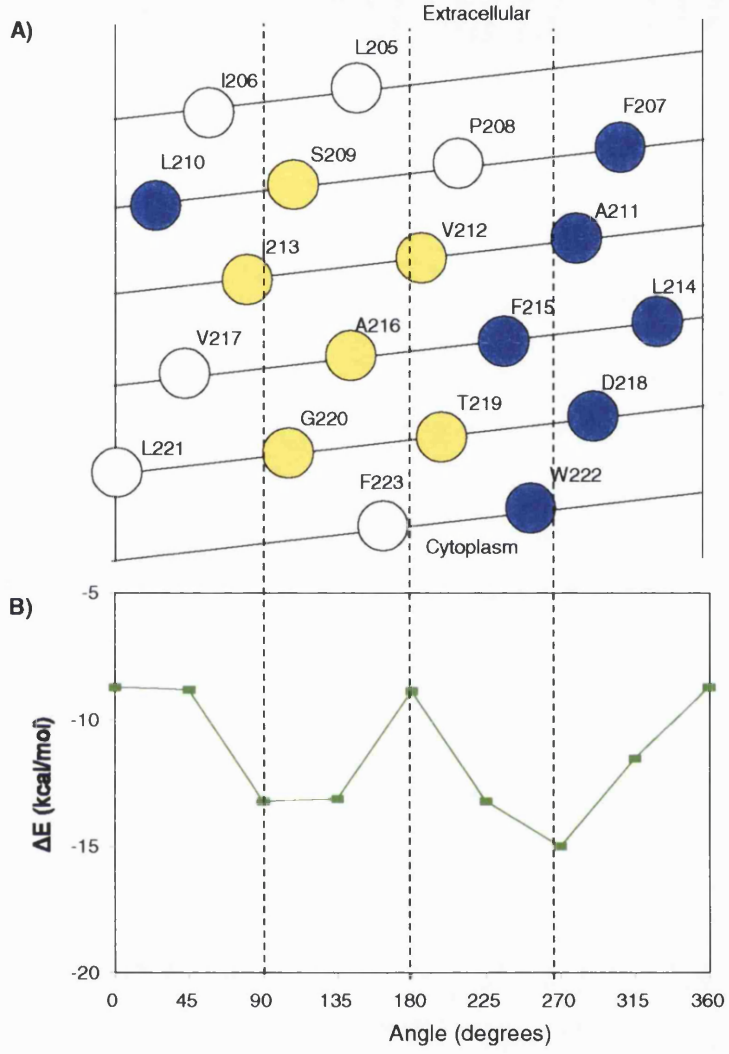

Figure 4.13 The hydrophobic surface mapping of the TM helix of the α-subunit of the FcεRI A) The helical net plot outlines the amino acid residues in the first most stable complex (depicted as blue circles) and second most stable complex (depicted as yellow circles). B) The interaction energy between the TM helix of the α-subunit of the FcεRI and dodecane as a function of the rotation of dodecane around helical axis as described in methods.

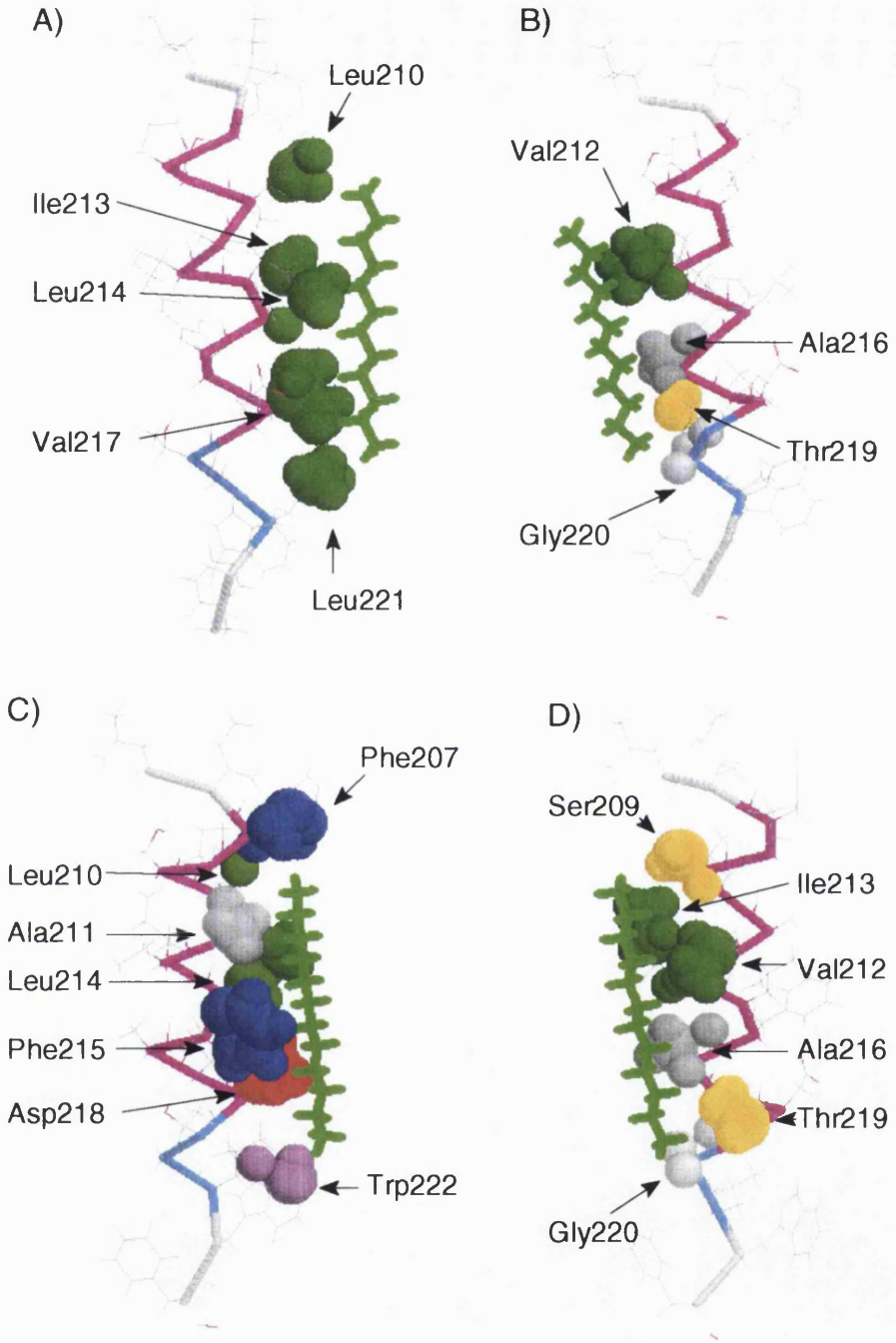

Figure 4.14 The complexes of TM helix of the α-subunit of the FcεRI and dodecane at rotational angles A) 0 degrees, B) 180 degrees (the least stable complexes), C) 270 degrees and D) 90 degrees (the most stable complexes).

4.3.3.2 The TM helix 1 of the β subunit:

The β-subunit of the FcεRI consists of the four TM helices that could form the 4 helix bundle that interacts with TM helices of the α- and γ-subunits. The rest of the bundle interacts with lipids. The TM helix 1 of the β-subunit, denoted as TM helix β1, (F^{60}LGVTQVLVGLICLCFGTVVC^{80}) is shown in Fiure 4.15A. The mapping of the helix surface by dodecane produced the interaction energy curve with one minimum and one maximum (Figure 4.15B), distinguishing the one hydrophobic (180° to 315°) and one less hydrophobic (0° to 180°) interfaces. The complex formed at the 0° rotational position (Figure 4.16A) with interaction energy of -8.7 kcal/mol was not stable, since the number of atoms of TM helix was small. Most residues V66, L70, L73 and T77 involved in the interaction were branched, and hence did not allow efficient packing of dodecane during complex formation. The most stable dodecane - TM helix β1 complex (at 270° - 315° rotational positions) was formed involving residues G62, Q65, V66, G69, C72, L73, G76 and T77 (depicted as a blue circles in helical net plot, Figure 4.15A). Interactions in the most stable complex are pressented in Figure 4.16B. Some of these residues were also involved in the forming of the least stable complex, but in the region of the 270 to 315° rotational position, the packing of the dodecane was satisfactory. Thus, there was an indication that both, packing of the hydrocarbon chain as well as the hydrophobicity of the interacting amino acid sidechains could be important aspects in the lipid - helix interaction.

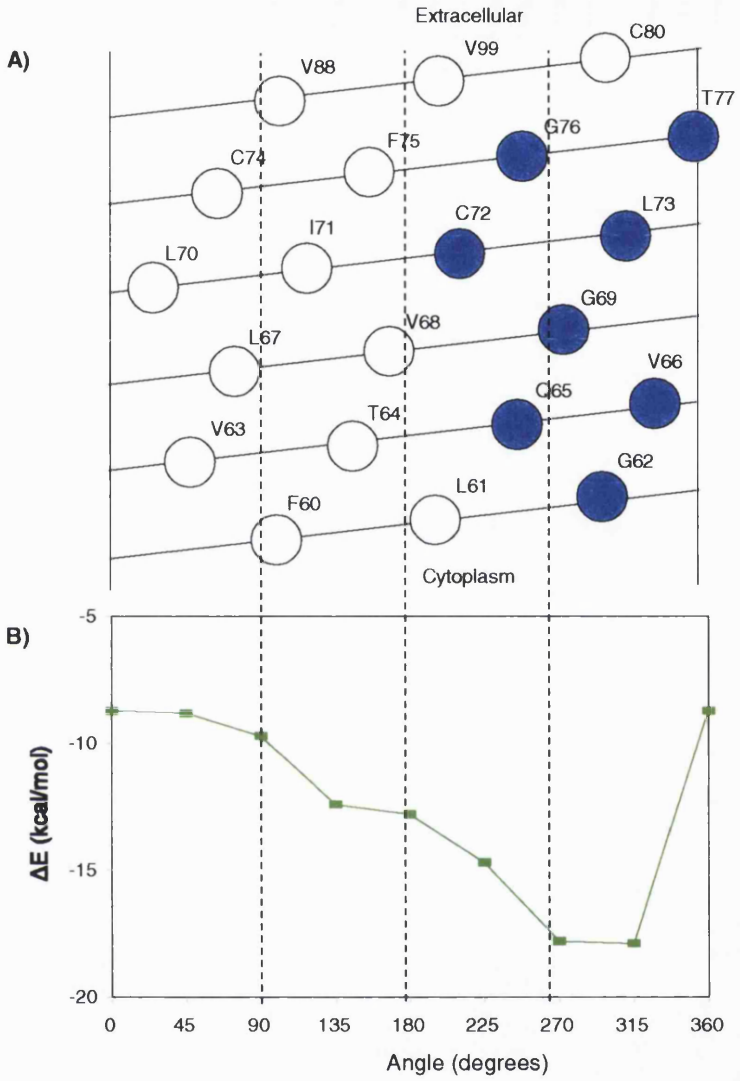

Figure 4.15 The hydrophobic surface mapping of the TM helix 1 of the β-subunit of the FcεRI A) The helical net plot outlines the amino acid residues in the first most stable complex (depicted as blue circles) and second most stable complex (depicted as yellow circles). B) The interaction energy between the TM helix 1 of the β-subunit of the FcεRI and dodecane as a function of the rotation of dodecane around helical axis as described in methods.

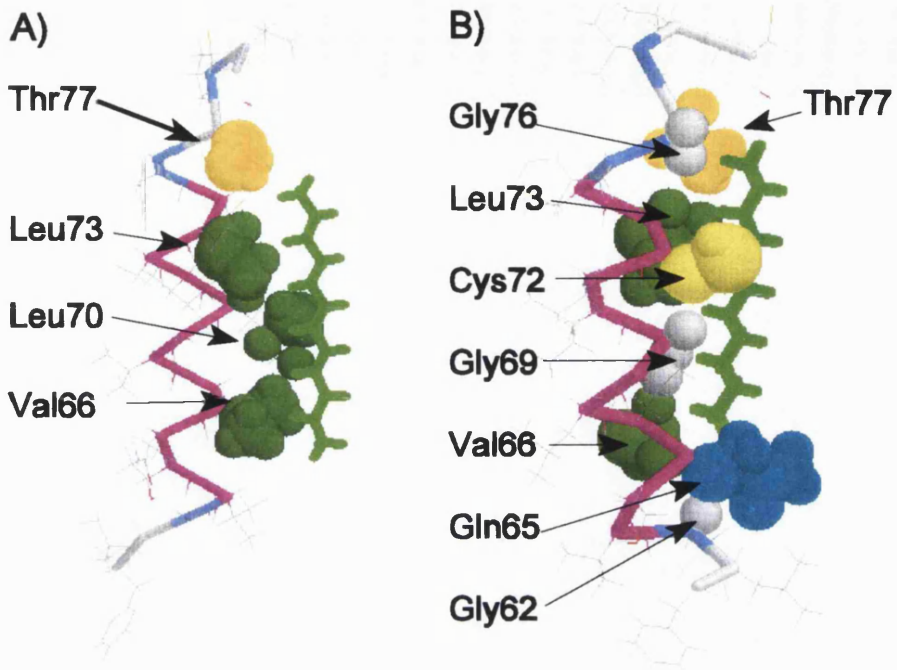

Figure 4.16 The complexes of TM helix 1 of the β-subunit of the FcεRI and dodecane at rotational angles A) 0 degrees (the least stable complex) and B) 315 degrees (the most stable complex).

However, the mapping of the helix hydrophobicity predicted only one lipid favourable surface (315° rotational position), which was described earlier and it was depicted in the helical net plot as a blue circles (Figure 4.15A). Corollary to the Section 4.3.2. that should be correct prediction of the lipid facing surface of the TM helix β1.

4.3.3.3 The TM helix 2 of the β-subunit:

The helical net plot of TM helix 2 of the β-subunit, depicted TM helix β2, (AGYPFWGAVLFVLSGFLSIM) is shown in Figure 4.17A. The calculation of the interaction energies between helix and dodecane in eight different rotational positions is presented in Figure 4.17B. Three minima and a three maxima in the interaction energy curve with dodecane were detected and it implied complicated behaviour of this helix. Only the interactions in two least stable complexes (Figure 5.19A and Figure 4.19B) and two most stable complexes (Figure 4.19C and 4.19D) were shown. The effect of the stabilization was in the range of 7 to 8 kcal/mol, when the least and most stable complexes were compared. Again the number of interacting atoms was much smaller in the least stable complexes, due to poorer packing in those complexes. The residues P101, G104, A105 and F108 (Figure 4.19A) and V109, G112 and F113 (Figure 4.19B) were involved in the forming least stable complexes, and subsequently lipid unfavourable sides. The most stable complexes were formed when W103, V106, L107, S111 and L114 (Figure 4.19C) and V106, V109, L110, F113 and L114 (Figure 4.19D) interacted with dodecane. In these situations, a high number of branched residues were involved in the interaction, but actually other residues like W103, S111 and F113 allowed the efficient packing and higher degree of interaction, thus stabilizing the complexes.

However, the mapping of the helix hydrophobicity predicted at least two lipid favourable surfaces, which were described earlier and they were depicted in the helical net plot (Figure 4.17A) as a blue (0° rotational position) and yellow (215° rotational position) circles. It was not possible to determine which one is correct prediction without additional information, and that will subject of the next Chapters .

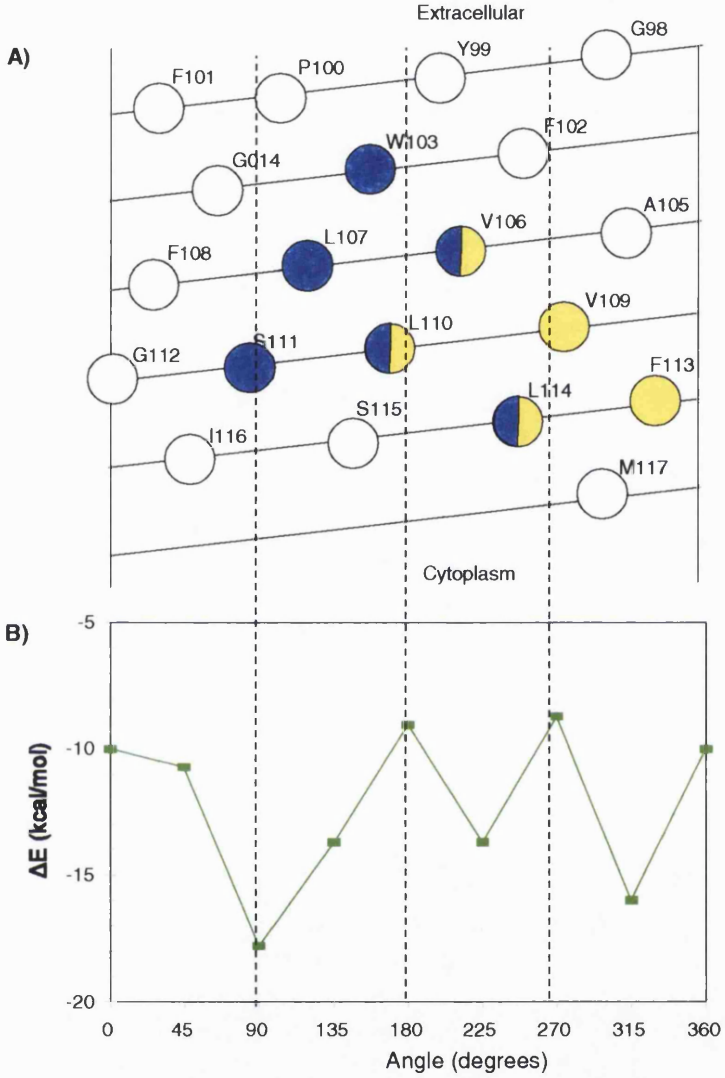

Figure 4.17 The hydrophobic surface mapping of the TM helix 2 of the β-subunit of the FcεRI A) The helical net plot outlines the amino acid residues in the first most stable complex (depicted as blue circles) and second most stable complex (depicted as yellow circles). B) The interaction energy between the TM helix 2 of the β-subunit of the FcεRI and dodecane as a function of the rotation of dodecane around helical axis as described in methods.

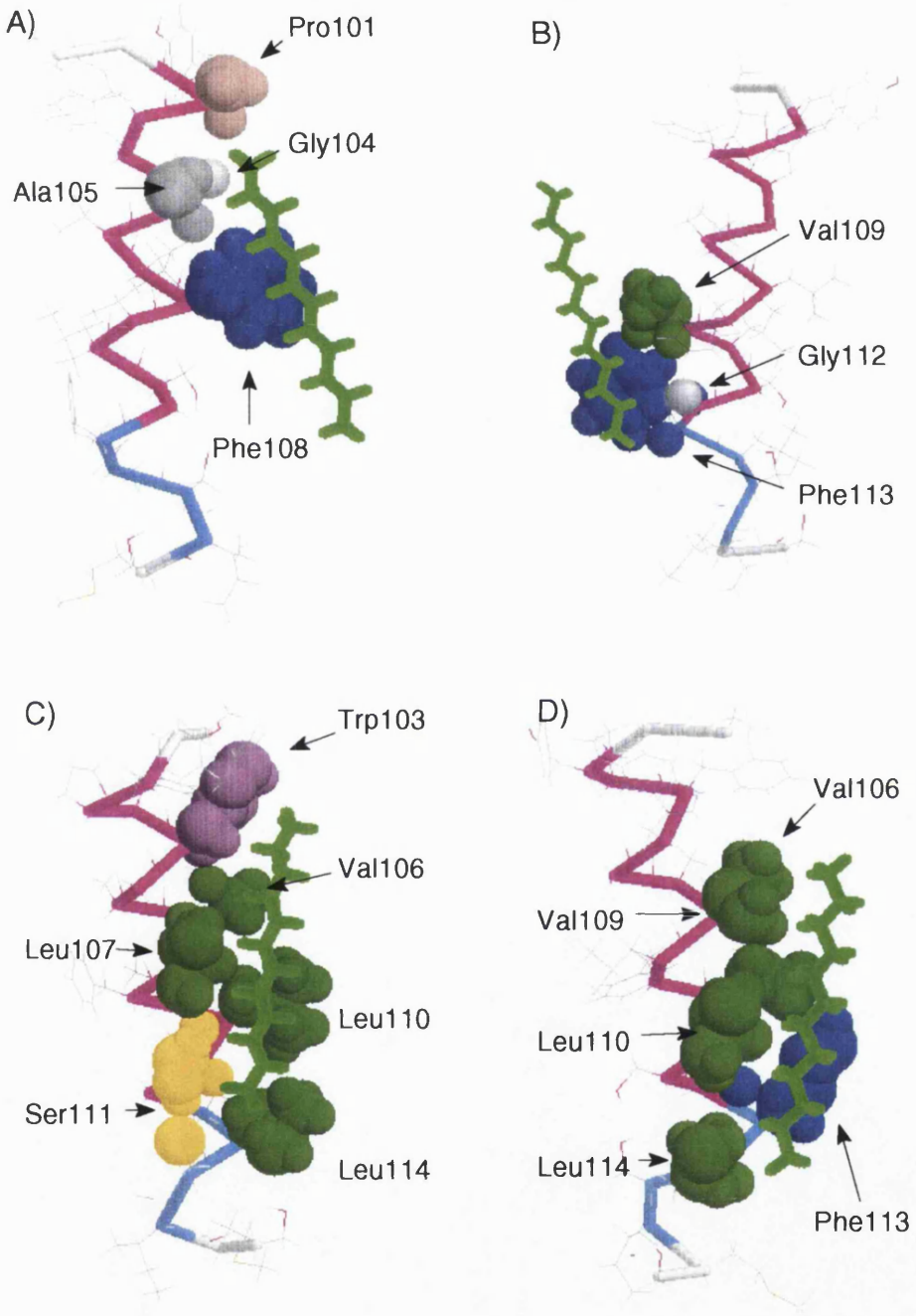

Figure 4.18 The complexes of TM helix 2 of the β-subunit of the FcεRI and Dodecane at rotational angles A) 90 degrees, B) 180 degrees (the least stable complexes), C) 0 degrees and D) 225 degrees (the most stable complexes).

4.3.3.4 The TM helix 3 of the β-subunit:

The helical net plot of the TM helix 3 of β-subunit, designated as TM helix β3, (LGANIVSSIAAGLGIAILIL) is shown in Figure 4.19A. The interaction energy curve between TM helix β3 and dodecane (Figure 4.19B) shows one least stable complex at rotational position of 0° and two stable complexes at 90 and 270°. The shape of the curve could implicated the two broad sides, one dodecane favourable and one dodecane unfavourable.

The least stable complex (at 0° rotational position with ΔE = -8.2 kcal/mol) consisted of branched hydrophobic residues; I135, V136, I139 and L143, again leading to poor packing of the hydrocarbon chain (Figure 4.20A). The two stable complexes had residues involved in the interaction that allowed efficient packing of dodecane, namely A133, V136, S137, A140, A141, G144 and L148 for complex at 90° and ΔE = -14.4 kcal/mol (Figure 4.21B), and L131, I135, S138, I139, G142, I145 and A146 for the complex at 270° and ΔE = -14.3 kcal/mol (Figure 4.21C). Both stable complexes had similar energies with the difference of ΔE for two complexes smaller than the threshold, which indicated the equivalent behaviour of two surfaces.

However, the mapping of the helix hydrophobicity predicted at least two lipid favourable surfaces, which were described earlier and they were depicted in the helical net plot (Figure 4.19A) as a blue (90° rotational position) and yellow (270° rotational position) circles. It was not possible to determine which one is correct prediction without additional information, and that will subject of the next Chapters.

4.3.3.5 The TM helix 4 of the β-subunit:

The TM helix 4 of the β-subunit, denoted as TM helix β4, (LVLMLLFLTILAFCSAVLLII) is shown in Figure 4.21A and it exhibited behaviour similar to the TM helix β3 with one least stable complex and having a broad surface favourable for the interaction with dodecane (Figure 4.21B). The least stable complex was formed when dodecane interacted with residues L187, L190, S194 and L198 (Figure 4.22A). The stabilization energy difference of -6.6 kcal/mol was observed between the most and the least stable complexes, indicating more interaction and better packing of dodecane in the most stable complex.

The interaction was observed between dodecane and TM helix β4 residues L184, T188, A191, P192 and A195 for rotational position of 135° (Figure 4.23B) and F186, I189, C193, V196 and L197 for the rotational position of 225° (Figure 4.23B).

Again, the mapping of the helix hydrophobicity predicted broad lipid favourable surfaces, which was desribed earlier and it was presented as a combination of two surfaces depicted in the helical net plot (Figure 4.21A) as a blue (135° rotational position) and yellow (225° rotational position) circles. It was not possible to determine which one is correct prediction without additional information, and that will subject of the next Chapters, but it might be possible to state that surface at 0° rotational position could be involved in the helix - helix interface.

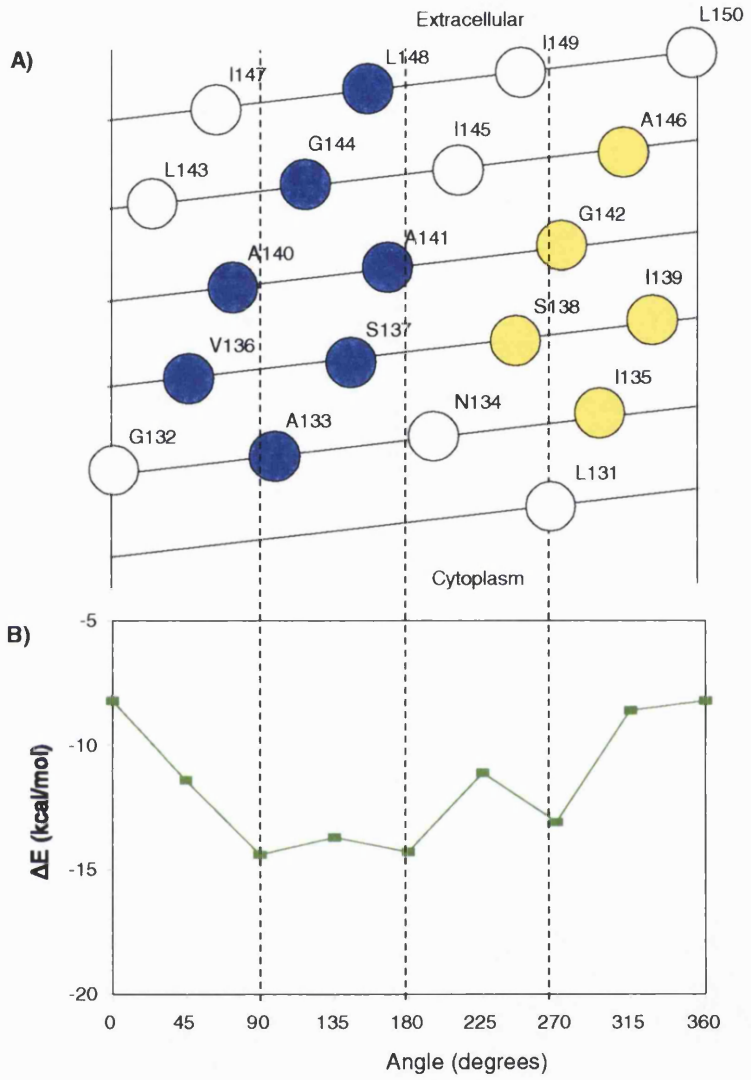

Figure 4.19 The hydrophobic surface mapping of the TM helix 3 of the β-subunit of the FcεRI A) The helical net plot outlines the amino acid residues in the first most stable complex at 90° rotational position (depicted as blue circles) and second most stable complex at 270° rotational position (depicted as yellow circles). B) The interaction energy between the TM helix 3 of the β-subunit of the FcεRI and dodecane as a function of the rotation of dodecane around helical axis as described in methods.

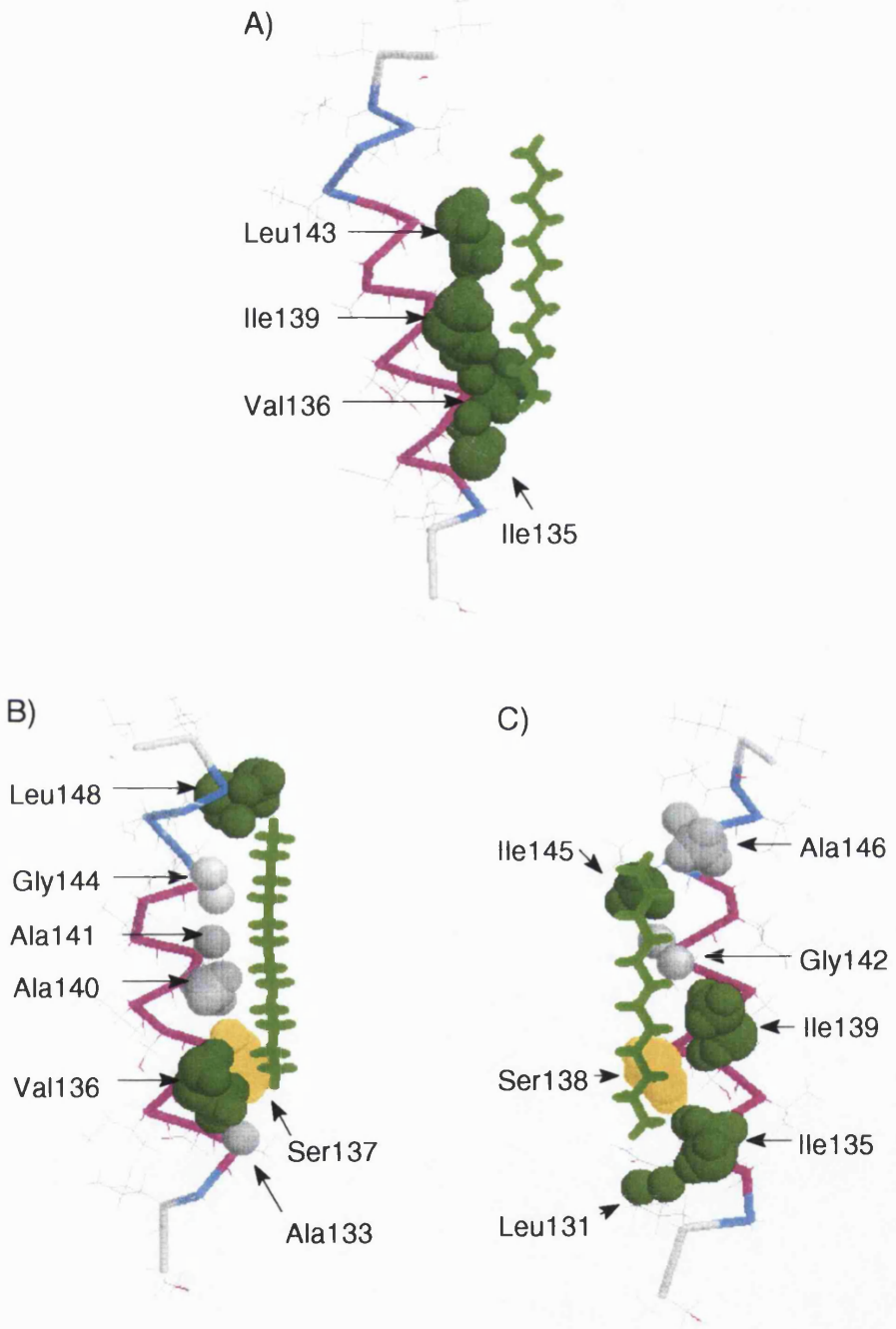

Figure 4.20 The complexes of TM helix 3 of the β-subunit of the FcεRI and Dodecane at rotational angles A) 0 degrees, (the least stable complex), B) 90 degrees and C) 270 degrees (the most stable complexes).

4.3.3.6 The TM helix of the γ-subunit:

The TM helix of γ-subunit, designated as TM helix γ, (CYILDAILFLYGIVLTLLYC) is shown in Figure 4.23A as a helical net plot. The interaction curve between the dodecane and the TM helix γ is shown in the Figure 4.23B. It displayed the two minima (at 0° and 135° rotational positions) and two maxima (at 90° and 270° rotational positions). The least stable complexes was formed residues when residues C7, Y8, D11, A12, F15 and I19 interacted with dodecane at 0° rotational position (Figure 4.25A). The branched residues L10, L14 and L21 were again involved in the interaction with dodecane in the complex at 135°rotational angle (Figure 4.25B). The most stable complex at 90° was formed when residues D11, L14, F15, G18, L21, T22 and C26 interacted with dodecane (Figure 4.25C). The dodecane interacted with residues A12, P15, L16, I19, V20 and L23 in the complex formed at 315° position (Figure 4.25D).

The mapping of the helix hydrophobicity predicted two lipid favourable surfaces, which were described earlier and they were depicted in the helical net plot (Figure 4.19A) as a blue (90° rotational position) and yellow (315° rotational position) circles. It was not possible to determine which one is correct prediction without additional information, and that will subject of the next Chapters.

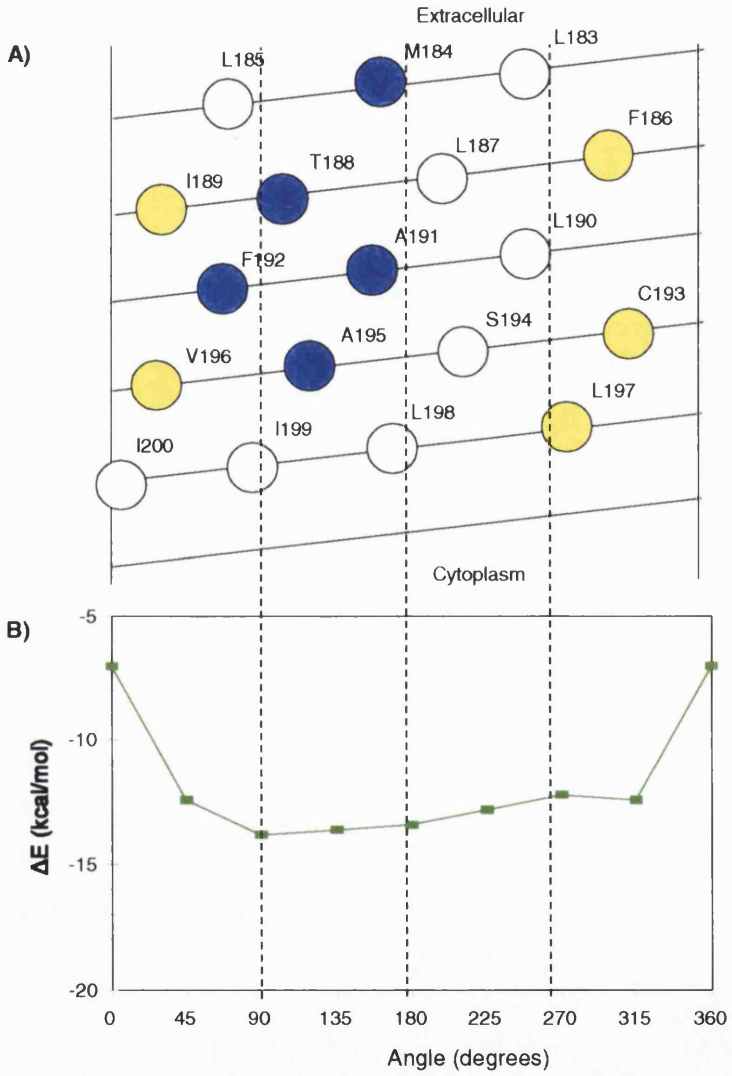

Figure 4.21 The hydrophobic surface mapping of the TM helix 4 of the β-subunit of the FcεRI A) The helical net plot outlines the amino acid residues in the first most stable complex (depicted as blue circles) and second most stable complex (depicted as yellow circles). B) The interaction energy between the TM helix 4 of the β-subunit of the FcεRI and dodecane as a function of the rotation of dodecane around helical axis as described in methods.

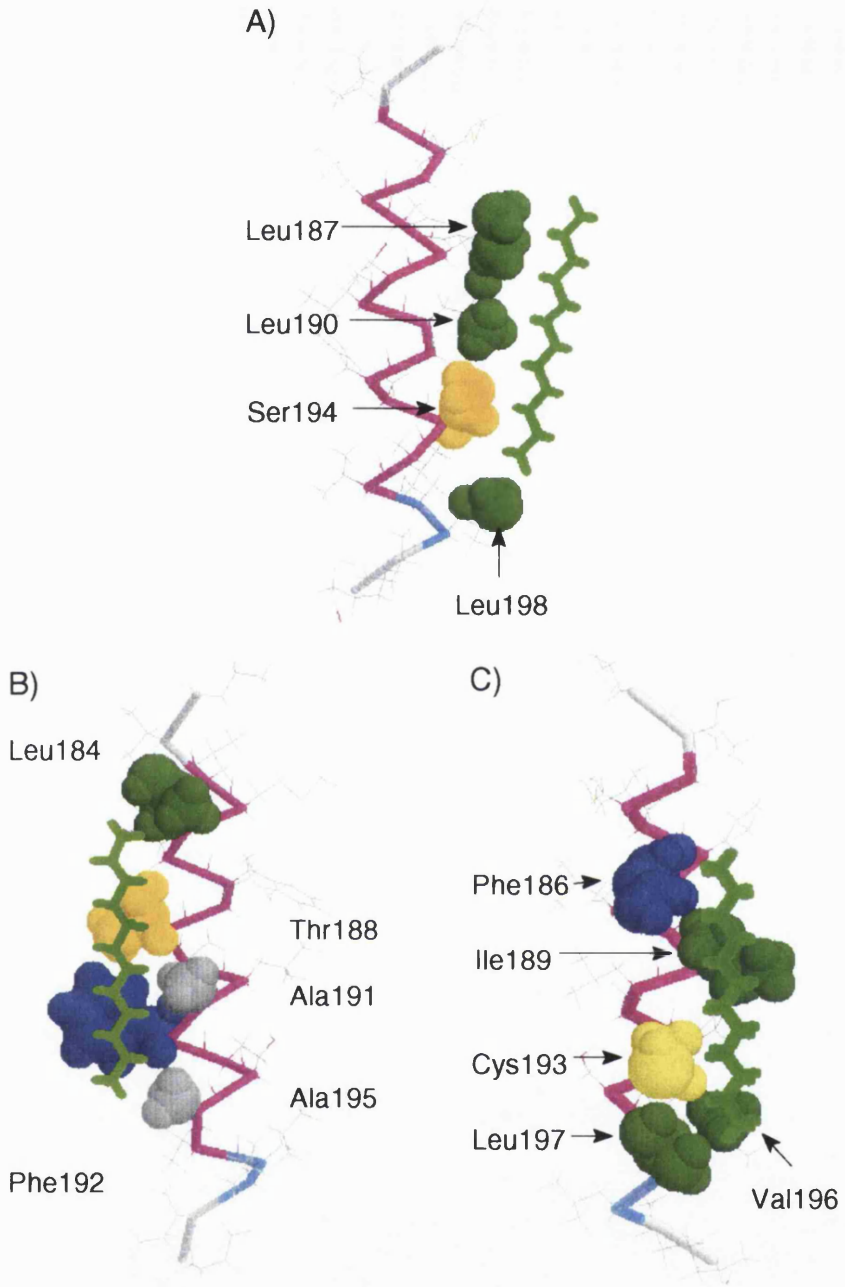

Figure 4.22 The complexes of TM helix 4 of the β-subunit of the FcεRI and Dodecane at rotational angles A) 0 degrees (the least stable complex), B) 135 degrees and C) 225 degrees (the most stable complexes).

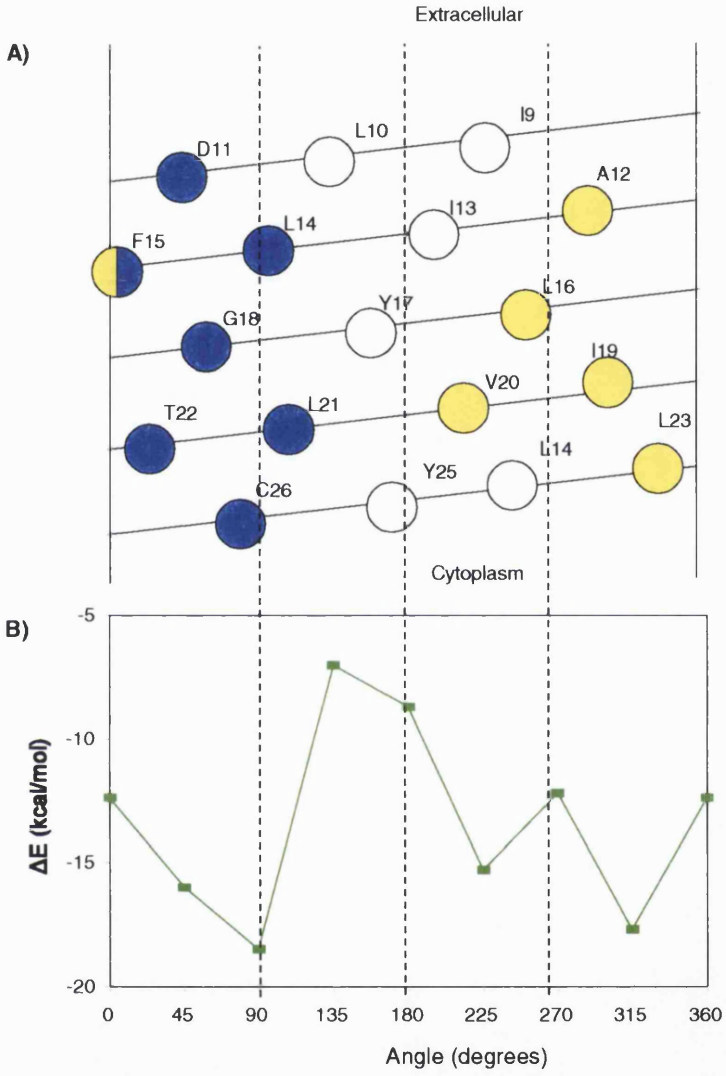

Figure 4.23 The hydrophobic surface mapping of the TM helix of the γ-subunit of the FcεRI A) The helical net plot outlines the amino acid residues in the first most stable complex (depicted as blue circles) and second most stable complex (depicted as yellow circles). B) The interaction energy between the TM helix of the γ-subunit of the FcεRI and dodecane as a function of the rotation of dodecane around helical axis as described in methods.

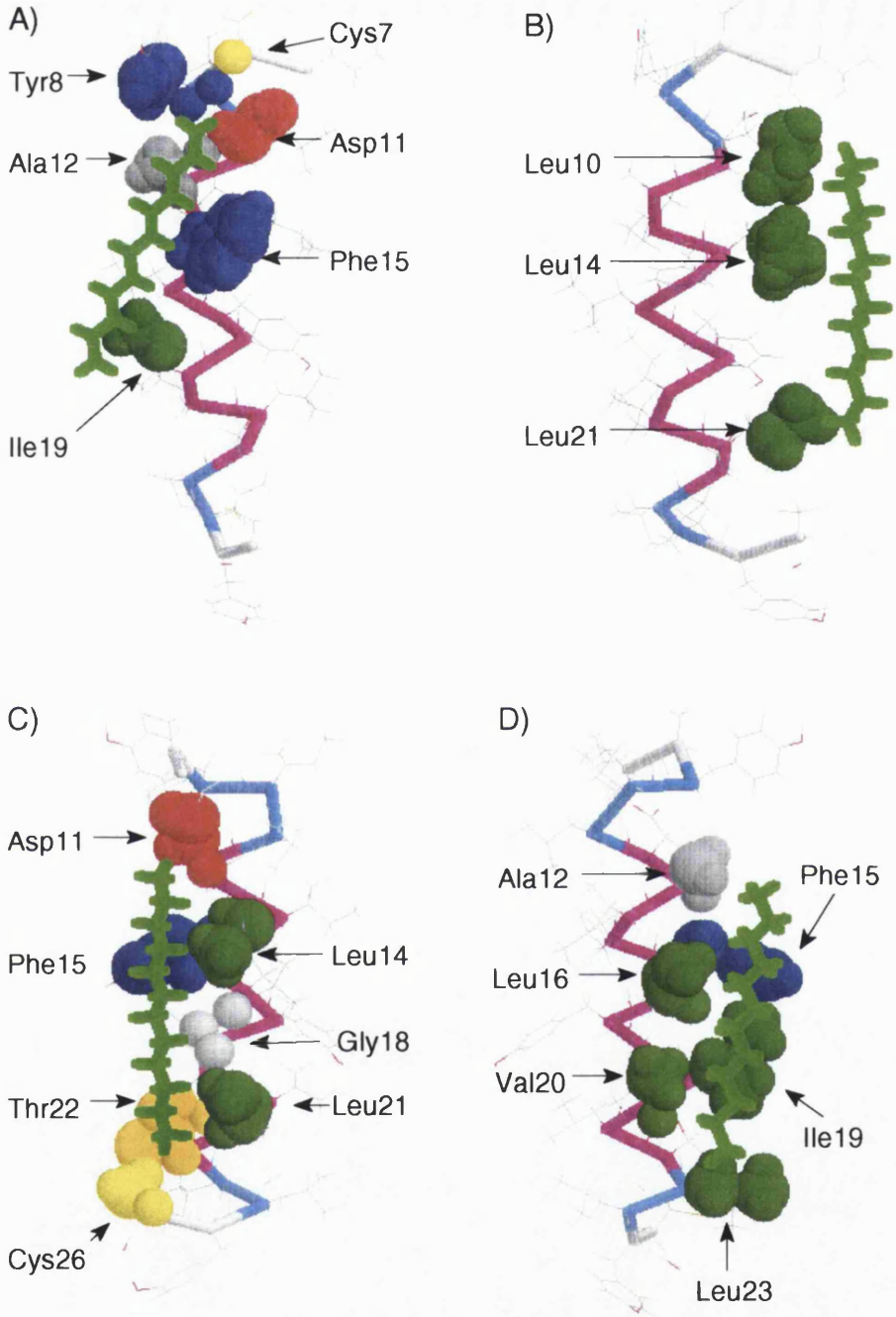

Figure 4.24 The complexes of TM helix of the γ-subunit of the FcεRI and Dodecane at rotational angles A) 0 degrees, B) 135 degrees (the least stable complexes), C) 90 degrees

4.4 Discussion

The strategy for these calculations was based on the distribution of the functional groups within the lipid bilayer - cell membrane (Figure 4.25 - modified from the White and Wimley, 1994). For most TM helices, middle part of the lipid facing side is exposed to the hydrocarbon chains of lipids, such as CH_2 and CH_3 groups. The certain amount of information on the possible prediction of the lipid favourable or hydrophobic surfaces of the TM helix could be obtained by molecular modelling.

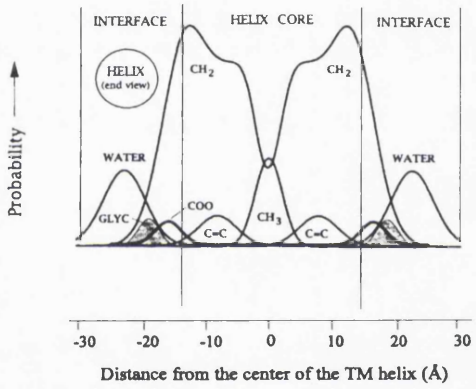

Figure 4.25 The time averaged distribution of the principal structural of the lipid projected onto axis normal to the bilayer plane.

The dodecane molecule was considered as a non-specific hydrophobic probe for mapping the selective interactions of the various TM helices. The relative energy of the interaction was studied for dodecane in the different positions around helices. There was no obvious conclusion which residues will not appear in lipid facing side of the TM helix, since the polar residues appeared in the surfaces involved in the most stable complexes between the TM helices and dodecane. It is known, that a charged residue brings a penalty

in energy when exposed to the hydrocarbon environment of lipid bilayer [Popot et al., 1994] and that the polar side chains (Ser, Thr, Asp and Arg) have the ability to make side-chain to backbone hydrogen bonds in order to satisfy the hydrogen bond potential of free N-H groups [Burley and Petsko, 1988]. Even if the N-H group is involved in the forming of TM helices, bifurcated hydrogen bonds could be formed [Burley and Petsko, 1988]. That could explain the possible appearance of polar amino acid sidechains in lipid facing sides of the TM helices.

On the other hand, the helix - helix packing in the integral membrane proteins is not much different than the helix - helix packing in water soluble proteins. The analysis was performed of the amino acid composition of residues involved in helix - helix contacts for the *Rhodob. sphaeroides* (RC) and water soluble protein [Rees et al., 1994]. RC has roughly comparable amino acid composition of the contact residues to the water soluble proteins, with some noticeable differences. RC exhibited the greater proportional abundance of Phe, Trp and Ala and deficiency of Val, with respect to water soluble proteins. A similar comparison was made for the amino acid composition of residues involved in TM helix - lipid and TM helix - TM helix contacts for the BR and RC (Figure 4.26). The higher proportional percentage of Gly, Ala, Val, Leu, Pro, Asn and Lys residues were observed in the lipid facing sides for the BR with the respect to RC, while higher percentage of Ile, Phe, Tyr, Met and Gln were observed for the RC (Figure 4.26A). Significantly, polar and even charged residues occurred in the lipid facing sides for both proteins. Since those residues were hydrophylic according the Eisenberg et al., 1982b scale, this made the hydrophobic moments of the helices smaller. The percentage of the hydrophobic residues in the helix - helix contacts was high for both proteins, thus resulting in a direction hydrophobic moment different from the lipid facing side (Figure 4.26B).

Therefore, it could be assumed that the hydrophobic moment might not be enough to correctly predict the lipid facing sides of membrane proteins, excluding ion channels. The TM helices of ion channels have high concentration of charged residues along the channel pore, thus having higher degree of amphipathic character of their TM helices and thus the hydrophobic moment could be enough to orient TM helices within ion channel.

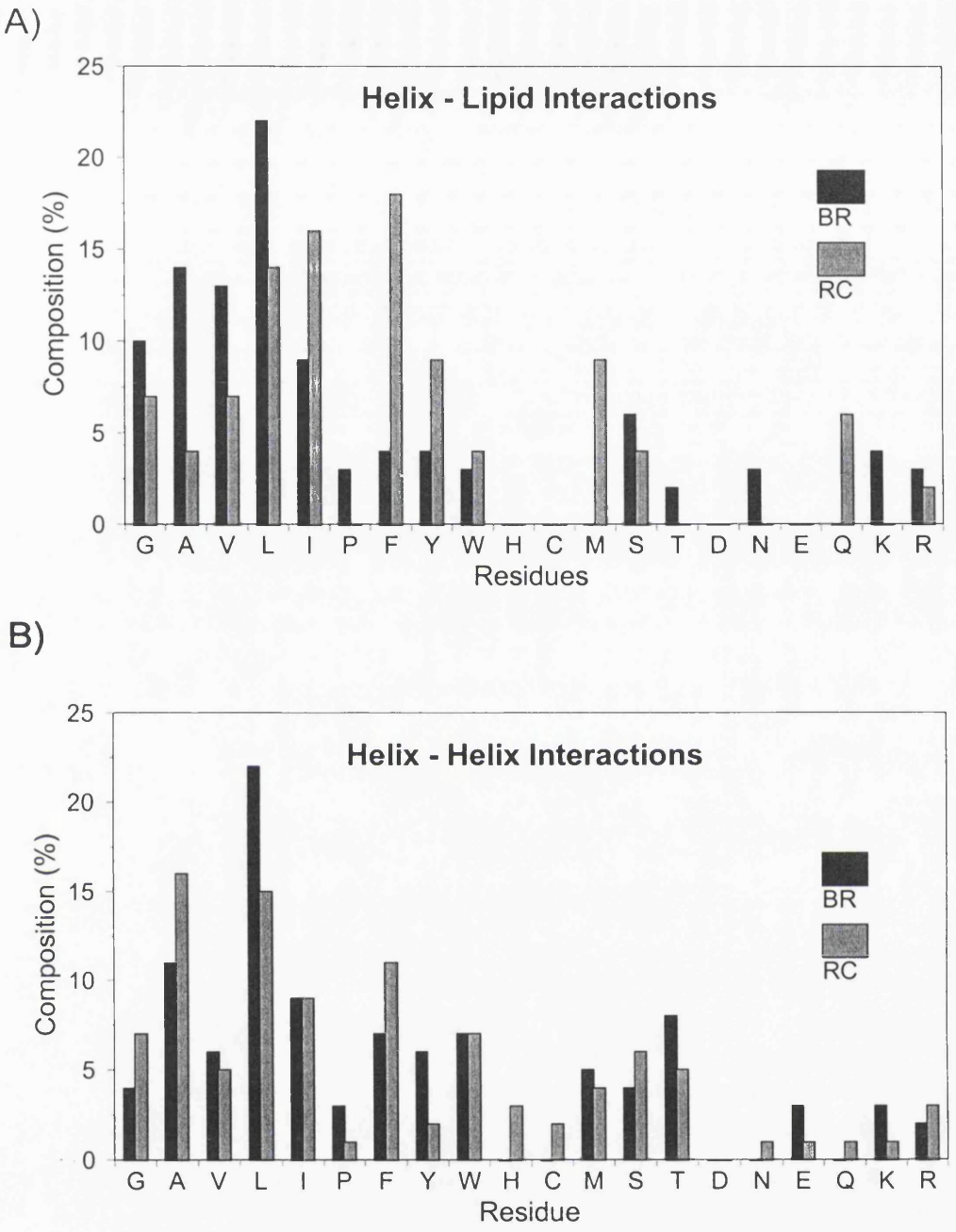

Figure 4.26 The amino acid composition of *Bacteriorhodopsin* (BR) and *Rhodob. Sphaeroides* (RC) residues involved in A) lipid -TM helix and B) TM helix - TM helix contacts.

and D) 315 degrees (the most stable complexes).

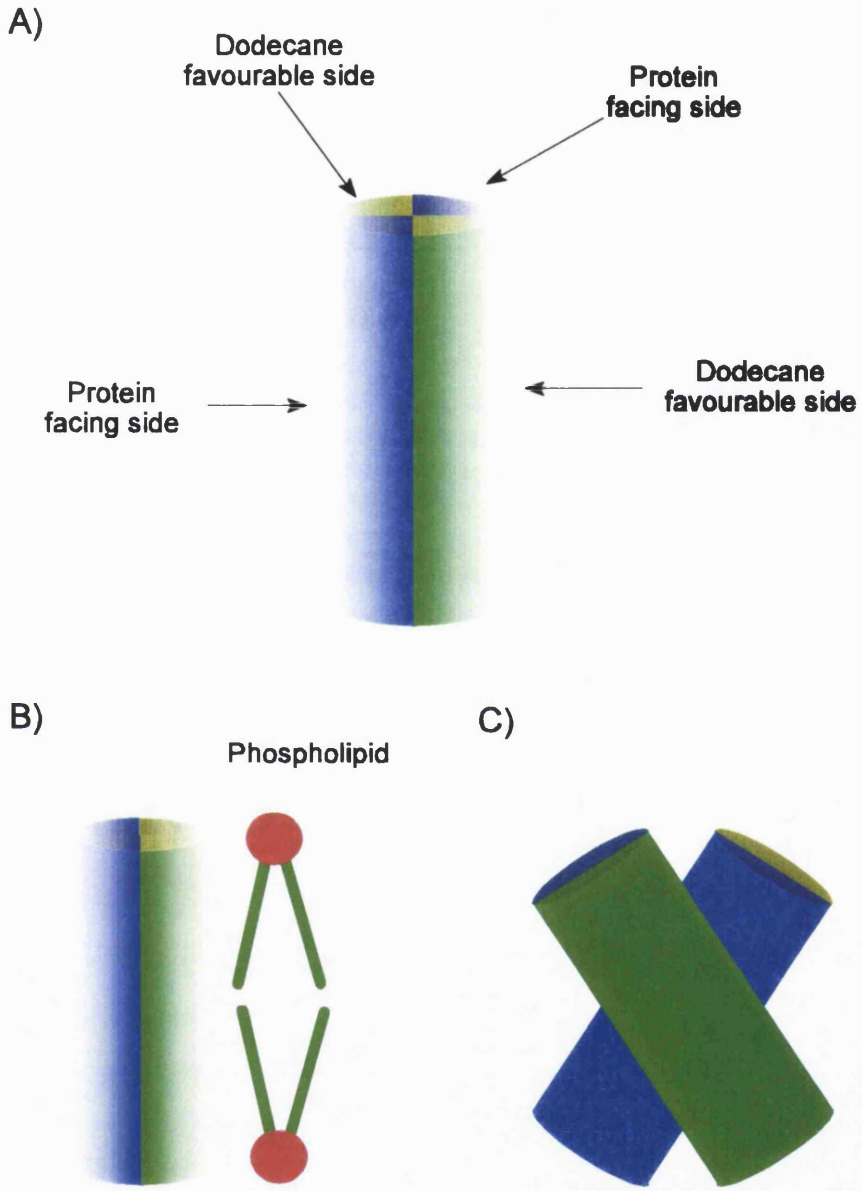

Figure 4.27 The schematic representation of the TM helix; A) the TM helix with two dodecane favourable (green surfaces) and protein favourable (blue surfaces) sides, B) TM helix facing phospholipid and C) TM helix - TM helix packing.

4.5 Summary

In this chapter the use of the dodecane as a probe of hydrophobicity and lipid facing sides of the TM helices were shown. For simplicity the fully symmetric hydrophobic dodecane molecule was chosen as a ligand instead of a phospholipid, since it has no polar groups, and only van der Waals interaction would be encountered. Dodecane is also an anaesthetic and studies could provide a basis for understanding its effect on anaesthetic receptors and ion channels. The poly-alanine helix has uniformly distributed nonpolar CH_3 groups, shielding the polar groups of the backbone, and therefore the essentially same interaction energies were expected for all eight rotational positions.The comparison between highest and lowest energy positions was the most important feature of this experiment. The difference of interaction energies between the highest and lowest energy positions bigger than 3.6 kcal/mol were considered as significant. These data/conclusions encouraged the study of more complex helices and lipids with same way, but particularly to apply this method to a known model system, where both the helix - helix and lipid - helix interfaces have been structurally defined by crystallography. *Bacteriorhodopsin* was chosen as the model system and the FcεRI as a structurally unknown example of a 7 helix integral membrane protein.

BR is a 7-helix membrane protein with known three dimensional structure.The outer surface of the *Bacteriorhodopsin* is very lipophylic, the three lipid molecules have to be between two bundles in order for crystals to be formed [Popot et al, 1994]. The ideal α-helix geometry of the TM helices of the BR, mimicking the transmembrane helices, were used to study the hydrophobic interaction with lipids and hence to map the surface as a test case. The calculated lipid facing surfaces of three TM helices (TM helix 1, TM helix 2 and TM helix 4) substantially agreed with lipid interacting surface of TM helices in crystal

structure. For the TM helices 3. 5, 6 and 7 the two hydrophobic surfaces were predicted. For each of those helices one surface was in excellent agreement with lipid facing surfaces determined by crystallography data. The other surface was poor prediction of the lipid facing surface, but the rest of the surface could be assigned as a helix - helix interface. The additional information, such as a hydrophobic moments, TM helix - TM helix docking, etc, would be necessary to fully determine lipid facing side. The corollary indicates that this approach was complementary to other methods when applied to TM helices of BR. More interestingly, it should provide extra information in determination of helix surfaces of the FcεRI with unknown three dimensional structure.

The six different TM helices of the FcεRI were subject to hydrophobicity mapping. The interaction energy differences between lowest and highest energy positions were in the range from -7 to -18 kcal/mol for these TM helices. Usually, two or three hydrocarbon interaction sites with lower energies were detected on the transmembrane helices as a function of rotation through 360° of dodecane around the helical axis and it is sketched in Figure 4.27A. The essential focus of the interaction between the dodecane and helix included the hydrophobicity of the amino acid residues and packing of the hydrophobic chain of the lipid (Figure 4.27B). The branched resides were usually involved in the non favourable dodecane sides, despite the fact they are hydrophobic. They could be involved in the TM helix -TM helix contacts (Figure 4.27C). Therefore, the hydrophobicity mapping using hydrophobe provides the basis for the correct orientation of TM helices in the helix bundles within membrane bilayer. It requires further refinement by using other data, like hydrophobic moments, TM helices docking, mutagenesis, etc.

Chapter 5.

INTERACTION OF TRANSMEMBRANE HELICES OF THE HIGH AFFINITY IgE RECEPTOR WITH PALMITIC FATTY ACID STUDIED BY MOLECULAR MODELLING

5. INTERACTION OF TRANSMEMBRANE HELICES OF THE HIGH AFFINITY IgE RECEPTOR WITH PALMITIC FATTY ACID STUDIED BY MOLECULAR MODELLING

5.1 Background

As described in the Chapter 4., a lipid molecule can interact with a protein in many different ways: hydrophilic, hydrophobic or mixed interactions can be established between the polar head groups or the apolar fatty acid side chains of a phospholipid and the amino acidic residues of the protein.

Palmitic acid (PFA) was used as a simplified representation of the amphipathic lipid, with a long hydrophobic chain and polar group at the end. Eight rotational positions and two different longitudal arrangements of the PFA respect to the transmembrane helix were considered and in all cases their long axis were parallel to each other, see Figure 5.1. The protonated carboxylic group of the PFA was placed near the N-terminal region of the TM helix in one case and near to the C-terminal region of the TM helix thus giving the possible sites for PFA - TM helix interaction across membrane. All six high affinity IgE transmembrane helices were studied in this way and results compared.

The hydrophobic contribution to the interaction between the saturated fatty acid chain of the phospholipid and all six TM helices was described in Chapter 4. using the dodecane molecule to mimic the hydrocarbon chain of the saturated fatty acid. This approach to hydrophobic surface mapping of TM helices yielded a simplified picture, yet

it provided a basis for designing the work described here. By using molecular modelling, the possible interaction of the six TM helices of the high affinity IgE receptor (FcεRI) with the apolar and the hydrophilic moieties of a phospholipid component such as palmitic fatty acid, were analysed. The resulting data not only contributed to the relative hydrophobic surface mapping around and along ends of the helix but have formed a data basis for calculating the relative interactions of more complex lipids and individual TM helices, coiled coils and bundles in receptors.

5.2 Methods

The interaction energies between the FcεRI helices and palmitic fatty acid 16:0 (PFA) were calculated by X-PLOR (Brunger, et al., 1987) using the CHARMM 22x parameter set and dielectric constant of 1.0. Helical backbone geometry was explicitly maintained during minimization through imposition of a one-sided distance restraint with an upper boundary of 3.2A between i oxygens and i+4 nitrogens along the length of the helix. The fully extended form of PFA was used as the starting geometry for the ligands. In fully extended form of PFA was 20.8 Å long, so it could stretched almost over the length of a whole bilayer leaflet. Thus, the probing of the hydrophobicity over length of the TM helices combined with the examination of polar interactions could be achieved. The helix peptide and PFA ligand were always oriented with thier long axes parallel and antiparallel to each other (Figure 5.1). The eight rotational positions were considered, each with a separation of a 5Å between the helix and ligand. An energy minimization protocol consisting of 2000 steps of Powell minimization steps was used.

The α-helical hydrogen bond restraints were also active during the minimization stage. The interaction energies between the PFA ligands and the peptide helices were calculated relative to those when the two molecules were far apart: E=E(close)-E(far). Thus, negative values of interaction energies corresponded to stabilization.

The figures in this chapter were created only for most and least stable complexes between PFA and TM helices in the same manner as in the Chapter 4.

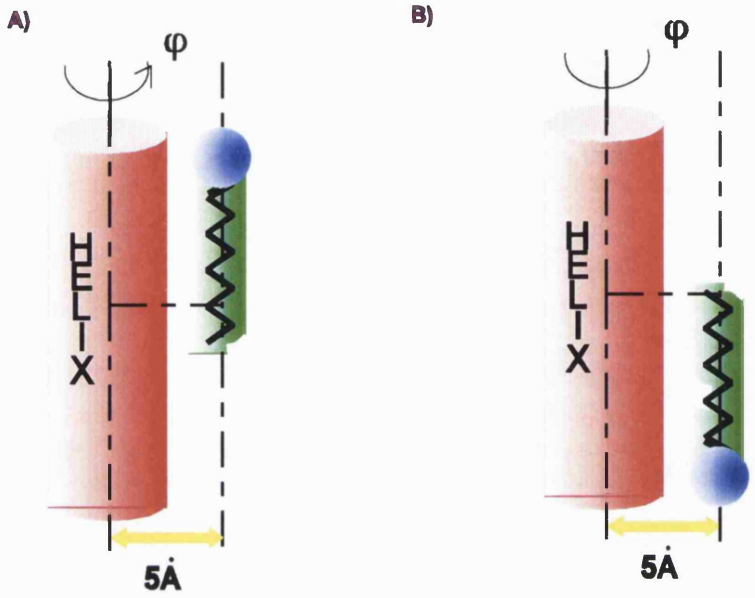

Figure 5.1 The schematic representation of the study of TM helix (red) and PFA (green), A) parallel and B) antiparallel orientation of the PFA in the respect to the TM helix. The rotational angle (φ) was varied in steps of 45° from 0° to 360°.

5.3 Results and Discussion

5.3.1 Interaction of transmembrane helix of α-subunit with palmitic acid.

The α-subunit contains a single TM helix (depicted as TM helix α), which is presented in Figure 5.2A (L^{205}IFPSLAVILFAVDTGLWF^{223}). The interaction energies as a function of rotational angle of the fatty acid around the axis of the TM helix of the α-subunit of the FcεRI is shown in Figure 5.2B. Generally, the two different longitudal positions of the palmitic acid molecule, corresponding to parallel and antiparallel axes led to similar results: two lower and two higher energy positions, but the magnitude of the stabilization energies was different. In some cases the results were more complex, but still comprehensible and useful.

Complexes between PFA and outer N-terminal region of TM helix α.

The N-terminal half of the TM helix α are considered to be located in the outer leaflet of the lipid bilayer [Blank et al., 1989]. The energy differences among the lowest and highest energy rotational positions for the antiparallel orientation of the PFA molecule and helix (Figure 5.2B) were in the range of 7 kcal/mol to 15 kcal/mol for the 0° and 270° positions; and for the 135° and 180° positions, respectively. The essential element of the interaction between PFA and a the TM helix included packing interactions involving the hydrophobic side-chains of the helix. Two fatty acid binding sites with lower energies were detected for this end of the transmembrane helix. Thus, PFA interacted with sidechains of L205, P208, S209, V212, A216, T219, G220 and F223 residues of the TM helix at lower energy 135° position and with the sidechains of residues F207, P208, A211, L214, F215, D218, T219, and W222 at the other 270° low energy position. The less stable complexes

were formed at rotational angles 0° and 180°. Those interaction sites involved the residues L210, L214, V217, L221 and P208; V212, F215, T219, W222, F223, respectively.

Complexes between PFA and inner C-terminal region of TM helix α.

Greater stabilisation (from 25 kcal/mol to 56 kcal/mol) of the PFA-TM helix α complex was observed for the fatty acid in the 270° antiparallel (Figure 5.3), when the carboxylic group of PFA was placed at the C-terminal end of the transmembrane helix. At the this low energy position the residues F207, P208, A211, L214, F215, D218 and W222 interacted with the PFA molecule with hydrogen bonds between the carboxylic group of the fatty acid and D218 and W222 located at the end of the TM helix α (Figure 5.3). This provided the extra stabilization energy for the 270° antiparallel position. The existence of these hydrogen bonds supported the hypothesis that the lowest energy position could correspond to the lipid facing side of the TM helix in the intact membrane. The indole N-H of tryptophane has been shown to form a hydrogen bond with the surface of bilayer [Shiffer, et al., 1992]. PFA interacted with L205, P208, S209, V212, A216, T219, G220 and F223 residues of the TM helix at other lower energy 135° position [Figure 5.2A].

At the high energy positions, 0° and 180° rotational angles, PFA interacted with Leu210, L214, V217, L221 (Figure 5.4); and P208, V212, F215, T219, W222, F223, respectively. The α-subunit of the FcεRI is a single polypeptide chain with one transmembrane α-helix. It is not known whether the TM helix of the α-subunit interacts with TM helices of the β-subunit and/or with TM helices of the γ-dimer and/or with lipids. The amino acid residues V206, L210, L214, V217 and L221 interacted with the PFA molecule producing the high energy complex at 0° (Figure 5.4). This amino acid sequence (xxLxxxLxxVxxxL) is homologous with the sequence required for forming a parallel coiled coil [Hodges et al., 1981]. One possibility is that this position at 0° could be the helix

facing side of the TM helix α, that could interact with parallel TM helices of other subunits of the FcεRI.

Essentially, the same behaviour was observed for the both orientations of the PFA in the respect to the TM helix α for almost all rotational positions. There was an extra stabilization when the hydrogen bond was formed between PFA and residues D218 and W222 in the 270° position. The most and least stable complexes were also formed at the same rotational positions between the TM helix α and dodecane (Figure 4.14), indicating the complementary of the two different investigations.

5.3.2 Interaction of the four transmembrane helices of β-subunit with palmitic acid

5.3.2.1 TM Helix β1.

The β-subunit of the FcεRI consists of the four TM helices that could form the four helix bundle that interacts with TM helices of the α- and γ-subunits [Blank et al., 1989]. The rest of the bundle can therefore interact with lipids. The TM helix 1 of β-subunit, denoted as TM helix β1, (F^{60}LGVTQVLVGLICLCFGTVVC^{80}) is shown in Figure 5.5A and mapping of the helix surface by PFA produced the interaction energy curve (Figure 5.5B) The interaction energy between PFA and the TM helix β1 again showed bimodal behaviour, with two low energy positions at 135° and 270° and two high energy positions at 0° and 180° for both orientations.

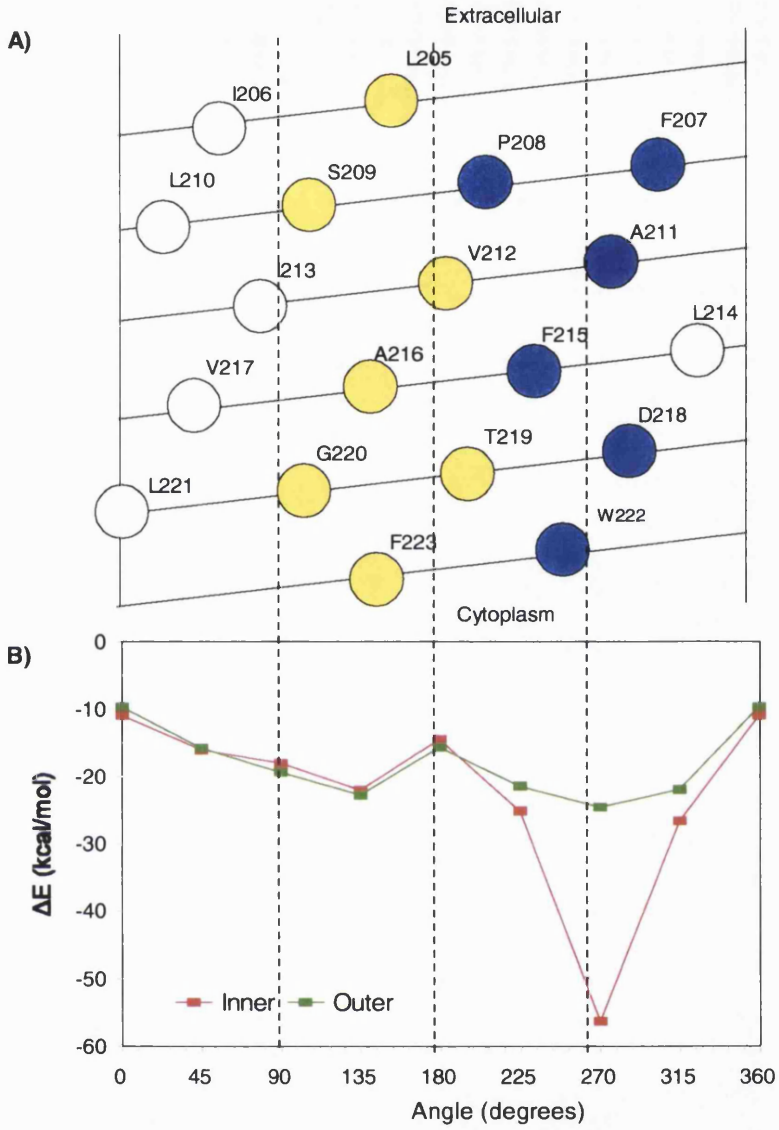

Figure 5.2 The PFA favorable surface mapping of the TM helix of the α-subunit of the FcεRI A) The helical net plot outlines the amino acid residues in the first most stable complex (depicted as blue circles) and second most stable complex (depicted as yellow circles) when carboxylic group was located near C-terminal region. B) The interaction energy between the TM helix of the α-subunit of the FcεRI and PFA as a function of the rotation of PFA around helical axis as described in methods (antiparallel - the carboxylic group located in the inner leaflet near C-terminal region, parallel - the carboxylic group located in outer leaflet near N-terminal region).

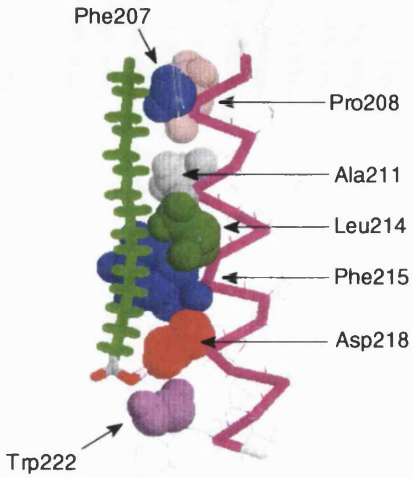

Figure 5.3 The lowest energy complex of TM helix of the α-subunit of the FcεRI and PFA at rotational angle 270°.

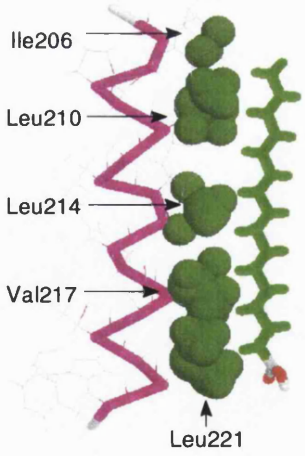

Figure 5.4 The least stable complex of TM helix of the α-subunit of the FcεRI and PFA at rotational angle 0°.

Complexes between PFA and outer C-terminal region of TM helix β1.

The C-terminal residues of TM helix β1 are located in the outer leaflet of the membrane bilayer. The calculated difference of interaction energy between the lowest and highest positions was between 10.6 and 17.3 kcal/mol which were outside the computational error, and indicated that two helix surfaces again had a preference towards the fatty acid. The low energy complexes were formed at the 90° and 270° rotational positions of PFA around TM helix β1. The 270° complex (stabilization energy of -25 kcal/mol) involved PFA interactions with G62, Q65, V66, G69, C72, L73, G76 and C80. The hydrogen bond between the carboxylic group of the PFA with C80 was detected in the lowest energy position, as reflected in the larger energy of the interaction of -25 kcal/mol. The interaction of PFA with the TM helix in the other lower energy position (rotational angle of 90°) was mainly hydrophobic and showed PFA interactions with V63, L67, L70, I71, C74 and V78.

The high energy complexes were observed at 0° and 180° rotational positions. The residues L61, T64, V68, F75 and V78 were in the contact with PFA at rotational position 0°. On the opposite side of the helix, PFA interacted with residues V63, V66, L70, and T77. The stabilization energy in this case was very low, about -7 kcal/mol, since PFA interacted with fewer residues. Those residues were branched at the β-carbon atom. The residue at position 73 in the sequence is leucine, and again the sequence motif xxVxxVxxxLxxLxxxT could be involved in the coiled coil type helix-helix interaction [Offer and Sessions, 1995].

Complexes between PFA and inner N-terminal region of TM helix β1.

The N-terminal residues of the TM helix 1 were located in the inner membrane leaflet and the difference in interaction energy between the lowest and highest positions was between 3.7 and 19.3 kcal/mol. In the lowest energy position (-29 kcal/mol at 270°),

the residues G62, Q65, V66, G69, C72, L73, and G76 interacted with the PFA molecule. A hydrogen bond was again detected, but this time between the hydroxyl hydrogen of carboxylic group of PFA and the C=O group of the sidechain of Q65 (Figure 5.6). The other low energy position was in the comparable range of the error determined by interaction of polyalanine and dodecane in Chapter 4., and so by comparison it could be regarded as non-specific and was not further considered. The less stable complexes were formed in the same rotational positions of the PFA (0° and 180°) as described in previous section.. The V63, V66, L70 and T77 residues interacted with PFA at 0° rotational position (Figure 5.7). Same sequence motif, that could be involved in the coiled-coil formation, was also involved in the interaction with PFA in other orientation.

Again, the same behaviour was observed for the both orientations of the PFA , except for an extra stabilization due to hydrogen bond at 270° rotational position. These results were in the excellent agreement with results of the hydrophobic surface mapping of the TM helix β1 with dodecane (Figure 4.16).

5.3.2.2 TM Helix 2.

The N-terminal region of the TM helix 2 of the β-subunit of FcεRI (designated as TM helix β2) was located in the outer leaflet of the membrane bilayer, with W103 in the second turn of the helix, while the C- terminal region was in the inner leaflet with S115 and M117 in the last turn of the helix. The helical net plot of TM helix β2(A^{98}GYPFWGAVLFVLSGFLSIM^{117}) is shown in Figure 5.8A. The graph of the calculated interaction energies between this helix and PFA in eight different rotational positions is presented in Figure 5.8B. In the case of this complexes, the energies of interaction between the parallel and antiparallel arrangements (Figure 5.8B) were different

for the same rotational angle. Thus the antiparallel arrangement generally provided more stable complexes due to the greater stabilizing polar interactions in the N-terminus of the TM helix β2.

Complexes between PFA and outer N-terminal region of TM helix β2.

The most stable complex between PFA and TM helix β2 was found at rotational angle 225°. Residues R97, P101, F102, A105, F108, V109, G112, and I116 of the TM helix β2 residues were involved in the interaction with PFA molecule (Figure 5.9). A hydrogen bond was formed between the carboxylic group of the PFA and R97. The other low energy position (angle 315°) involved polar interaction between the PFA carboxylic group and Y100 and W103 but with no hydrogen bonds. But this position was not so different from the rest of the helix, since for all the rotational positions of PFA around the TM helix β2 there was a stabilization, with energies of stabilization above of ca -20 kcal/mol.

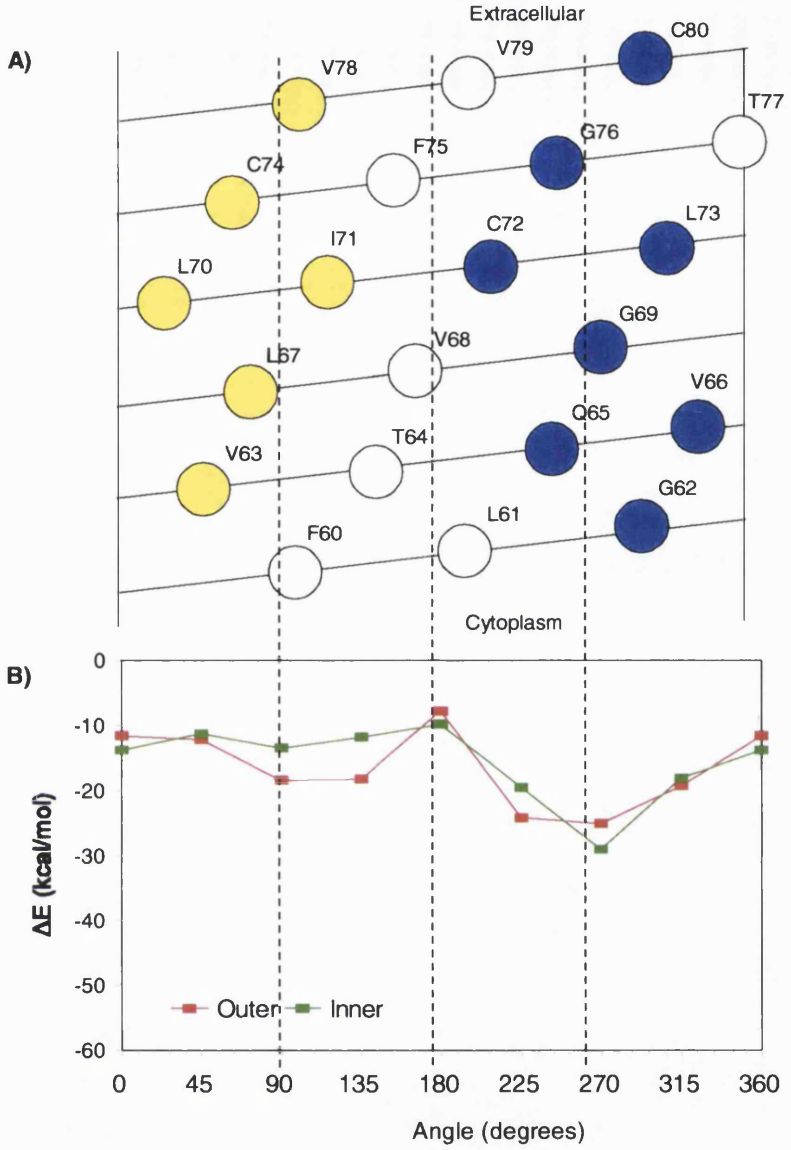

Figure 5.5 The PFA favorable surface mapping of the TM helix 1 of the β-subunit of the FcεRI A) The helical net plot outlines the amino acid residues in the first most stable complex (depicted as blue circles) and second most stable complex (depicted as yellow circles) when carboxylic group was located in inner leaflet near N-terminal region. B) The interaction energy between the TM helix 1 of the β-subunit of the FcεRI and PFA as a function of the rotation of PFA around helical axis as described in methods (parallel - the carboxylic group located in the inner leaflet near N-terminal region, antiparallel - the carboxylic group located in outer leaflet near C-terminal region).

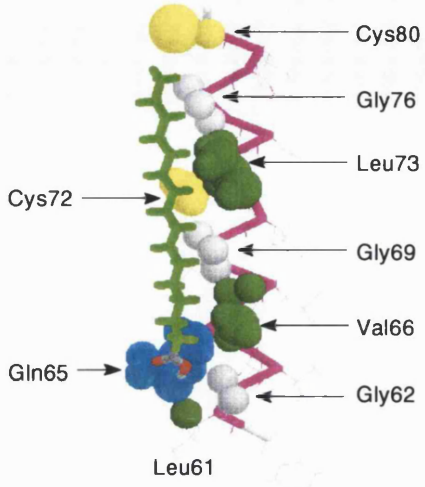

Figure 5.6 The lowest energy complex of TM helix 1 of the β-subunit of the FcεRI and PFA at rotational angle 270°.

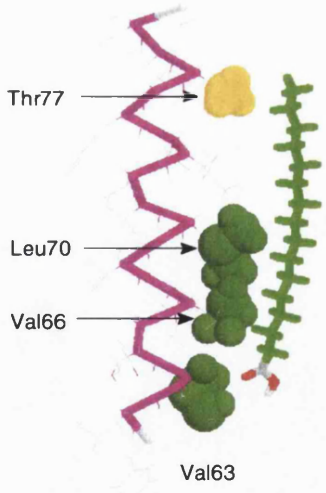

Figure 5.7 The least stable complex of TM helix 1 of the β-subunit of the FcεRI and PFA at rotational angle 0°.

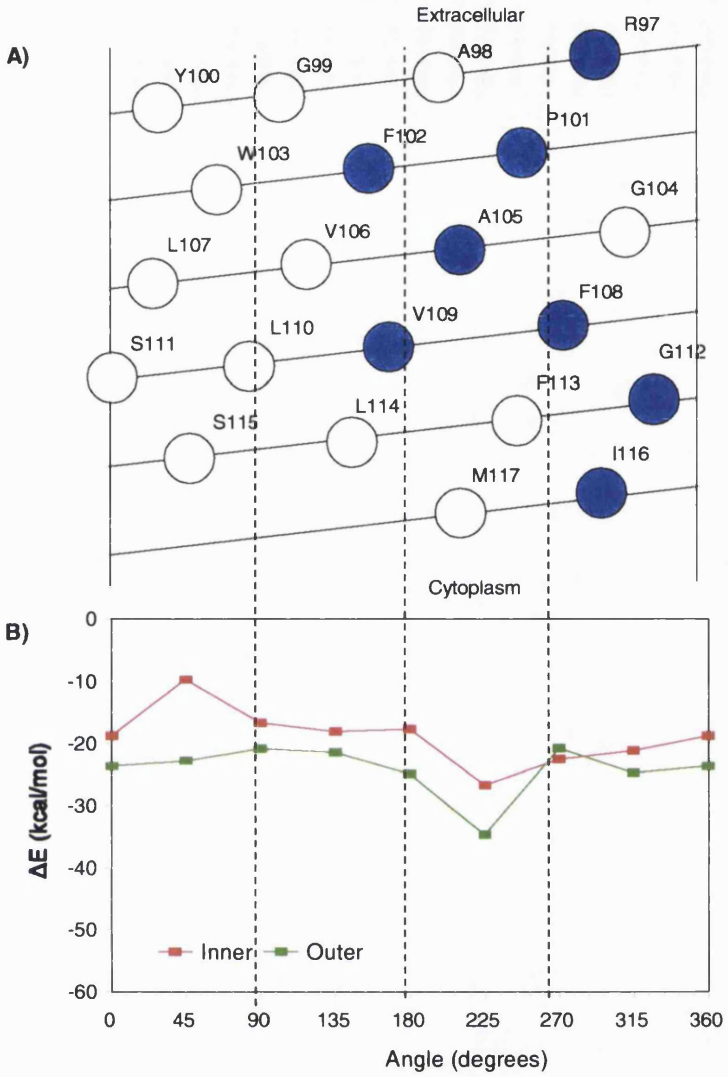

Figure 5.8 The PFA favorable surface mapping of the TM helix 2 of the β-subunit of the FcεRI A) The helical net plot outlines the amino acid residues in the first most stable complex (depicted as blue circles) when the carboxylic group was located in the outer leaflet near N-terminal region. B) The interaction energy between the TM helix 2 of the β-subunit of the FcεRI and PFA as a function of the rotation of PFA around helical axis as described in methods (antiparallel - the carboxylic group located in the inner leaflet near C-terminal region, parallel - the carboxylic group located in outer leaflet near N-terminal region).

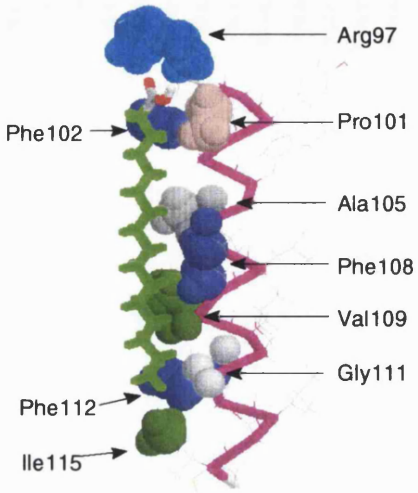

Figure 5.9 The lowest energy complex of TM helix 2 of the β-subunit of the FcεRI and PFA at rotational angle 225°.

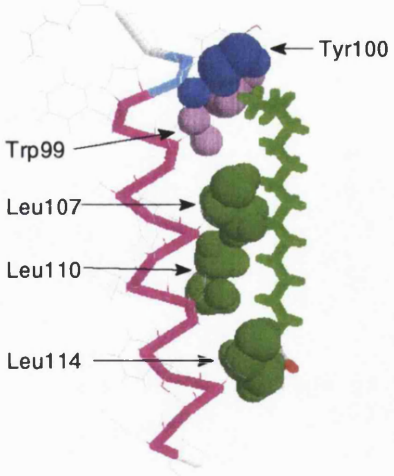

Figure 5.10 The least stable complex of TM helix 2 of the β-subunit of the FcεRI and PFA at rotational angle 45°.

Complexes between PFA and inner C-terminal region region of TM helix β2.

The most stable complex between TM helix β2 and PFA was formed in the 225° rotational position. Residues P101, F102, A105, F108, G112, and S115 were interacted with PFA in that complex. In the lowest energy position (-34.6 kcal/mol at 225° position) the -OH group of S115 formed the hydrogen bond with the -C=O group of the PFA molecule.

The low energy complex was formed at rotational angle of 45° (stabilization energy of -9.7 kcal/mol). In latter complex PFA interacted with residues Y100, W103, L107, L110, and L114 of the TM helix β2 (Figure 5.10). Again, there was a noticeable appearance of the leucine residues in the side of the helix that had a low affinity towards PFA - lipids (sequence motif LxxLxxxL).

The significant differences in the nature of the N- and C-terminal ends of the TM helix β2 /PFA complexes are not easily could not be explained at the moment. Also, the different mapping of the TM helix β2 surface was observed for the dodecane and PFA as ligands. One explanation could be that with PFA, we have introduced the mapping of the end of the helix and studied the role of "anchor" residues. In this case R97, that could serve to orient the TM helix towards lipids in the bilayer.

5.3.2.3 TM Helix β3.

TM helix 3 of the β-subunit (depicted as TM helix β3) is antiparallel to the TM helix β2, and parallel to the TM helix β1, and thus its N-terminal region was located in the inner leaflet of the membrane bilayer, and its C-terminal resided in the outer leaflet. The helical net plot of the TM helix β3 (L^{131}GANIVSSIAAGLGIAILIL^{150}) is shown in Figure 5.11A. Interaction energy profiles for two longitudal directions of the PFA were similar in the most of the rotational positions, except for the rotational positions 135° and 225° in

which the interactions of between TM helix and PFA in parallel direction were less stabilizing (Figure 5.11B).

Complexes between PFA and outer C-terminal region of TM helix β3.

Three stable complexes between the PFA molecule and the TM helix β3 in a parallel position were observed (Figure 5.11B) with similar ΔE of -14.4, -14.3 and -13.1 kcal/mol. Each complex was stabilised by hydrophobic interactions of PFA with sidechains, and by weak polar interactions with backbone atoms. The stabilizing complex at 90° involved the following residues: I135, S138, I139, G142, A146, I149 and L150, at the 180°: N134, S138, A141, I145 and L148, while at the position of 270°: A133, S137, A140, G144, I147 and L148. The less favourable positions were at 0° rotational angle: V136, L143, I147 and L150; at 135° rotational angle: N134, I135, S138, G142, I145 and I 149; and at rotational angle of 225°: N134, S137, A141, I145, and L148. Some of the residues found interacting in both, favourable and less favourable lipid binding sites, and the only difference was probably the packing of those residues in different positions of PFA with respect to the TM helix β3.

Complexes between PFA and inner N-terminal region of TM helix β3.

Generally, the interaction energy curve was bimodal, there was again a region associated with low energy complexes, in the region of 135° and 270°, and a region of the less stable complexes around 0° and 225° rotational position (Figure 5.11B). In 135° PFA / TM helix 3 complex, the following residues were involved in the interaction: L131, N134, I135, S138, G142, I145, A146 and I149 (Figure 5.12), and there was a hydrogen bond formed between the backbone oxygen of Leu131 and the PFA carboxylic group. The

neighbours of L131, such as S130 and G132 are small in the volume, and therefore the formation the hydrogen bonds between the backbone acceptor atoms and carboxylic group was possible. At the 270° rotation position PFA interacted with A133, V136, S137, A141, G144, I147 and L148 residues of the TM helix β3. The interaction was mainly hydrophobic in nature.

The less stable complex at 0° rotational position involved V136, L143, I147 and L150 residues, and again the sequence motif xxVxxxAxxLxxxIxxL was present (Figure 5.13). The other less stable complex at 225° rotational position involved residues N134, S137, A141, I145 and L148 in the PFA interaction. The stabilization energy of this complex was -16.8 kcal/mol, and therefore it was stabilized. This side of the TM helix could be therefore considered as favourable towards lipids. The whole region from 90° to 315° of rotational positions was in fact favourable towards lipids, leaving only one side of the TM-helix as helix favourable side.

The difference in the behaviour of N- and C-terminal was observed and that needs further attention. In fact, the hydrophobic surface mapping of the TM helix β3 with dodecane (Figure 4.19) gave an essentially same results as the mapping of the N-terminal end with PFA, meaning that the C-terminal part of the helix exhibits different properties that could be important in the folding of the β-subunit.

5.3.2.4 TM Helix β4.

The TM helix 4 of the β-subunit, designated as TM helix β4, (L^{180}VLMLLFLTILAFCSAVLLII^{200}) is shown in Figure 5.14A and its N terminal region is located in the outer leaflet of the membrane. The interaction energy profiles for the two longitudal directions of the PFA molecule were the essentially same for both parallel and

antiparallel orientations, each having three minima and therefore implying three stable complexes (Figure 5.14B).

Complexes between PFA and outer N-terminal region of TM helix β4.

The stable complex at the 45° and ΔE = -21.4 kcal/mol position involved hydrophobic interactions between the PFA molecule and residues V181, L185, P186, I189, L190, C193 and L197. The other stable complex at a position 180° (ΔE = -22.7 kcal/mol) possessed a hydrogen bond between the hydroxyl group of PFA and the backbone oxygen of L180, and hydrophobic interaction with residues V181, L185, T188, F192, A195 and I199 residues (Figure 5.16). The third complex at 310° was significantly lower in stabilization energy than the 45° and 180° complexes (ΔE = -17.4 kcal/mol). The less stable complexes were at 0° rotational position: F186, L190, and L197; at 90°: V181, L185, F186, I189, V196; and at 270° rotational position: L184, L187, A191, S194 and L198. Again, some of the residues found interacting in both, favourable and less favourable PFA binding sites, and the only difference was probably the packing of those residues in different positions of PFA with respect to the TM helix β4.

Complexes between PFA and inner C-terminal region of TM helix β4.

The interaction energy curve for this parallel longitudal complex had the same shape as that corresponding to the antiparallel longitudal position of the PFA molecule. Again the complex at 45° was mainly hydrophobic in nature with interactions of PFA with the following residues: V181, L185, F186, I189, L190, C193, and L197. The position at 180° had extra stabilization due to a polar interaction between the PFA and backbone atoms and the residues that had hydrophobic interaction with PFA were: L185, T188, F192, A195, and I199.

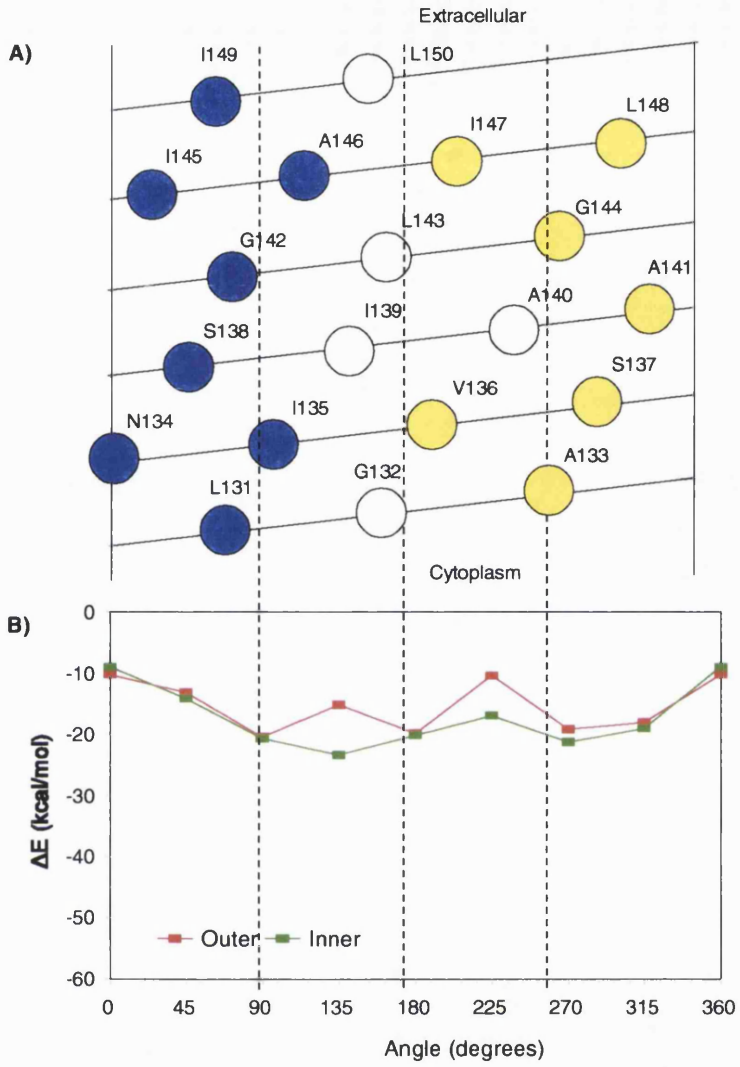

Figure 5.11 The PFA favorable surface mapping of the TM helix 3 of the β-subunit of the FcεRI A) The helical net plot outlines the amino acid residues in the first most stable complex (depicted as blue circles) and second most stable complex (depicted as yellow circles) when the carboxylic group located in the outer leaflet near C-terminal region. B) The interaction energy between the TM helix 3 of the β-subunit of the FcεRI and PFA as a function of the rotation of PFA around helical axis as described in methods (parallel - the carboxylic group located in the inner leaflet near N-terminal region, antiparallel - the carboxylic group located in outer leaflet near C-terminal region).

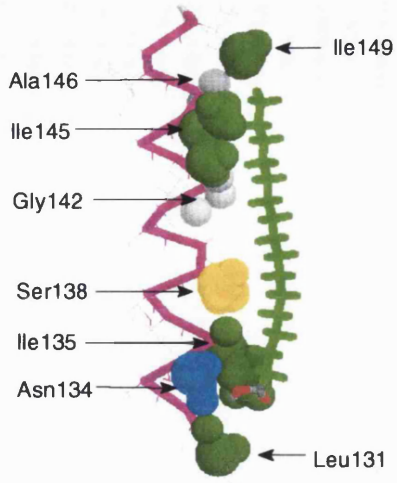

Figure 5.12 The lowest energy complex of TM helix 3 of the β-subunit of the FcεRI and PFA at rotational angle 135°.

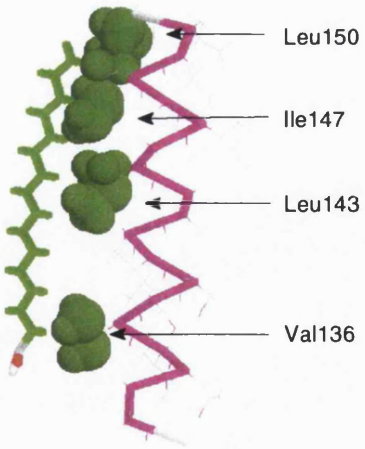

Figure 5.13 The least stable complex of TM helix 3 of the β-subunit of the FcεRI and PFA at rotational angle 0°.

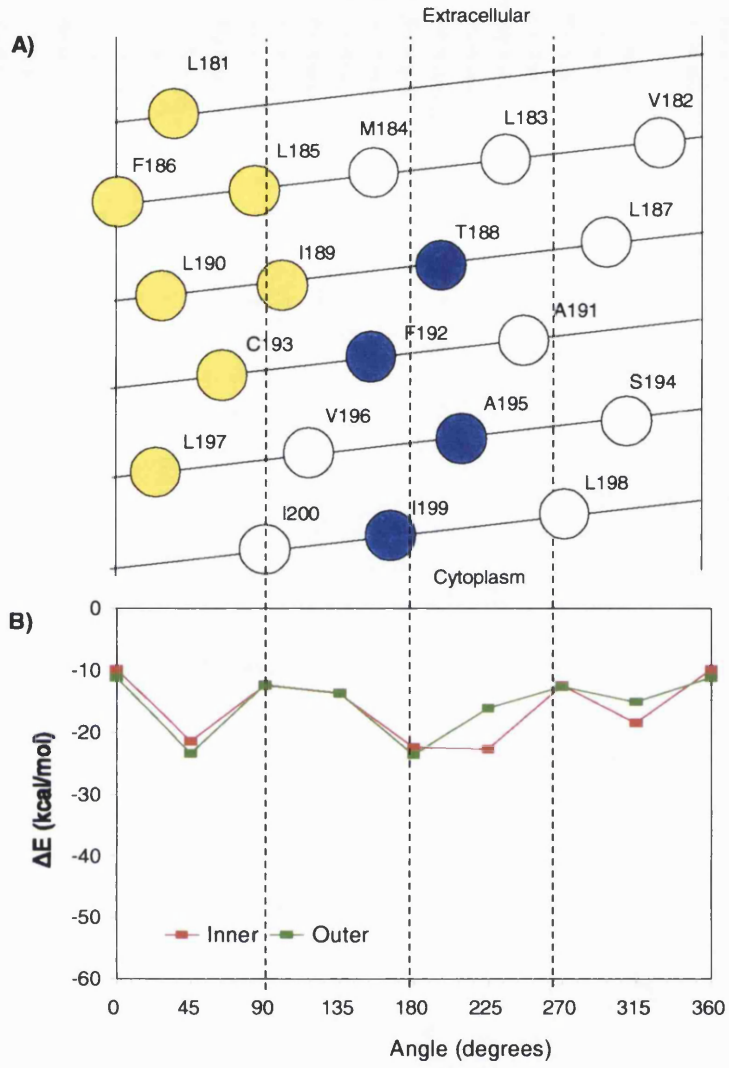

Figure 5.14 The PFA favorable surface mapping of the TM helix 4 of the β-subunit of the FcεRI A) The helical net plot outlines the amino acid residues in the first most stable complex (depicted as blue circles) and second most stable complex (depicted as yellow circles) when the carboxylic group located in the inner leaflet near C-terminal region. B) The interaction energy between the TM helix 4 of the β-subunit of the FcεRI and PFA as a function of the rotation of PFA around helical axis as described in methods (antiparallel - the carboxylic group located in the inner leaflet near C-terminal region, parallel - the carboxylic group located in outer leaflet near N-terminal region).

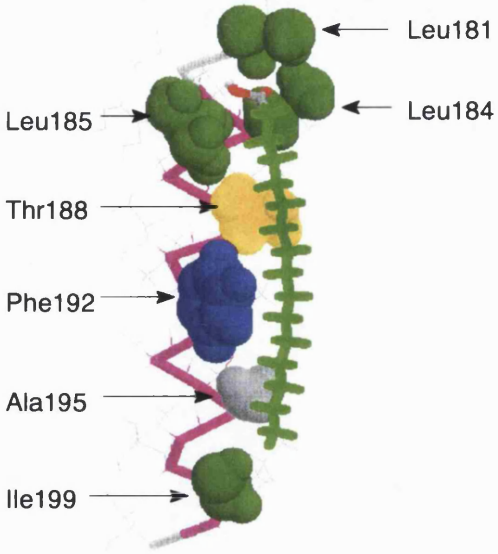

Figure 5.15 The lowest energy complex of TM helix 4 of the β-subunit of the FcεRI and PFA at rotational angle 180°.

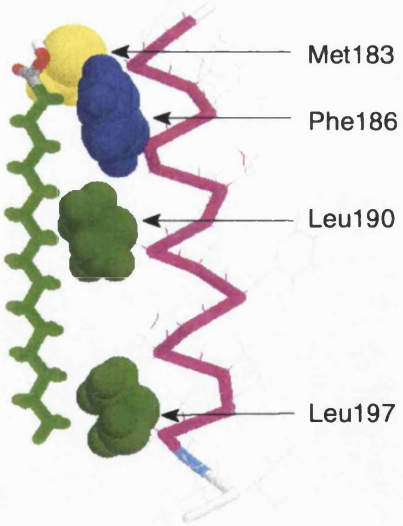

Figure 5.16 The least stable complex of TM helix 4 of the β-subunit of the FcεRI and PFA at rotational angle 0°.

The less favourable binding surfaces of TM helix β4 were at 0° and involved residues F186, L190 and L197; at 90°: V181, L185, F186, I189, V196 and I200; at 270° rotational position: L184, L187, A191, S194 and L198. In the case of the TM helix β4, there was a difference in the packing of the PFA and sidechains. Many of the same residues were involved in both stable and less stable complexes.

The same behaviour was observed for both orientations of the PFA in the respect to the TM helix β4, and it was in good agreement with results obtained for the hydrophobic surface mapping using dodecane (Figure 4.22).

5.3.3 Interaction of transmembrane helix of the γ-subunit with palmitic fatty acid.

The TM helix of γ-subunit, denoted as TM helix γ, (C^{7}YILDAILFLYGIVLTLLYC^{26}) is shown in Figure 5.17A as a helical net plot. The N-terminal region of the TM helix γ was located in the outer leaflet of the membrane bilayer. Their interaction curve between the PFA and the TM helix γ is shown in the Figure 5.17B. Their interaction energy curves for TM helix PFA complexes were complicated and showed one main minimum for both longitudal orientations of the molecule (Figure 5.17B), and two extra less stable complexes for the parallel - inner orientation of the PFA molecule.

Complexes between PFA and outer N-terminal region of TM helix γ.

Greatest stabilisation effect was found at the 90° rotational position of the PFA around the TM helix γ. The PFA interacted with the following residues of the TM helix: Y8, D11, L14, F15, G18, L21, T22 and Y25 (Figure 5.18). A hydrogen bond was formed

between the carboxylic group of the fatty acid and the hydroxy group of Y8 of the γ-subunit. The other stable complex was formed at rotational position of 180°, involving the I9, L10, I13, L14, Y17, L20 and L23. There was a whole range of rotational angles between 270° and 45°, in which the stabilizing interactions occurred. The following residues were involved in the interaction at 315° position: Y8, A12, F15, L16, I19 and L23. The least stable complex was at 135° rotational position, in which C7, L14, L21 and Y25 residues interacted with PFA (Figure 5.19).

Complexes between PFA and inner C-terminal region of TM helix γ.

Similar behaviour was observed in the parallel orientation of PFA in respect to the TM helix γ. The main difference was that carboxylic group of PFA in the parallel orientation was found in close proximity to Y25, without forming a hydrogen bond, but the stabilization of the complex occurred due to the polar interactions. Generally, same results were obtained when hydrophobic surface was mapped with dodecane (Figure 4.24).

This lowest energy position was far from of the C7 and C26, leaving those sides for the helix-helix interaction. It is known that the γ-subunit forms a parallel coiled-coil homo-dimer, covalently bound by disulfide bond but it is not known which pair of cysteine residues is involved in the interaction C7-C7 or C26-C26. The PFA - TM helix calculations predicted that Y8 and Y25 would be involved in the lipid facing side, and that left both cysteine residues of the TM helix γ accessible for the disulfide bond formation. The question which pair of cysteine residues forms the disulfide bond could not still be resolved by these calculations.

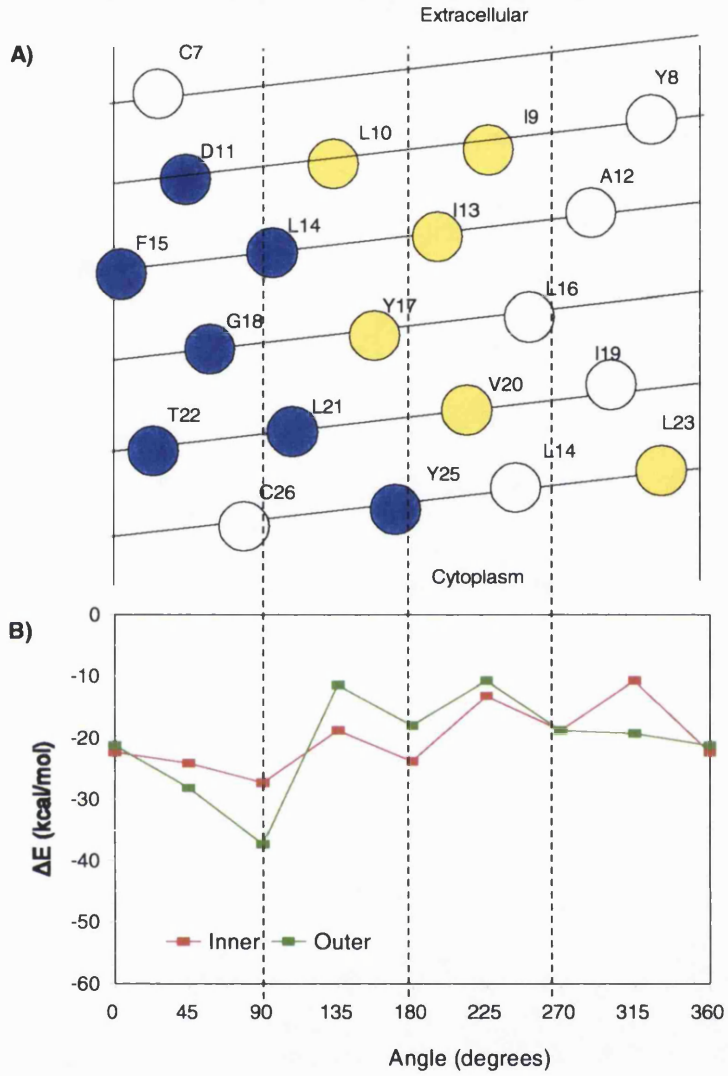

Figure 5.17 The PFA favorable surface mapping of the TM helix of the γ-subunit of the FcεRI A) The helical net plot outlines the amino acid residues in the first most stable complex (depicted as blue circles) and second most stable complex (depicted as yellow circles) the carboxylic group was located in outer leaflet near N-terminal region. B) The interaction energy between the TM helix of the γ-subunit of the FcεRI and PFA as a function of the rotation of PFA around helical axis as described in methods (antiparallel - the carboxylic group located in the inner leaflet near C-terminal region, parallel - the carboxylic group located in outer leaflet near N-terminal region).

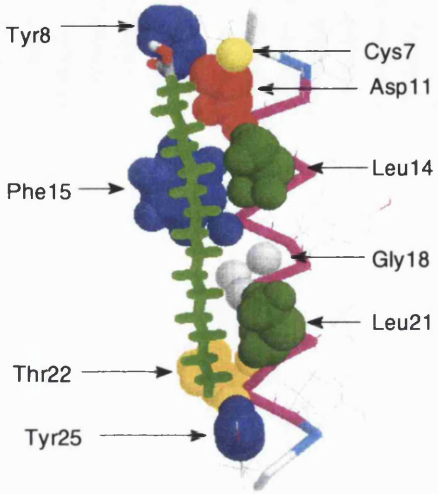

Figure 5.18 The lowest energy complex of TM helix of the γ-subunit of the FcεRI and PFA at rotational angle 90°.

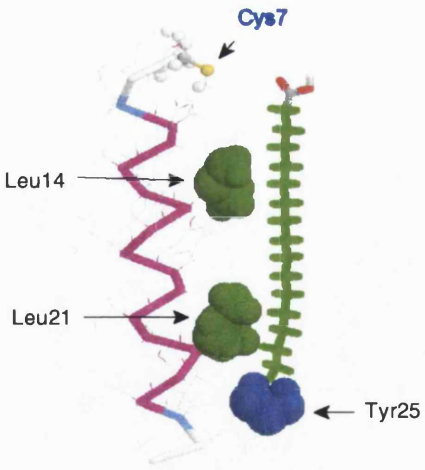

Figure 5.19 The least stable complex of TM helix of the γ-subunit of the FcεRI and PFA at rotational angle 135°.

5.3.4 Homology and similarity studies

All residues involved in forming the more stable complexes between the six different helices of FcεRI and PFA are shown in Table 5.1. There was no obvious sequence motif specific for the helix residues and PFA interactions. In addition, the presence of the polar residues in PFA favourable surfaces collided with hypothesis that generally polar residues should be buried in the interior of helix bundle.

However, residues involved in forming the least stable complex are shown in the Table 5.2. These residues were mostly hydrophobic and branched. The sequence alignment of four parallel transmembrane helices of the FcεRI is presented in Table 5.3. These transmembrane helices had their N-terminal residues located in the outer leaflet of the membrane bilayer. The sequence LxxxxxxL was conserved in three of these four TM helices, but in the fourth helix (TM helix β4) the first leucine was replaces with another hydrophobic residue alanine (AxxxxxxL). This conserved sequence was involved in forming the least stable complexes between TM helices and PFA. Similar conserved sequence occurs in the four TM helices of *Bacteriorhodopsin* (Table 5.4.) and some of these sequences were involved in the helix-helix packing of the *Bacteriorhodopsin* molecule. While the IgE receptor transmembrane domains were set to be ideal α-helices for this study, the helices in the *Bacteriorhodopsin* were tilted, kinked and twisted (or deviated from axial symmetry) in the crystall structure. Still, the sequences of the "PFA unfavourable surfaces" of the IgE TM helices coincided with the sequences involved in the TM helix - TM helix contacts of *Bacteriorhodopsin*, and this signified the possibility that the "PFA unfavourable surfaces" of the IgE TM helices could favour in the helix-helix contacts in the 7 helix bundle.

Table 5.1. Table of the TM helix residues of the FcεRI involved in forming stable complexes with PFA. Position denotes the rotational angle of the PFA in respect to the TM helix, ↑↑ and ↑↓ denote the parallel and antiparallel position, respectively; x marks the residues not involved in the interaction.

TM helix	Position and orientation	Sequence	Interaction energy (kcal/mol)
α	135↑↑	LxxPSxxxVxxxAxxTGxxF	-22
	135↑↓	LxxPSxxxVxxxAxxTGxxF	-22.7
	270↑↑	xxFpxxAxxLFxxDTxxWxx	-56.3
	270↑↓	xxFPxxAxxLFxxDTxxWxx	-24.5
β1	90↑↑	xVxxxLxxLIxxCxxxVxxx	-18.3
	270↑↑	GxxQVxxGxxCLxxGxxxCx	-25
	270↑↓	GxxQVxxGxxCLxxGxxxxx	-29
β2	225↑↑	RxxxPFxxAxxFVxxGxxxI	-34.6
	225↑↓	xxxxPFxxAxxFxxxGxxSx	-26.6
β3	90↑↑	xxxxIxxSIxxGxxxAxxIL	-14.4
	180↑↑	xxxNxxxSxxAxxxIxxLxx	-14.3
	135↑↓	LxxNIxxSxxxGxxIAxxIx	-23.3
	270↑↑	xxAxxxSxxAxxxGxxILxx	-13.1
	270↑↓	xxAxxVSxxxAxxGxxILxx	-21.2
β4	45↑↑	xxVxxLFxxILxxCxxxLxx	-21.4
	45↑↓	xxVxxLFxxILxxCxxxLxx	-22.4
	225↑↑	CYxLxxILxxYxxLxxLxxx	-22.7
	180↑↓	xxxxxLxxTxxxFxxAxxxI	-23.6
Y	90↑↑	CYxxDxxLFxxGxxLTxxYx	-27.3
	90↑↓	xxxxDxxLFxxGxxLTxxYx	-37.3
	180↑↑	CYxLxxILxxYxxLxxLxxx	-23.8
	315↑↑	xYxxxAxxFLxxIxxxLxxx	-22.3

Table 5.2. Table of the TM helix residues of the FcεRI involved in forming least stable complexes with PFA. Position denotes the rotational angle of the PFA in respect to the TM helix, ↑↑ and ↑↓ denote the parallel and antiparallel position, respectively; x marks the residues not involved in the interaction.

TM helix	Position and orientation	Sequence	Interaction energy (kcal/mol)
α	0↑↑	xxxxxLxxxLxxVxxxLxx	-10.8
	0↑↓	xxxxxLxxxLxxVxxxLxx	-9.6
	180↑↑	xxxPxxxVxxFxxxTxxWF	-14.4
	180↑↓	xxxPxxxVxxFxxxTxxxF	-15.6
β1	0↑↑	xLxxTxxxVxxxxxxFxxVxx	-11.5
	180↑↑	xxxVxxVxxxLxxxxxxTxxx	-7.6
β2	45↑↑	AGxxxWxxxLxxLxxxLxxx	-9.7
β3	0↑↑	xxxxxVxxxxxxLxxxIxxL	-10.1
	0↑↓	xxxxxVxxxxxxLxxxIxxL	-8.9
	135↑↑	xxxNxxSxxxAxxxIxxxIx	-15.3
	180↑↓	xxxNxxSxxxAxxxIxxLxx	-10.3
	225↑↑	xxxNxxSxxxAxxxILxxxx	-16.8
β4	0↑↑	xxxxxxFxxLxxxxxxLxxx	-9.8
	0↑↓	xxxxxxFxxLxxxxxxLxxx	-11.4
	180↑↑	xxxxLxxLxxxAxxSxxxLx	-12.4
	180↑↓	xVxxxLFxxLxxxxxVxxxI	-12.4
Y	135↑↑	xxxxxxxxLxxxxxxLxxxYx	-13.4
	225↑↑	xxILxxIxxYxxVxxLxxxxx	-13.1

Table 5.3. Sequence alignment of the TM helices of the FcεRI (four parallel helices, with N-terminal residues in the outer leaflet of the bilayer). Amino acid residues in bold letters were appearing in the least stable complexes of TM helices with PFA.

TM helix	Sequence
α	LIFPS**L**AVI**L**FA**V**DTG**L**WF
γ	LC**Y**ILD**A**ILF**L**YG**I**VLT**L**LYC
β2	**AG**YPF**W**GAV**L**FV**L**SGF**L**SIM
β4	VLM**L**LF**L**TIL**A**FC**S**AVL**L**II
	* *
Conserved sequence	L L

Table 5.4. Sequence alignment of the TM helices of the *Bacteriorhodopsin* (four parallel helices, with N-terminal residues in the inner leaflet of the bilayer) helices.

TM helix	Sequence
1	EWIWL**A**LGTA**L**MGLGT**L**YFLVKGM
5	WWAISTAAM**L**YILYV**L**FFGFT
3	EQNPIYWARYADW**L**FTTPL**L**LLDALL
7	NIETLLFMVLDVSAKVGFG**L**ILLR
	* *
Conserved sequence	L L

5.4 Summary

Molecular mechanics and dynamics to were used to study helix-lipid interactions in receptor 3D modelling, specifically, on the complex system represented by the FcεRI. This 7-helix receptor has a four polypeptide subunits ($\alpha\beta\gamma_2$) and its integration in the bilayer depends on the lipid-protein and protein-protein interfaces. The competition between helix-helix and lipid-helix interactions is considered to determines the correct fold of the receptor. Membrane lipids were found necessary to preserve the interactions between the α- and β-subunits during FcεRI purification (Rivnay, et al., 1982).

In this study of the interactions between the six different helices (α, β1, β2, β3, β4 and γ) of the 7-helix FcεRI with palmitic fatty acid, distinct differences in the hydrophobic surface of each helix was detected as a function of rotation of the PFA ligand around the helix axis. The PFA-TM helix interactions were generally hydrophobic, but stabilizing polar interactions between Trp, Ser, Tyr residues and sometimes CONH backbone groups and the fatty acid COOH group were detected. This type of data should contribute to a better understanding and modelling of helix-helix and helix-lipid interaction within a bilayer. PFA could interact with either end of a helix and therefore these studies contributed to understanding PFA complexes with each end of helix within a bilayer leaflet.

The above approach to mapping the relative hydrophobicity of helix surfaces, both along the helix and around the helix, produced interesting and potentially useful results for the FcεRI. Generally, as a function of rotational angle, a bimodal curve resulted with two low affinity and two high affinity surfaces per helix. In some helices, only one predominant high affinity surface was discovered, but sometimes there were three surfaces. The results obtained here were in good agreement with the hydrophobic surface mapping of the TM helices with dodecane (Chapter 4.). Although there were exceptions, the same surface

properties were observed in both outer and inner leaflets. The exceptions usually involved surfaces in which Trp, Ser, Thr, and Tyr residues occurred at the TM helix ends. These residues formed hydrogen bonds with the COOH group of the palmitic acid. It is proposed that these TM helices surface of high lipid affinity could be facing lipids and possibly, by corollary, would not usually form the helix-helix contact surfaces.

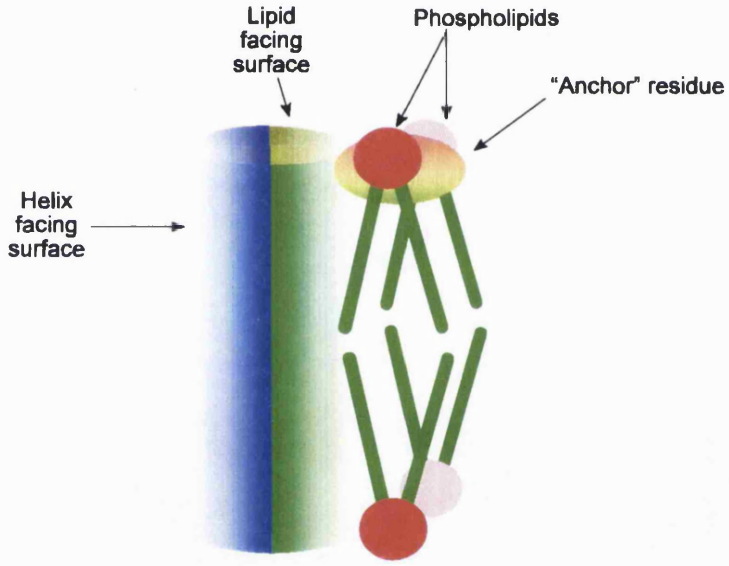

Figure 5.20 The schematic representation of the amphipatic TM helix surrounded by phospholipids with helix facing side (blue), lipid facing side (green) and anchor residue (Trp, Tyr, Ser and Thr) in the hydrophilic-hydrophobic interface.

For example, it is known that Trp [Shiffer, et al., 1992; Hu et al., 1993; Hu and Cross, 1995; Hu et al., 1995] and Tyr [Weiss et al., 1991] residues at the end of the TM helix are oriented at the hydrophobic - hydrophilic interface and therefore define the lipid facing side of the TM helix. Polar residues at the ends of the TM helix could therefore serve as anchors for lipids. Thus it could be one of the factors that drives the TM helix into the correct fold of the transmembrane bundles (Figure 5.20). The results of this chapter were used as part of the data basis in the Chapter 7, in order to propose the putative model of the β-subunit.

Chapter 6.

DOCKING OF THE TM HELICES OF THE HIGH AFFINITY IGE RECEPTOR

6. DOCKING OF THE TM HELICES OF THE HIGH AFFINITY IGE RECEPTOR

6.1 Background

The basic structural building block in plasma membrane proteins of both prokaryotic and eukaryotic cells is the apolar, often slightly amphipathic, transmembrane α-helix. A major problem in membrane protein structure prediction is the transmembrane helix arrangement and how to effectively calculate this from the amino acid sequence [von Heijne and Manoil, 1990]. At present, this is best attempted using hydrophobicity analysis algorithms, where the amino acid sequence is scanned to locate segments rich in apolar residues. The most suitable helix-helix packing arrangements are then sought using rules derived from soluble helical proteins and by rotating the helices such that the most hydrophobic sides face the lipids [von Heijne, 1992]. While the apolar surfaces of the transmembrane helices provide a surface for interaction with the lipid environment, the more polar character of the inward-facing amino acids favours the spontaneous formation of helical bundles with polar surfaces removed from lipid environment [Rees et al., 1989].

Helix-helix packing also plays an important role in the forming of TM helix bundles. This type of interaction has been studied by molecular modelling and mutagenesis, and revealed the dimerization motif for the transmembrane helices of the glycophorin A [Lemmon et al., 1994]. Mingaro et al., 1997 later showed that duplication of the critical interface (dimerization motif) on the lipid exposed side of the TM helix of glycophorin induced the tetramer formation. Their results suggested that the amino acid

sequence of TM helices contains information which directs specific interactions. The docking of the TM helices was also used to study the arrangement in TM helix bundles [Vakser, 1995; Vakser, 1996a; Vakser, 1996b].

The high affinity IgE receptor consists of four subunits, α, β and two indentical γ, and it has been proposed to possess 7 TM helices. The arrangement of the TM helices within the membrane is unknown and it could, in principle, adopt any arrangement (some examples are shown Figure 6.1). The three dimensional structures of the individual TM helices, and the helix - helix interactions in the high affinity IgE receptor are also unknown. Since the direct experimental structure determination of the intact receptor is generally beyond the capability of modern experimental technology, other ways often hybrid theory with experiments have to be used to elucidate the 3D structure. The TM helices of the high affinity IgE receptor do not contain the previously described dimerization motif [Lemmon et al., 1992; Lemmon et al., 1994] in their sequences and the sequences of its subunits are not homologous to the *Bacteriorhodopsin* GPR receptor family or any other membrane protein of known structure.

The computational search described by Lemmon et al., 1994 is also not practical for this receptor, since it would lead to 1920 combinations to be studied by the simulated annealing approach. The three dimensional structures of the TM helices, as well as, the helix - helix interactions in the high affinity IgE receptor were therefore studied, at first, using a low resolution docking procedure [Vakser, 1995; Vakser, 1996a; Vakser, 1996b]. All possible pairs of the six TM helices , namely β1 - β2; β1 - β3; β1 - β4; β2 - β3; β2 - β4; β3 - β4, α - γ, α - β1, α - β2, α - β3, α - β4, γ - β1, γ - β2, γ - β3, γ - β4, and γ - γ, were docked and the results yielded 10 lowest energy complexes for each pair varying from -353.4 to -149.2 kcal/mol.

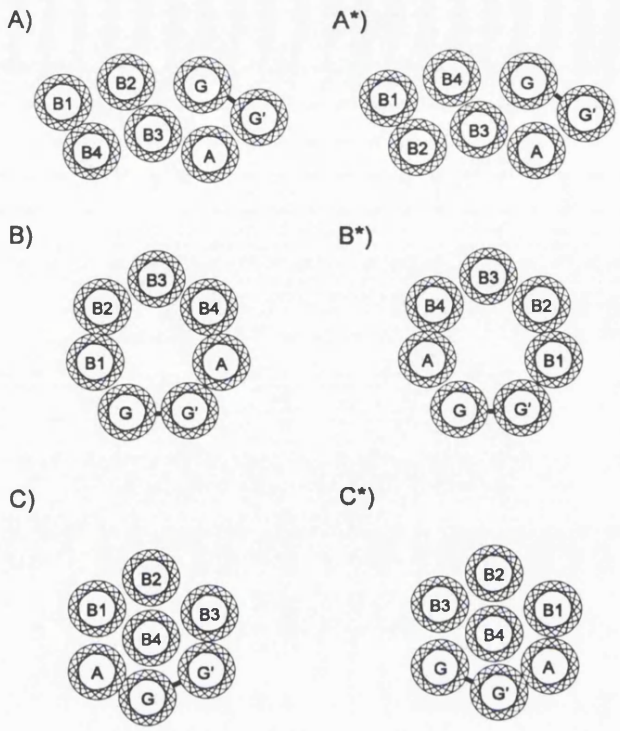

Figure 6.1 Some examples of the possible clockwise and anticlockwise arrangements of the TM helices of the high affinity IgE receptor: A) *Bacteriorhodopsin* type, B) channel type, and C) circular type arrangements (* denotes the anticlockwise arrangement).

The procedure for the docking of the TM helices into a four helix bundle for the β-subunit was chosen in such way to explore possible combinations of the helix - helix packing. In the first instance, all possible combinations of the TM helix pairs were used (β1 - β2; β1 - β3; β1 - β4; β2 - β3; β2 - β4; and β3 - β4). For every one of these 6 pairs, 10 dimeric structures were obtained which were then divided into clusters using NMRCLUST. The representative (lowest energy) structures of each cluster were chosen to add a third helix, so that three helix bundles were formed. For example, some bundles were listed: β1 - β2 - β3; β1 - β2 - β4; β1 - β4 - β2; β1 - β4 - β3; β3- β2 - β4; etc (the order of helices in

the bundles corresponded to the order in which helices were added). The clusters of each three helix bundle were obtained and representative structures were chosen for further docking. The fourth (missing helix) was docked to each structure and four helix bundles were obtained. Some were listed in this example: β1 - β2 - β3 - β4; β1 - β2 -β4 -β3; β1 - β3 - β2 - β4; β1 - β3 - β4 - β2; etc. No distance or any other constraints were used during this docking procedure. The bundles were analysed for the correct orientation .The NMRCLUST program was used to choose the 19 representative bundles out of 35 were chosen for further modelling.

6.2 Methods

6.2.1 Docking of the TM helices of the high affinity IgE receptor

All calculation described in this section were performed on the SGI O2 workstation with 64 MB RAM and 6 GB hard disk. The TM helices were constructed in the same manner as described in the previous section. In this work the version 6.3 and 6.4 of SYBYL were used. The GRAMM software was used for the low resolution docking of the TM helices [Vakser, 1995; Vakser, 1996a; Vakser, 1996b]. Parameters for the low resolution docking were: the matching mode = helix, grid step = 4.1, angle for the rotation = 20°, representation = all, potential range type = grid step, repulsion = 11, attraction double range = 0, number of the produced low energy structures = 10. Orientation of the TM helices was same as in the topographical model shown in the Figure 1.2.

The analysis of the resulting structure was performed with NMRCLUST and Webmol [Walter, 1997] software. Hydrophobic moments in units of hydrophobicity values for TM helices were calculated according to Eisenberg et al. 1982.

The helix packing parameters were shown and defined in Figure 6.2. The crossing angle (Ω) values were calculated as a dihedral angle defined by four points; one at the end of each helix axis, and two the two points of closest approach on the helix axis by WebMol software [Walter, 1997]. A positive crossing angle represents the left-handed supercoil helix pair, and a negative value is the right-handed supercoil helix structure.

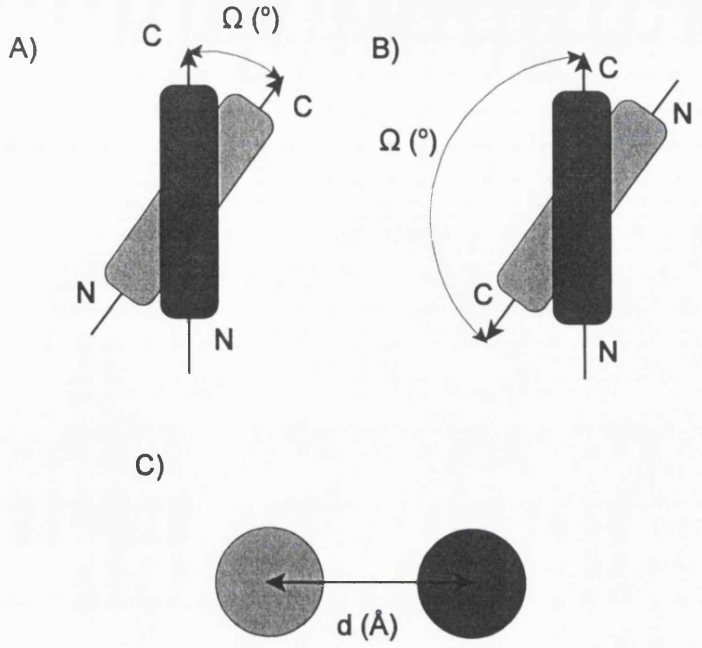

Figure 6.2 Definition of the helix packing parameters A) torsion (crossing, Ω) angle and smallest distance between helix axes. Note, Ω = 0° corresponds to exactly parallel helices and Ω = ±180 ° corresponds to exactly antiparallel helices. Therefore, Ω = 0° is quasi-equivalent to Ω = -180°.

6.3 Results and Discussion

6.3.1 Docking the TM helices of the β-subunit into helix pairs

All the results obtained by the docking procedure were analysed for the energy of interaction, geometry of packing and for the arrangement of the hydrophobic moments. The contact surfaces formed between the pairs of the TM helices were also compared to the helix exposed surfaces as determined by calculations in Chapter 5.

6.3.1.1 Interaction between TM helix β1 and TM helix β2 of β-subunit

The ten lowest energy complexes of TM helices 1 and 2 of the β-subunit produced by GRAMM software are shown in Figure 6.3. One specific surface on TM helix β1 interacted with essentially same surface of TM helix β2 in all 10 structures. The resulting ten structures were then subjected to simulated annealing calculations and the most stable complex was analysed (E_{VDW} = -31.6 kcal/mol; E_{elec}=-4.4 kcal/mol). In this helix dimer, the distance of the closest approach between two helix axes was 8.7 Å and the dihedral (crossing) angle was -173°. This was essentially an antiparallel left-handed orientation of the helix pair with the hydrophobic moments of the two helices oriented as in Figure 6.3. The hydrophobic moment of the TM helix 1 was oriented towards the TM helix 2, while hydrophobic moment of the TM helix 2 was oriented away from the TM helix 1.

The unique interface on the TM helix 1 included Phe60, Val63, Thr64, Leu67, Leu70, Ile71, Cys74, Thr77, Val78 and Ser81. These residues were partially in the potential lipid exposed side as determined in the calculations with PFA (Figure 5.5A), but they were not part of the contact between helix and lipid in the most stable complex of TM helix 1 and PFA.

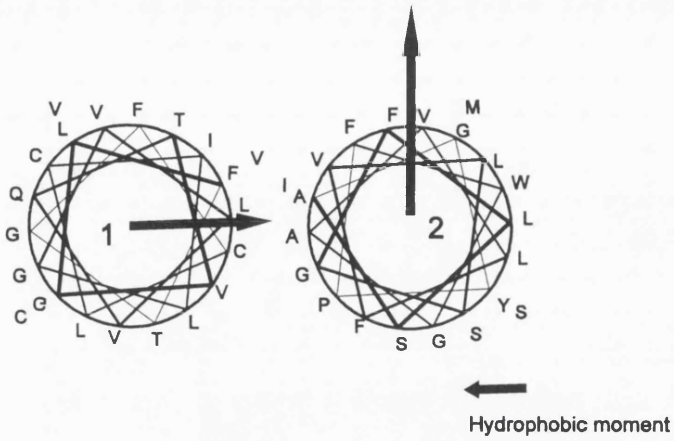

Figure 6.3 The helical wheel of the complex between TM helix 1 and TM helix 2 of the β-subunit of the high affinity IgE receptor calculated by GRAMM. The direction and size of the hydrophobic moment of each helix is represented by an arrow in the helical wheel plots.

The residues of the TM helix 2 involved in the interaction were G99, P101, F102, A105, F108, V109, G112, S115, I116 and M117. This contact surface was the same as the PFA interaction site as determined in the Chapter 5 (Figure 5.8A). The information from two different experiments, namely lipid mapping and helix-helix docking, were not in agreement for the coiled-coils calculated in this section. Such disagreement of the two experiments indicated that this unique interface prediction required modification. This was partly done by adding a further data set.

6.3.1.2 Interaction between TM helix β1 and TM helix β3 of the β-subunit

The result of the above docking procedure was also applied to the TM helix β1 and TM helix β3(Figure 6.4). The interaction between TM helices 1 and 3 was not specific,in the sense that several surfaces of TM helix β1 formed complexes with several TM helix β3 surfaces. This reflects the probability that TM helix β1 and TM helix β3 would have little contact if the β-subunit form a 4 helix bundle? These results were therefore not considered in the further modelling of the four helix bundle.

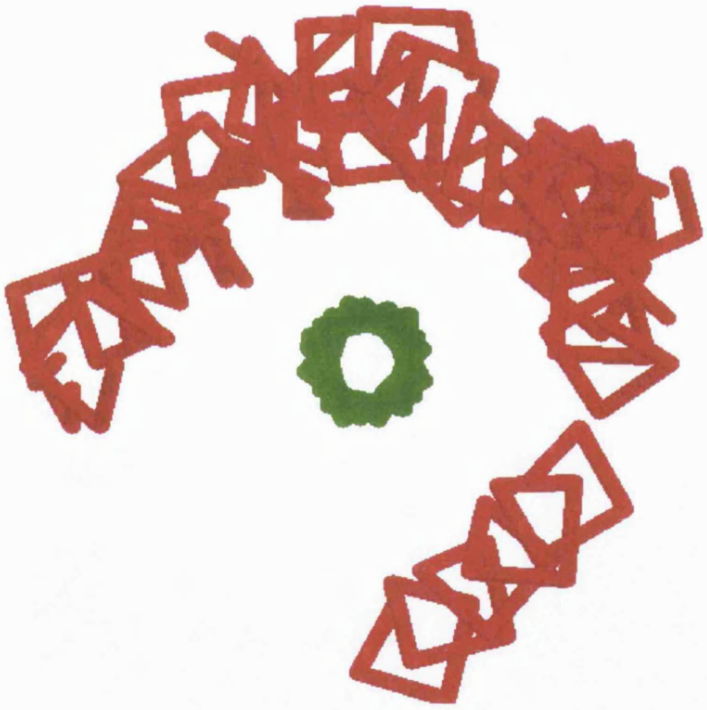

Figure 6.4 The overlap of the complexes between TM helix β1 (green) and TM helix β3 (red) of the β-subunit of the high affinity IgE receptor calculated by GRAMM.

6.3.1.3 Interaction between TM helix β1 and TM helix β4 of the β-subunit

The results of the docking procedure applied to the TM helix β1 and TM helix β4 are shown in Figure 6.5. The most stable complex produced by the simulated annealing protocol (E_{VDW} = -46.5 kcal/mol and E_{elec} = -4.7 kcal/mol) was again analysed. The distance of closest approach between two helix axes was 10.4 Å and dihedral (crossing) angle was -177° which indicated the antiparallel orientation of the helix pair. The hydrophobic moments of the two helices were oriented as shown in Figure 6.5. and should be compared with Figure 6.3 for β1-β2 helix pair.

The Phe60, Thr64, Leu67, V68, L70, Ile71, Cys74, Phe75, T77, Val78 and Ser81 residues of the TM helix β1 were involved in the interaction with TM helix β4. Those residues were also involved in the interaction with the TM helix β2. There could therefore be a possible competition between TM helix β2 and TM helix β4 for the same binding interface on the TM helix 1.

The V181, Leu182, Leu185, Ile189, Phe192, A195, Val196 and Ile199 residues of the TM helix 4 were involved in the interaction with TM helix 1. Many of these TM helix 4 residues were involved in forming both stable and less stable complexes with PFA, but still it could be concluded that the helix surface at the 90° rotational position (when interacted with PFA) preferred interaction with the another helix and with the lipid?

6.3.1.4 Interaction between TM helix 2 and TM helix 3 of the β-subunit

The NMRCLUST software was used to evaluate ten low energy β2-β3 helix pairs. Examination of these helix pairs revealed that TM helix β3 had only two surfaces that interacted with the TM helix β2 (Figure 6.6). Further examination revealed that three β2

helix surfaces could interact with "surface I" of TM helix β3, whereas only one β2 surface interacted with "surface II" of TM helix β3. In all this meant that there were four possible β2-β3 helix pairs (clusters of helix pairs).

The energy of the interaction in the representative structure of the first cluster was E_{VDW} = -23.3 kcal/mol and E_{elec} = -6.8 kcal/mol. The distance of closest approach between the helix axes was 9.6 Å and the crossing angle was 158°, indicating a antiparallel right - hand oriented helix pair. The hydrophobic moments were oriented away from the helix - helix interface (Figure 6.6A). Such arrangement was consistent with usual orientation of the TM helices when the helix bundles were constructed, but the further data are necessary to choose correct orientation.

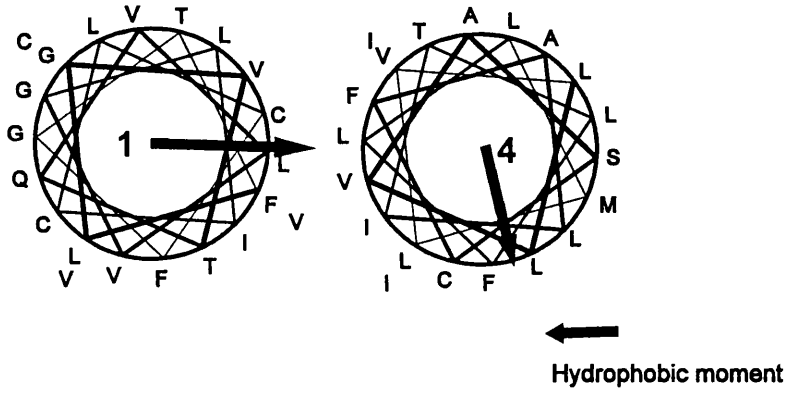

Figure 6.5 The helical wheel presentation of the complex between TM helix β1 and TM helix β4 of the β-subunit of the high affinity IgE receptor calculated by GRAMM. The direction and size of the hydrophobic moment of each helix is represented by an arrow in the helical wheel plots.

The A98, G99, F102, W103, V106, L110 and F113 residues of the TM helix 2 interacted with the N134, I135, S138, I139, G142, L143, I145, A146 and I149 residues of TM helix 3 of the β-subunit in first cluster. The interacting interface of the TM helix 2 could be partially involved in the interaction with lipids as determined in the Chapter 5 (Figure 5.8A), so it might not be the best choice as the helix interaction surface. The contact interface of the TM helix 3 was involved in the forming least stable complex with PFA, and in that sense could be a good preference for the β2 helix - β3 helix interface?

The helical wheel presentation of the second cluster is shown in Figure 6.6B, together with hydrophobic moments of the TM helices. The energy of the interaction in the representative structure of this cluster was E_{VDW} = -18.5 kcal/mol and E_{elec} = -22.8 kcal/mol. The distance of closest approach was 9.6 Å and the dihedral (crossing) angle was 151°. Again, it was an antiparallel right-hand oriented helix pair and the hydrophobic moments did not face the helix-helix interface. The residues A98, G99, F102, W103, V106, V109, L110 and F113 were involved in the interaction with TM helix 3. Some of those residues formed the stable complex with PFA, but they could also be involved in the helix - helix contact. The V136, S137, A140, L143, G144, I147 and L148 residues of the TM helix 3 were in the contact with TM helix 2 in the second cluster. These residues were not involved in the forming the most stable complex between the helix and PFA (Figure 5.11A), but since the energy difference was small, it could be difficult to accept or reject this cluster as a correct solution for the docking problem.

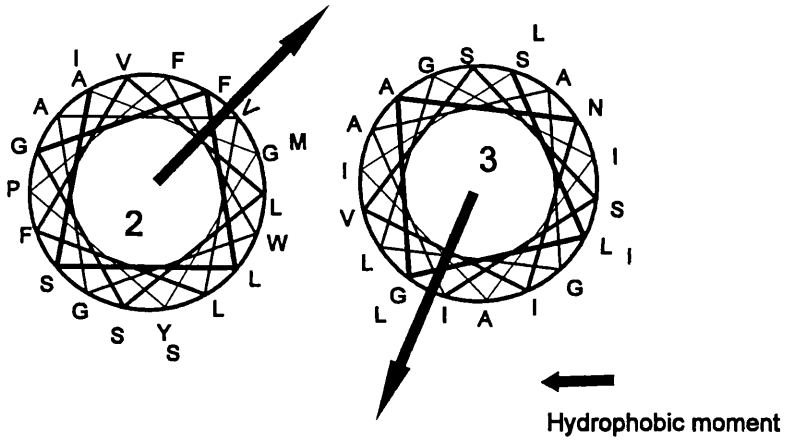

Figure 6.6A The helical wheel presentation of the first complex between TM helix β2 and TM helix β3 of the β-subunit of the high affinity IgE receptor calculated by GRAMM. The direction and size of the hydrophobic moment of each helix is represented by an arrow in the helical wheel plots.

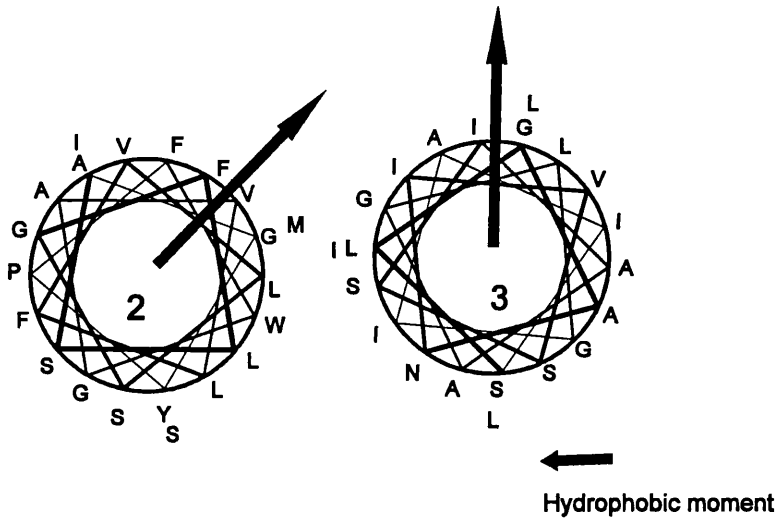

Figure 6.6B The helical wheel presentation of the second complex between TM helix β2 and TM helix β3 of the β-subunit of the high affinity IgE receptor calculated by GRAMM. The direction and size of the hydrophobic moment of each helix is represented by an arrow in the helical wheel plots.

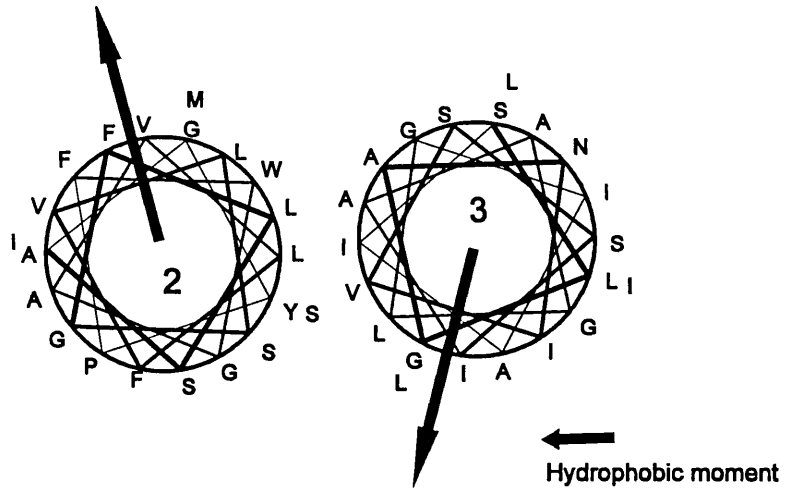

Figure 6.6C The helical wheel presentation of the third complex between TM helix β3 of the β-subunit of the high affinity IgE receptor calculated by GRAMM. The direction and size of the hydrophobic moment of each helix is represented by an arrow in the helical wheel plots.

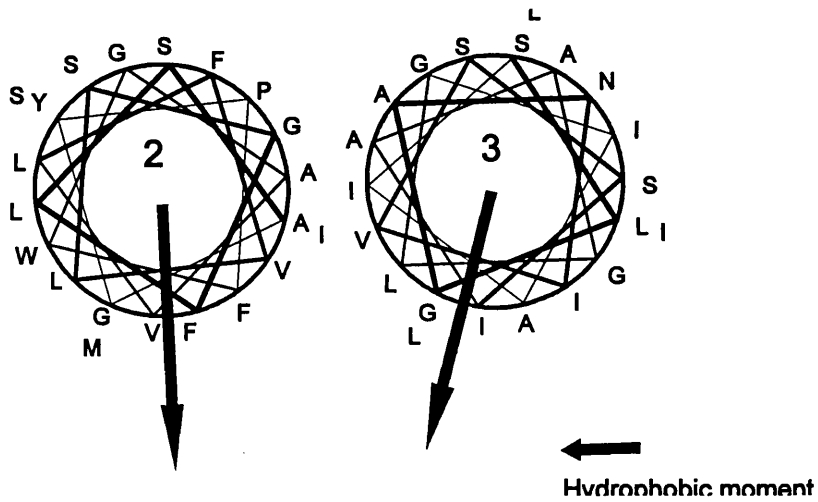

Figure 6.6D The helical wheel presentation of the fourth complex between TM helix β2 and TM helix β3 of the β-subunit of the high affinity IgE receptor calculated by GRAMM. The direction and size of the hydrophobic moment of each helix is represented by an arrow in the helical wheel plots.

The third cluster of the TM helix 2 and TM helix 3 complex is shown in Figure 6.6C. The energy of the interaction in the representative structure of this cluster was E_{VDW} = -16.3 kcal/mol and E_{elec} = -23.9 kcal/mol. The distance of closest approach was 9.6 Å and the dihedral (crossing) angle was 151°. The energy of interactions and geometry of packing values were same as for the second complex, but the interaction interface was different, with the hydrophobic moments orientation not facing contact interface. The P101, F102, L107, F108, S111, L114, S115 and M117 residues of the TM helix β2 were involved in this contact interface. If we compare with results from Chapter 5 (Figure 5.8A), we found that some of these residues (P101, F102 and F108) could be involved in the fatty acid interaction site, but most could be involved in the interaction with other helices. The TM helix β3 residues, L131, G132, N134, I135, S138, I139, I145, A146, I149 and L150, were involved in the interaction with TM helix β2 in the third complex. Comparison with results from Chapter 5 (Figure 5.11A) showed that only some residues could be involved in the helix-helix interaction (I139 and L150) and the rest of them could be part of the fatty acid binding site? Following this, the third complex should not be appropriate as a solution for the docking of the TM helices 2 and 3. Still, the representative structure was also used as a starting structure in the docking of the four helix bundle of the β-subunit.

The representative structure of the fourth cluster (Figure 6.6D) was the most stable with largest interaction energies (E_{VDW} = -34.5 kcal/mol and E_{elec} = -45.3 kcal/mol). The distance of closest approach was 9.0 Å and the dihedral (crossing) angle was 140°. The contact interface in that cluster on the TM helix β3 was the similar to a contact surfaces on TM helix β3 in the first and third clusters (it involved residues N134, I135, S138, I139, G142, I145, A146, I149, L150), with most residues that could be part of the fatty acid binding site. The contact interface on the TM helix 2 was different (G99, Y100, P101,

F108, V109, G112, F113 and I116) from that in the other three clusters. According to Chapter 5. results (Figure 5.8A), most of the these residues should be involved in the fatty acid binding site. Since the contact interface of both helices could be a lipid binding site, this fourth cluster might not be a proper solution for the docking problem despite the high stabilization energy of the complex. The competition between helix - helix and lipid - helix interactions could determine the correct folding of the four helix bundle.

6.3.1.5 Interaction between TM helix 2 and TM helix 4 of the β-subunit

Again, as with the β2-β3 helix pair two distinct interaction surfaces were detected on the TM helix β2 for the TM helix β4, but only one β4 surface was found to interact with the two β2 surfaces. This clearly predicted two possible interfaces between these two TM helices. The energy of the interaction in the representative structure of the first cluster was E_{VDW} = -25.6 kcal/mol and E_{elec} = -6.4 kcal/mol and the distance of closest approach was 9.0 Å and the dihedral (crossing) angle was -40° (parallel right-handed helix pair). The hydrophobic moments were oriented outside of the helix - helix interface (Figure 6.7A). The interface of the representative structure of the first cluster involved A98, G99, F102, W103, V106 and L110 of the TM helix β2 and L184, L187, T188, L190, A191, F192, S194 and A195 residues of TM helix β4. Most of these residues were not predicted as a part of the fatty acid binding site (Figures 5.8A and 5.14A), and therefore this cluster could be considered as a correct prediction of the arrangement of TM helices β2 and β4.

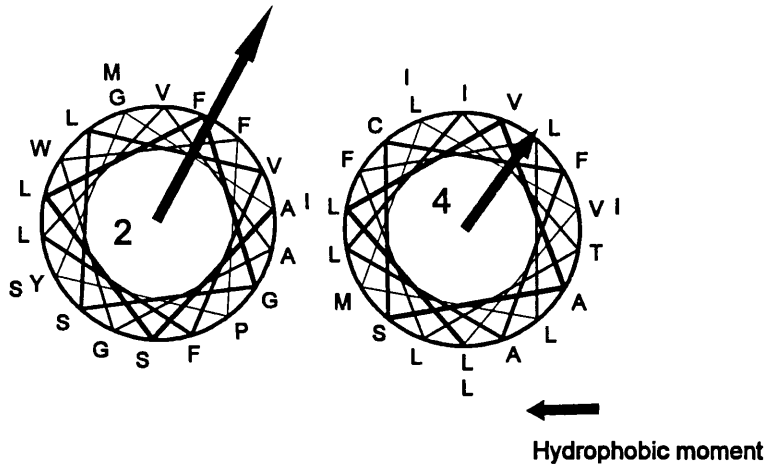

Figure 6.7A The helical wheel presentation of the first complex between TM helix β2 and TM helix β4 of the β-subunit of the high affinity IgE receptor calculated by GRAMM. The direction and size of the hydrophobic moment of each helix is represented by an arrow in the helical wheel plots.

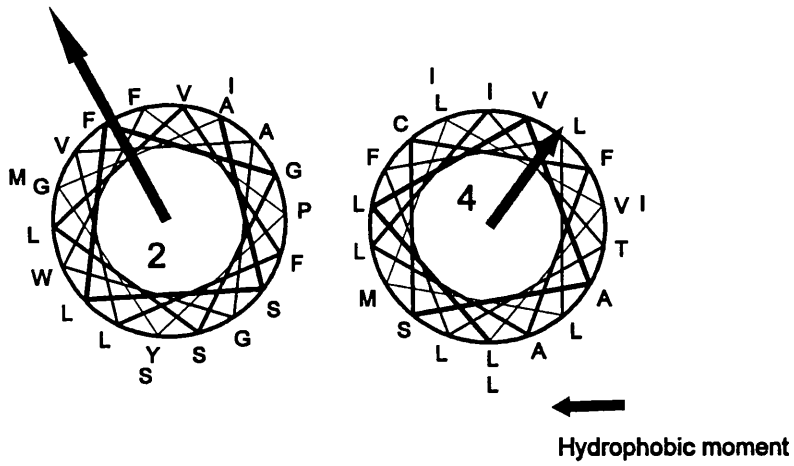

Figure 6.7B The helical wheel presentation of the second complex between TM helix β2 and TM helix β4 of the β-subunit of the high affinity IgE receptor calculated by GRAMM. The direction and size of the hydrophobic moment of each helix is represented by an arrow in the helical wheel plots.

The energy of the interaction in the representative structure of the second cluster was E_{VDW} = -34.7 kcal/mol and E_{elec} = -4.3 kcal/mol. The distance of closest approach was 9.5 Å and the dihedral (crossing) angle was 21° (parallel left-handed helix pair). The hydrophobic moments were again oriented outside of the helix - helix interface (Figure 6.7B). The contact interface included the residues Y100, W103, G104, L107, F108, L110, S111 and L114 of TM helix β2 despite the fact that the two clusters differed by 90° in selective orientation. Again, most of these residues were not predicted as part of the fatty acid binding site, and therefore this cluster could be also considered as a correct prediction of the arrangement of TM helices β2 and β4.

The representative structure of second cluster had a greater stabilization interaction energies between two helices and it could therefore be a better prediction for the correct orientation of the this two helices in the four helix bundle. However, both structures were latter used for constructing four helix bundles as described earlier.

6.3.1.6 Interaction between TM helix β3 and TM helix β4 of the β-subunit

The antiparallel arrangement of the TM helices β3 and β4 in the four helix bundle was preserved during the docking procedure. The result was 10 lowest energy complexes, that belonged to one cluster (Figure 6.8). In other words, only one surface on β3 helix and one on β4 helix interacted with to form ten β3-β4 helical pairs. The distance of closest approach between the helix axes was 8.4 Å and the torsion (crossing) angle was 163° (the antiparallel right-handed helix pair). The most stable complex (E_{VDW} = -35.0 kcal/mol and E_{elec} = -37.05 kcal/mol) had the interface between two helices constructed of Ser138, Ile139, Ala141, Gly142, Ile145, Ala146, Ile149 and Leu150 residues from TM helix β3 and L185, T188, F192, V196, I200 residues from TM helix β4. The TM helix β3 contact

surface was similar to the PFA unfavourable surface at 135° rotational position as predicted by calculation (Figure 5.11A). The contact surface of the TM helix β4 would be partially involved in the PFA binding site (residues L185, T188 and F192) as determined by calculation in Chapter 5 (Figure 5.14A). These docking results were in reasonable agreement with the molecular mechanics calculations of the interaction between TM helices and PFA as shown in the Chapter 5, and the representative structure was used as a starting structure in the docking of the four helix bundle of the β-subunit.

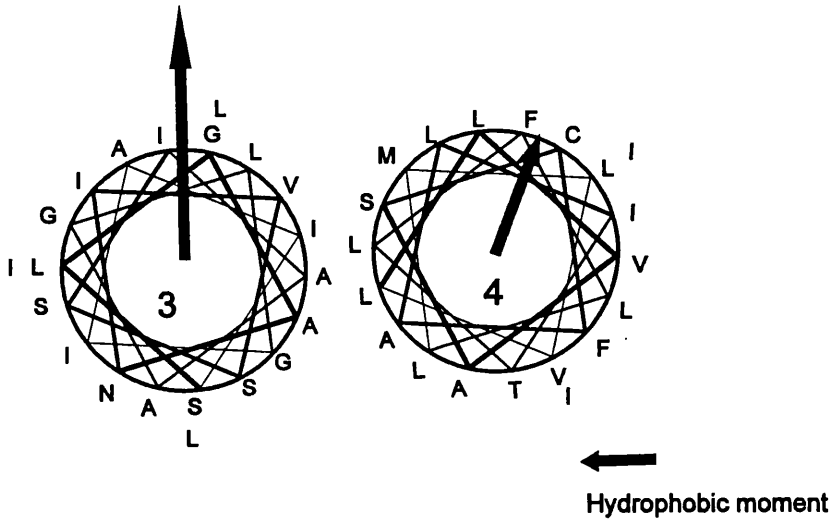

Figure 6.8 The helical wheel presentation of the complex between TM helix β3 and TM helix β4 of the β-subunit of the high affinity IgE receptor calculated by GRAMM. The direction and size of the hydrophobic moment of each helix is represented by an arrow in the helical wheel plots.

Table 6.1 Interaction energies and contact surfaces between TM helices of the β-subunit of high affinity IgE receptor obtained by docking with GRAMM software (β1, β2, β3, β4 - β-subunit; one letter amino acid code was used in the table).

Helix Pair	Cluster No.	Energy vdw; elec (kcal/mol)	Residues involved in the contact interface.
β1-β2	1	-31.7; -4.4	**β1** - F60, V63, T64, L67, V68, L70, I71, C74, T77, V78, S81; **β2** - G99, P101, F102, A105, F108, V109, G112, S115, I116, M117
β1-β3	-	-	nonspecific
β1-β4	1	-46.5 -4.7	**β1** - F60, T64, L67, V68, L70, I71, C74, F75, T77, V78, S81; **β4** - V181, L182, L185, I189, F192, A195, V196, I199
β2-β3	1	-23.3; -6.8	**β2** - A98, G99, F102, W103, V106, L110, F113; **β3** - N134, I135, S138, I139, G142, L143, I145, A146, I149
	2	-18.5; -22.8	**β2** - A98, G99, F102, W103, V106, V109, L110, F113; **β3** - V136, S137, A140, L143, G144, I147, L148
	3	-16.3; -23.9	**β2** - P101, F102, L107, F108, S111, L114, S115, M117; **β3** - L131, G132, N134, I135, S138, I139, I145, A146, I149, L150
	4	-34.5; -45.3	**β2** - G99, Y100, P101, F108, V109, G112, F113, I116; **β3** - N134, I135, S138, I139, G142, I145, A146, I149, L150
β2-β4	1	-25.6; -6.4	**β2** - A98, G99, F102, W103, V106, L110; **β4** - L184, L187, T188, L190, A191, F192, S194, A195
	2	-34.7; -4.3	**β2** - Y100, W103, G104, L107, F108, L110, S11, L114; **β4** - L185, T188, A191, F192, A195; V196, L198, I199
β3-β4	1	-35.0; -37.05	**β3** - I,135, S138, I139, G142, I145, A146, I149, L150; **β4** - L185, T188, F192, V196, I200

6.3.1.7 Summary

The docking of the six different TM helical pairs of the β-subunit studied by Gramm software yielded nine different clusters and their representative structures were analysed. The summary of the interactions between different helices in all nine clusters is shown in Table 6.1. Despite the different interaction energies observed between different helix pairs in Table 6.1, it was difficult a priori to decide which helix pair was most suitable as a starting point for further docking. The representative structure of the fourth cluster of the β2-β3 helix pair had the greatest electrostatic stabilisation energy, but the β3 - β4 cluster had a stabilisation interaction with a similar range of energies. Thus, it would be to restrictive to use the energies of interaction as the only criteria for selection of the correct orientation of the helix pairs.

The second problem encountered during this docking procedure was the non-unique selection of the helix surfaces. For example, the TM helices 2 and 4 of the β-subunit interacted with the same surface of the TM helix β1 (the surface composed of F60, V63, T64, L67, V68, L70, I71, C74, T77, V78, S81 residues). At the same time the A98, G99, F102, W103, V106, L110 residues of the TM helix 2 were preferred by all three TM helices in most representative structures. The surface composed of the S138, I139, G142, L143, I145, A146, I149 residues of the TM helix 3 was also a good target for the interaction with all other helices. In the similar fashion, the surface of the TM helix 4 containing the residues F192 and A195 was a good target for the helix - helix interaction. These predicted surfaces of the helix - helix interaction (Table 6.1) were in good agreement with the helix - helix interaction surfaces predicted in the Chapter 5 through calculation of TM helix - PFA interaction. Anyway, the correct arrangement of the four helix bundle of the β-subunit

could not be deduced using only the information obtained only from the docking of the helix pairs, and the docking of four helix bundle had to be performed.

6.3.2 Docking the TM helices of the β-subunit into four helix bundle.

The procedure for the docking of the TM helices into four helix bundle of the β-subunit was chosen in such way to explore possible combinations of the helix - helix packing and to avoid subjective criteria. The strategy of the docking protocol is outlined in Figure 6.9 using β2 - β3 helices as starting TM helix pair. In the first instance, all representative structures of clusters of the TM helix pairs were used, namely, one cluster of β1 - β2 helix pair; one cluster of β1 - β4 helix pair; four clusters of β2 - β3 helix pair; two clusters of β2 - β4 helix pair and one cluster of β3 - β4 helix pair (namely Stage I, Figure 6.9). To every one of these 9 structures, a third helix was docked, so that putative three helix bundles were formed. Example of some of these bundles are listed: β1 - β2 - β3; β1 - β2 - β4; β1 - β4 - β2; β1 - β4 - β3; β3- β2 - β4; etc (Stage II, Figure 6.9). The order of helices in the bundles corresponded to the order in which helices were added. The clusters of each three helix bundle were obtained and representative structures were chosen for further docking. The fourth (missing helix) was docked to each representative structure and four helix bundles were obtained (Stage III, Figure 6.9). Some were listed in this example: β1 - β2 - β3 - β4; β1 - β2 - β4 - β3; β1 - β4 - β2 - β3; β1 - β4 - β3 - β2; β3- β2 - β4 -β1; etc. The resulting helix bundles were different depending on the order in which the helices were added, as shown for β2 - β3 helices as starting TM helix pair in Figure 6.9.

Figure 6.9 The schematic representation of the strategy for building the four helix bundle, using the TM helix β2 and TM helix β3 as a starting helix pair in this example.

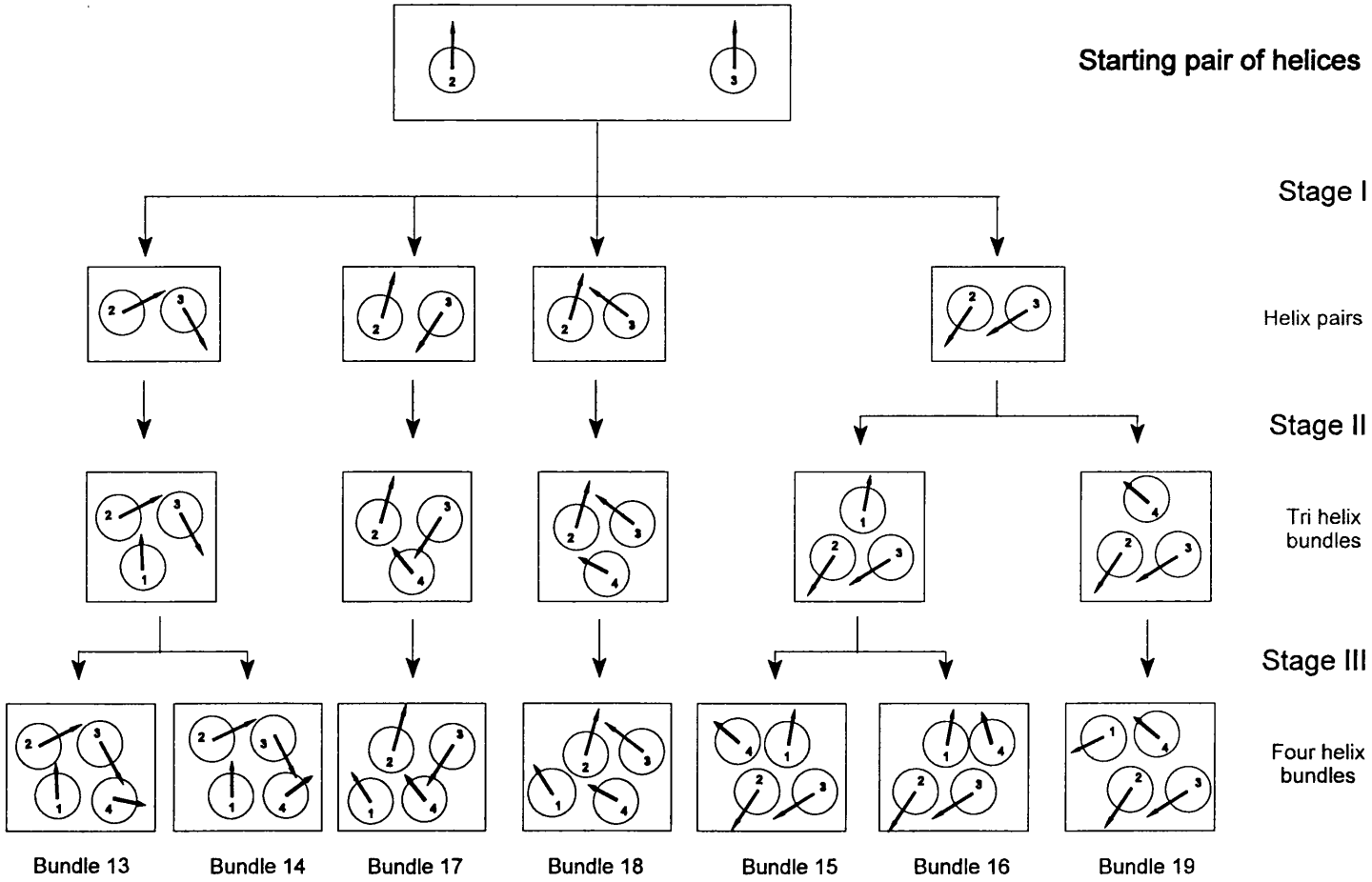

The summary of the interaction energies and geometry of the four helix bundles of the β-subunit is presented in Table 6.2. The order of adding helices to the bundle is shown as a number, for example, the 1423 means that in the first instance the TM helices β1 and β4 were docked, then the helix β2 was added and the four helix bundle was formed by docking TM helix 3. The clusters obtained during docking of pairs are denoted as I, II, III or IV, and clusters of the three helix bundles are denoted as small letters (a or b). Some four helix bundles formed more than one cluster and their representative structures were minimized and analysed. The energies of the interaction between helices within four helix bundle were denoted as E_{vdw} - van der Waals. The Ω(°) - torsion (crossing) angle and d(Å) - distance of the closest approach between helix axes were calculated by WebMol software. The orientation was assigned using the view from the top of the membrane. The crossed loop term was used to describe the arrangement of the TM helices in which two non-neighbouring helices in the sequence were neighbours in the bundle; even the loops were not present in the bundles at this stage. The clusters of the four helix bundles, in which the orientation of the TM helices were not in agreement with the proposed topology by Blank et al, 1989, were discarded.

The representative structures of thirty five different clusters of four helix bundles of the β-subunit are presented in Table 6.2. Sixteen structures with crossed loops were observed. The distance between the ends of TM helices could be greater than the length of the loop peptides in folded conformation. According to statistical criteria [Finkelstein et al., 1995] such helix bundles are less likely to appear in the nature. Crossing of loops is very rare; it either demands additional loop bending or dehydrates a peptide group. Such "defects" may demand a few kcal/mol [Finkelstein, 1987]. Therefore, those bundles with crossed loops have not been analysed further in this work. This included those structures

which had interaction energies similar to those of the clockwise or anticlockwise arrangements. Twelve structures after docking had the clockwise arrangement of the four helix bundle, while only seven had the anticlockwise arrangement. The four helix bundle structures with clockwise arrangements had van der Waals energy of the interactions in the region of -142 to -180 kcal/mol, while the anticlockwise four helix bundle had van der Waals energy of the interaction in the range of -141 to -171 kcal/mol. The contribution of the electrostatic interaction energies was low, ranging from +10 to -15 kcal/mol for both arrangements. This could be explained by the general absence of the charged residues in the sequences of the TM helices of the β-subunit. For example, it has been proposed that charged interactions, if present, can dominate the final arrangement of the TM helices within membrane proteins [Green, 1991]. Since charge interaction constraints were absent, there were no obvious charged constraints in the arranging of the bundles. According the previous deductions, the clockwise arrangement could have the higher probability of appearing in the final structure of the four helix bundle of the β-subunit.

The Ω (crossing) angle was observed for all combinations of the helix pairs and it was shown in Table 6.2. The crossing angle was in the range of -176 to -121° and 125 to 175° for the pair of TM helices 1 and 2. It indicated that the antiparallel topology , and both, left and right-handed helix bundle orientations were possible. Similar observations were found for the other TM helix pairs; they had the correct topology, but they could have left-handed or right-handed helix bundle orientations. Therefore, both, left-handed and right-handed helix bundle orientations could be observed in the bundles and no generalisation could be drawn from these structures. That was expected since the starting structures (helix pairs) in the docking procedures were left-handed or right-handed helix pairs.

Table 6.2 Energetic and orientation analysis of the four helix bundles of the beta subunit of high affinity IgE receptor formed by Gramm software; E_{vdw} - van der Walls interaction energies between TM helices of the four helix bundles, Ω(°) - torsion (crossing) angle between helix axes, d(Å) - distance of the closest approach between helix axes, arrangement was assigned as observed from the top of the membrane.

Bundle	Order of adding helices	Four helix bundle clusters	E_{vdw} (kcal/mol)	TM helix pairs within bundle												Arrangement
				1-2		1-3		1-4		2-3		2-4		3-4		
				Ω(°)	d(Å)	Ω(°)	d(Å)	Ω(°)	d(Å)	Ω(°)	d(Å)	Ω(°)	d(Å)	Ω(°)	d(Å)	
1	1234	1	-170.0	-173	8.7	22	12.4	-160	11.4	-164	9.1	27	17.4	-166	10.9	OK - clockwise
2	1234	2	-172.4	-173	8.7	22	12.4	-162	9.5	-164	9.1	34	12.6	177	10.3	OK - clockwise
3	1234	3	-173.0	-173	8.7	22	12.4	-172	11.5	-164	9.1	17	17.6	-170	9.7	OK - clockwise
4	1234	4	-159.0	-173	8.7	22	12.4	-156	10.8	-164	9.1	23	16.1	-154	10.3	OK - clockwise
5	1243	1	-172.3	-173	8.7	42	20.0	-159	12.3	-171	10.9	11	9.1	-164	9.4	OK - clockwise
6	1243	2	-189.5	-173	8.7	11	11.0	-159	12.7	26	14.5	11	9.1	-160	8.2	Crossed loops
7	1243	3	-174.2	-173	8.7	20	9.9	-159	12.3	18.8	16.0	11	9.1	-177	10.3	Crossed loops
8	1423IIa	1	-145.8	-153	11.4	19	8.5	-153	10.6	-168	9.2	19	11.6	-146	18.8	Crossed loops
9	1432Ia	1	-158.9	178	10.5	1	9.9	-158	10.8	167	9.6	14	20.8	-165	13.8	OK- anticlockwise
10	1432Ia	2	-149.6	-153	15.2	1	9.9	-158	10.8	-155	9.9	9	18.9	-167	13.8	Crossed loops

11	1432IIa	1	-162.4	-165	19.7	45	11.8	-153	10.1	157	9.8	-5	9.1	176	8.8	Crossed loops
12	1432IIa	2	-129.8	-151	10.6	45	11.8	-153	10.1	173	9.8	-10	18.8	176	8.8	OK- anticlockwise
13	2314Ia	1	-166.3	157	9.6	-32	10.4	160	11.4	173	9.1	32	16.8	-142	12.5	OK - clockwise
14	2314Ib	2	-150.2	157	9.6	-32	10.4	160	11.2	173	9.1	33	17.3	-145	10.2	OK - clockwise
15	2314IVa	1	-173.2	-168	11.5	-43	10.4	151	9.1	-164	9.8	44	16.1	-159	9.9	Crossed loops
16	2314IVb	2	-161.3	151	11.5	-43	10.3	145	10.9	160	9.2	-33	9.4	120	17.3	Crossed loops
17	2341IIb	1	-156.7	-132	13.7	48	15.4	174	10.6	-145	9.1	62	9.8	-124	8.6	OK - clockwise
18	2341III	1	-142.1	178	9.2	-12	18.6	-162	11.4	-164	9.5	15	10.8	156	10.8	OK - clockwise
19	2341IV	1	-144.8	-121	14.6	56	9.2	-163	20.2	146	10.7	-40	12.8	154	10.6	OK- anticlockwise
20	2413Ia	2	-165.1	-157	9.5	25	9.6	-160	10.9	-139	17.0	26	9.0	-154	10.6	Crossed loops
21	2413IIa	1	-143.6	125	11.3	-32	9.8	143	10.8	118	22	-22	8.8	-154	10.6	Crossed loops
22	2431Ia	1	-147.9	-130	11.6	41	20.1	-141	10.1	-164	9.4	26	9.0	-164	10.2	OK- anticlockwise
23	2431Ia	2	-170.5	-154	17.0	19	10.4	-165	10.3	-164	9.4	26.4	9.0	-164	10.2	Crossed loops
24	2431IIa	2	-163.4	128	17.6	-19	10.5	152	11.4	145	10.4	-41	9.8	150	12.3	Crossed loops
25	3412Ia	1	-179.9	172	8.2	-10	11.7	-170	10.0	-163	10.2	18	11.8	164	8.4	OK - clockwise
26	3412Ia	2	-156.0	-175	20.0	-10	11.7	-170	10	176	10.5	-10	10.0	164	8.4	Crossed loops
27	3412Ib	1	-165.8	-154	12.3	6.5	10.5	178	10.1	-155	9.6	19	10.3	164	8.4	OK- anticlockwise
28	3412IIa	1	-164.1	162	6.3	-33	9.8	159	9.5	-174	18.6	21	10.3	154	8.2	Crossed loops

29	3412IIb	1	-171.0	-176	7.8	12	12.4	172	11.5	179	10.6	24	16.9	154	8.2	OK- anticlockwise
30	3412IIIa	1	-162.8	162	10.4	-39	10.2	140	9.8	135	19.0	-45	11.7	159	8.8	Crossed loops
31	3421Ia	1	-154.6	179	19.7	-13	11.6	-164	9.5	176	11.7	-10	9.9	164	8.4	Crossed loops
32	3421IIa	1	-168.6	157	9.1	-29	1.9	166	11.8	-179	11.5	-18	10.0	154	8.2	OK - clockwise
33	3421IIIa	1	-170.9	153	10.2	-60	19.2	142	9.6	138	9.2	-37	7.9	159	8.8	OK- anticlockwise
34	3421IIIb	1	-161.5	155	8.5	-10	10.2	172	10.8	155	12.2	-12	10.1	159	8.8	Crossed loops
35	3421IIIb	2	-153.8	169	10.9	-30	19.3	168	10.9	155	12.2	-12	10.1	159	8.8	OK - clockwise

Table 6.3 Analysis of interactions in the four helix bundles of the beta subunit of high affinity IgE receptor formed by Gramm software. ΔSASA (%) - change in the solvent accessible surface area upon formation of four helix bundle.

Bundle	ΔSASA (%)	Residues of the beta subunit interacting in the four helix bundles			
		TM Helix 1	TM Helix 2	TM Helix 3	TM Helix 4
1	37.0	F60, V63, T64, V66, L67, V68, L70, I71, L73, C74, T77, V78, S81	A98, G99, Y100, P101, F102, G104, A105, L107, F108, S111, S115, I116, M117, S118	N134, V136, S137, A140, A141, L143, I147, L148	L185, T188, I189, F192, A195, V196, I199, I200
2	37.3	F60, V63, T64, V66, L67, L70, I71, C74, T77, V78, V79, S81	A98, G99, Y100, P101, F102, G104, A105, F108, G112, S115, I116, M117, S118	A133, N134, V136, A140, A141, L143, I145, I147, L148,	L184, L187, T188, L190, A191, F192, S194, A195
3	37.6	F60, V63, T64, V66, V68, L70, I71, L73, L67, C74, T77, V78, V79, S81	A98, G99, P101, F102, G104, A105, F108, V109, S111, G112, S115, I116, M117, S118	A133, V136, A140, L143, I145, I147, L148	L185, T188, I189, F192, A195, I199

4	34.4	F60, V63, T64, L67, V68, L70, I71, L73, C74, T77, V78, V79, C80, S81	A98, Y100, P101, F102, G104, A105, L107, F108, S111, S115, I116, M117, S118	V136, A140, A141, L143, I145, I147, L148	V181, L184, L185, T188, I189, F192
5	38.0	F60, V63, T64, L67, V68, L70, I71, C74, T77, V78 S81	A98, G99, Y100, P101, F102, W103, G104, A105, L107, F108, V109, S111, G112, L114, S115, I116, M117, S118	A133, V136, S137, L143, G144, I147, L148	V181, L184, T188, I189, A191, F192, A195, L198, I199
9	36.8	F60, G62, V63, T64, V66, L67, G69, L70, I71, C74, T77, S81	F108, I109, I116	L131, G132, I135, S138, I149	V181, M183, F186, L187, L190, L197, L198, I199
12	31.7	V63, L67, L70, I71, C74, T77, V78, C80, S81	P101, A105, F108, G112, S115, I116	I135, V136, S138, I139, L143, I145, A146, I147, I149	V181, L182, L184, F186, L187, T188, I189, A191, F192, A195, V196, I199
13	36.8	Q65, V66, G69, L70, L73, G76, T77, V79, C80	A98, G99, F102, W103, V106, V109, L110, F113	L143, I147	M183, L187, L190, A191, L198
14	33.9	Q65, V66, V68, G69, L70, L73, G76, T77, V79, C80	A98, G99, Y100, F102, W103, V106, L107, V109, L110, S111, F113, L114	N134, I135, S138, I139, G142, L143, I145, A146, I147, I149, L150	L187, L190, A191, F192, L198

17	35.9	L67, L70, I71, C74, T77, V78	Y100, F102, W103, A105, V106, L107, V110, F113, L114, S115, M117, S118	L131, N134, I135, S137, S138, A141, I145, I149, L150	T188, I189, A191, F192, S194, A195, V196, L198, I199, I200
18	34.7	L67, I71, C74, T77, V78, S81	A98, G99, Y100, F102, W103, G104, V106, L107, F108, V109, L110, F113, L114, S115, I116, M117, S118,	A133, V136, A140, L143, G144, I147, L148, I149, L150	L182, L185, T188, I189, F192, V196, L197
19	32.4	G62, Q65, V66, G69, L73	A98, G99, Y100, P101, A015, F108, V109, G112, F113, S115, I116, M117	N134, I135, V136, S137, S138, I139, A141, G142, I145, L148, I149, L150	L185, I189, F192, V196, L197, I200
22	33.5	Q65, V66, V68, G69, G76, V79	Y100, W103, G104, V106, L107, F108, L110, S111, G112, L114, S115, I116	I135, V136, S138, I139, G142, I145, I149	L184, L185, L187, T188, I189, A191, F192, A195, V196, L198, I199, I200
25	39.5	G62, Q65, V66, V68, L73, G76, V79, C80	P101, A105, L107, F108, V109, S111, G112	L131, G132, N134, I135, S137, S138, I139, G142, I145, I149, L150	L182, L184, L185, T188, F192, V196, L198, I199, I200
27	38.5	T64, L67, V68, I71, C74, F75, V78, V79, S81	L107, L110, S111, L114	L131, N134, I135, V136, S138, I139, A140, G142, L143, I145, A146, I147, I149, L150	L182, M183, L184, L185, F186, I189, F192, C193, V196, I199, I200

29	38.9	F60, V63, V66, L70, I71, L73, C74, V78	G104, L107, F108, S111, G112, S115, I116, S118	L131, G132, N134, I135, V136, S138, I139, G142, L143, I145, A146, I149, L150	M183, L184, F186, L187, L190, C193, S194, L197, L198, I199, I200
32	39.8	Q65, V68, C72, L73, F75, G76, V79	A98, Y100, P101, F102, G104, L107, F108, V109, S111, G112, S115, I116	L131, G132, N134, I135, S138, I139, G142, L143, I145, A146, I149, L150	M183, F186, L187, L190, C193, S194, L197, L198, I199, I200
33	37.5	L61, T64, Q65, V68, I71, C72, F75, V79	W103, A105, L107, F108, V109, S111, G112, F113, L114, S115, I116, S118	L131, N134, I135, S137, S138, I139, A141, L143,I145, A146, I149, L150	M183, L184, L187, T188, I189, L190, F192, S194, A195, V196, L198, I199
35	35.9	V63, V66, L70, L73, T77	Y100, L107, F108, S111, S115, I116,	L131, N134, I135, S137, S138, A141, I145, A146, I149, L150	V181, M183, L184, L187, I189, L190, C193, S194, A195, V196, L197, L198, I199, I200

The distance of closest approach between helix pairs was in the range of 8.6 to 13.8 Å for the neighbouring helix pairs in the helix bundles with anticlockwise and clockwise arrangements. Such a range of distances between TM helices allowed the addition of the connecting loop peptides. It was found in the Chapter 2, that even the shortest, 11 amino acid residue, loop (loop 2-3) could be connected to these TM helix ends. Only the distances between the neighbouring helix pairs in the bundles with crossed loops deviated out of that range, and this was therefore the reason for excluding them from further analysis.

The summary of the interaction between TM helices in the clockwise and anticlockwise helix bundles is presented in Table 6.3. The numbering of the bundles corresponds to Table 6.2. Table 6.3 shows the residues of one TM helix involved in the interaction with the rest of the bundle. In these 19 bundles, every residue of the four TM helices appeared in the contact interfaces and no obvious surface could be pointed to as specific for the helix - helix interaction. The appearance of the residues in the contact interfaces in the clockwise and anticlockwise bundles is presented in Figure 6.10. Certain residues appeared more frequently than others, implying they are possible markers for the helix - helix contact interfaces.

For example, some of the markers for the TM helix β1 could be residues whose frequency of appearances were greater than average plus standard deviation. V66, L70, I71, C74 and T77 (figure 6.10A) are such marker residues. By analogy marker residues for the TM helix 2 were: L107, F108, S115 and I116 (Figure 6.10B); for TM helix 3 - I135,S138, L143, I145 and I149 (Figure 6.10C); and for TM helix 4 - I189, F192 and I199 (Figure 6.10D).

By corollary, the residues with the smallest frequency of appearances (below the average minus standard deviation) could be markers for (say) the lipid facing sides. These

residues were: L61, G62, C72, F75, G76, V106, L110, F113, G132, A133, G144, V181, L182, F186, C193 and were comparable to the predicted PFA binding sites from Chapter 5. The best such agreement was found for TM helix β1, where five residues could be markers and three of them (G62, C72 and G76) were predicted to be only on the lipid facing side by both hydrophobicity mapping and docking calculations. These three residues are situated at the 270° rotational position of the helix surface, where the interaction energy between PFA and TM helix β1 was largest (Figure 5.5). For the TM helix β3 and β4, the agreement between the two calculations was only for the few residues, while for the TM helix 2 none of the residues from the docking calculations coincided with the predicted PFA binding site from the Chapter 5. This deduction must be taken with caution, since bundles which were compared had a little in common.

The number of the residues per helix involved in the helix-helix interactions was in the range of 2 to 12, with average of 10 residues per helix for all analysed 19 bundles. On the average, up to the half of TM helix surface was buried in the four helix bundle. At the same time some of those residues involved in the helix - helix interaction could be partially exposed to the lipids as well, which could lead to the conclusion that at least half of the TM helix surface could be exposed to the lipids.

A)

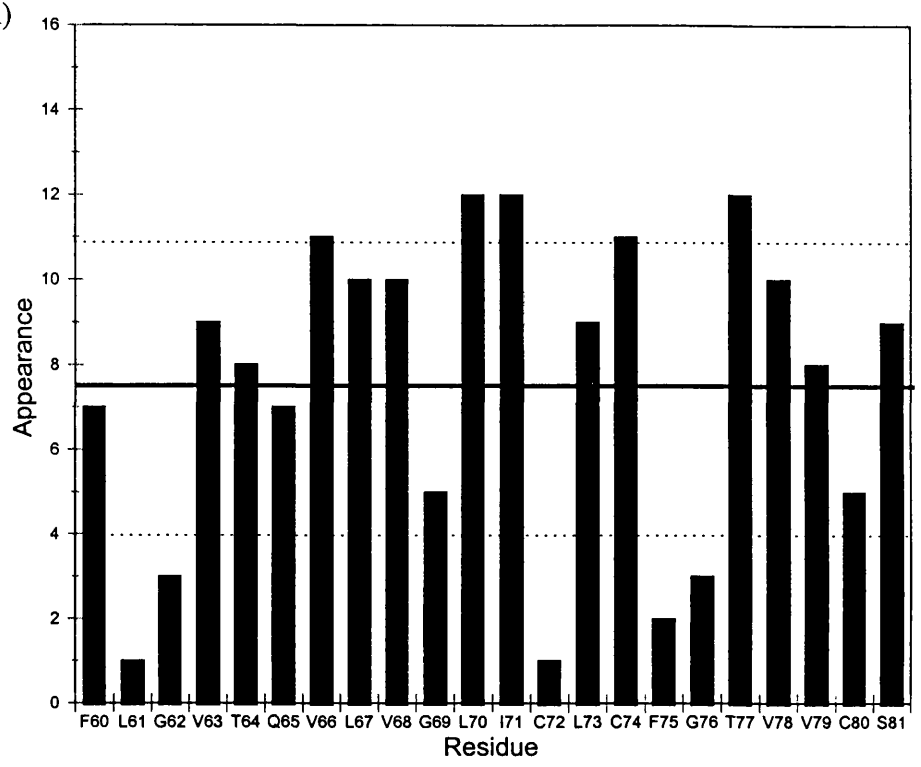
Appearance
0
2
4
6
8
10
12
14
16
F60 L61 G62 V63 T64 Q65 V66 L67 V68 G69 L70 I71 C72 L73 C74 F75 G76 T77 V78 V79 C80 S81
Residue

B)

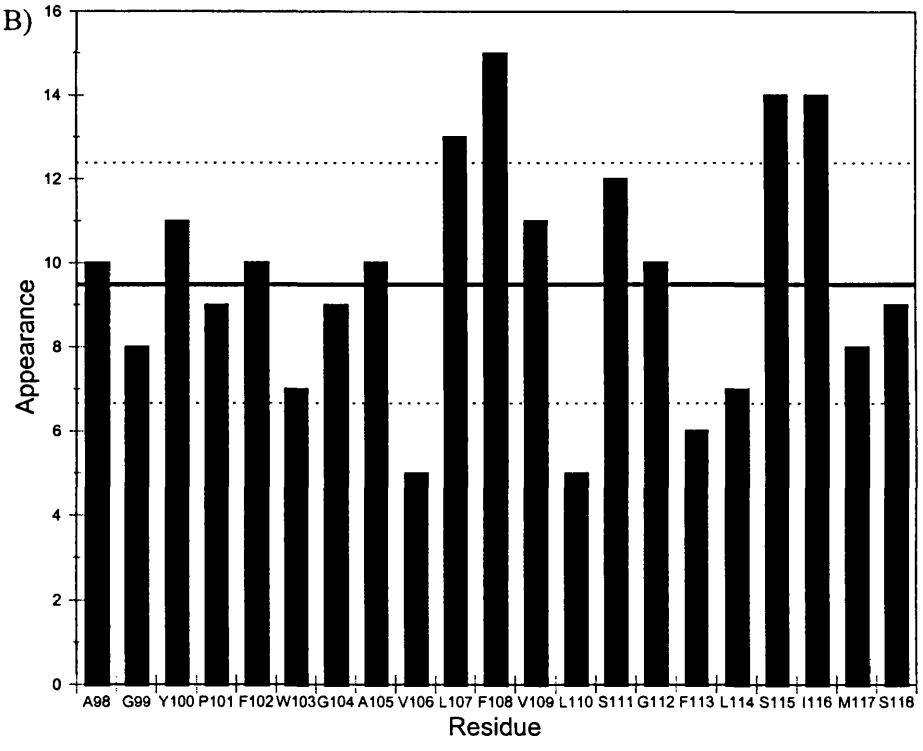
Appearance
0
2
4
6
8
10
12
14
16
A98 G99 Y100 P101 F102 W103 G104 A105 V106 L107 F108 V109 L110 S111 G112 F113 L114 S115 I116 M117 S118
Residue

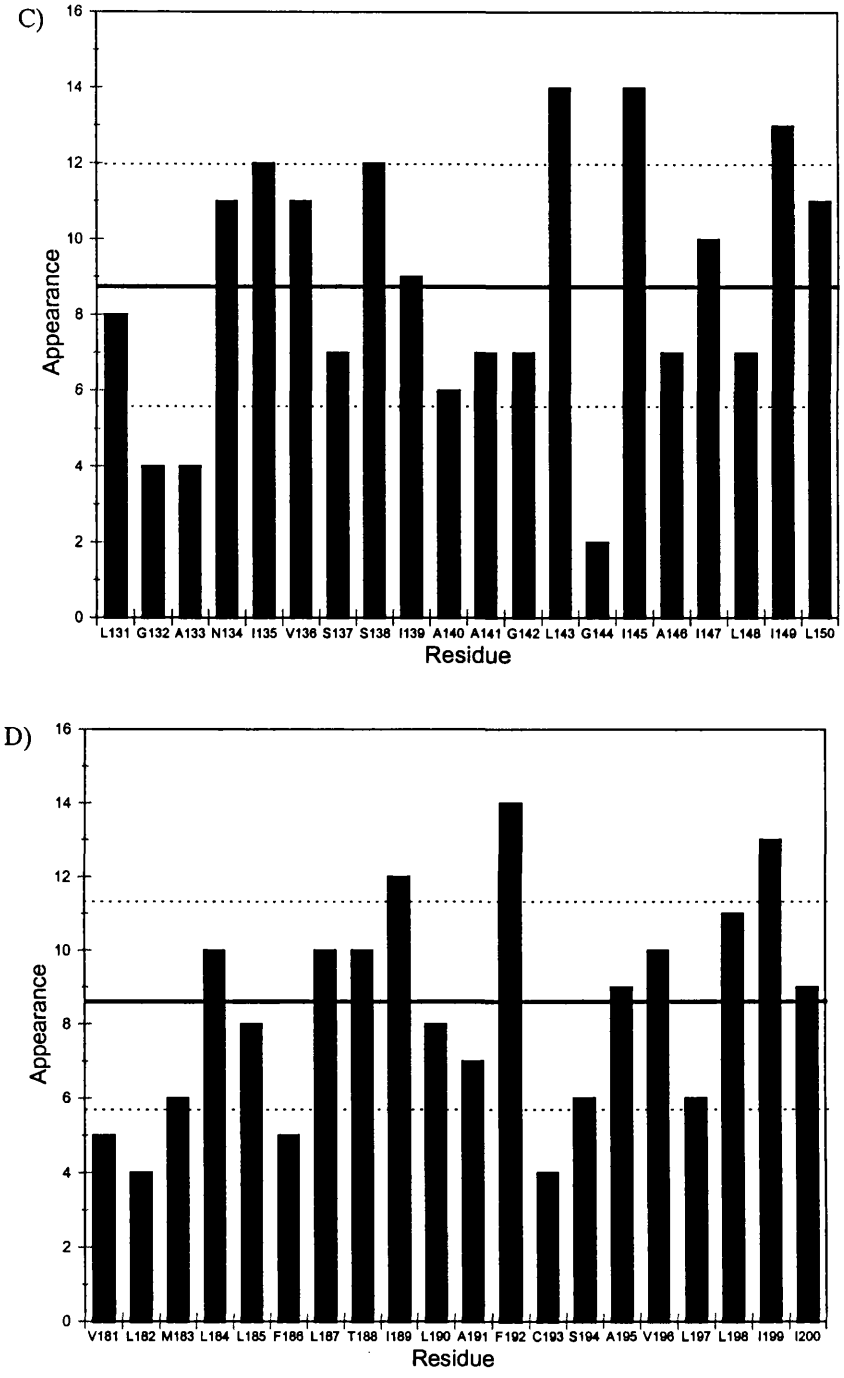

Figure 6.10 The appearance of the residues in all docked four helix bundles of the β-subunit; A) TM helix 1; B) TM helix 2; C) TM helix 3) and D) TM helix 4. Solid line represents the average number of appearances per residue, dotted lines depict standard deviation.

The solvent accessible surface area (SASA) of the four helix bundles were calculated by MolMol software (Table 6.3). Those calculations indicated that the area buried upon formation of the helix bundle is about 40 % of the total SASA of the isolated helices for the bundle 25 (bundle with highest interaction energy between helices). This again suggested that each helix loses about 20% to the interface with each of two neighbours. This figure is similar to that determined for *Bacteriorhodopsin* [Henderson et al., 1990] and a synthetic parallel four-helix coiled-coil [Harbury et al., 1993]. The other bundles with lower interaction energies between helices had lower change in SASA, for example that the area buried upon formation of the helix bundle 12 was 32% which suggested poor packing between the structural components of the four helix bundle. This was also reflected in low van der Waals interaction energy.

A further approach to analysing the data considered the relative orientation of the hydrophobic moments of the helices within the bundles. All 19 bundles are shown in Figure 6.10 had four circles with arrows depicting the hydrophobic moments. Many different orientations of the moments were observed; and sometimes the hydrophobic moments faced the inside of the bundle. The usual assumption in modelling a membrane receptor is that the hydrophobic moments are directed to outside of the bundle, and actually face the lipid bilayer. The human opoid [Habibi-Nezhad, et al, 1996] and $5HT_{2c}$ receptors [Kristiansen et al., 1993; Kristiansen and Dahl, 1996; Sytle et al., 1993; Sytle et al., 1996] were modelled using that approach. This assumption narrows the choice of the four helix bundles obtained as a result of docking procedure. Four helix bundles numbered 19, 22, 25, 32, 33 and 35 have passed the criteria of the orientation of hydrophobic moments (Figure 6.10), and thus these listed bundles could be starting structure for further modelling of the

7 helix bundle. The modelling of the 7 helix bundle was not subject of this work, but it will be part of the further work in this field.

Still, the possibility of the seven helix bundle with a circular arrangement of the TM helices (Figure 6.1C) leaves one of the TM helix inside of the bundle. In that case the hydrophobic moment of that TM helix should face inside of the TM bundle interior, and not face the lipid environment? This extended the possible combinations for the four helix bundle of the β-subunit, with bundles depicted as 2, 4, 5, 13, 14 and 18 (Figure 6.11).

6.3.3 Analysis of the four helix bundle 25 of the β-subunit of high affinity IgE receptor

Since, the many possibilities are open, the bundle numbered 25 was chosen for further analysis. It was a bundle with highest van der Waals interaction energy (-180 kcal/mol) and it satisfied the hydrophobic moment orientation criteria (Figure 6.10). The calculations of the SASA indicated that the area buried upon formation of the helix bundle was 39.5 % of the total SASA of the isolated helices for this bundle. It was second highest change of the solvent accessible surface, but this bundle had the highest interaction energy. Furthermore, the residues not involved in the interaction between helices (lipid facing residues) were in good agreement with the PFA favourable surfaces according the Chapter 5. As mentioned before, some of the residues could be in the interaction with helices and with lipids at the same time. The ribbon presentation of bundle 25 is shown in Figure 6.12.

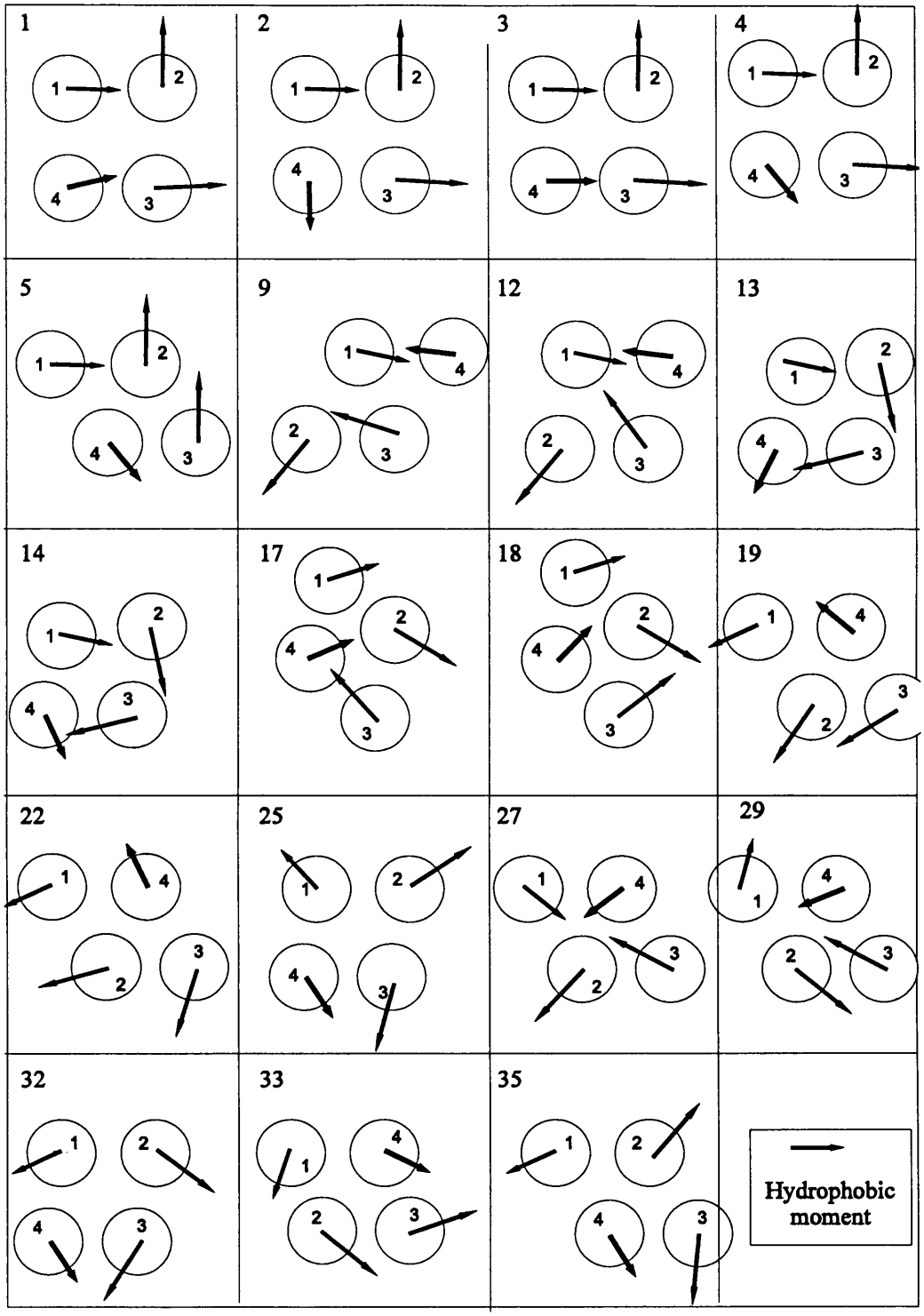

Figure 6.11 The orientation of the helix hydrophobic moments in the anticlockwise and clockwise four helix bundles (perpendicular view to the plane of the membrane). Arrows depicted the hydrophobic moments.

The distances between neighbouring helices was between 8.2 and 10.2 Å (Table 6.3), which was similar to the mean inter-helical distance observed in protein crystal structures of 9.4 Å [Clothia,et al., 1981] or the mean inter-helix distance of 9.9 Å in integral membrane proteins. The Ω angle for the TM helix 2 and 3 was -163°, indicating the antiparallel arrangement, and which would be quasi-equal to 17°. Such crossing angle of 23° reflects the common arrangement in the CLASS 3-4 packing, in which the i,i+3 ridge on one helix interacts with i,i+4 on the second helix. This type of the interaction, which is similar to the "knobs in holes" packing described by Crick, 1953, characterizes the helix - to - helix packing found in coiled - coil structures, such as the leucine zipper [O'Shea et al., 1991]. This is different packing than CLASS 4-4, the packing found in the globular proteins, where crossing angle is about -50°. The quasi-crossing angle resembles this packing, but it is more comparable to the packing in the Rhodob. Sphaeroides RC. [Rees et al, 1995], where crossover interaction between two ridge type (3-4 and 4-4) is present. The crossing angle of 20° enables better packing than -50°, when its helix axes are closer to parallel orientation more residues can interact between each other.

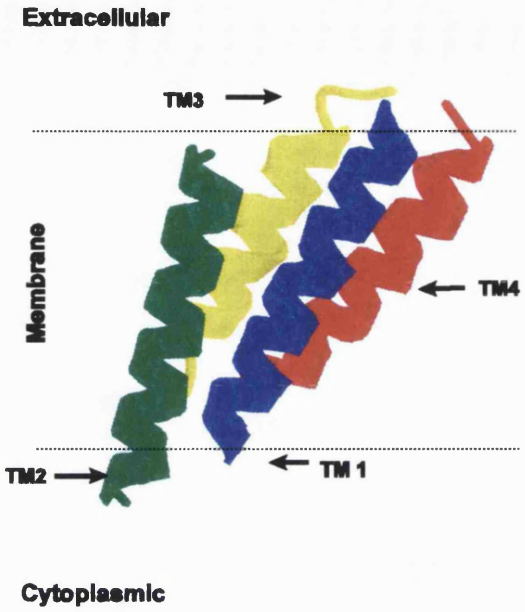

Figure 6.12 The ribbon presentation of the four helix bundle of β-subunit of high affinity IgE receptor.

The crossing angles between other helix axes in the four helix bundle 25 were similar to those previous discussed. Again, due to the more parallel alignment of the helix axes, CLASS 3-4 contacts generated an extensive contact interface between helices. Most of the compact structures, in well-studied cases of water soluble protein domains, like four helix bundles (Weber and Salleme, 1988) are based on the CLASS 3-4 contacts. The similar values of the crossing angle indicated the compact folded structure of the four helix bundle. It is a striking feature that TM helix β2 of the bundle 25 was about 6.5 Å below the putative membrane. In such ways several residues were not involved in the interaction, and still produced the highest interaction energy of all "correctly" folded (clockwise and anticlockwise) bundles.

The absolute values of the crossing angles were in the range of 9 to 20 °, comparable to the values of crossing angles in the predicted four helix bundle in tetrameric GCN-4 coiled-coil structures [Delano and Brunger, 1994]. Beside, the left-handed helix bundle with 20 °crossing angle, the right-handed coiled-coil structures were also observed [Lin et al, 1995].

The presence of many large branched hydrophobic residues in the helix contact interfaces could be significant (19 out of 35), since that could be the driving force for the helix bundle formation. It was shown that leucine zipper type structure could be formed if positions "a" and "d" of the heptapad repeat were filled with hydrophobes. [Sodek et al, 1972], with the most stable coiled-coil structures with Leu residues in position "a" and "d" [Hodges et al., 1981, Zhou et al., 1992]. The stability of the coiled-coils decreased by replacing all Leu residues with Val, Phe, Tyr, and Ala [Hodges et al., 1990]. The decrease in stability was in the order of Leu>Ile>Val>Phe>Tyr>Ala. Therefore, bundle 25 of the four helix bundle with its high presence of hydrophobes in the interface, could be described as a sequence with potency to form a coiled-coil superstructure, even when all geometry factors were not satisfied. The reason was that starting geometries for the docking procedure were modules with ideal α-helix structures. Only energy minimization was performed on the results of the docking. This minimization protocol was not enough to induce change from α-helix to coiled-coil geometry of the four helix bundle. Also, the imperfection in the coiled-coil formation could have biological importance, as found by studying the discontinuities in several proteins [Oas and Endow, 1994].

6.3.4 Interaction between other TM helices of the high affinity IgE receptor

The docking procedure described in the Section 6.3.1 was applied to all possible combinations involving the TM helices of the α- and γ-subunit. The interaction energy and residues involved in the interactions are shown in Table 6.4.

Blank et al., 1989 found that the two γ-subunit were connected by a disulfide bond, but it was not proven which pair of the cysteine residues were involved. The docking procedure produced one cluster, which had a van der Waals interaction energy of -32.8 kcal/mol. The geometric analysis of the lowest energy structure showed that distance of the closest approach between helix axes was 8.8 Å. This value was very similar to the mean inter-helical distance observed in protein crystal structures of 9.4 Å [Clothia,et al., 1981], but not so close to the mean inter-helix distance of 9.9 Å in integral membrane proteins [Rees et al., 1995]. The crossing angle was found to be -66.8°, implying the right-handed coiled-coil and it was similar to the crossing angle of -50°, found in the CLASS 4-4 packing in the coiled-coil of annexin [Huber et al, 1990]. These geometric features were not refined, since only minimization protocol was performed; further refinement should produce more exact values. Both pairs of cysteine residues faced and formation of disulfide bond would be possible for any of the two pairs. The distance between C26-C26' pair was 6.5 Å, while the distance between C7-C7' residues was 14.0 Å. According to these values, the C26-C26' disulfide bond would be more plausible, but since structure was not refined, the deduction would be not fully true.

The TM helix of the monomeric γ-subunit could be in contact with TM helices of other subunits, but it more likely that the dimer interacts with them. The docking between the four helix bundle, the γ-dimer TM helical coil and the single TM helix of α-subunit should be studied, but this was not the subject of this work.

The rest of the results in this section will discussed having in mind bundle 25 from the previous section. The β-subunit was considered independently of the α- and γ-dimer subunits in the previous section. This assumption mimicks the *in vivo* membrane situation since the β-subunit probably spans the membrane independently before interaction with other subunits [Jacobs and White, 1988]. The residues of the TM helices of β-subunit involved in the four helix bundle are presented in Table 6.3. The TM helix of α-subunit would not be able to interact with TM helices 3 and 4 of the β-subunit, since the surfaces were involved in the interaction within four helix bundle. So, there is possibility of the TM helix of α-subunit interacting with the free surfaces of TM helix 1 (L67, I71, C74, T77, V78) and 2 (A98, G99, F102, W103, V106, L110, F113, L114, M117). Those two surfaces were not adjacent in the bundle 25, therefore, TM helix of α-subunit could interact with either one. Interaction energies were similar, so there is no clear preference for any surface.

The TM helix of γ-subunit could only interact with TM helix 3 of the β-subunit, but the study of γ-dimer should be performed and problem is more complex and it is outside scope of this work.

Table 6.4 Interaction energies and contact surfaces between TM helices of the high affinity IgE receptor obtained by docking with GRAMM software (α - α-subunit; γ - γ-subunit; β1, β2, β3, β4 - β-subunit; one letter amino acid code was used in the table).

Helix Pair	Cluster No.	Energy (kcal/mol)	Residues involved in the contact interface.
α-β1	1	-42.4	α - F207, A211, L214, F215, D218; β1 - L67, I71, C74, T77, V78
	2	-21.3	α - S209, V212, I213, F215, A216, T219, G220, F223, S224; β1 - V66, G69, L73, T77, C80, S81
α-β2	1	-40.9	α - L205, I206, S209, L210, V212, I213, A216, T219, G220, F223, S224; β2 - A98, G99, F102, W103, V106, L110, F113, L114, M117
	2	-29.1	α - A211, L214, F215, V217, D218, L219, W222, T225; β2 - Y100, G104, L107, F108, L110, S111, L114
α-β3	1	-30.9	α - V212, A216, T219, F223, S224; β3 - S138, A141, G142, I145, A146, I149
α-β4	1	-34.5	α - F207, F215, D218, W222, T225; β4 - L182, L185, F186, I189, F192, C193, V196, I199
α-γ	-	-	nonspecific
γ-β1	1	-42.1	γ - L6, Y8. I9. A12, F15, I19, T22; β1 - Q65, C72, L73, G76, V19, C80
γ-β2	1	-35.7	γ - D11, L14, F15, G18, L21, T22, Y25, C26; β2 - F102, W103, V106, L110, F113, L114, M117
	2	-34.5	γ - Y8. I9. D11, A12, F15, I19, T22; C26 β2 - Y100, P101, G104, L107, F108, S111, L114
	3	-33.2	γ - I9, A12, I13, L16, I19, V20, L23, L24; β2 - A98, F102, W103, V106, L107, L110, F113, M117
γ-β3	1	-39.1	γ - Y8, I9, F15, L16, V20, L24; β3 - N134, S138, I139, A141, G142, I145, A146, I149, L150
γ-β4	1	-35.3	γ - Y8. I9, A12, L16, I19, V20, L23, L24, C26; β4 - L185, I189, F192, C193, V196; L197, I199, I200
γ-γ	1	-32.8	γ - L14, F15, G18, I19, L21, Y22; G' - L14, F15, Y17, G18, L21, Y25

6.4 Summary

The TM helices of the β-subunit of the high affinity IgE receptor were amphiphatic, but the absence of the charged residues was noticeable. Such sequences led to the absence of the salt bridges and presented difficulties for predicting the TM helix arrangement in the native receptor structure since only polar residues contributed to the forming of amphipathic surfaces, and polar interactions not yielded a unique prediction. Therefore, the nonsubjective procedure was employed that involved low resolution docking of the TM helices. The results of this procedure gave 35 four helix bundles, that were divided into three categories, "clockwise", "anticlockwise" and "crossed loop" arrangements. The latter "crossed loop" bundles were discarded as statistically less favourable [Finkelstein et al., 1995] and thus 19 "clockwise"and "anticlockwise" four helix bundles were selected for further consideration.

The folding of integral membrane proteins clearly differs from that of soluble proteins since the lipid bilayer imposes constraints on polypeptide secondary and tertiary structural features quite different from those imposed by an aqueous environment. The formation of the dimer of helices results in an increase in helix-helix and lipid-lipid interactions and a loss of helix-lipid interactions. The entropy of the lipids is expected to increase, with a concomitant decrease in the entropy of the helices. The value of the equilibrium constant will depend on the magnitudes of these entropic terms and on the enthalpic terms that arise from the detailed helix-helix, helix-lipid, and lipid-lipid contacts. The association of the hydrophobic helices into a specific structure is expected to be also influenced by the covalent linkages imposed by extramembraneous loops.

One four helix bundle, denoted as a bundle 25, was chosen as a solution that satisfies most of the criteria, such as: agreement with proposed topology by Blank et al.,

1989, correct TM helix arrangement, greatest interaction energy between TM helices, appropriate orientation of the hydrophobic moments towards lipid bilayer. Furthermore, the exposed surfaces were available to interact with TM helices of other subunits and lipids.

The exposed surfaces of the bundles used in the further modelling of the complete β-subunit were in good agreement with possible lipid interaction sites as determined by calculation of interaction energies between PFA and TM helices. Specifically, the bundle 18, had an excellent agreement between prediction of lipid facing surface on the TM helices by these two different approaches. The lipid favourable surfaces calculated in the Chapters 4. and 5. (residues depicted as a blue circles in Figures 5.5A, 5.8A, 5.11A and 5.14A) were not involved in the helix-helix contact interface determined by docking procedure (Table 6.3). There was an exception for seven residues out of thirty seven, namely F102, F108, V109, I116, I149, T188 and F192. However, those were involved in both, helix - helix and helix - lipid interfaces. Similarly, the lipid facing surfaces of bundle 25 calculated using two different methods were also in a good agreement, but in this case the second most stable complexes between PFA and TM helices 1and 3(residues depicted as a yellow circles in Figures 5.5A and 5.11) were not involved in helix - helix contacts (Table 6.3).

It was encouraging that very good agreement was obtained between the determination of lipid binding sites and helix-helix docking procedures, despite the fact that the ideal geometries of TM helices were used in all calculations. Inclusion of more experimental facts in these procedures would lead to the results with more certainty. As in any modelling study, the theoretical results are is no substitute for a high resolution three-dimensional structure; however, the insights obtained suggest a number of avenues for further study and form a framework for rational strategies for possible site-directed mutagenesis and other experimental approaches.

Chapter 7.

MODELLING THE 3D STRUCTURE OF THE β-SUBUNIT OF THE HIGH AFFINITY IgE RECEPTOR

7. MODELLING THE 3D STRUCTURE OF THE β-SUBUNIT OF THE HIGH AFFINITY IgE RECEPTOR

7.1 Background

The amino acid sequence of the high affinity IgE receptor has been cloned and its amino acid sequence deduced [Blank et al., 1989], but its 3D structure is not known. The basic structural building-block in plasma membrane proteins of both prokaryotic and eukaryotic cells is the apolar, often slightly amphipatic transmembrane α-helix. For multi-spanning membrane proteins with most of their mass buried within the bilayer in the form of transmembrane helices, the insertion event is decisive. The best attempts to predict the topology and structure of receptor used hydrophobicity analysis algorithms, where the amino acid sequence was scanned to locate segments rich in apolar residues. The most suitable helix-helix packing arrangements were then sought using rules derived from helical soluble proteins and by rotating the helices such that the most hydrophobic sides faced the lipids [von Heijne, 1992], to dock TM helices [Vakser, 1996] or to use homology with membrane proteins with known structure [Habibi-Nezhad et al., 1996]. While the apolar surfaces of the transmembrane helices provide a good interface for the membrane lipids, it is believed that the hydrophylicity of the polar amino acids within a helix should favour the spontaneous formation of helical bundles with polar surfaces interacted and removed from the lipid environment [Rees et al., 1989]. It was proposed that the structure of short extramembraneous loops connecting contiguous helices should be predictable using libraries of known loop-structures [Rooman et al., 1989], biophysical data of peptides with

the same sequence of these loops and molecular mechanics and dynamics calculations of the loops.

Since the size of the receptor subunits as well as the existence of both lipophilic and hydrophillic domains in the same subunit have not yet permitted a direct experimental structure determination, characterisation of the receptor subunits by cutting them into smaller domains or structural units has been performed. The anisotropic environment of membrane receptors leads to their natural division in terms of environment. Thus each membrane receptor, including the high affinity IgE receptor, can be classified into extracellular, transmembrane and cytoplasmic domains. This domain approach to structure determination of large proteins has been pioneered by Campbell and workers [Baron et al., 1991] and used by others [Anderson et al., 1992; Musco et al., 1995]. The novel method of cutting large protein into small to medium size peptides was used to determine the secondary structure of vaccinia virus thymidine kinase, porcine adenylate kinase and yeast guanylate kinase [Behrends et al., 1996; Behrends et al., 1997]. Using this approach several domains of the high affinity IgE receptor have been studied [Anderson et al., 1992, 1994/95; Thomas et al., 1993; Zloh et al., 1994a; Zloh et al., 1994b; Padlan and Helm, 1993; McDonnell et al., 1997].

The motif or domain approach was used to calculate the 3D structure(s) of the β-subunit, but it was modified by utilizing spectroscopic data and/or calculations of the structures of the loop peptides, the TM helices and the cytoplasmic tail peptides. Specifically, the β-subunit calculations were carried out in a historical/chronological context by adding the following data as it became available over a 4 year period:

1) CD and prediction based structures of the loop peptides;

2) CD and prediction based structures of the cytoplasmic tails;

3) NMR-based structures of loop 1-2 and loop 2-3;

4) Calculation of the hydrophobic moments;

5) Dodecane mapping of the relative hydrophobicity of the TM helices;

6) Palmitic fatty acid mapping of the relative hydrophobicity of the TM helices;

7) Docking of TM helices.

The sophistication of the molecular mechanics and dynamics calculations of the 3D structure of the whole β-subunit (243 residues) enhanced with the availability of the above data. In the final analysis, the calculations yielded three subunit structures probably more realistic than those which would be calculated purely by a comparison with *Bacteriorhodopsin* crystal structure.

7.2 Methods

7.2.1 Molecular modelling of the β-subunit. Model I - use of the hydrophobic moments.

Energy minimizations and molecular dynamics were performed using the Sybyl program, version 6.0A [Tripos Association, 1993]. All calculations were performed on the SUN Sparc workstation with 16 MB Ram memory. Due to workstation limitations at that time and available CPU time, all molecular dynamics calculations were short, and they could be consider more as simulated annealing preformed to remove bad contacts and improve packing in chosen TM arrangements. The summary of the model building and MM/MD protocol is shown in Table 7.1. The TM helices of the β-subunit were constructed with the ideal α- helix geometry (ϕ = -57° and ψ = -47°), and they were subjected to the initial 1000 steps of Powell energy minimization, then short dynamics at 600 K for 0.5 ps, followed by 1 ps simulation at 300K and 2000 steps of Powell energy minimization. The Kollman force field with Kollman charges was used, with following parameters: a 8 Å nonbonded cutoff , time step of 1 fs during molecular dynamics, with NVT ensemble, coupling every 100 fs and non bonded interactions update every 25 fs. The dielectric constant of 10 Db was used to emulate the lipidic environment. The TM helices were manually docked into the four helix bundle, so that the hydrophobic moment of each TM helix faced the lipid environment and the centres of the four helices were placed at interhelical distances of 11.5 A. The helical axes were parallel to each other. The 2000 steps of the Powell energy minimization were performed on the bundle. The three interconnecting loops, with the defined α- helical structure in the middle of the sequence, were added to the four helix bundle. The previously described procedure was performed on this structure, with added 20 steps of Simplex minimization, and simulation at 300 K

was 2 ps. All parameters were the same, except that dielectric constant was set to 80 Db, to describe the polar environment out of the membrane. The TM four helix bundle was fixed during this procedure. The 2000 steps of the Powell energy minimization were performed on the β-subunit without cytoplasmic tails.

Table 7.1 Model building and MM/MD protocol for the β-subunit without cytoplasmic tails- model I. Detailed parameters are listed in the text above.

Stage	Notes	Temperature (K)	Constraints	Time (ps)	Steps
1	Helix building	-	$\phi = -57°$; $\psi = -47°$	-	-
2	Powell minimization	-	-	-	1000
3	Molecular dynamics	600	-	0.5	-
4	Molecular dynamics	300	-	1.0	-
5	Powell minimization	-	-	-	2000
6	Four helix bundle building	-	Hydrophobic moments orientation	-	-
7	Powell minimization	-	-	-	2000
8	Adding connecting loops	-	CD spectra + Secondary Structure Prediction	-	-
9	Simplex minimization	-	Fixed helix bundle	-	20
10	Molecular dynamics	300	Fixed helix bundle	2.0	-
11	Powell minimization	-	-	-	2000

7.2.2 Molecular modelling of the β-subunit. Model II - use of the docked four-helix bundle and the addition of the loops and tails in two stages.

The simulated annealing / molecular dynamics protocol (SA/MD) was applied to 12 out of 19 four helix bundles (see Chapter 6.) with added connecting loop sequences. All calculation described in this section were performed on the SGI O2 workstation with 64 MB RAM and 6 GB hard disk, thus allowing longer molecular dynamics calculations, but CPU time was limited. The protocol is shown in Table 7.2. The TM helices were constructed in the same manner as described in the previous section. In this work the version 6.3 and 6.4 of SYBYL [Tripos Association, 1994-1997] were used. The loops between helices and parts of N- and C-terminal tails were constructed, based on the available structural data (NMR based structures for loop 1-2 and loop 2-3 as described in Chapter 2 and 3; secondary structure prediction data for loop 3-4 as described in Appendix 1.) by biopolymer module of SYBYL. The structures were converted into X-PLOR PDB and PSF files. Those loops were manually docked into the four helix bundle. The 10 residues were added at both N- and C- terminal corresponding to the sequence of the β-subunit. These residues were added to prevent electrostatic interaction of the terminal groups in the four helix bundle. The described SA/MD protocol was modified from [Kerr et al., 1994], originally used to model ion channels.

The simulated annealing was performed on such truncated models of the β-subunit. During this phase the Cα atoms of the TM helix bundle were kept fixed to retain a "scafold" formed by the docking procedure. The initial minimization (5 cycles of Powell minimization) relieved the highly strained conformation. The annealing started at 1000 K, with initial velocities assigned on the basis of a Maxwellian distribution. All atomic masses are set to 10 atomic mass units (Nilges et al., 1988a). NOE type constraints were applied

to keep secondary structure of the loops and cytoplasmic tails. The annealing temperature, T, was maintained throughout by coupling the atomic velocities to an external heat bath using the algorithm of Berendsen et al. (1984). Frictional coefficients for all atoms were set to 100 ps^{-1} (Nilges and Brünger, 1991). Unless noted otherwise all step sizes were 1 fs. The 1000 K simulation was performed for a period of 3.7 ps. Molecular dynamics at 1000 K continued for a further period of 32 ps. A repulsive van der Waals term was slowly introduced after an initial delay. The system was then annealed slowly to 300 K in decrements of 25 K every 300 fs, giving a cooling period of 8.4 ps. This slow cooling, which contrasted with the rather faster cooling used in similar ab initio simulated annealing procedures (from 1000 K to 300 K in 1.4 ps; Nilges and Brünger, 1991; Treutlein et al., 1992) is believed to give more accurate refinement of structures during X-ray crystallographic refinement with fewer deviations from ideality of bond lengths and angles (Brünger et al., 1990). The system was then subjected to 2000 cycles of conjugate gradient energy minimisation. During the minimisation all energy weighting terms were as in the cooling period and the full Lennard-Jones potential with the Charmm22X force field was employed. This procedure was repeated 3 times and generated a set of models for MD refinement.

The resultant 3 models were each the subject of independent molecular dynamics runs, thus resulting in an ensemble of 3 final models. Throughout the MD phase all weighting factors in equation were set to 1.0. This procedure was a 4.0 ps cooling from 500 K to 300 K during which the Cα atoms of the molecule were gradually released from initial restraints [Bruccoleri and Karplus, 1986]. The electrostatic energy term was also introduced during this stage by scaling partial charges of polar sidechains. Minimisation (unrestrained) consisted of 5 ps of unrestrained MD at 300 K. The models were then subjected to 1000

cycles of energy minimisation to produce the final truncated models. The introduction of an electrostatic term in the dynamics phase together with the implementation of distance restraints on backbone hydrogen bonding groups caused the peptide to adopt a regular right-handed α-helical structure. The computational intensity of the dynamics phase was reduced by performing the calculations in the absence of any solvent (such as explicit representation of the lipid bilayer). Solvent screening of electrostatic charges was mimicked by using a distance-dependent dielectric constant. The electrostatic potential was further screened by the reduction of sidechain partial charges. A switching function (Brooks et al., 1983) was employed between 5 Å and 9 Å, with a non-bonded interaction cut-off distance of 9.5 Å. MD studies of X-ray crystal structures of globular proteins such as myoglobin [Loncharich and Brooks, 1989] suggested that a combination of distance-dependent dielectric and switching function is appropriate for MD simulations. A direct comparison of electrostatic models employed in SA/MD studies of isolated TM helices indicated that ensembles of lower RMSD were produced using a distance-dependent dielectric and a switching function similar to that employed here (Sankararamakrishnan and Sansom, 1994). During some stages, sets of restraints, dependent on the initial conformation, were applied to the loop and tails of the molecule. The restraints take the form of distance restraints and were treated computationally as if they were NOE distance restraints from an NMR experiment [Brünger, 1992]. Only intra-helical restraints were applied. These are applied between the backbone carbonyl oxygen of residue i and the backbone amide hydrogen at residue i+4 ie. restraining the backbone hydrogen bonding distance to retain helicity. This restraint is further subdivided into three regions of the helix since the mean observed O - H hydrogen bonding distance in well-defined protein structures varies at the termini [Baker and Hubbard, 1984; Jeffrey and Saenger, 1991].

Those 12 x 3 models were filtered further using hydrophobic moments orientation, lipid facing sides and interaction energy in the TM helix bundles. A bundle, with low energy, hydrophobic moment orientation and lipid facing surfaces criteria fulfilled, was chosen for further model building.

The addition of the whole cytoplasmic tails was carried out only on the one chosen bundle. In the absence of the detailed experimental results, the structures of the both tails were set to the predicted by the secondary structure algorithms (Appendix 1.). The dielectric constant was set to $\epsilon = 80$ Db, to emulate the polar environment in water. The stages 15 to 23 were performed on the selected bundle

7.2.3 Molecular modelling of the β-subunit. Model III - use of the four helix bundle and the addition of the loops and tails in one stage.

All calculation described in this section were performed on the SGI O2 workstation with 64 MB RAM and 6 GB hard disk, thus allowing longer molecular dynamics calculations, but CPU time was limited. The TM helices were constructed in the same manner as described in the previous section. In this work the version 6.3 and 6.4 of SYBYL [Tripos Association, 1994-1997] were used.

The outline of the β-subunit building from the bundle with highest interaction energy between TM helices is presented in Table 7.3. The loops between helices and parts of N- and C-terminal tails were constructed, based on the available structural data (NMR based structures for loop 1-2 and loop 2-3 as described in Chapter 2 and 3; secondary structure prediction data for loop 3-4 as described in Appendix 1.) using the biopolymer module of SYBYL. The structures were converted into X-PLOR PDB and PSF files.

The starting model of the β-subunit was constructed by manual rotation and translation of the loops and tails and docking them into four helix bundle 25 (Chapter 6. of this work).

The molecular dynamics protocol was applied in order to sample the conformational space of the constructed model. The first stage of the 1000 steps of Powell minimization was performed in order to remove initial bad contacts. The rest of the protocol is same as the protocol steps 15 to 22 described in the 7.2.2 Section.

Table 7.2 Model building and MM/MD protocol for the β-subunit - model II. Detailed parameters are listed in the text above. This protocol is based on the SA/MD protocol for building ion channels [Kerr et al., 1994]. Stages 1 to 13 were performed on all twelve four-helix-bundles, while the rest of the protocol was applied only to one selected model.

Stage	Notes	Temperature (K)	Constraints	Time (ps)	Steps
1	Helix building	-	$\phi = -57°$; $\psi = -47°$	-	-
2	Four helix bundle building	-	Docking procedure (Chapter 6.)	-	-
3	Loops 1-2 and 2-3 building	-	NMR based models (Chapters 2. and 3.)	-	-
4	Loop 3-4 and truncated tails building	-	Secondary structure prediction (Append. 1)	-	-
5	Manual docking of loops and truncated tails into bundle	-	All structures fixed	-	-
6	Energy minimization	-	-	-	5
7	Molecular dynamics	1000	Fixed Cα of bundle + NOE constraints	3.7	-
8	Molecular dynamics	1000	Fixed Cα of bundle + NOE constraints	32.0	-
9	Molecular dynamics Cooling	from 1000 to 300	Fixed Cα of bundle + NOE constraints	8.4	
10	Energy minimization	-	-	-	2000
11	Molecular dynamics Cooling	from 500 to 300	Gradually releasing bundle constraints	4.0	-
12	Molecular dynamics	300	-	5.0	-
13	Energy minimization	-	-	-	1000
14	Building whole subunit	-	Secondary structure	-	-

15	Energy minimization	-	-	-	1000
16	Molecular dynamics Cooling	from 800 to 300	NOE constraints + fixed Cα of bundle	10.0	-
17	Energy minimization	-	-	-	1000
18	Molecular dynamics Cooling	from 350 to 300	Fixed Cα of bundle	10.0	-
19	Molecular dynamics	300	Gradually releasing bundle constraints	25.0	-
20	Energy minimization	-	-	-	1000
21	Molecular dynamics	300	-	100.0	-
22	Energy minimization	-	-	-	1000

Table 7.3 Model building and MM/MD protocol for the β-subunit - model III. Detailed parameters are listed in text above. Protocol is based on the SA/MD protocol for building ion channels [Kerr et al., 1994].

Stage	Notes	Temperature (K)	Constraints	Time (ps)	Steps
1	Helix building	-	$\phi = -57°$; $\psi = -47°$	-	-
2	Four helix bundle building	-	Docking procedure (Chapter 6.)	-	-
3	Loops 1-2 and 2-3 building	-	NMR based models (Chapters 2. and 3.)	-	-
4	Loop 3-4 and cytoplasmic tails building	-	Secondary structure prediction (Append. 1)	-	-
5	Manual docking of loops and tails into bundle	-	All structures fixed	-	-
6	Energy minimization	-	-	-	1000
7	Molecular dynamics Cooling	from 800 to 300	NOE constraints + fixed Cα of bundle	10.0	-
8	Energy minimization	-	-	-	1000
9	Molecular dynamics Cooling	from 350 to 300	Fixed Cα of bundle	10.0	-
10	Molecular dynamics	300	Gradually releasing bundle constraints	25.0	-
11	Energy minimization	-	-	-	1000
12	Molecular dynamics	300	-	100.0	-
13	Energy minimization	-	-	-	1000

7.3 Results and discussion

7.3.1 Molecular modelling of the β-subunit. Model I - using the hydrophobic moments.

As a first step to the modelling of the β-subunit of FcεRI, the four transmembrane helices of the β-subunit were chosen as these should be close in space due to the interconnecting loops that bring them together.

7.3.1.1 Four helix bundle

The four 21 residue helices were accommodated initially by considering the following assumptions:

1) the β-subunit was considered to be independent of the α- and γ-dimer subunits. This assumption mimicks the *in vivo* membrane situation since the β-subunit probably spans the membrane independently before interaction with other subunits [Jacobs and White, 1989].

2) An 'inside-out' pattern of residue hydrophobicity, in which the interior residues are more polar than the membrane-exposed surface residues, was assumed in order to select the most probable sets of relative orientations of the helices between themselves. One of these dispositions of the helices is presented in Figure 7.1. The hydrophobic moment, defined as

$$\mu = \Sigma H_n S_n$$

in which H_n is the numerical hydrophobicity of the n-th residue and S_n is a unit vector in direction from the nucleus of the α carbon towards the geometric centre of the side chain, is used to study folding of globular [Eisenberg et al., 1982a, 1982b] and membrane [Taylor et al., 1994] proteins. The hydrophobic moment of the peptide can be predicted from the

primary sequence using hydrophobicity values for each residue [Eisenberg et al, 1982b]. The hydrophobic moment of each TM helix was calculated and oriented so as to face the lipidic environment.

3) Minimizations were performed using a dielectric constant of 10 Db so as to simulate the lipidic environment.

4) TM1, TM2, TM3 and TM4 were initially positioned regularly with axes that were exactly parallel. The centres of the four helices were placed at interhelical distances of 11.5 A on the corners of a square in a plane perpendicular to the axes. This distance is the sum of the maximal peripheral radii of two poly(Ala) α- helices, assuring the absence of repulsive overlaps in the starting structure [Chou et al, 1994].

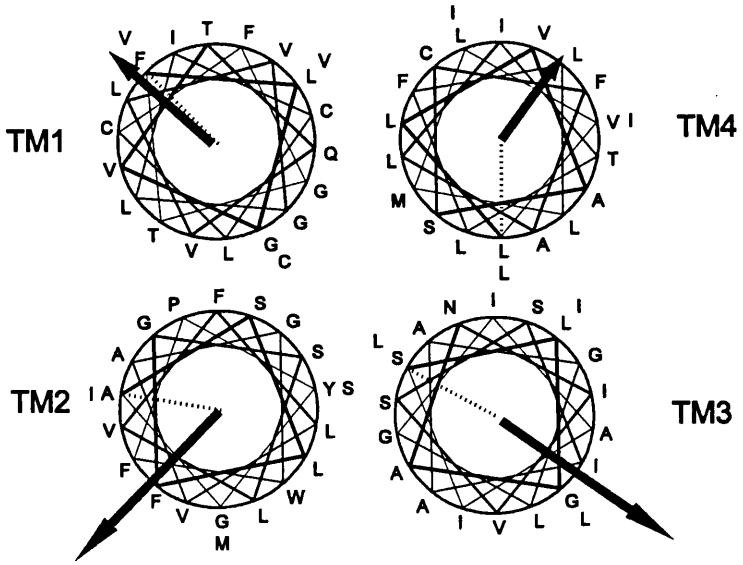

Figure 7.1 The calculated four-helix bundle conformation for the β subunit transmembrane domains of $Fc_{\epsilon}RI$. Wheel diagram of the four helices as seen from above showing the hydrophobic moment vector (arrow). The first residue of each helix is indicated by a dashed line.

After energy minimization and molecular dynamics the helical structure of all the transmembrane domains was conserved. The lowest energy conformation was a four helix bundle arrangement. The principal non-covalent interactions between the constituent helices for the most stable of these arrangements are presented in Figure 7.2. These interactions were mainly Van der Waals and no inter-helix hydrogen bonds were present in this model. The packing was efficient and it resembled the packing in the proteins of class '3-4', as defined by [Clothia et al., 1981]

7.3.1.2 Conformational motifs for the β-subunit involving the transmembrane helices and extracellular loops

The three interconnecting loops were added to the calculated four-helix bundle and molecular dynamics calculations were performed. The secondary structure of the loops was based on the evaluation of CD spectra. The molecular dynamics calculations were carried out by heating up to 600 K, cooling down to 300 K and then energy minimization for the lowest energy structures.

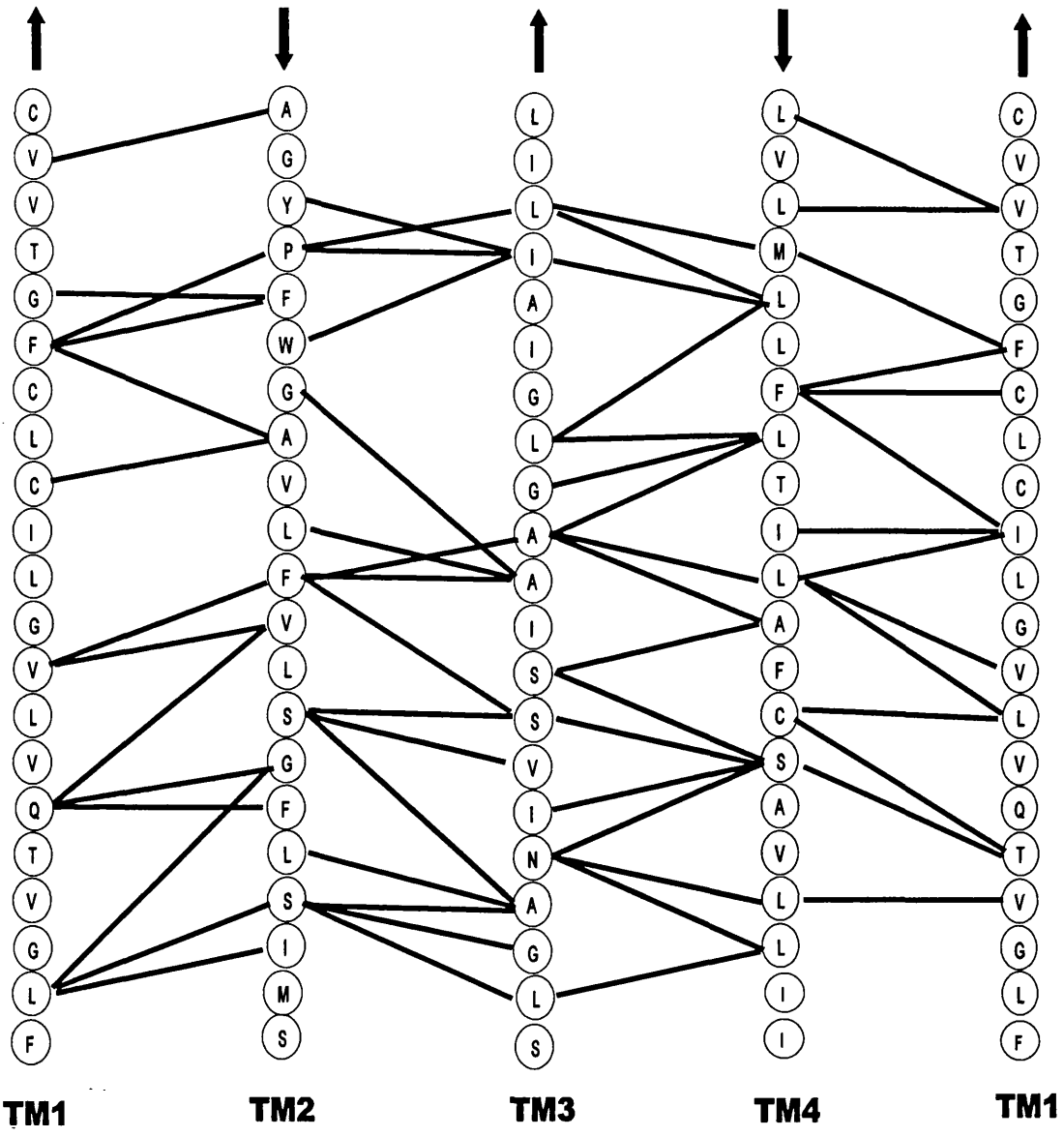

Figure 7.2 Diagram of the four β transmembrane domains where inter-helix interactions are indicated with full lines (residues up to 4 Å apart). The arrows represent the orientation of the TM helices, from N- to C-terminal end.

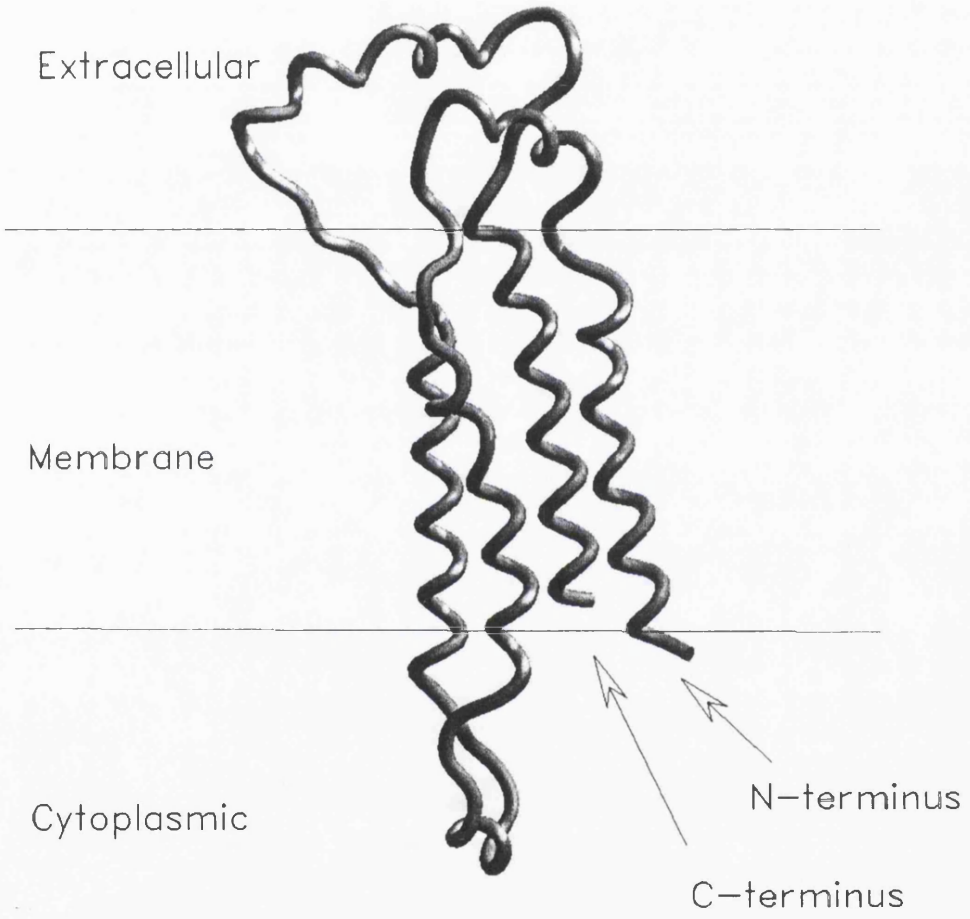

Figure 7.3 The conformation of the four-helix bundle and three interconnecting loops of high affinity IgE receptor, determined from molecular mechanics and dynamics calculations and CD spectroscopy of the component loop peptides.

Table 7.4 Geometric and energetic analysis of transmembrane helix - helix packing in the partially truncated model of β-subunit of high affinity IgE receptor. E_{VDW} represents the van der Waals interaction energy between helix pairs, respectively, while d (distance of closest approach) and Ω (crossing angle) are helix packing parameters defined in the Chapter 5., Figure 6.2.

Helix pair	E_{VDW} (kcal/mol)	d (Å)	Ω (degrees)
1 - 2	-27.3	8.9	-175
1 - 3	-2.5	15.3	12
1 - 4	-36.5	10.7	179
2 - 3	-29.3	8.5	-169
2 - 4	-6.5	12.5	15
3 - 4	-33.1	8.5	-161

The most stable conformation of the four-helix bundle including the three interconnecting loops, after molecular dynamics and energy minimization calculations, is presented in Figure 7.3. The interaction energies between neighbouring helices was highest, with negligible interaction between non-neighbouring helices (Table 7.4). Best interaction was found between TM helix 1 and TM helix 4. The helix packing in the four helix bundle was found to correspond to the left handed coiled coil superstructure. The crossing angles (Ω) between helix axes were in the range of 10 to 15 ° for parallel orientation and between -161 to -175° [quasi 19 to 5°] for antiparallel helix arrangement (Table 7.4). Those values correspond to crossing angle of 20° found for the left handed parallel coiled coil [Clothia et al., 1981]. This crossing angle is found usually in proteins with class 3-4 packing, indicating good interaction between helices.

The distance between the axes of neighbouring helices was smaller than that corresponding distances found in helix bundles in protein crystal structures of 9.4 Å [Clothia,et al., 1981] or the mean inter-helix distance of 9.9 Å in integral membrane proteins. The short distances of 8.5 Å were observed, even when the helices were 11.5 Å apart in the starting structure. However, the repeating conformational motif "TM helix-bend - loop helix - bend -TM helix" occurred three times in this structure (Figure 7.3). This motif was predicted independently by two groups: for the high affinity IgE receptor [Zloh et al., 1995] and for *Bacteriorhodopsin* [Yeagle et al., 1995]. In Figure 7.4, the helical wheels of the connecting loop helices based on the calculated model is presented. Later, the NMR studies confirmed that the helical content in the loop structures were overestimated. However, both extracellular loops, loop 1-2 and loop 3-4, did have their predominantly negatively charged side of their central helices facing the membrane lipidic interface. This was consistent with the "positive-inside" rule [von Heijne and Gavel, 1988], in which the cytoplasmic interface of the membrane would be predominantly negatively charged whereas the exoplasmic interface would be predominantly positively charged. Loop 2-3 exhibited the opposite behaviour, although to a lesser extent, probably due to the smaller size of its helical region. In this model the two linear cytoplasmic tail peptides attached to TM helices 1 and 4 could interact with each other as well as with the membrane surface.

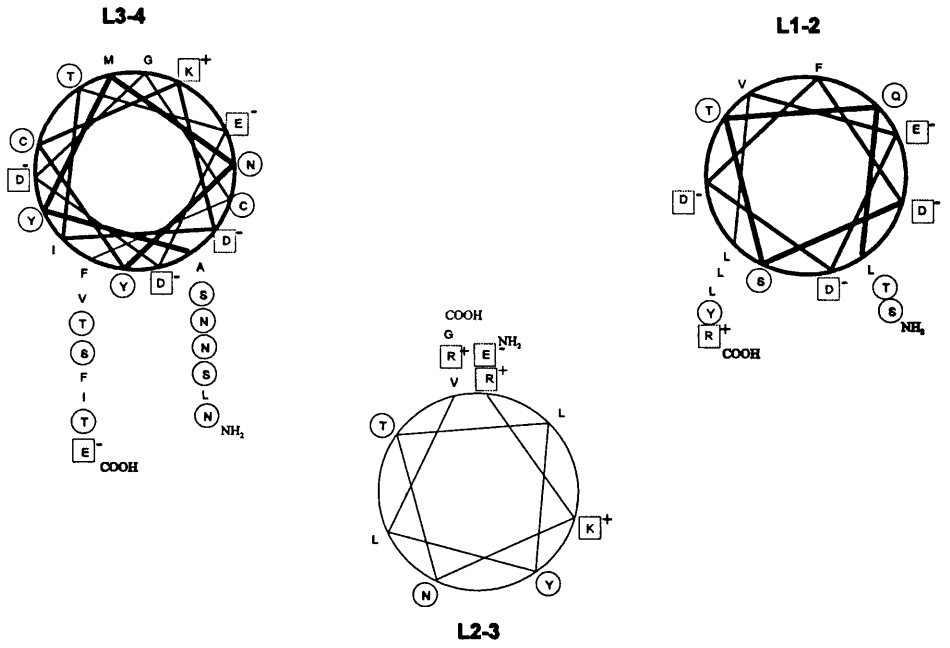

Figure 7.4 Helical wheel representation of connecting loop helices based on the calculated model of the four-helix bundle and three interconnecting loops of high affinity IgE receptor. Charged and polar amino acids are indicated with a square and with a circle respectively.

7.3.1.3 Summary of Model I

This first β-subunit model had weaknesses, since only small number of experimental and theoretical constraints were available to be incorporated in the short molecular dynamics simulations. For example, the helix - helix arrangement was based only on the intuitive orientation of the hydrophobic moments and vertical docking of the TM helices was not allowed. The secondary structures of the connecting loops were based

only on the CD spectra with some information from the secondary structure predictions. Therefore, further refinement in the model building was carried out.

7.3.2 Molecular Modelling of the β-subunit. Model II -use of the docked four-helix bundle and the addition of the loops and tails in two stages

The uncertainties found in the previous model, had led to expanding the work in the several directions. The secondary structures of the loops (1-2 and 2-3) were examined further by NMR and NMR based molecular modelling (Chapters 2. and 3.). The absence of the experimental knowledge in the transmembrane has channelled this work towards helix - helix and helix - lipid interaction studies, as described in Chapters 6., 4. and 5. These experimental and calculated data were therefore used in new calculation of the β-subunit.

7.3.2.1 Partially truncated models of the β-subunit

The twelve helix bundles formed in the Chapter 5. were chosen for the further modelling. To the 12 four helix bundles the loop peptides and 10 residues of each cytoplasmic tails were added. These were subjected to the SA/MD protocol described in the Section 7.2.2 (stages 1-15). Three independent models for each bundle were obtained as a result of the SA/MD protocol. The interaction energies between TM helices within bundles were calculated for all resulting structures. The greatest interaction energies of the lowest energy models for each bundle are shown in Table 7.5.

The adding of the loops and truncated 10 residue tails was therefore utilized to constraint the four helix bundle, since the distance between N- and C- terminals of two

consecutive TM helices could not be larger than the distance between the two terminal ends of the loop that connects those helices (Figures 2.22 and 3.10). In such a way, the structure of the loop could aid the TM bundle folding. Also, new interactions were introduced which could lead to construction of a more detailed model, hopefully closer to reality. In the *Bacteriorhodopsin*, the flexibility of the connecting loops prevented the experimental elucidation of their conformation. Therefore, modelling of the some receptors homologous to the BR (human opoid receptors) was constricted to the modelling of the helix bundle [Habibi-Nezhad et al., 1996]. In the case of 5-HT_2 receptor, the ligand interaction site was identified within the extracellular region. In the absence of the experimental data, the secondary structure prediction results were used as a starting conformation for the loop and tail regions in the building 3-D models and explaining ligand - receptor interactions [Kristiansen et al., 1993; Kristiansen and Dahl, 1996; Sytle et al., 1993; Sytle et al., 1996].

In this work, the experimental (NMR & CD) data of loops were combined with molecular mechanic calculations of lipid - helix interaction sites and secondary structure prediction to build the subunit model. The fulfilling of the experimental and empirical constraints should be therefore criteria for choosing the correct model out of the twelve partially truncated models of the β-subunit. In this case, the TM helix - TM helix packing, expressed through interaction energy between helices within the transmembrane bundle, was also an important determinant. The orientation of the hydrophobic moments and lipid binding sites (determined in Chapters 4. and 5.) were additional and influential factors in making the decision of which model should be subjected to further modelling.

The bundle 5 had greatest individual interaction energy (ΔE_{VDW} = -123.6 kcal/mol), but it was not chosen as a suitable model for further modelling. The lipid facing side of TM helix β4, as predicted by dodecane and PFA molecular mechanics calculations (Figures

4.23B and 5.14), was involved in the TM helix - TM helix contact surface (Table 6.3). However, this bundle could be considered in the future work as a low energy structure.

The bundle 18 (as constructed in the Chapter 6.) had the second greatest interaction energy (ΔE = -107.6kcal/mol). Bundle 18 had the hydrophobic moment of TM 4 facing inside the bundle, not the lipid exterior (Figure 6.10), which could be explained by the small value of the hydrophobic moment for this helix, and this model of the β-subunit could be a good basis for the circular type of the 7 helix bundle of the high affinity IgE receptor (Figure 6.1C).

The overlap of three models for the partially truncated β-subunit based on this bundle is shown in Figure 7.5. The RMSD for the Cα of the bundle was 4.5 Å, indicating a substantial difference in the three models - even the starting point was same. The sampling of the conformational space using this approach could be considered wide varying. The important feature of these models, was that the helical structure of the TM helices was conserved during SA/MD protocol.

The bundle 18 had an excellent agreement between prediction of lipid facing surface on the TM helices by two the different approaches used independently in this work. The lipid favourable surfaces calculated in the Chapters 4. and 5. (residues depicted as a blue circles in Figures 5.5A, 5.8A, 5.11A and 5.14A) were not involved in the helix-helix contact interface determined by docking procedure in the Chapter 6. (Table 6.3). There was an exception for residues (seven residues out of thirty seven), namely F102, F108, V109, I116, I149, T188 and F192. However, those were involved in both, helix - helix and helix - lipid interfaces.

Table 7.5 The interaction energies between the TM helices of the lowest energy four helix bundles of the partially truncated β-subunit of high affinity IgE receptor. The bundle formation was explained in the Chapter 6. The schematic arrangement of the helices within bundles was shown in Figure 6.10

Bundle	E_{VDW} (kcal/mol)
1	-99.9
2	-87.2
5	-123.6
9	-72.2
12	-95.2
17	-103.2
18	-107.6
25	-93.6
27	-81.6
29	-86.5
33	-90.1
35	-89.7

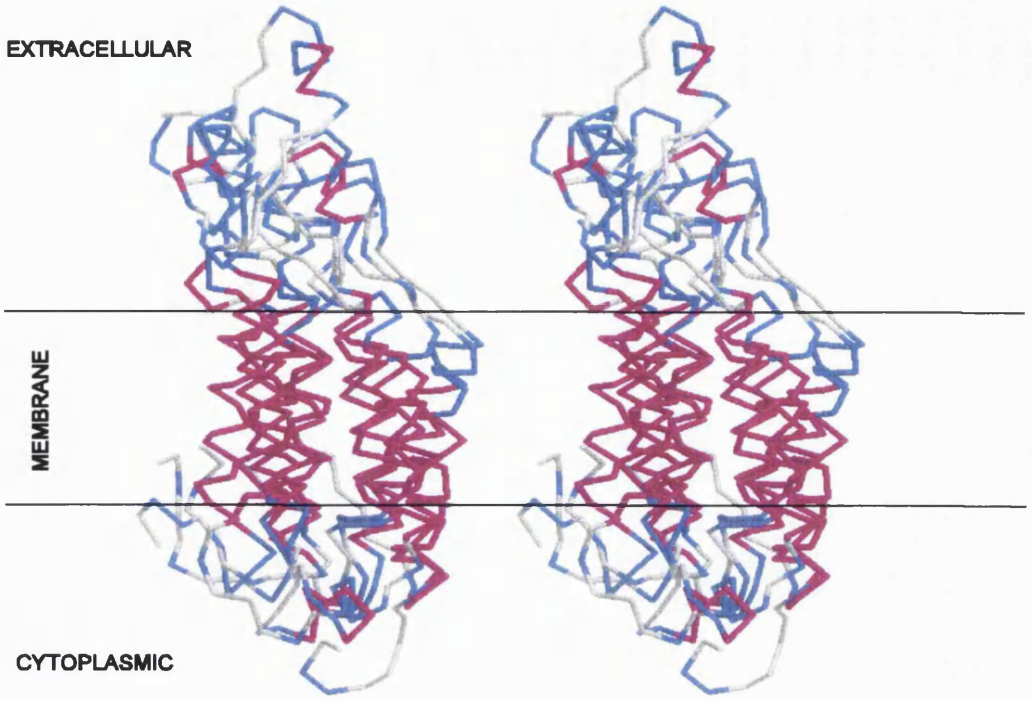

Figure 7.5 Stereoview of the three truncated models overlap of the β-subunit of high affinity IgE receptor built starting from bundle 18 of Chapter 5. Overlapping was done on the Cα of the four helix bundle using Profit software. Secondary structure assignments were colour coded (red - α- helix; blue - β-turn).

7.3.2.2 Complete model of the β-subunit

This model of the truncated β-subunit, based on the bundle 18, was completed by adding the cytoplasmic tails with conformation based principally on secondary structure prediction (Appendix 1.). The initial minimization, followed by several different runs of molecular dynamics (stages 15 to 22 in Table 7.3) were applied to this model. Proteins, including integral membrane proteins, in cells have constantly changing geometries, with movements occurring on a femtosecond to millisecond (10^{-15} to 10^{-3} s) time scales.

Molecular dynamics simulations, which combine molecular mechanics energy functions with Newton's equations of motions, have been used to study the internal movements in proteins, and also to refine 3D molecular structure. For example, a seven helix protein model can change from an initial circular arrangement (Figure 6.1B) into a *Bacteriorhodopsin*-like shape (Figure 6.1A) during 20-25 ps of molecular dynamics simulation in vacuo [Edvardsen et al., 1992; Jahnig and Edholm, 1992]. In this work, molecular dynamics calculations were used to study changes in molecular conformations, since upon addition of kinetic energy to the molecular system, a structure may move across conformational barriers and undergo substantial changes during such simulations.

The geometric changes during molecular dynamics were followed through displacement of the Cα atoms. The RMS deviation from the starting conformation were calculated and presented in different forms (Figures 7.6 and 7.7). In these diagrams, there were an initial molecular dynamics stages of cooling and minimizations (stages 15-18; Table 7.2) after model building, and before simulation at 300 K presented as 0 ps in the graphs 7.6. and 7.7. Also, there was an energy minimization at 25 ps (depicted as a vertical bar in the graphs), after all constraints were removed from the simulation process and dielectric constant was changed to 80 Db.

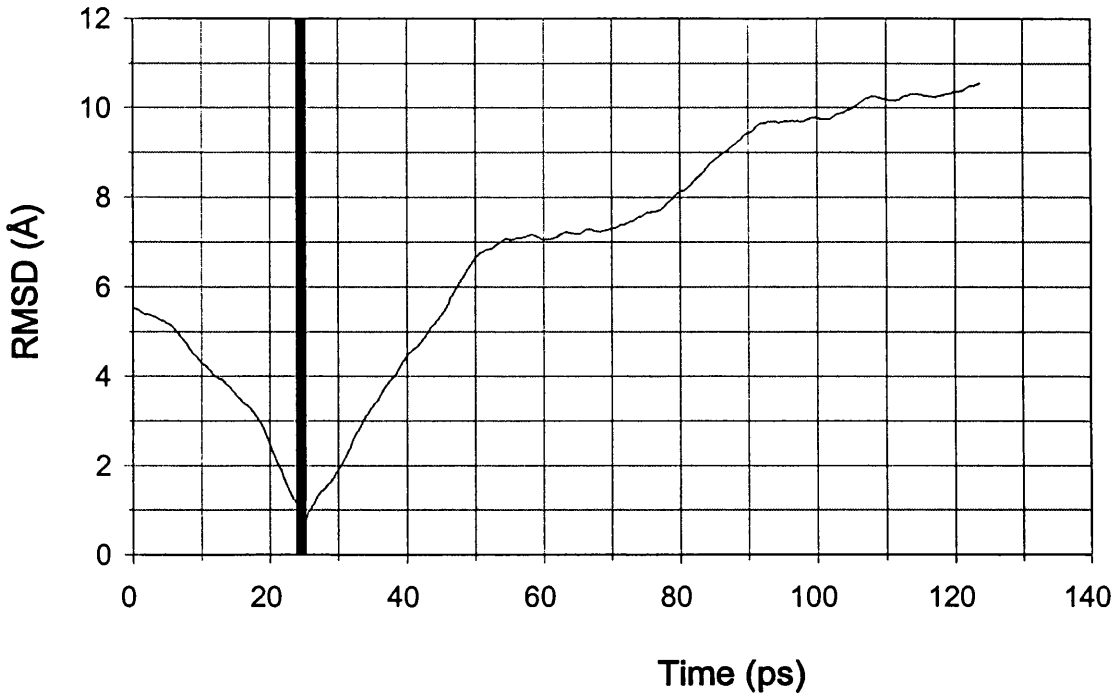

Figure 7.6 Geometric analysis of the β-subunit based on bundle 18, at each 0.25 ps of the molecular dynamics run at 300 K. RMSD was calculated against starting conformation. Cα of the whole subunit were used for the calculations.

The RMSD calculations were performed against the initial model of the β-subunit based on the bundle 18. The conformation of the whole subunit changed considerably and the average structure would not be a good representative, since averaging of the model during simulation could lead to unrealistic geometries. The RMSD for the all atoms of the β-subunit is presented in Figure 7.6. The initial displacement of the atoms during stages 15-18 was around 5.5 Å. This was followed by decrease in the RMSD in the first 25 ps of the simulation (stage 19, Table 7.2), while the dielectric constant was set to 1Db. The α-helical hydrogen bonding constraints (called NOE constraints) were absent, and Cα atom

constraints applied on the bundle were gradually relaxed. The simulation conditions directed changes towards the initial conformation before heating the structure to 500 K as seen in Figure 7.6. After the first 25 ps, the dielectric constant was changed, and the RMSD of all Cα atoms gradually increased to the 10.5 Å, indicating substantial change in the conformation.

The details of RMSD changes was followed both by behaviour of the bundle and of the helical motifs within connecting loop . The bundle and connecting loops parts did not change significantly during the first 25 ps (Figure 7.7A-D), indicating that the cytoplasmic tails were principally responsible for the change. Between 25 and 125 ps of the simulation the bundle conformation did not change (RMSD fluctuated around 0.6 Å). The helical secondary structural elements of loops 1-2 and 2-3 (as determined by NMR based modelling) behaved similarly with an RMSD fluctuation between 0.4 and 0.5 Å. This implied that they possessed conformation similar to the initial model structures based on experimental data. Loop 3-4 exhibited a different behaviour, since the RMSD increased to the 2.3 Å, and structure changed significantly from the initial conformation (based on structure prediction). The structure of loop 3-4 was not significant for docking to bundle 18. Specifically, the distance between the C-terminus of the TM helix 3 and N-terminus of the TM helix 4 was 20.1 Å in bundle 18, which could not be accomodated by the initial conformation of loop 3-4. Unfolding of loop 3-4 was thus observed. The presence of the two cysteine residues (C162 and C171) in the loop 3-4 further complicated the secondary structure prediction, since it has never been established whether or not they form a disulfide bridge.

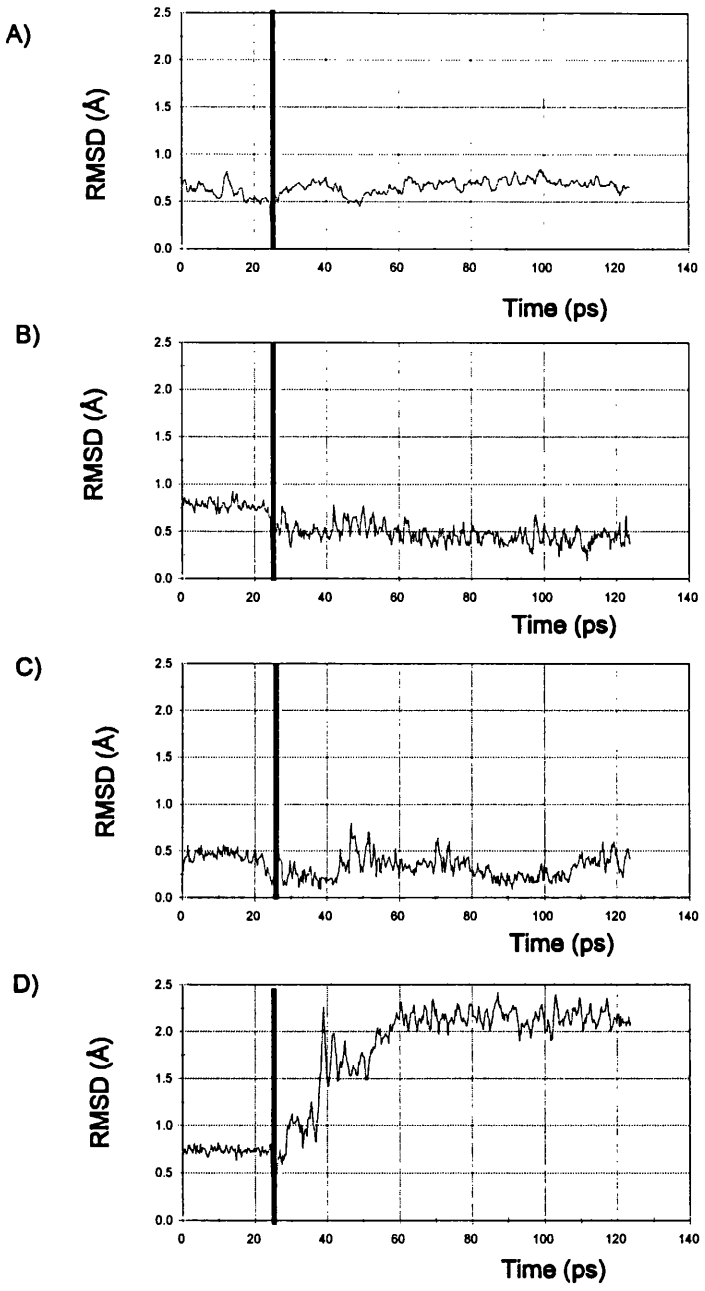

igure 7.7 Geometric analysis of the β-subunit based on bundle 18, at each 0.25 ps of the molecular dynamics run at 300 K. RMSD was calculated against the starting conformation, for the secondary structure elements set during building of the initial model . A) bundle -

residues 60-80, 98-117, 130-150 and 180-200; B) Loop 1-2 - residues 86-91; C) Loop 2-3 - residues 121-126; D) Loop 3-4 - 156-164). Cα atoms were used for the calculations.

The snapshot structures from the beginning and the end of the simulation are shown in Figure 7.8. In the agreement with the above arguments, the biggest change in the structure was observed for the cytoplasmic tails.

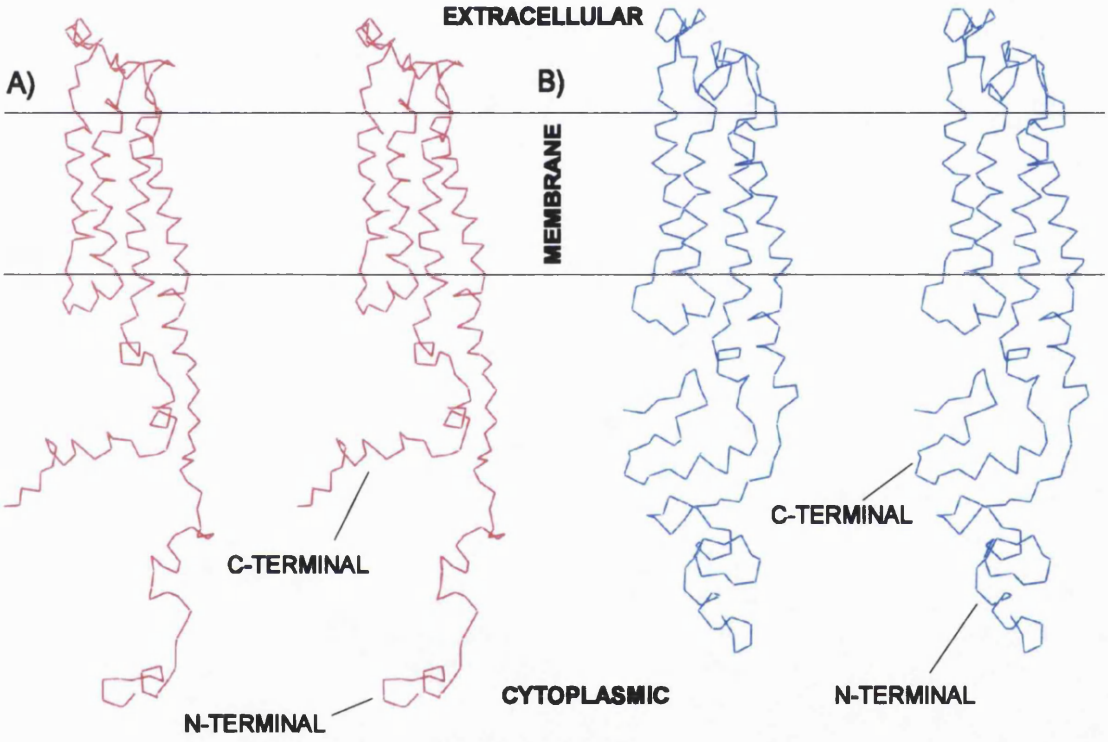

Figure 7.8 Stereoview of the Cα atoms representation of the β-subunit models based on the bundle 18. Snapshot from the molecular dynamics simulation at A) 0 ps and B) 125 ps as defined for the Figure 7.6.

The relevant biological feature (cell signalling) of the β-subunit detected experimentally was phosphorylation of the cytoplasmic C-terminal tail (Chapter 1.), which then interacted with Lyn SH2 domain of tyrosine kinase [Kihar and Siraganian, 1994].

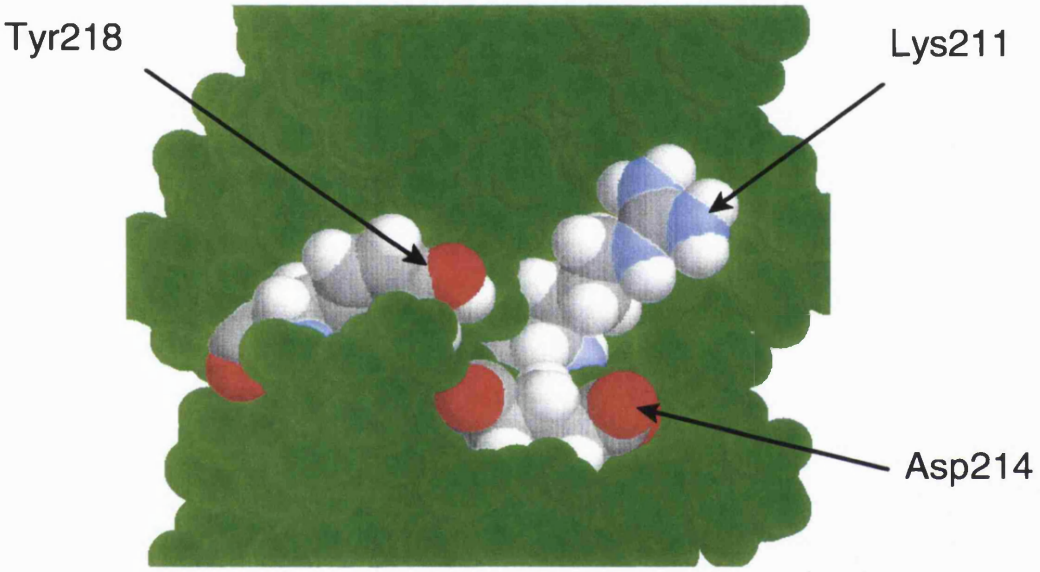

Figure 7.9 The van der Waals surface presentation of the cytoplasmic tails of the β-subunit model II based on the bundle 18. All residues were coloured in green, except residues belonging to tyrosine phosphorylation sites, namely K211, D214 and Y218, which were coloured according to the CPK scheme.

The search of the PROMOTIF database detected two motifs - containing tyrosine phosphorylation sites in the C-terminal sequence. Both motifs had the sequence which appears twice in β-subunit, cytoplasmic C-terminal tail:

[RK]-x(2,3)-[DE]-x(2,3)-Y.

These were:

Site I - $\mathbf{K}^{211}$VP$\mathbf{D}^{214}$DRL$\mathbf{Y}^{218}$;

Site II - $\mathbf{R}^{216}$LYE$\mathbf{E}^{220}$LHV$\mathbf{Y}^{224}$.

The analysis of the van der Waals surface of the cytoplasmic domains in this work found that the relevant residues belonging to tyrosine phosphorylation site I were exposed to the solvent (Figure 7.9) and available for the interaction with signal transduction kinases. The other site was not fully exposed in this model. However, the model was refined in the absence of the water molecules and lipid bilayer, so the further refinement would be necessary, before studying phosphorylated subunit - SH2 protein interaction.

7.3.2.3 Summary of Model II

The generated molecular model is modelled in such way, that during procedure environment could not be explicitly included. The absence of the lipid bilayer - surrounding water molecules, and rest of the high affinity IgE receptor could present the problem that could lead to a wrong result. In this work, the used approach should avoid some of these obstacle by accepting following:

- a combination of distance-dependent dielectric and switching function is appropriate for MD simulations in the absence of any solvent [Loncharich and Brooks, 1989; Sankararamakrishnan and Sansom, 1994].

- parts of the receptor could be replaced by a truncated receptor model and used in the ligand - receptor interaction studies [Habibi-Nezhad et al, 1996; Sansom et al, 1998].

Formed four helix bundle could have both anticlockwise and clockwise when viewed from the extracellular side, and that question could be answered by site-directed mutagenesis or by obtaining detailed crystal structure. Owing to the relatively small structural changes during model refinement, the validity of such models depends heavily on the starting structure. In principle, the model could have correct shape, but it would be premature to draw firm conclusions about the fine structure of the receptor from such models. It has been maintained that it may not even be reasonable to ask how close these models are to the real receptor structure due to the lack of the experimental data [Dale and Edvardson, 1994]. At this stage, the main purpose of molecular model could be to use resulted model to interpret biological data, create new ideas and design new experiments. Molecular models have already proven to be useful for this purposes [Dale and Edvardson, 1994].

However, few interesting features of this model could be pointed out:

- The resulted model of the β-subunit presented here was based on the docking of the TM helices and in every attempt the result was the four helix bundle, without introducing any constraints during docking procedure.

- The excellent agreement between calculated lipid-facing surfaces by helix - helix docking and molecular mechanics hydrophobic surface mapping.

- The NMR based structure of the connecting loops fit well into four helix bundle.

- The C-terminal tail of the β-subunit in this model possessed the conformation adequate for the possible explanation of the signal transduction mechanism, but further work would be required in this direction.

7.3.3 Molecular modelling of the β-subunit. Model III - use of the docked four helix bundle and the addition of the loops and tails in one stage.

The other approach cited in the literature were also applied to the dopamine receptor [Dahl and Edvardsen, 1994] and to the 5-HT_2 receptor [Kristiansen et al., 1993; Kristiansen and Dahl, 1996; Sytle et al., 1993; Sytle et al., 1996]. The loops and tails with predicted secondary structure were added to the 7-helix bundle, and resulting models were subjected to the molecular dynamics simulation.

The work presented in this section was based on the similar approach. The use of the experimental data (NMR based structure of the loops 1-2 and 2-3) gives the extra strength to this work. According to the results of the Chapter 6, the bundle depicted as 25 could be most suitable subject for the modelling.

7.3.3.1 Molecular dynamics simulation of the whole β-subunit

The geometric changes during molecular dynamics were again followed through displacement of the Cα atoms. The RMS deviations from the starting conformation were calculated and presented in different forms (Figures 7.10 and 7.11). There were initial molecular dynamics stages of cooling and minimizations (stages 6-10; Table 7.3)

after model building, and before simulation at 300 K presented as 0 ps in the graphs 7.10 and 7.11. Also, there was an energy minimization at 25 ps (depicted as a vertical bar in the graphs), after all constraints were removed from the simulation process and dielectric constant was changed to 80 Db.

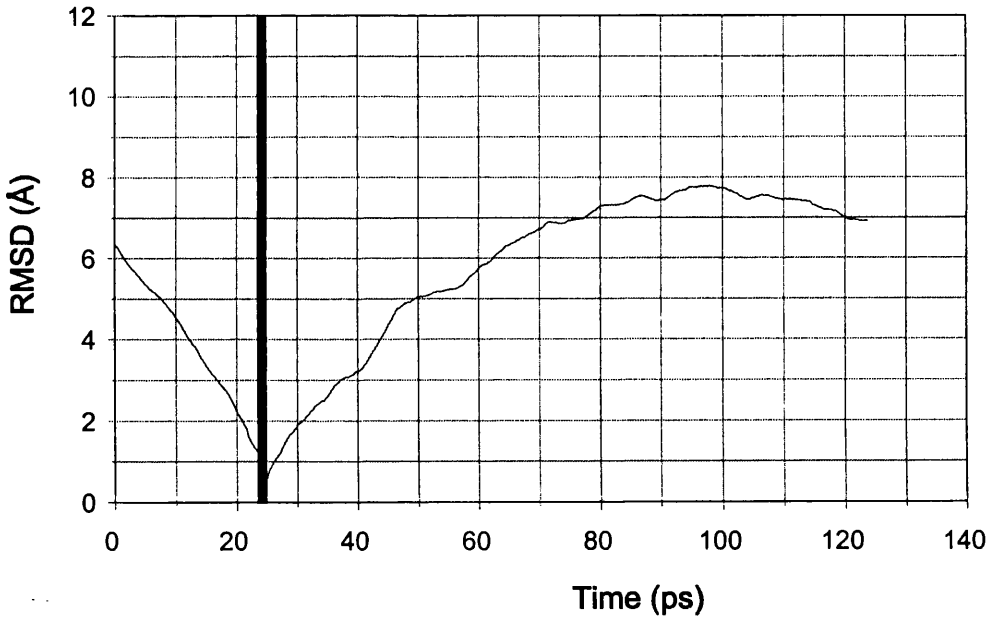

Figure 7.10 Geometric analysis of the β-subunit based on the bundle 25, at each 0.25 ps of the molecular dynamics run at 300 K. RMSD was calculated against starting conformation. Cα atoms of the whole subunit were used for the calculations.

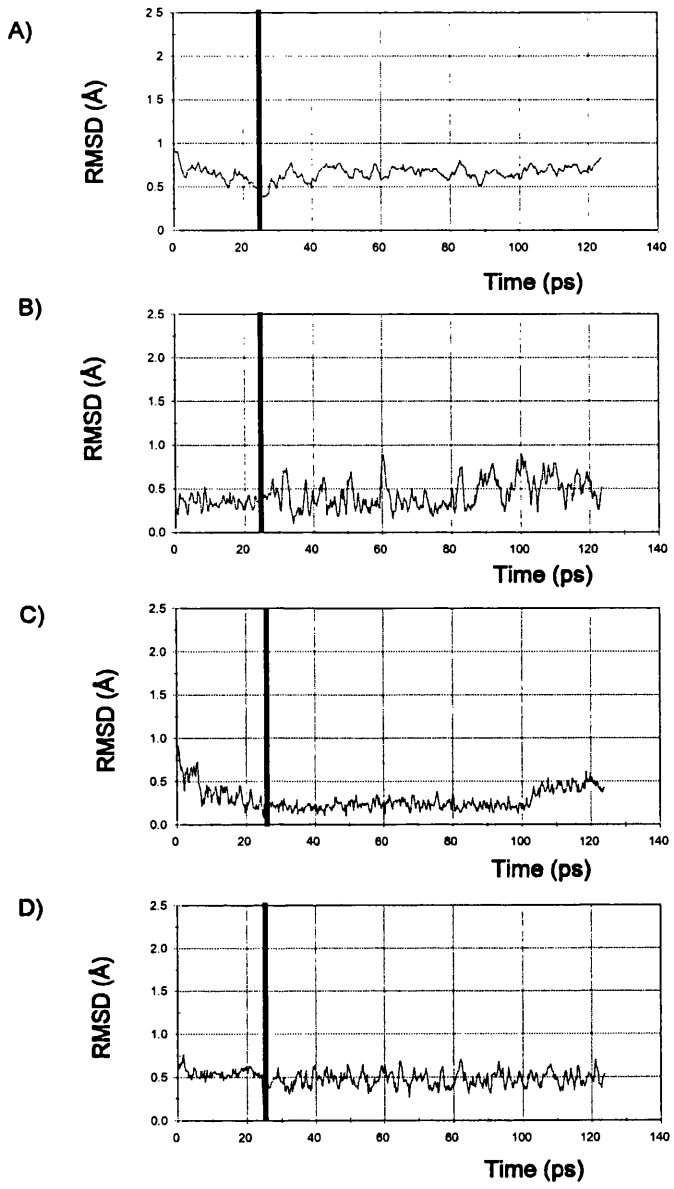

Figure 7.11 Geometric analysis of the β-subunit based on the bundle 25, at each 0.25 ps of the molecular dynamics run at 300 K. RMSD was calculated against starting conformation, for the secondary structure elements set during building initial model . A) bundle - residues 60-80, 98-117, 130-150 and 180-200; B) Loop 1-2 - residues 86-91; C) Loop 2-3 - residues 121-126; D) Loop 3-4 - 156-164). Cα atoms were used for the RMSD calculations.

The RMSD calculation were performed against the initial model of the β-subunit. The RMSD for the all atoms of the β-subunit is presented in Figure 7.10. The initial displacement of the atoms during stages 6 to 9 (Table 7.3) was around 6.0 Å. This was followed by decrease in the RMS in the first 25 ps of the simulation (stage 10), while the dielectric constant was set to 1Db. The NOE type constraints were absent, and Cα atom constraints applied on the bundle were gradually relaxed. These simulation conditions directed changes towards the initial conformation. After the first 25 ps, the dielectric constant was changed to 80 Db (as for the model II). The RMSD gradually increased to the 7.5 Å during this procedure, indicating changes in the conformation of the whole subunit. This RMSD change was smaller than the corresponding change of RMSD for the β-subunit model (model II) based on the bundle 18 (Section 7.3.2.1).

The details of the RMSD changes were once again followed by monitoring both the behaviour of the bundle and the helical motifs of the connecting loops. The bundle and connecting loops helices did not change significantly during period of the first 25 ps (Figure 7.11A-D), indicating that the cytoplasmic tails must have been changing. In the later stages of the simulation the bundle conformation did not change (RMSD fluctuated around 0.7 Å). The helical secondary structure elements of all three loops exibited similar behaviour, with their RMSD fluctuating between 0.2 and 0.7 Å. This implied that they had similar conformations to the initial models based on the experimental and theoretical data. The results for loop 3-4, however, were different from the results in the model II section, where the RMSD increased to the 2.3 Å,. In this case, structure did not deviate far from of the initial conformation (based on the structure prediction). The initial structure prediction of loop 3-4 was not suitable for the conformation bundle 18, where the distance between the C-terminus of the TM helix 3

and the N-terminus of the TM helix 4 was 20.1 Å. The distance between C-terminus of the TM helix 3 and N-terminus of the TM helix 4 for the bundle 25 was by comparison only 5.4 Å. The loop 3-4 initial conformation was therefore more suitable to bundle 25 than bundle 18. The unfolding of this loop was not observed when attached to bundle 25.

A comparison of the snapshot structures from the beginning and the end of the simulation were shown in Figure 7.12. Again, the biggest change in the structure was observed at cytoplasmic tails.

The analysis of the van der Waals surface of the cytoplasmic domains revealed that residues belonging to tyrosine phosphorylation site II (Section 7.3.2.2) were exposed to the solvent (Figure 7.13) and available for the interaction with signal transduction proteins. The other site was not fully exposed in this model as it was in model II. Again, the model was refined in the absence of the water molecules and lipid bilayer, and thus further refinement would be necessary in order to study phosphorylated subunit - SH2 protein interaction.

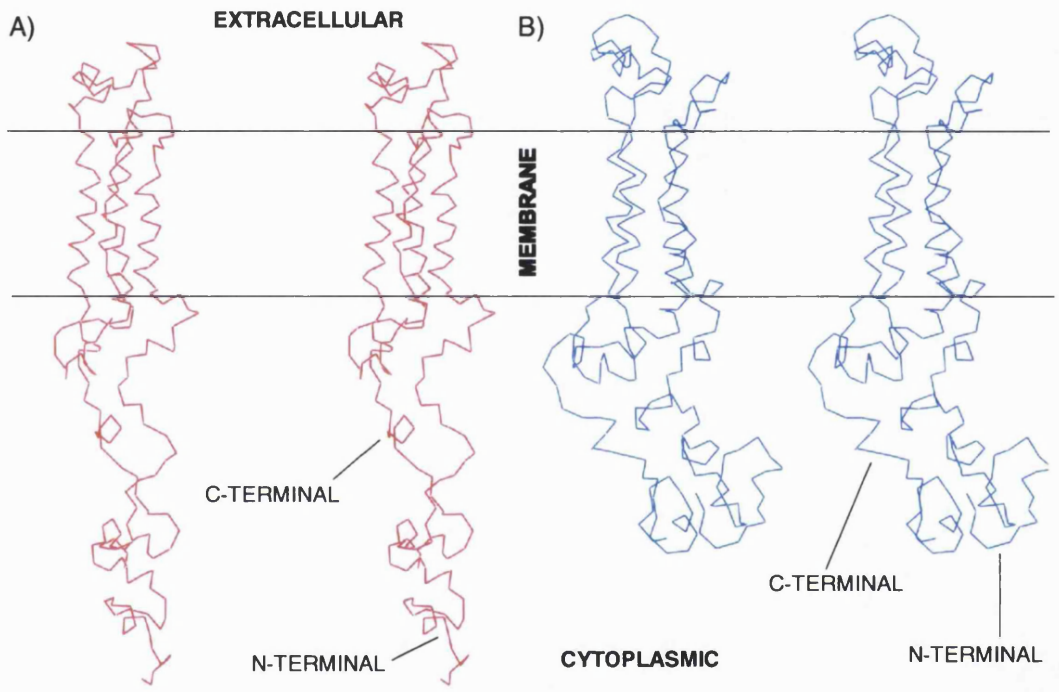

Figure 7.12 Stereoview of the Cα presentation of the β-subunit models based on the bundle 25. Snapshots from the molecular dynamics simulation at A) 0 ps and B) 125 ps as defined for the Figure 7.10.

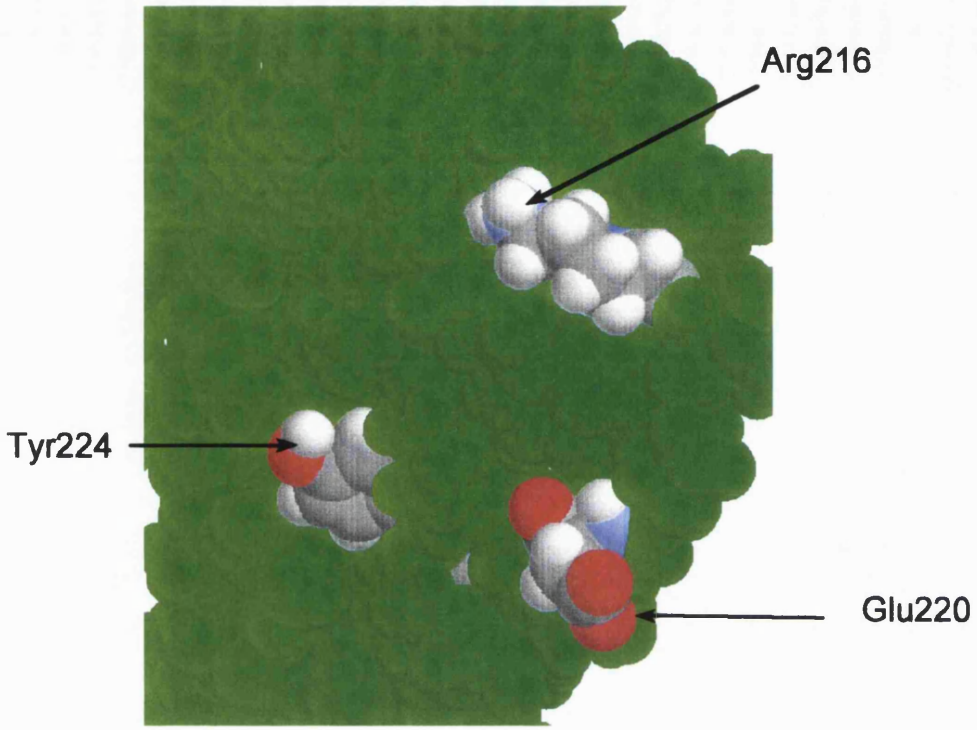

Figure 7.13 The van der Waals surface presentation of the cytoplasmic tails of the β-subunit model based on the bundle 25. All residues were coloured in green, except residues belonging to tyrosine phosphorylation sites, namely R216, E220 and Y224, which were coloured according to the CPK scheme.

7.3.3.2 Summary of Model III.

The conclusions from the Section 7.3.2.2 could be drawn for this model.

- The resulted model of the β-subunit presented here had the four helix bundle motif in the transmembrane domain.

-It had a clockwise arrangement of the four helix bundle as viewed from the extracellular side, but the question of the clockwise or anticlockwise arrangement is still not resolved.

- The very good agreement between calculated lipid-facing surfaces by helix - helix docking and molecular mechanics hydrophobic surface mapping.

- The NMR based structure of the connecting loops fit well into four helix bundle.

- The C-terminal tail of the β-subunit in this model possessed the conformation adequate for the possible explanation of the signal transduction mechanism, but further work would be required in this direction.

This and previous models have to be tested for the correctness and accuracy through obtaining further experimental data and explaining the biological and biochemistry facts described in the Chapter 1.

7.4 Summary

In this chapter, three different approaches were used in the modelling of the transmembrane protein, β-subunit of the high affinity IgE receptor. Three different, and in the same time similar models were produced and their properties discussed.

Through CD and NMR spectroscopy, the conformational behaviour of the three interconnecting loop peptides of the β-subunit of the high affinity IgE receptor was studied. In the three cases some degree of helical content was found.

The calculation of the three-dimensional structure of the four membrane-spanning segments of the β-subunit using rules of helix-helix packing arrangements and molecular dynamics yielded a four-helix bundle with specific Van der Waals interactions between the TM helices. This four-helix bundle was used as a framework upon which to calculate the conformation of the β-subunit. For each pair of consecutive transmembrane helices and their interconnecting loop peptide, a **TM helix - turn - loop helix - turn - TM helix** motif was found to be stable and within the range of possibilities of secondary structure elements shown by the CD and NMR spectroscopy of the peptide loops. Three models were proposed using three different approaches in the constructing the initial conformation.

In these calculations it was assumed that the β-subunit existed as a single monomeric species. However, the spatial arrangement of the transmembrane domains and disposition of helices of the β-subunit could change when interacting with α- and γ-dimer structural subunits. The relationship to these other subunits, which probably occurs after the folding of the β-subunit, is at present unknown and could be due to both intra and extramembraneous interactions, some of which can be hypothesized from the present data.

The other important feature of this chapter is the possible explanation for signal transduction mechanism was proposed for these the models. The tyrosine phosphorylation motif, found twice in the sequence of the C-terminal tail of the β-subunit, was on the exterior of the van der Waals surface of the cytoplasmic domains in molecular models. The solvent exposed residues of the motif would be available for the interactions with the signal transduction proteins. Thus, these models could be basis for the studying of the signal transduction pathways in allergy and inflammation.

The elucidation of domain conformations opens new possibilities for exploring in vitro a model system of high affinity IgE receptor for investigating the mechanisms of immediate hypersensitivity and the general mechanisms that mediate stimulus-secretion coupling. The next step in this set of calculations will be the addition of the α-subunit and of the γ-dimer TM helices. The determination of the mode of packing of the seven helices of the receptor should allow the modelling of all the exoplasmatic and cytoplasmatic loops and tails of the four subunits, as it was partially described in this chapter. A better understanding of the topology of the receptor is crucial for improving drug design targets related to allergy inflammations.

Chapter 8.

CONCLUSIONS

Chapter 8. Conclusions

8.1 Introduction

The objectives of this thesis were both experimental and theoretical and involved, as the long term objective, the complete determination of the 3D structure the peptides, domain peptides, individual subunits and the intact FcεRI, high affinity receptor for immunoglobulin E. The approach that was adopted was analogous to that used for spectroscopy-based structure determination of complex proteins, including some signal transduction proteins and complexes. The present work has been successful in elucidating the structural properties of the high affinity IgE receptor domains and incorporating experimentally-derived information into plausible molecular models for the β-subunit. The potential limitations of the methods employed was discussed and improvements suggested. The final chapter of this thesis has three aims:

a) To integrate the main findings of the work, discussing the results in the context of structure.

b) To evaluate the experimental and modelling approaches adopted, highlighting both their advantages and drawbacks.

c) To suggest refinements and indicate potential future work.

8.2 Integrated results summary

The high affinity IgE receptor is a polytopic membrane protein, and based upon its gene sequence, was divided, into its α-, β- and γ-dimer subunits ($\alpha\beta\gamma_2$), with an unknown 3D structure. Even if molecular biology could produce sufficient quantity of each of its four subunits (α, β, γ and γ-dimer) it would be difficult to assemble the structure of intact receptor after purification. A combination of both experimental and theoretical approaches was therefore applied to this complex problem. The solution to the 3D structure determination of the whole receptor was divided into several different, yet complementary, steps:

- spectroscopic determination of the 3D structure of the domain peptides;
- molecular mechanics probing of the relative hydrophobicity of the individual TM helical domains;
- prediction of the lipid facing surface of the TM helices using molecular mechanics;
- determination the TM helix - TM helix packing and orientation by docking;
- and finally, combination of all the above data sets to form plausible molecular models of the β-subunit of the high affinity IgE receptor.

The dissecting of the receptor into its domains and structure elucidation of those domains has been used as an alternative to whole receptor structure determination. Such approach was also used in determination of the connecting loops structures of another 7 helix membrane protein - bovine rhodopsin [Yeagle et al., 1995; Yeagle et al., 1997]. The NMR spectroscopic studies of the domain peptides of FcεRI, showed that generally the

connecting loop peptides of FcεRI contained an α-helical moiety. The middle part of the loops 1-2 and 2-3 peptides were thus folded into an α-helix structure in solution.

The loop peptides were studied in the absence of the rest of the protein and lipid bilayer, and that was biggest disadvantage of this approach. The peptide was free to adopt any conformation. The common difficulty in cases like this is that any particular conformation is adopted in only a small fraction of molecules at any time. A useful technique to magnify these tendencies is to use other organic solvents, like TFE. This enhances the helicity of the peptide segments, but apparently only if the residues have an intrinsic propensity to adopt that conformation [Nelson and Kallenbach, 1989; Lehrmann et al., 1990; Storrs et al., Sonnichensen et al., 1992; Jasanoff and Fersht, 1994; Shiraki et al., 1995; Kemmink and Creighton, 1995; Behrends et al., 1996; Behrends et al., 1997].

The ends of the peptides in these spectroscopic experiments were not restricted by TM helices, as indicated by the high RMSD in NMR based models. The N and C terminal portions of the loop peptide were flexible (which links between the parts with defined structure) and could therefore take on other structures when covalently connected to the two transmembrane helices of the receptor. Based on the results discussed in this thesis, it was reasonable to deduce that the structure of the loops observed by NMR are like the structure of the loops of the high affinity IgE receptor in the biological membrane and that they probably form a **TM helix- bend - loop helix - bend - TM helix** motifs, described earlier in the Chapters 2. and 3. It is possible that this motif is commonly found in 7 helix receptors and other integral membrane proteins.

One question that has arisen concerns the influence of the loop conformation on the orientation of transmembrane helices, and vice -versa, since both the loop conformation and the helix-helix interactions may be important [Rees et al., 1989; von Heijne, 1992] or

even complementary. One hypothesis suggested that loop formation is driven by packing and transmembrane location of the transmembrane helices, which in turn forces the loop to adopt a specific conformation, this was discussed for the loop 2-3 in this work (Chapter 2.). Engelman et al., 1981 suggested that a substructure forms initially with two transmembrane helices connected by a loop, which then inserted into the membrane. The structural information obtained here for the loop 1-2 is more consistent with the latter hypothesis than the former. Much of the sequence of the loop 1-2 is incorporated in a defined structure in the absence of a transmembrane helices and in the absence of the membrane and the rest of the protein (Chapter 3.).

It was important to have this experimental data, especially for the loop peptides, where the conformation (usually helical) determined the end to end distance. The latter distance of course, could be a critical distance for choosing between different, calculated, helix bundles.

Helix - helix interactions guide folding of the TM helices to form higher order structures of high affinity IgE receptor. TM helices were not available either by synthesis or biosynthesis and a purely modelling approach was adopted to determine the possible formation of coiled-coils helix bundles and full 3D structure of the subunits and whole receptor. Molecular mechanics calculations and protein docking were therefore used to study both lipid - TM helix and TM helix - TM helix interactions and methods used are complementary to the method based on the hydrophobic moment orientation.

The first preliminary calculations involved using dodecane to map the lateral (rotational) surface of the individual helices. Thus the total helix surface was characterized by its hydrophobicity of its component surfaces relative to each other. This was called "relative hydrophobic surface mapping of TM helices". To test the validity or usefulness

of this approach, the "7 helix bundle" of *Bacterirhodopsin* was mapped. Fortunately, this methodology clearly delineated the outer lipid facing surfaces of each helix of *Bacteriorhodopsin*.

To make helix surface mapping more relevant, palmitic fatty acid was also utilized. This gave essentially the same results as hydrophobic mapping with dodecane but added further insight into helix surface mapping. Thus it was seem that helix-residues such as Trp (its indole ring NH) and other residues could form stabilizing hydrogen bond with COOH group of palmitic fatty acid.

The corollary to the mapping and identification of the relative hydrophobic surfaces that would interact with membrane bilayer (leaflet) lipids was that other helix surfaces would be more prone to interacting in helix - helix contacts.

To test this and to provide evidence for surfaces favourable (energetically) for helix - helix contacts each of the six different helices of IgE receptor were subjected to docking procedure. This yielded an additional data base for calculating coiled-coils and helix bundle structures. The results proved supportive and complementary to the lipid- helix results.

The results of three complementary approaches were combined to build, for example, four helix bundle of the β-subunit. The helix - helix docking protocol was designed to be as objective as possible, such that subjective input was minimal. The helix packing parameters found in the four helix bundles that were formed in the β-subunit, ie. the inter-helix distance and the helix crossing angle, were consistent with those observed in the *Bacteriorhodopsin* and photosynthetic reaction centre and therefore the docking protocol used here was a plausible approach to determine packing in helix bundles. It was found that several calculated bundles also fulfilled the hydrophobic moment orientation and low energy criteria. Less complicated receptors homologous to *Bacteriorhodosin* [Green,

1991; Dale and Edvardson, 1994], by the latter two criteria yielded more than one possible helix bundles. This was also true in this work.

These four sets of data 1) experimental, 2) lipid - helix contact surface mapping, 3) helix - helix contacts and 4) hydrophobic moments were used as input data in the final calculations of the β-subunit or filter to choose between low energy helix bundles.

Two different lowest energy four helix bundle were therefore used to construct the complete model of the β-subunit and the latter subjected to SA/MD protocol. The potential energy surface of such a complex subunit (243 residues) is highly irregular, and it was explored more efficiently by high temperature molecular dynamics combined with simulated annealing [Kirkpatrik et al., 1983]. The protocol used here took no explicit account of the effects of the lipid bilayer and solvent water, consequently a global minimum could not be exactly defined. Charge screening due to the low dielectric medium of the lipid bilayer was mimicked by the use of a distance-dependent dielectric constant. The complexity of the problem rises, since there are three phases with different properties, that could not be represented by simply changing the dielectric constant. Therefore, lipid bilayer and water molecules has to be included during simulation, to create model closer to reality.

However, the resulting models of the β-subunit presented were had several exciting features. The excellent agreement was achieved between calculated lipid-facing surfaces by helix - helix docking and molecular mechanics hydrophobic surface mapping. The NMR based structure of the connecting loops fitted well into docked four helix bundle. Not only did these calculations led to interesting β-subunit and helix bundles models and could provide a basis for calculation provisional 3D structures for the whole receptor, but they indicated that a common structural motif for coiled coils and helix bundles in 7 helix

receptors existed. This motif involved (TM helix - bend - loop helix - bend - TM helix). In the proposed models of the β-subunit it was found 3 times. In the a single polypeptide chain having 7 helices in the form of coils or bundles it could occur a maximum of six times.

The potential explanation for the structure/function relationship was also found for this models of the β-subunit, but further work would be required to expand these data. Until a detailed experimental structure of the high affinity IgE receptor is available, models may provide insight into receptors mechanisms and be used to design new experiments.

8.3 Future work

The results of present work naturally suggest several directions of the future research of the structure of the high affinity IgE receptor and in the field of the drug design against allergy and inflammation.

- Obtaining the further structural information for the cytoplasmic tails and third connecting loop of the β-subunit by spectroscopic methods;

- Generating seven helix bundle of the receptor;

- Automating the combination of the helix docking protocol and hydrophobic surface calculations.

- Incorporating known structural data for the α- and γ-subunits into plausible molecular model of the whole receptor;

- Molecular dynamics simulations of the whole receptor in the presence of the lipid bilayer and water molecules;

- Producing the high affinity IgE receptor models of other species by mutations of initial model using molecular modelling;

- Design of experiments to evaluate the molecular models;

- Rationalize the receptor aggregation mechanism;

- Study of the Interaction of the γ- and β-cytoplasmic tails with SH2 domain of the tyrosine kinase by molecular dynamics simulation;

- Rational drug design based on the prevention of receptor aggregation or breaking the signal transduction pathways in allergy process.

The model building depends greatly on the experimentally derived restraints [van Gunsteren and Mark, 1992]. The knowledge of the protein secondary structure could be obtained through spectroscopic studies of domains (CD, FT-IR and solution NMR spectroscopy), which identify the percentage and location of secondary structure of proteins, could aid the construction of initial models. The more complex domains, like TM domain - extracellular loop - TM domain, could be synthesized (or expressed in the bacteria) and studied.

The best source of structural restraints would be a crystallography or cryo-EM, if expression and purification of the whole receptor or β-subunit would be achieved. This has been obtained for both halorhodopsin [Havelka et al., 1993], *Bacteriorhodopsin* [Grigorieff et al., 1996] and rhodopsin [Schertler et al., 1993], when the number of TM segments was identified, their secondary structure, and the overall topology of the molecule solved (eg. a 7 TM helix bundle in both the referred cases). Combination of EM projections and neutron diffraction studies (which rely on the differential scattering of neutrons by hydrogenated and deuterated amino acids) can aid in the determination of TM helix

orientation [eg. Samatey et al., 1994]. Solid state NMR could also produce distance restraints that could be incorporated in the model building.

Interpretation of biochemical data would give powerful constraints, like:

i) The identification of disulphide bridges can be interpreted as a powerful inter-atomic distance restraint.

ii) Interpretation of site-directed mutagenesis data, as demonstrated in modelling of globular proteins [Jin et al., 1994] and in transmembrane domains [Adams et al., 1995].

The SA/MD procedure was the subject of a number of studies designed to counter the possible drawbacks discussed above. While the omission of the lipid bilayer is a drawback to the present calculations, the inclusion of explicit lipid molecules in the molecular dynamics simulations would be beneficial after building initial models. That would lead to the increased computational requirement. At the moment a full lipid simulation is beyond our facilities. The determinations of lipid bilayer structures [Weiner and White, 1992] and molecular dynamics simulations of lipid bilayers surrounded by water [Egberts et al., 1994] indicate how a "bilayer" potential might be included in the SA/MD protocol. Molecular dynamics of individual alpha-helices of bacteriorhodopsin was performed in dimyristoyl phosphatidylcholine bilyaer [Woolf, 1997].

The evaluation of molecular models is an import step in modelling procedures. The ensembles of models generated by SA/MD studies could be used to predict inter-residue distances (or the upper and lower limit of an inter-residue distance). Such data could be incorporated into the design of NMR studies, the results of which would be included into further modelling studies, or model could aid to design mutagenesis or biochemistry experiments.

8.4 Summary

The work in this thesis has shown how a combination of experimental and theoretical approaches can be used to propose structure for domains and subunits of high affinity IgE receptor. Additionally, such studies have also led to the development of calculation procedures complement to current molecular modelling methods suitable for application to larger and more complex systems. Despite the improving techniques for the determination of the structure of integral membrane proteins other approaches are still required. It is concluded that combinations of approaches, including structural, biochemical and molecular modelling studies will lead to the development of plausible model structures for receptor proteins.

REFERENCES

REFERENCES

Abagyan, R., and Argos, P., (1992) "Optimal protocol and trajectory visualization for conformational searches of peptides and proteins." *J. Mol. Biol.*, **225**, 519-532.

Adams, P.D., Arkin, I.T., Engelman, D.M. and Brunger A.T., (1995) "Computational searching and mutagenesis suggest a structure for the pentameric transmembrane domain of phospholamban." *Nature Structural Biology*, **2**, 154-162.

Anderson, G.J., Biekofsky, R.R., Zloh, M., Toth, G.K., Toth, I., Benedetti, E., and Gibbons, W.A., (1994/95) "Spectroscopy and modelling of the cytoplasmic domain of the γ-subunit of the high affinity immunoglobulin E receptor." *Biomedical Peptides, Proteins and Nucleic Acids,* **1**, 31-38.

Anderson, G.J., Harris, P.I., Chapman, D., Romer, J.T., Toth, G.K., Toth, I. and Gibbons, W.A. (1992) "Synthesis and spectroscopy of membrane-receptor proteins - the gamma subunit of the IgE receptor." *Eur. J. Biochem.*, **207**, 51-54.

Baker, E.N., and Hubbard, R.E., (1984) "Hydrogen bonding in globular proteins." *Prog. Biophys. Molec. Biol.*, **44**, 97-179.

Baldwin, E.T., Weber, L.T., Charles, R.St., Xuan, J.-C., Appella, E., Yamada, M., Matsushima, K., Edwards, B.F.P., Clore, G.M., Gronenberg, A.M., and Wlodawer, A. (1991) "Crystal-structure of Interleukin-8 - symbiosis of NMR and crystallography." *Proc. Natl. Acad. Sci. USA*, **99**, 502-506.

Baldwin, J.M., Schertler, G.F.X., and Unger, V.M. (1997) "An alpha-carbon template for the transmembrane helices in the rhodopsin family of G-protein-coupled receptors." *J. Mol. Biol.*, **272**, 144-164.

Baron, M., Norman, D.G.,. and Campbell, I.D. (1991) "Protein modules."*Trends Biochem. Sci.*, **16**, 13-17.

Barsukov, I.L., Abdulaeva, G.V., Arseniev, A.S., and Bystrov, A.S."Sequence-specific H-1-NMR assignment and conformation of proteolytic fragment 163-231 of *Bacterioopsin.*" *Eur . J. Biochem.* 1990., **192,** 321-327.

Bax, A., and Davis, D. G. (1985) "MLEV-17-based two-dimensional homonuclear magnetization transfer spectroscopy." *J. Magn. Reson.*, **65**, 355-360.

Beaven, M.A. and Metzger, H. "Signal-transduction by Fc-receptors - the Fc-epsilon-RI case." *Immunol.Today* 1993, **14**, 222-226.

Beaven, M. A., Moore, J. P., Smith, G.A., Hesketh, T. R., and Metcalfe, J. C. (1984) "The calcium signal and phosphatidylinositol breakdown in 2H3 cells." *J. Biol. Chem.*, **259**, 7137-7142.

Beavan, M.A., and Baumgartner, R.A. (1996) "Downstream signals initiated by FcεRI and other receptors." *Curr. Opin. Immunol.*, **8**, 766-772.

Beavil, A.J., Beavil, R.L., Chan, C.M.W., Cook, J.P.D., Gould, H.J., Henry, A.J., Owens, R.J., Shi, J., Sutton, B.J., and Young, R.J. (1993) "Structural basis of the IgE-FceRI interaction" *Biochemical Society Transitions,* **21**, 968-972.

Bechinger, B., Zasloff, M., and Opella, S.J. (1993) "Structure and orientation of the antibiotic peptide magainin in membranes by solid-state nuclear magnetic resonance spectroscopy." *Prot. Scien.*, **2**, 2077-2084.

Behrends, H.W., BeckSickinger, A.G., and Folkers G. (1996) "Evaluation of the secondary structure of vaccinia-virus thymidine kinase by circular-dichroism spectroscopy of overlapping synthetic peptides." *Eur. J. Biochem.*, **241**, 126-132.

Behrends, H.W., Folkers, G., and BeckSickinger, A.G. (1997) "A new approach to secondary structure evaluation: Secondary structure prediction of porcine adenylate kinase and yeast guanylate kinase by CD spectroscopy of overlapping synthetic peptide segments." *Biopol.*, **41**, 213-231.

Benhamou, M., Stephan, V., Robbins, K. C., and Siraganian, R. P. (1992) "High-affinity IgE receptor-mediated stimulation of rat basophilic leukemia (RBL-2H3) cells induces early and late protein-tyrosine phosphorylations." *J. Biol. Chem.*, **267,** 7310-7314.

Berendsen, H.J.C., Posta, J.M.P., van Gunsteren, W.F., DiNola, A., and Haak. J.R., (1984) "Molecular dynamics with coupling to an external bath." *J. Chem. Phys.*, **81**, 3684-3690.

Bertrand, D., Galzi, J-L., Devillers-Thiéry, A., Bertrand, S., Changeux, J-P. (1993). "Stratification of the channel domain in neurotransmitter receptors." *Curr. Opin. Cell. Biol.*, **5**, 688-693.

Billeter, M., and Xia, T., (1997) "MolMol" Ver. 2.5.1, ETH Zurich, Switzerland.

Blank, U., Ra C., Miller, L., White, K., Metzger, H. and Kinet, J-P. (1989) "Complete structure and expression in transfected cells of High-affinity IgE receptor." *Nature*, **337**, 187-189.

Böhm, G., (1997) "CDNN" v. 2.0c

Bonnefoy, J-Y., Aubry, J-P., Gauchat, J-F., Graber, P., Life, P., Flores-Romo, L. and Mazzei, G. (1993) "Receptors for IgE." *Curr.Opin. in Immunol.*, **5**, 944-949.

Brahms, S., and Brahms, J. (1980) "Determination of Protein Secondary Structure i Solution by Vacuum Ultraviolet Circular Dichroism ." *J. Mol. Biol.*, **138**, 149-178.

Breed, J., Kerr, I.D., Molle, G., Duclohier, H., and Sansom, M.S.P. (1997) "Ion channel stability and hydrogen bonding - Molecular modelling of channels formed by synthetic alamethicin analogues." *Biochim.Biophys Acta-Biomembr.*, **1330**, 103-109.

Bruccoleri, R.E., and Karplus, M. (1986) "Spatially constrained minimisation of macromolecules." *J. Comp. Chem.*, **7**, 165-175.

Brunger, A.T., Kurian, J. and Karplus M. (1987) "Crystallographic R-factor refinement by
molecular-dynamics." *Science*, **235**, 458-460.

Brunger, A.T., Krukowski, Ericson, J.W. (1990) "Slow-cooling protocols for crystallographic refinement by simulated annealing." *Acta Cryst.*, **A46**, 585-593.

Brünger, A.T., (1992) "Free R-value - a novel statistical quantity for assessing the accuracy of crystal structures." *Nature*, **355**, 472-475.

Brünger, A.T., Clore, G.M., Gronenberg, A.M., Saffrich, R., and Nilges, M., (1993) "Assessing the quality of solution nuclear-magnetic-resonance structures by complete cross-validation." *Science*, **261**, 328-331.

Brünger, A.T., (1993) X-PLOR version 3.1: "A System for X-ray crystallography and NMR." Yale University Press, New Haven, CT.

Burley, S.K., and Petsko, G.A., (1988) in "Advances in Protein Chemistry." (Anfinsen, C.B., Edsall, J.T., Richards, F.M., and Eisenberg, D.S., Eds.) **39**, 125-189, Academic Press, New York.

Campbell, I.D., Dobson, C.M., and Williams, R.J.P. (1985) "The study of conformational states of proteins by nuclear magnetic resonance." *Biochem J.*, **231**, 1-10.

Chang, C-H., Tiede, D., Tang, J., Smith, U., Norris, J., Schiffer, M. (1986) "Structure of Rhodopseudomonas sphaeroides R-26 reaction center." *FEBS Lett.*, **205**, 82-86.

Chou, K.-C., Carlacci, L., Maggiora, G.M., Parodi, L.A., and Schulz, M.W., (1992) "An energy-based approach to packing the 7-helix bundle of Bacteriorhodopsin." *Protein Science,* **1**, 810-827.

Chou, P.Y. and Fasman, G.D. (1974) "Prediction of protein conformation." *Biochem.*, **13**, 211-222.

Clore, G.M., Appella, E., Yamata, M., Matsushima, K., and Gronenberg, A.M. (1990) "3-dimensional structure of Interleukin-8 in solution." *Biochem.*, **29**, 1689-1696.

Clothia, C., Levitt, M., and Richardson, D. (1981) "Helix to helix packing in proteins." *J. Mol. Biol.*, **145**, 215-250.

Clubb, R.T., Omichinski, J.G., Clore, G.M., and Gronenberg, A.M. (1994) "Mapping the binding surface of Interleukin-8 complexed with an N-terminal fragment of the type-1 human Interleukin-8 receptor." *F.E.B.S. Lett.*, **338**, 93-97.

Cosette, P., Kerr, I.D., LaRocca, P., Duclohier, H., and Sansom, M.S.P. (1997) "Secondary structure of an isolated P-region from the voltage-gated sodium channel: a molecular modelling dynamics study." *Biophys. Chem.*, **69**, 221-232.

Cowan, S.W., Shirmer, T., Rummel, G., Steiert, M., Ghosh, R., Pauptit, R.A., Jansonius, J.N., and Rosenbusch, J.P. (1993) "Crystal structures explain functional properties of two E. coli porins." *Nature*, **358**, 727-733.

Crick, F.H.C. (1953) "The packing of α-helices: simple coiled - coil." *Acta Crystallogr.*, **6**, 689-697.

Cserhati, T., and Szogyi, M. (1991) "Interaction of phospholipids with proteins and peptides - new advances. 1." *Int. J. Biochem.*,**23**, 131-145.

Cserhati, T., and Szogyi, M. (1992) "Interaction of phospholipids with proteins and peptides - new advances. 2." *Int. J. Biochem.*,**24**, 525-537.

Cserhati, T., and Szogyi, M. (1993) "Interaction of phospholipids with proteins and peptides - new advances. 3." *Int. J. Biochem.*,**25**, 123-146.

Dahl, S.G., and Edvardsen, O. (1994) "Molecular modelling of dopamine receptors." in "Dopamine receptors and transporters" (Ed. Niznik, H.B.), Marcel Dekker, Inc., New York.

Deisenhofer, J., Epp, O., Miki, K., Huber, R., Michel, H. (1985) "Structure of the protein subunits in the photosynthetic reaction centre of Rhodopseudomonas viridis at 3 Å resolution." *Nature*, **318**, 618-624.

Deleage, G., and Roux, B. (1987) "An algorithm for protein secondary structure prediction based on class prediction." *Prot. Eng.*, **1**, 289-294

Delano, W.L., and Brunger, A.T., (1994) "Helix packing in proteins: prediction and energetic analysis of dimeric, trimeric and tetrameric GCN4 coiled coil structures." *Proteins, Structure, Function, and Genetics*, **20**, 105-233.

Derome, A.E. (1987) "Modern NMR techniques for chemistry research." Pergamon Press, Oxford.

Doyle, D.A., Cabral, J.M., Pfeutzner, R.A., Kuo, A., Gulbis, J.M., Cohen, S.L., Chait, B.T., and Mackinnon, R., (1998) "The structure of the potassium channel: molecular basis of K^+ conduction and selectivity." *Science*, **280**, 69-77.

Drake, A.F., Siligardi, G. and Gibbons, W.A. (1988) "Reassessment of the electronic circular-dichroism criteria for random coil conformations of poly(L-lysine) and the implications for protein folding and denaturation studies." *Biophys. Chem.*, **31**, 143-146

Edvardsen, O., Sylte, I., and Dahl, S.G. (1992) "Molecular dynamics of serotonin and ritaserin interacting with 5-HT2 receptor." *Mol. Brain. Res.*, **14**, 166-178.

Egberts, E., Marrink, S-J., and Berendsen, H.J.C., (1994) "Molecular dynamics simulation of a phospholipid membrane." *Eur. Biophys. J.*, **22**, 371-374.

Eisenberg, D., Weiss, R.M. and Terwilliger T.C. (1982a) "The helical hydrophobic moment - a measure of the amphiphilicity of a helix." *Nature*, **299**, 371-37

Eisenberg, D., Weiss, R.M., Terwilliger T.C. and Wilcox, W. (1982b) "Hydrophobic moments and protein-structure." *Faraday Symp. Chem. Soc.*, **17**, 109-120.

Elling, C.E., Nielsen, S.M., and Schwartz, T.W. (1995) "Conversion of antagonist-binding site to metal-ion site in the Tachykinin NK-1 receptor.", *Nature*, **374**, 74-77.

Engelman, D.M., and Steitz, T.A.(1981) "The spontaneous insertion of proteins into and across membranes - the helical hairpin hypothesis." *Cell*, **23**, 411-422.

Fasman, G.D., (1995) "The measurement of transmembrane helices by the deconvolution of CD spectra of membrane-proteins - a review." *Biopol.*, **37**, 339-362.

Fersht, A.R., (1984) "Basis of biological specificity." TIBS, **9**, 145-147.

Field, K.A., Holowka, D., and Baird, B. (1997) "Compartmentalized activation of the high affinity immunoglobulin E receptor within membrane domains." *J. Biol. Chem.*, **272**,4276-4280.

Finkelstein, A.V., and Pitsin, O.B., (1987) "Why do globular proteins fit to the limited set of folding patterns?" *Progr. Biophys. Mol. Biol.*, **50**, 171-190.

Ford, J.J. and Gibbons, W.A. (1979) "Conformational studies of neuropeptides using through-space and through-bond interactions." In: "Peptides: Structure, biology, function," Proceedings of the 6th American Peptide Symposium, (E. Gross and J. Meienhofer, eds.), Pierce Chemical Com. Publications, Rockford, 857-859.

Finkelstein, A.V., Badretdinov, A.Y., and Gutin, A.M. (1995) "Why do proteins have Boltzman-like statistics?" *Proteins:Structure, Function, and Genetics,* **23**, 142-150.

Gao, B., Anderson, G.J., Brammer, M.J., James, C.H., Danton, M., Toth, G., Toth, I., Gibbons, W.A. (1993) "Sequence-specific antipeptide antibodies that recognize different subunits of the high-affinity IgE receptor." *Biochem. Soc. Trans.*, **21**, 302-304.

Gao, B., Toth, I., Clark-Lewis, I and Gibbons, W.A. (1994) "Topology studies and immunoreactive forms of the beta subunit of the high affinity IgE receptor using site-specific antibody." *Innovation & Perspectives in Solid Phase Synthesis,* **65,** 423-428.

Garcia-Gil, M., and Siraganian, R. P. (1986) "Phospholipase-A2 stimulation during cell secretion in rat basophilic leukemia-cells." *J. Immunol.* **136**, 259-263.

Garnier, J., Osgurthorpe, D.J., and Robson B. J. (1978) "Analysis of the accuracy and implications of simle methods for predicting the secondary structure of globular proteins." *Mol. Biol.*, **120**, 97-120.

Geourjon, C., and Deleage, G. (1994) "SOPM: a self optimised prediction method for protein secondary structure prediction." *Protein Engineering*, **7**, 157-164.

Geourjon, C., and Deleage, G. 1995, "SOPMA: Significant improvements in protein secondary structure prediction by prediction from multiple alignments." *Comput. Applic. Biosci.*, **11**, 681-684.

Gibrat, J.F., Garnier, J., and Robson, B. (1987) "Further developments of protein secondary structure prediction using information theory - new parameters and consideration of residue pairs." *J.Mol.Biol.*, **198**, 425-443.

Gibbons, W.A., Crepaux, D., Delayre, J., Dunand, J. and Wyssbrod, H.R. (1975) "The study of peptides by INDOR, difference NMR and time-resolved double resonance. In: "Peptides: Chemistry, Structure, Biology, " Proceedings of 4th American Peptide Symposium, (R. Walter and J. Meienhofer, eds.), Ann Arbor Science Publications, 127-137.

Grasberger, B.L., Gronenberg, A.M., and Clore, G.M. (1993) "Analysis of the backbone dynamics of Interleukin-8 by N-15 relaxation measurements." *J. Mol. Biol.*, **230**, 364-372..

Green, M. (1991) "The semiotics of charge" *Nature*, **351**, 349-350.

Grigorieff, N., Ceska, T.A., Downing, K.H., Baldwin, J.M. and Henderson, R.J. (1996) "Electron-crystallographic refinement of the structure of Bacteriorhodopsin." Mol. Biol., **259**, 393-421.

Grobner, G., Choi, G., Burnett, I.J., Glaubitz, C., Verdegem, I.J.E., Lugtenburg, J., and Watts, A. (1998) "Photoreceptor rhodopsin: structural and conformational study of its chromophore 11-cis retinal in oriented membranes by deuterium solid state NMR." *FEBS Lett.*, **.422**, 201-204.

van Gunsteren, W.F., and Berendsen, H.J.C. (1977) "Algorithms for macromolecular dynamics." *Mol. Phys.*, **34**, 1311-1327.

van Gunsteren, W.F., and Mark, A.E., (1992) "On the interpretation of biochemical data by molecular dynamics simulation." *Eur. J. Biochem.*, **204**, 947-961.

Habibi-Nezhad, B., Hanifan, M., and Mahmoudian, M. (1996) "Computer-aided receptor modelling of human opoid receptors - (Mu, Kappa and Delta)." *J. Mol. Model.*, **2**, 362-369.

Harbury, P,B., Zhang T., Kim, P.S., Alber T. (1993) "A switch between two-, three-, and four stranded coiled coils in GCN4 leucine zipper mutants." *Science*, **262**, 1401-1407.

Harris, N. T., Goldstein, B., Holowka, D., and Baird., B. (1997) "Altered patterns of tyrosine phosphorylation and Syk activation for sterically restricted cyclic dimers of IgE-Fc epsilon RI." *Biochemistry,* **36**, 2237-2242.

Havel, T. and Wuthrich, K. (1984) "A Distance geometry program for determining the structures of small proteins and other macromolecules from nuclear magnetic-resonance measurements of intramolecular H-1-H-1 proximities in solution." *Bulletin of Mathematical Biology*, **46**, 673-698.

Havel, T.F., Wüthrich, K. (1985) "An evaluation of the combined use of nuclear magnetic resonance and distance geometry for the determination of protein conformation in solution." *J. Mol. Biol.*, **182**, 281-294.

Havelka, W.A., Henderson, R., Heymann, J.A., and Oesterhelt, D., (1993) "Projection structure of halorhodopsin from *Halobacterium halobium* at 6 Å resolution obtained by electron-cryomicroscopy." *Nature*, **257**, 28-32.

Heberle, J., Buldt, G., Koglin, E., Rosenbusch, J.P., and Landau, E.M. (1998) "Assessing the functionality of a membrane protein in a three-dimensional crystal." *J. Mol. Biol.*, **281**, 587-592.

Henderson, R., Baldwin, J.M., Ceska, T.A., Beckmann, E., and Downing, K.H (1990) "Model for the structure of Bacteriorhodopsin based on high-resolution electron cryomicroscopy." *J. Mol. Biol.*, **213**, 899-929.

von Heijne, G. and Gavel, Y. (1988) "Topogenic signals in integral membrane-proteins." *Eur.J.Biochem.*, **174**, 671-678 .

von Heijne, G. and Manoil C.(1990) "Membrane-proteins - from sequence to structure." *Protein Engineering* 1990, **4**, 109-112.

von Heijne, G. (1992) "Membrane-protein structure prediction - hydrophobicity analysis and the positive-inside rule." *J. Mol. Biol.*, **225**, 487-494.

Hennessey, J. P., and Johnson, W. C., Jr. (1981) "Information-content in the circular-dichroism of proteins." *Biochem.*, **20**, 1085-1094.

Herzyk, P., and Hubbard, R.R., (1995) "Automated-method for modeling 7-helix transmembrane receptors from experimental-data." *Biophys. J.*, **69**, 2419-2442.

Heyn, M.P. (1989) "Circular dichroism for determining secondary structure and state of aggregation of membrane proteins." *Methods Enzymol.*, **172**, 575-584.

Hirasawa, N., Santini, F., and Beaven, M. A. (1995) "Activation of the mitogen-activated protein-kinase cytosolic phospholipase A(2) pathway in a rat mast-cell line - indications of different pathways for release of arachidonic-acid and secretory granules." *J. Immunol.*, **154**, 5391-5402.

Hodges, R.S., Saund, A.K., Chong, P.C.S., StPierre, S.A., and Reid, R.E. (1981) "Synthetic model for two-stranded α-helical coiled-coil: design, synthesis and characterization of an 86-residue analog of tropomyosin.." J. Mol. Chem., **256**, 1214-1224.

Hodges, R.S., Zhou, N.E., Kay, C.M., and Semchuk, P.D. (1990) "Synthetic model proteins: contribution of hydrophobic residues and disulfide bonds to protein stability." *Peptide Research*, **3**, 123-137.

Housset, D., Mazza, G., Gregoire, C., Piras. C., Malissen, B., and FontecillaCamps, J.C. (1997) "The three-dimensional structure of a T-cell antigen receptor V alpha V beta heterodimer reveals a novel arrangement of the V beta domain." *EMBO J.*,.**16**, 4205-4216.

Hu, W., and Cross, T.A. (1995) "Tryptophan hydrogen-bonding and electric-dipole moments - functional roles in the gramicidin channel and implications for membrane-proteins." *Biochem.*, **34**, 14147-14155.

Hu, W., Lazzo, N.D., and Cross, T.A. (1995) "Tryptophan dynamics and structural refinement in a lipid bilayer environment - solid-state NMR of the gramicidin channel." *Biochem.*, **34**, 14138-14146.

Hu, W., Lee, K.-C., and Cross, T.A. (1993) "Tryptophans in membrane-proteins - indole ring orientations and functional implications in the gramicidin channel." *Biochem.*, **32**, 7035-7047.

Huber,R., Romisch, J., and Paques, J.P. (1990) "The crystal and molecular structure of human annexinV, an anticoagulant protein that binds to calcium and membranes." *EMBO J.*, **9**, 3867-3874.

Inouye, M. (1974) "A three-dimensional molecular assembly model of a lipoprotein from the Escherichia coli outer membrane." *Proc. Natl. Acad. Sci.*, **71**, 2396-2400.

Jacobs, R. and White, S. (1988) "The nature of the hydrophobic binding of small peptides at the bilayer interface - implications for the insertion of transbilayer helices." *Biochem.*, **28**, 3421-3437.

Jackson, R.M., Gabb, H.A., and Sternberg, J.E. (1998) "Rapid refinement of protein interfaces incorporating solvation: Application to the protein docking." *J. Mol. Biol.*, **276**, 265-285.

Jahnig, F., and Edholm, O. (1992) "Modeling of the structure of Bacteriorhodopsin - a molecular-dynamics study." *J. Mol. Biol.*, **226**, 837-850.

Jeener, J., Meier, B. H., Bachmann, P., and Ernst, R. R. (1979) "Investigation of exchange processes by two-dimensional NMR spectroscopy." *J. Chem. Phys.*, **71**, 4546-4553.

Jeffrey, G.A., and Saenger, W. (1991) "Hydrogen bonding in biological structure." Springer-Verlager, Berlin.

Jin, L., Cohen, F.E., and Wells, J.A. (1994) "Structure from function: screening structural models with functional data." *Proc. Natl. Acad. Sci.*, **91**, 113-117.

Johnson, W.C. (1990) "Protein secondary structure and circular-dichroism - a practical guide." *Proteins-Structure Function and Genetics*, **7**,205-214.

Jones, C.R., Sikakana, C.T., Kuo, M. and Gibbons, W.A. (1978a) "Interproton distances for the ß-turn residues of the peptide gramicidin S determined from nuclear Overhauser effect ratios." *J. Amer. Chem. Soc.*, **100**, 5960-5961.

Jones, C.R., Sikakana, C.T., Hehir, S., Kue, M. and Gibbons, W.A. (1978b) "The quantitation of nuclear Overhauser effect methods for total conformational analysis of peptides in solution: application to gramicidin S." *Biophysics. J.*, **24**, 815-832.

Jones, G., Willett, P., and Glen, R.C. (1995) "Molecular recognition of receptor sites using a genetic algorithm with a description of desolvation." *J. Mol. Biol.*, **245**, 43-53.

Kahn, T.W., Sturtevant, J.M, and Engelman, D.M. (1992) "Thermodynamic measurements of the contributions of helix-connecting loops and of retinal to the stability of Bacteriorhodopsin." *Biochem.*, **31**, 8829-8839.

Katchalski-Katzir, E., Shariv, I., Eistein, M., Friesam, A.A., Aflalo, C., and Vakser, I.A. (1992) "Molecular surface recognition: Determination of geometric fit between proteins and their ligands by correlation techniques." *Proc. Natl. Acad. Sci. USA*, **89** 2195-2199.

Kelley, L.A., Gardner, S.P. and Sutcliffe, M.J. (1996) "An automated approach for clustering an ensemble of NMR- derived protein structures into conformationally-related subfamilies.", *Protein Engineering*, **9**, 1063-1065.

Kemmink, J., and Creighton, T.E. (1995) "Effects of trifluoroethanol on the conformations of peptides representing the entire sequence of bovine pancreatic trypsin-inhibitor" *Biochem.*, **34**, 12630-12635.

Kerr, I.D., Sankararamakrishnan, R., Smart, O.S., and Sansom, M.S.P. (1994) "Parallel helix bundles and ion channels - molecular modelling via simulated annealing and restrained molecular dynamics." *Biophys. J.*, **67**, 1501-1515.

Kerr, I.D., Doak, D.G., Sankararamakrishnan, R., Breed, J., and Sansom, M.S.P. (1996)"Molecular modelling of Staphylococcal delta-toxin ion channels by restrained molecular dynamics." *Prot. Eng.*, **9**, 161-171.

Kahn, T.W. and Engelman, D.M. (1992) "Bacteriorhodopsin can be refolded from two independently stable transmembrane helices and the complementary five-helix fragment." *Biochem.*, **31**, 6144-6151.

Ketchem, R.R., Roux, B., and Cross, T.A. (1997) "High-resolution polypeptide structure in a lamellar phase lipid environment from solid state NMR derived orientational constraints." *Struct.*,.**5**, 1655-1669.

Kihara, H., and Siraganian, R.P., (1994) "Src homology-2 domains of syk and lyn bind to tyrosine- phosphorylated subunits of the high-affinity IgE receptor." *J. Biol. Chem.*, **269**, 22427-22432.

Kinet, J.P. (1990) "The high-affinity receptor for IgE." *Curr. Opin. Immun.*, **2**, 499-505.

King, R.D., Saqi. M., Sayle, R., and Sternberg, M.J.E. (1997) "Identification and application of the concepts important for accurate and reliable protein secondary structure prediction." *Computer Applications in the Biosciences*, **13**, 473- 474.

Kirkpatrik, S., Gellat, C.D., and Vecchi, M.P. (1983) "Optimization by simulated annealing." *Science*, **220**, 671-680.

Knegtel, M.A.,Knutz, I.D., and Oshire, C.M. (1997) " Molecular docking to ensembles of protein structures." *J. Mol. Biol.*, **266**, 424-440.

Kreusch, A., Neubüser, A., Schiltz, W., Wekesser, J., and Schulz, G.E. (1994) "The structure of the membrane channel porin from Rhodopseudomonas blastica at 2.0 Å resolution." *Protein Science*, **3**, 58-63.

Kristiansen, K., Edvardsen, O., and Dahl, S.G. (1993) "Molecular modelling of ketansterin and its interaction with the 5-HT_2 receptor." *Med. Chem. Res.*, **3**, 370-385.

Kristiansen, K., and Dahl, S.G., (1996) "Molecular modelling of seratonin, ketansterin, ritanserin and their and its interaction with the 5-HT_{2c} receptor." *E. J. Pharmacol.*, **306**, 195-210.

Kumar, A., Ernst, R. R., and Wüthrich, K. (1980) "A two-dimensional nuclear Overhauser enhancement (2D NOE) experiment for the elucidation of complete proton-proton cross-relaxation networks in biological macromolecules." *Biochem. Biophys. Res. Commun.* **95**, 1-6.

Kumashiro, K.K., SchmidtRohr, K., Murphy, O.J., Ouellette, K.L., Cramer, W.A. and Thompson, L.K. (1998) "A novel tool for probing membrane protein structure: Solid-state NMR with proton spin diffusion and X-nucleus detection." *J. Amer. Chem. Soc.*, **120**, 5043-5051.

Kuntz. I.D., Blanley, J.M.,Oatley, S.J., Langridge, R.L., and Ferrinn, T.E. (1982) "A geometric approach to macromolecule-ligand interactions." *J. Mol. Biol.*, **161**, 269-288.

Kuster, H., Thompson, H., and Kinet, J-P. (1990) "Characterization and expression of the gene for the human Fc receptor-gamma subunit - definition of a new gene family." *J. Biolog. Chem.*, **265**, 6448-6452.

Kuo, M. and Gibbons, W.A. (1979) "Total assignments, including four aromatic residues, of the decapeptide tyrocidin A using difference double resonance." *J. Biol. Chem.*, **254**, 6278-6287.

Kühlbrandt, W., and Wang, D.N. (1991) "Three-dimensional structure of plant light-harvesting complex determined by electron crystallography." *Nature*, **350**, 130-134.

Kühlbrandt, W., Wang, D.N. and Fujiyoshi, Y. (1994) "Atomic model of plant light-harvesting complex by electron crystallography." *Nature*, **367**,: 614-621.

Labadia, M.E., Jakes, S., Grygon, C.A., Greenwood, D.J., Schrembri-King, J. Lukas, S.M., warren, T.C., and Ingreaham, R.H. (1997) "Interaction between SH2 domains of ZAP-70 and the tyrosine-based activation motif 1 sequence of the ζ subunit of the T-Cell receptor." *Arch. Biochem. Biophys.*, **342**, 117-125.

Lau, F.W., and Bowie, J.U. (1997)"A method for assessing the stability of a membrane protein." *Biochem.*, **36**, 5884-5892 .

Levitt, M. (1982. "Protein conformation, dynamics, and folding by computer simulation." *Ann. Rev. Biophys. Bioeng.*, **11**, 251-271.

Lemmon, M.A., Flanagan, J.M., Treutlein, H.R., Zhang, J., and Engelman, D.M. (1992) "Sequence specificity in the dimerisation of transmembrane α-helices." *Biochem.*, **31,** 12719-12725.

Lemmon, M.A., Treutlein, H.R., Adams, P.D., Brünger, A.T., and Engleman, D.M.(1994) "A dimerization motif for transmembrane alpha-helices." *Nature Structural Biology*, **1**, 157-163.

Levin et al., Robson, B., and Garnier, J. (1986) "An algorithm for secondary structure determination in proteins based on sequence similarity." *Febs Lett.*, **205**, 303-308.

Lewis, R.A., and Austen, K.F. (1981) "Mediation of local homeostasis and inflammation by leukotrienes and other mast cell-dependent compaunds." *Nature*, **293**, 103-108.

Lichtenstein, L.M., (1993) "Allergy and the immune-system." *Scien. Amer.*, **269**, 85-93.

Li, H.L., Sui, H.X., Ghanshani, S., Lee, S., Wallan, P.J., Wu, C.L., Chandy, K.G., and Jap, B.K. (1998) "Two-dimensional crystallization and projection structure of KcsA potassium channel." *J. Mol. Biol.*, **282**, 211-216.

Li, W., Deanin, G. G., Margolis, B., Schlessinger, J., and Oliver, J. M. (1992) "FC-epsilon-R1-mediated tyrosine phosphorylation of multiple proteins, including phospholipase c-gamma-1 and the receptor beta-gamma-2 complex, in RBL-2H3 rat basophilic leukemia-cells." *Mol. Cell. Biol.*, **12**, 3176-3182.

Lim, V.I. (1974) "Algorithms for prediction of α-helical and β-structural regions in globular proteins." *J. Mol. Biol.*, **88**, 873-894.

Lin S.L., Tsai, C.J., and Nussinov, R. (1995) "A study of four helix bundles: investigating protein folding via similar architectural motifs in protein cores and in subunit interfaces." *J. Mol. Biol.*, **248**, 151-161.

Liu, Y., Zhao, D.Q., Altman, R., and Jardetzky, O. (1992) " A systematic comparison of 3D structure determination methods from NMR data - dependence upon quality and quantity of data." *J. Biomol. NMR*, **2**, 373-388.

Lomize, A.L., Pervushkin, K.V., and Arseniev, A.S. (1992) "Spatial structure of (34-65) bacterioopsin polypeptide in SDS micelles determined from nuclear magnetic resonance data." *J. Biol. NMR*, **2**, 361-372.

Loncharich, R.J., and Brooks, B.R., (1989) "The effects of truncating long-range forces on protein dynamics." *Proteins: Structure, Function and Genetics*, **6**, 32-45.

Lovy, D. (1994-1996) WinDig, v. 2.50.

Manavalan, P., and Johnson, W. C., Jr. (1983) "Sensitivity of circular dichroism to protein tertiary structure class." *Nature*, **305**, 831-832.

Manavalan, P., and Johnson, W. C., Jr. (1987) " Variable selection method improves the prediction of protein secondary structure from circular-dichroism spectra." *Anal. Biochem.*, **167**, 76-85.

Manning, M.C. and Woody, R.W. (1989) "Theoretical-study of the contribution of aromatic side-chains to the circular-dichroism of basic bovine pancreatic trypsin-inhibitor." *Biochem.*, **28**, 8609-8613.

Marsh, D., (1993) in "Protein Lipid Interactions", (Neuberger, A. and van Deenen, L.L.M., Eds.) Elsevier, Amsterdam.

McCammon, J.A., Harvey, S.C. (1987). "Dynamics of Proteins and Nucleic Acids.". Cambridge University Press, Camb.

McDonnell, J.M., Beavil, A.J., Mackay, G.A., Jameson, B.A., Korngold, R., Gould, H.J., and Sutton, B.J. (1996) "Structure based design and characterisation of peptides that inhibit IgE binding to its high-affinity IgE receptor." *Nature Struc. Biol.*, **3**, 419-426.

McDonnell, J.M., Fushman, D., Cahill, S.M., Sutton, B.J., and Cowburn, D., (1997) "Solution structures of FcεRI α-chain mimics: A β-hairpin peptide and its retroenantiomers" *J. Am. Chem. Soc.*, **119**, 5321-5328.

Menon, A. K., Holowka, D., Webb, W. W., and Baird, B. (1986a) "Clustering, mobility and triggering activity of small oligomers of Immunoglobulin E on rat basophilic leukemia cells." *J. Cell. Biol.*, **102**, 534-540.

Menon, A. K., Holowka, D., Webb, W. W., and Baird, B. (1986b) "Cross linking ofreceptor-bound IgE to aggregates larger than dimer leads to rapid immobilization." *J. Cell. Biol.*, **102**, 541-555.

Metcalfe, D. D., Costa, J. J., and Bard, P. R. (1992) in "Inflammation: Basic Principles and Clinical Correlates" (Gallin, J. I., Goldstein, I. M., and Snyderman, R., Eds) pp 709-725, Raven Press, New York.

Millard, P. J., Ryan, T. A., Webb, W. W., and Fewtrell, C. (1989) "Immunoglobulin-E receptor cross-linking induces oscillations in intracellular free ionized calcium in individual tumor mast-cells." *J. Biol. Chem.*, **264**, 19730-19739.

Mingarro, I., Elofsson, A., and von Heijne, G. (1997) "Helix-helix packing in a membrane-like environment." *J. Mol. Biol.*, **272**,633-641

Musco, G., Tziatzios, C., Schuck, P. and Pastore, A. (1995) "Dissecting titin into its structural motifs - identification of an alpha-helix motif near the titin N-terminus." *Biochem.*, **34**, 553-561.

Molecular Simulations Inc (1998) " WebLab Viewer Lite, 3.10".

Nilges, M., Gronenborn, A.M., Brunger, A.T., and Clore, G.M. (1988a) "Determination of three-dimensional structures of proteins by simulated annealing with interproton distance restraints. Application to crambin, potato carboxypeptidase inhibitor and barley serine proteinase inhibitor 2." *Protein Engineering*, **2**, 27-38.

Nilges, M., Clore, G.M., and Gronenborn, A.M. (1988b) "Determination of three-dimensional structures of proteins from interproton distance data by dynamical simulated annealing from a random array of atoms." *FEBS Lett.*, **239**, 129-136.

Nilges, M., and Brunger, A.T., (1991) "Automated modelling of coiled coils: application to the GCN4 dimerazition region." *Prot. Eng.*, **4**, 649-659.

Nilges, M. (1995) "Calculation of protein structures with ambiguous distance restraints-automated assignment of ambiguous NOE crosspeaks and disulfide connectivities." *J. Mol. Biol.* **245**, 645-660.

Offer, G., and Sessions, R., (1995) "Computer modelling of the alpha-helical coiled-coil - packing of side-chains in the inner-core." *J. Mol. Biol.*, **249**, 967-987.

Oas, G.T., and Endow, S.A., (1994) "Spring and hinges: dynamic coiled coils and discontinuities." TIBS, **19**, 51-54.

O'Shea, E.K., Klemm, J.D., Kim, P.S., and Alber, T. (1991) "X-ray structure of GCN4 leucine zipper, a two stranded, parallel coiled coil." *Science*, **254**, 539-544.

Ozawa, K., Szallasi, Z., Kazanietz, M.G., Blumberg, P.M., Mischak, H., Mushinski, J.F., and Beaven, M. A. (1993) "Ca2+-dependent and Ca2+-independent isozymes of protein-kinase-C mediated exocytosis in antigen-stimulated rat basophilic RBL-2H3 cells - reconstitution of secretory responses with Ca2+ and purified isozymes in washed permeabilized cells." *J. Biol. Chem.*, **268,** 1749-1756.

Padlan, E.A., and Davies, D.R. (1986) "A model of the Fc of immunoglobulin-E." *Mol. Immunol.*, **23**, 1063-1075.

Padlan, E.A., and Helm, B.A. (1993) "Modelling study of IgE/receptor interactions." *Biochem. Soc. Trans.*, **31**, 963-967.

Paolini, R., Jouvin, M-H., and Kinet, J-P. (1991) "Phosphorylation and dephosphorylation of the high-affinity receptor for immunoglobulin-E immediately after receptor engagement and disengagement." *Nature*, **353**, 855-858.

Paolini, R., and Kinet, J. P. (1993) "Cell-surface control of the multiubiquitination and deubiquitination of high-affinity immunoglobulin-E receptors" *EMBO J.* **12**, 779-786.

Pinto, L.H., Holsinger, L.J., Lamb, R.A. (1992) "Influenza virus M2 protein has ion channel activity." *Cell,* **69**, 517-528.

Popot, J.-L., and Engleman, D.M. (1990) "Membrane protein folding and oligomerization - the 2-stage model." *Biochem.*, **29**, 4031-4037.

Popot, J.-L., De Vitry, C., and Atteia, A., (1994) in "Membrane Protein Structure" (White, S.H., Ed.), 41-96, Oxford University Press, Oxford.

Presnell, S.R., Cohen, F.E. (1989) "Topological distribution of four-α-helix bundles." *Proc. Natl. Acad. Sci.*, **86**, 6592-6596.

Provencher, S., and Glockner, J. (1981) "Estimation of globular protein secondary structure from circular dichroism." *Biochem.*, **20**, 33-37.

Prusis, P., Schioth, H.B., Muceniece, R., Herzyk, P., Afshar, M, Hubbard, R.E., and Wikberg, J.E.S. (1997) "Modelling of the three-dimensional structure of the human melanocortin 1 receptor, using an automated method and docking of a rigid cyclic melanocyte-stimulating hormone core peptide." *J. Mol. Graph. & Model.*, **15**, 307-319.

Rance, M., Sørensen, O. W., Bodenhausen, G., Wagner, G., Ernst, R. R., and Wüthrich, K. (1983) "Improved spectral resolution in COSY 1H NMR spectra of proteins via double quantum filtering." *Biochem. Biophys. Res. Commun.*, **117**, 479-485.

Ranatunga, K.M., Kerr, I.D., Adcock, C., Smith, G.R., and Sansom, M.S.P. (1998) "Protein-water ion interactions in a model of the pore domain of a potassium channel: a simulation study." *Biochim. Biophys. Acta-Biomembranes,* **1370**, 1-7.

van Rhee, A.M., Fischer, B., and Jacobson, K.A. (1995) "Molecular probes for muscarinic receptors - functionalized congeners of selective muscarinic antagonists." *Drug Design Discovery,* **13**, 133-154.

Rarey, M., Kramer, B., Lengauer, T., and Klebe, G. (1996) "A fast flexible docking method using an incremental construction algorithm." *J. Mol. Biol.*, **261**, 470-489.

Reddy, B.V.B., Blundell, T.L. (1993) "Packing of secondary structural elements in proteins. Analysis and prediction of inter-helix distances." *J. Mol. Biol.*, **233**, 464-479.

Rees, D.C., Chirino, A.J., Kim, K.H., and Komiya, H., (1994) "The nature of the membrane protein structure problem" in "Membrane Protein Structure" (White, S.H., Ed.), 3-26, Oxford University Press, Oxford.

Rees, D.C., DeAntionio, L. and Eisenberg, D. (1989) "Hydrophobic organization of membrane-proteins." *Science*, **245**, 510-513.

Reth, M., (1989) "Antigen receptor tail clue." *Nature*, **338**, 383-384.

Rigby, A.C., Grant, C.W.M., and Shaw, G.S. (1998) "Solution and solid state conformation of the human EGF receptor transmembrane region." *Biochim. Biophys. Acta-Miomemb.*, **1371**, 241-253.

Rivnay, B., Wank, S.A. Poy, G. and Metzger, H. (1982) "Phospholipids stabilize the interaction between the alpha-subunit and beta-subunit of the solubilized receptor for immunoglobulin-E." *Biochem.*, **21**, 6922-6927.

Rooman, M.J., Woodak, S.J. and Thornton, J.M. (1989) "Amino-acid sequence templates derived from recurrent turn motifs in proteins - critical evaluation of their predictive power." *Protein Engineering*, **3**, 23-27.

Rost, B., and Sander, C. (1993) "Prediction of protein secondary structure at better than 70-percent accuracy." *J. Mol. Biol.*, **232**, 584-599.

Rost, B., and Sander, C. (1994) "Combining evolutionary information and neural networks to predict protein secondary structure." *Proteins-Structure Function And Genetics*, **19**, 55-72.

Samatey, F.A., Zaccai, G., Engelman, D.M., Etchebest, C., and Popot, J-L. (1994) "Rotational orientation of transmembrane helices in bacteriorhodopsin. A neutron diffraction study." *J. Mol. Biol.*, **236**, 1093-1104.

Samso,M., and Wagenknecht, T. (1998) "Contributions of electron microscopy and single-particle techniques to the determination of the ryanodine receptor three-dimensional structure." *J. Struc. Biol.*, **121**, 172-180.

Sankararamakrishnan, R., and Sansom, M.S.P. (1994) " Kinked structures of isolated nicotinic receptor M2 helices - a molecular-dynamics study." *Biopol.*, **34**, 1647-1657.

Sansom, M.S.P., Adcock, C., and Smith, G.R. (1998) " Modelling and simulation of ion channels: Applications to the nicotinic acetylcholine receptor." *J. Struct. Biol.*, **121**, 246-262.

Saudek, V., Pastore, A., Castiglione, M.A., Frank, R., Gausepohl, H., Gibson, T., Weih, F., and Roesch, P. (1990) "Solution structure of the DNA-binding domain of the yeast transcriptional activator protein GCN4 " *Protein Eng.*, **4**, 3-10.

Sayle, R. (1992-1995) Rasmol Version 2.6b2, Glaxo Wellcome Research and Development Stevenage, Hertfordshire, U.K.

Schetler, G.F.X., Villa, C., and Henderson, R. (1993) " Projection structure of rhodopsin." *Nature*, **362**, 770-772.

Schiffer, M., Chang, C.-H. and Stevens, F.J., (1992) "The functions of tryptophan residues in membrane-proteins." *Prot. Eng.*, **5**, 213-214.

Schultz, G.E., and Schrimmer, R.H. (1979) "Principles of protein structure" Spinger-Verlag, New York.

Shiraki, K., Nishikawa, K., and Goto, Y. (1995) "Trifluoroethanol-induced stabilization of the alpha-helical structure of beta-lactoglobulin - implication for non-hierarchical protein-folding." *J. Mol. Biol.*, **245**, 180-194.

Siligardi, G., Drake, A.F., Mascagni, P., Rowlands, D., Brown, F. and Gibbons, W.A. (1991) "Correlations between the conformations elucidated by CD spectroscopy and the antigenic properties of 4 peptides of the foot-and-mouth- disease virus." *Eur.J.Biochem.*, **199**, 545-551.

Siligardi, G., Samori, B., Melandri, S., Visconti and Drake, A.F. (1994) "Correlations between biological-activities and conformational properties for human, salmon, eel, porcine calcitonins and elcatonin elucidated by CD spectroscopy." *Eur.J.Biochem.*, **221**, 1117-1125.

Sodek, J., Hodges, R.S., Smillie, L.B., and Jurasek, L., (1972) "Amino acid sequence of rabbit skeletal tropomyosin and its coiled-coil structure." *Proc. Natl. Acad. Sci.*, **69**, 3800-3804.

Sreerama, N., and Woody, R. W. (1994) "Poly(Pro)II helices in globular-proteins - identification and circular dichroic analysis." *Biochem.*, **33**, 10022-10025.

Stern, A., Gibbons, W.A., and Craig, L. (1968) "A conformational analysis of gramicidin S-A by nuclear magnetic resonance." *Proc. Natl. Acad. Sci.*, **61**, 734-741.

von Stosch, A.G., Jimenez, M.A., Kinzel, V., and Reed J., (1995) "Solvent polarity-dependent structural refolding - a CD and NMR-study of a 15 residue peptide." *Prot: Struc. Func. and Gen.*, **23**, 19-203.

Street, I.P., Armstrong, C.R., and Withers, S.G. (1986) "Hydrogen-bonding and specificity - fluorodeoxy sugars as probes of hydrogen-bonding in the glycogen-phosphorylase glucose complex." *Biochem.*, **25**, 6021-6027.

Sutton B.J., and Gould, H.J. (1993) "The human IgE network." *Nature*, **366**, 421-428.

Sybyl 6.0A, 6.2, 6.3, 6.4 *Tripos Association inc.* 1993-1997.

Sylte, I., Edvardsen, Ø., and Dahl, S.G., (1993) "Molecular-dynamics of the 5-HT(1a) receptor and ligands." *Prot. Eng.*, **6**, 691-700.

Sylte, I., Edvardsen, Ø., and Dahl, S.G., (1993) "Molecular modeling of UH-301 and 5-HT1a receptor interactions." *Prot. Eng.*, **9**, 149-160.

Taylor, W.R., Jones, D.T. and Green, N.M., (1994) "A method for alpha-helical integral membrane-protein fold prediction." *Proteins: Structure, Function and Genetics,* **18**, 281-294.

Tedder, T.F. Klejman, G., Disteche, C.M., Adler, D.A., Schlossman, S.F. and Saito, H. (1988) " Cloning of a complementary-DNA encoding a new mouse lymphocyte-B differentiation antigen, homologous to the human B1 (CD20) antigen, and localization of the gene to chromosome-19."*J. Immun.*, **141**, 4388-4394.

Treutlein, .R., Lemmon, M.A., Engelman, D.M., and Brunger, A.T., (1992) "The glycophorin A transmembrane domain dimer: Sequence specific propensity for a right-handed supercoil of helices." *Biochem.*, **31**, 12726-12733.

Thomas, R.C., Anderson, G.J., Toth, I., Zloh, M., Ashton, D. and Gibbons, W.A. (1993) in "Conformational analysis of peptides from the high affinity receptor for IgE." *Proceedings of the 13th American Peptide Symposium*, 785-787.

Unwin, N. (1993) "Nicotinic acetylcholine receptor at 9Å resolution." *J. Mol. Biol.*, **229**, 1101-1124.

Vakser, I.A., and Afalo, C. (1994) "Hydrophobic docking - a proposed enhancement to molecular recognition techniques." *Prot.: Struc. Func. and Gen.*, **20**, 320-329.

Vakser, I.A. (1995a) "Protein docking for low-resolution structures." *Prot. Eng.*, **8**, 371-377.

Vakser, I.A. (1995b) "Long-distance potentials - an approach to the multiple-minima problem in ligand-receptor interaction." *Prot. Eng.*, **9**, 37-41.

Vakser, I.A. (1996) "Low-resolution docking - prediction of complexes for underdetermined structures." *Biopol.*, **39**, 455-464.

Verlet, L. (1967) "Computer experiments on clasical fluids. 1. Thermodynamical properties of Lennard-Jones molecules" *Phys. Rev.*, **159**, 98-103.

Wallace, B.A., and Janes, R.W. (1991) "Co-crystals of gramicidin-A and phospholipid - a system for studying the structure of a transmembrane channel." *J .Mol. Biol.*, **217**, 625-627.

Walther D. (1997) "WebMol - a Java based PDB viewer." *Trends Biochem Sci*, **22**, 274-275.

Wang, J. and Pullman, A., (1991) " Do helices in membranes prefer to form bundles or stay dispersed in the lipid phase?" *Biochim. Biophys. Acta*, **1070**, 493-406.

Wang, J.X., Balazs, Y.S., Thompson, L.K. (1997) "Solid-state REDOR NMR distance measurements at the ligand site of a bacterial chemotaxis membrane receptor." *Biochem.*, **36**, 1699-1703.

Weber, P.C., and Salleme, F.R. (1980) "Structural and functional diversity in 4-α-helical proteins." *Nature*, **287**, 82-84.

Weiner, M.C., and White, S.H. (1992) "Structure of fluid dioleoylphosphatidylcholine bilayer determined by joint refinement of X-ray and neutron diffraction data. III." *Biophys. J.*, **61**, 379-382.

Weiss, M.S., Abele, U., Weckesser, J., Welte, J., Schiltz, E., and Schulz, G.E., (1991) "Molecular architecture and electrostatic properties of a bacterial porin." *Science*, **254**, 1627-1630.

White, S.H., and Wimley, W.C. (1994) "Peptides in lipid bilayers - structural and thermodynamic basis for partitioning and folding." *Current Opinion in Structural Biology*, **4**, 79-86.

White, K. N., and Metzger, H. (1988)"Translocation of protein kinase-c in rat basophilic leukemic-cells induced by phorbol ester or by aggregation of IgE receptors." *J. Immunol.* **141**, 942-947.

Williamson, P.T.F., Grobner, G., Spooner, P.J.R., Miller, K.W., and Watts, A. (1998) "Probing the agonist binding pocket in the nicotinic acetylcholine receptor: A high-resolution solid-state NMR approach." *Biochem.*, **37**, 10854-10859.

Wishart, D.S., Sykes, B.D., and Richards, F.M. (1992) "The chemical shift index - a fast and simple method for the assignment of protein secondary structure through NMR-spectroscopy." *Biochem.*, **31**, 1647-1651.

Woody, R. W. (1991) *Adv. Phys. Chem.*, **2**, 1.

Woody, R. W. (1995) "Circular Dichroism" *Methods. Enzymol.* 246, 34-71.

Woolf, T.B. (1997) "Molecular dynamics of individual alpha-helices of bacteriorhodopsin in dimyristoyl phosphatidylcholine. 1. Structure and dynamics." *Biophys. J.*, **73**, 2376-2392.

Wüthrich, K., Wider, G., Wagner, G., and Braun, W. (1982) "Sequential resonance assignments as a basis for determination of spatial protein structures by high resolution nuclear magnetic resonance." *J. Mol. Biol.*, **155**, 311-319.

Wüthrich,, K. in 'NMR of the Proteins and Nucleic Acids', Wiley, New York, 1986.

Xing, J. and Scott, H.L. (1992) "Monte-Carlo studies of a model for lipid-gramicidin-A bilayers." *Biochim. Biophys. Acta*, **1106**, 227-232.

Yeagle, P.L., Alderfer, J.L., and Albert, A.D. (1995) "Structure of the 3rd cytoplasmic loop of bovine Rhodopsin." *Biochem.*, **34**, 14621-14625.

Yeagle, P.L., Alderfer, J.L., Salloum, A.C., Ali, L. and Albert, A.D. (1997) "The first and second cytoplasmic loops of the G-protein receptor, rhodopsin, independently form beta-turns." *Biochem.*, 36, 3864-3869.

Yeagle, P.L., Alderfer, J.L., and Albert, A.D. (1998) "The three dimensional structure of the G protein receptor, rhodopsin: the structures of the extracellular domains." *Biophys. J.*, **74**, A290

Zloh, M., Anderson, G.J., Clark-Lewis, I., Nicolaou, A., Thomas, R.C., Toth, I. and Gibbons, W.A. "Spectroscopic and conformational studies of the C-terminal cytoplasmic beta subunit 46-peptide of the high affinity IgE receptor." (1994a) *Biochem. Soc. Trans.*, **22**, 450S.

Zloh, M., Anderson, G.J., Clark-Lewis, I., Thomas, R.C., Toth, I. and Gibbons, W.A. "N.M.R. studies of the cytoplasmic C-terminal β-subunit domain of the high affinity IgE receptor." (1994b) *Biochem. Soc. Trans.*, **22**, 1027-1029.

Zloh, M., Anderson, G., Clark-Lewis, I., Thomas, R., Toth, I. and Gibbons, W.A. (1997) "NMR-based modelling revealed an alpha helical structure for cytoplasmic domain of the

alpha subunit of FcεRI, the high affinity IgE receptor. " *Biochem. Soc. Trans.*, **22**, 1027-1029.

Zloh, M., Biekofsky, R.R., Duret, J.-A., Danton, M. and Gibbons, W.A. (1995) "Conformational studies of the β-subunit of the high affinity IgE receptor: Circular dichroism and molecular modelling." *Biomedical Peptides, Proteins and Nucleic Acids*, **1**, 101-108.

Zloh, M. and Gibbons, W.A. (1996) "Lipid-helix interactions in membrane receptor." *Biochem. Soc. Trans.*, **24**, 305S.

Zloh, M., Thomas, R., Reid, R.E. and Gibbons W.A. (1997) "NMR-Based Modelling Revealed an Alpha Helical Structure for Cytoplasmic Domain of the Alpha Subunit of FcεRI, the High Affinity IgE Receptor" *Biochem. Soc. Trans.*, **25**, 55S.

Zloh, M., Esposito, D. and Gibbons, W.A. (1998) "NMR studies of the extracellular loop of the beta subunit of the high affinity IgE receptor." *Biochem.*, **26**, S34.

Zhou, N.E., Kay, C.M., and Hodges, R.S. (1992) "Synthetic model proteins: The relative contribution of leucine residues at the nonequivalent positions of 3-4 hydrophobic repeat to the stability of t the two-stranded a-helical coiled-coil." *Biochem.*, **31**, 5739-5746.

Appendix 1.

Protein structure prediction

Appendix 1. Protein prediction

A.1.1 Background

The prediction of the protein structure is part of the general protein folding problem. It is most general method of obtaining some structural information from the protein sequence. There exist a wide variety of methods for the predicting of secondary structure, but those methods could be roughly divided into statistical, knowledge-based and hybrid systems. Statistical methods are based in the studies of the database of proteins of known primary and secondary structure. They are finding the empirical relationship between two types of structure. The amount of the of available data is very important for statistical predication methods for the globular proteins (Chou Fasman, GOR, neural networks.). The transmembrane proteins can not be studied, since the number of membrane proteins with known structure is small for reliable statistical analysis.

Physico-chemical methods are based on the knowledge about the physical and chemical basis of the protein structure. Important structural features have been recognised to be useful in predicting the protein structure, like helical wheels, hydrophobicity profiles [Lim, 1974].

A neural net learning system is a network of non-linear processing units that have adjustable connection strengths. All work on the secondary structure predictions has been based on the feed-forward networks, using back-propagation learning rule. Learning consists of altering the wigths of connections between the units in response to a teaching signal which provides information about correct classification in input terms (primary and

secondary structure). The goal is to find a good input-output mapping which can then be applied for the prediction of the test set. Some methods are using the homology information, comparing analyzed sequence with proteins that secondary structure is known [King et al., 1997].

As there is as yet no clear best prediction method, especially for the membrane protein domains, it is sensible to apply a few different prediction methods to AA sequence. Regions where the prediction methods agree are more likely to be correctly predicted than other areas.

A.1.2 Cytoplasmic N-terminal tail of the β-subunit of FcεRI

The N-terminal domain of the β-subunit is located in the cytoplasm of the cell according to the proposed topography by Blank et al., 1989. The sequence together with the results of the secondary structure predictions are listed in Table A.1.1. It is a proline rich sequence. The methods used to obtain the consesus of predicted secondary structure had used different approaches that were mentioned above.

The consesus sequence predicted the α-helical structure for the A9-D10-L11-A12-; I25-E26-L27-L28; and Q51-S52-F53-L54-K55-K56-E57-L58-E59-F60-L61-G62. The molecular model of the peptide with N-terminal sequence was built based on the predicted structure and it was incorporated into the models of the β-subunit of FcεRI.

A.1.3 Cytoplasmic C-terminal tail of the β-subunit of FcεRI

The C-terminal tail of the β-subunit is located in the cytoplasm of the cell according to the proposed topography by Blank et al., 1989. The peptide with sequence of this domain was synthesized and the solvent titration from water to TFE was followed by CD. The structure

in TFE contained the alpha helix structure [Zloh et al., 1994a; Zloh et al; 1994b]. The sequence together with the results of the secondary structure predictions are listed in Table A.1.3. The methods used to obtain the consesus of predicted secondary structure had used different approaches that were mentioned above.

The consesus sequence predicted the α-helical structure for the Q205-E206-F207; R216-L217-Y218-E219-E220-L221-H222; I227-Y228-S229-A230-L231-E232-D233-T234-R235-E236 and β-sheet for the I200-Y201-R202-I203.The molecular model of the peptide with C-terminal sequence was built based on the predicted structure and it was incorporated into the models of the β-subunit of FcεRI.

Table A.1.1 The secondary structure prediction of the N-terminal cytoplasmic tail of the β-subunit of FcεRI. Methods used were: Gibrat - Gibrat et al., 1987; Levin - Levin et al., 1986; DPM -Deleage & Roux, 1987; SOPMA - C. Geourjon & G. Deleage, 1995; PhD - Rost & Sander, (1994); DSC - King et al., 1997. Secondary strucutures are denoted as: H - α-helix; E - β-sheet; T - β-turn; C - random coil.

Sequence / Method	1 10 20 30 40 50 60 MDTENKSRADLALPNPQESPSAPDIELLEASPPAKALPEKPASPPPQQTWQSFLKKELEFLG
Gibrat	HCHHHHHHHHHHCCCCCCCCCCCCHHHHHHHHCCHHHHCCCCCCCCCCCCHHHHHHHHHHHHHHHH
Levin	CCCCCCSSCEECCCCCCCCCCCCCCCEEECCCCCCTCCCCCCCCCCCCCCHHHHHHHHHHHTT
DPM	CCCHTCCHHHHHHCTTCCTCCCCCHHHHHHCCCHHHHCCCCCTCCCCCCCHHHHHHHHHHCC
SOPMA	CCCCCCCCEEEECCCCCCCCCCCCCEEEECCCCCCCCCCCCCCCCCCCCCCCHHHHHHHHHHHC
PHD	EE HHHHHHHHHHHH
DSC	HHHHHHHHHC
Concesus	CCCCCCCCHHHHCCCCCCCCCCCCCHHHHCCCCCCHCCCCCCCCCCCCCCCCHHHHHHHHHHHH

Table A.1.2 The secondary structure prediction of the C-terminal cytoplasmic tail of the β-subunit of FcεRI. Methods used were: Gibrat - Gibrat et al., 1987; Levin - Levin et al., 1986; DPM -Deleage & Roux, 1987; SOPMA - C. Geourjon & G. Deleage, 1995; PhD - Rost & Sander, (1994); DSC - King et al., 1997. Secondary strucutures are denoted as: H - α-helix; E - β-sheet; T - β-turn; C - random coil.

Sequence / Method	200 210 220 230 240 LIIYRIGQEFERSKVPDDRLYEELHVYSPIYSALEDTREASAPVVS
Gibrat	EEEEEECCCCCCCCCCCCHHHHHHEECCCCECEHHHHHHHCCCEEE
Levin	CCCHHHHHHHHTTSCCCTCCETTCCECCCHHHTHHHHHHTHCCCEH
DPM	CCEEEECHHHHHCCCCCCHHHHHHHEECCECCHHHHHHHHHHCECC
SOPMA	EEEEEEHHHHCCCCCCCCHHHHHHHHHCCHHHHHCCCCCCCCCEEE
PHD	EEEEEE EE HHHHHHHHH E
DSC	CCCCCCCHHHCCCCCCCCCCHHEEEECCCCCCCCCCCCCCCCCCC
Concesus	CCEEEECHHHCCCCCCCCHHHHHHHECCCHHCHHHHHHHHCCCEEE

A.1.3 Extracellular loop 3-4 of the β-subunit of FcεRI

The loop 3-4 of the β-subunit is located outside of the cell according to the proposed topography by Blank et al., 1989. The peptide with sequence of this domain was synthesized and the preliminary CD data indicated the presence of an alpha helix structure [Zloh et al., 1995]. The sequence together with the results of the secondary structure predictions are listed in Table A.1.3. The methods used to obtain the consesus of predicted secondary structure had used different approaches that were mentioned above.

The consesus sequence predicted the α-helical structure for the residues Y158-M159-N160-Y161-C162-K163 and β-sheet for F172-V173-T174-S175-F176-I177-T178. The molecular model of the peptide with loop 3-4 sequence was built based on the predicted structure and it was incorporated into the models of the β-subunit of FcεRI.

Table A.1.3 The secondary structure prediction of the extracellular loop 3-4 of the β-subunit of FcεRI. Methods used were: Levin - Levin et al., 1986; DPM -Deleage & Roux, 1987; SOPMA - C. Geourjon & G. Deleage, 1995. Secondary strucutures are denoted as: H - α-helix; E - β-sheet; T - β-turn; C - random coil; ? - unassigned.

Sequence / Method	151 160 170 180 | | | | NLSNNSAYMNYCKDITEDDGCFVTSFITE
Levin	CCCSCCHHHHHHHHCHTTTSCEEEEEEES
DPM	CTTTTCCCHTCCHCECTTTCCEEEEEECC
SOPMA	ECCCCCHHHHHHHCCCCCCCEEEEEEEHC
Concesus	CCCCCC?HHHHHHCCCCCCC?EEEEEEEC

Appendix 2.

Publications resulting from the work in this thesis

Appendix 2. Publications resulting from the work in this thesis

Zloh, M., Esposito, D. and Gibbons, W.A. (1998) " NMR Studies of the Extracellular Loop of the Beta Subunit of the High Affinity IgE Receptor" *Biochemical Society Transactions*, **26**, S34.

Zloh, M., Biekofsky, R.R. , Benedetti, E., Danton, M., Toth, I. and Gibbons, W.A. (1996) "NMR Studies of the 11-residue Cytoplasmic Peptide that Bridges Two Transmembrane Helices of the High Affinity IgE Receptor" *Innovation and Perspectives in Solid Phase Synthesis and Combinatorial Libraries: Peptides, Proteins and Nucleic Acid* (Ed. R. Epton), Mayflower Scientific Limited, Birmingham, 253-257.

Zloh, M. and Gibbons, W.A. (1996) "Lipid-Helix Interactions in Membrane Proteins" *Biochemical Society Transactions*, **24**, 305S.

Zloh, M. and Gibbons, W. A. (1996) "Lipid - Helix Interactions in Membrane Proteins Studied by Molecular Mechanics and Molecular Dynamics Calculations" *Proceedings of 24th EPS Conference* (Ed. R. Epton), Mayflower Scientific Limited, Birmingham, 937-938.

Gibbons, W.A., Anderson, G.J., Reid, R., Toth, G. and M. Zloh (1996) "Progress in Total Conformational Analysis by NMR and Modelling of the 7 Helix Membrane Receptor for

IgE "*Proceedings of 24th EPS Conference* (Ed. R. Epton), Mayflower Scientific Limited, Birmingham, 119-122.

Zloh, M., Biekofsky, R.R., Duret, J.-A., Danton, M. and W.A. Gibbons (1995) "Conformational Studies of the β-subunit of the High Affinity IgE Receptor: Circular Dichroism and Molecular Modelling" *Biomedical Peptides, Proteins & Nucleic Acids*, **1**, 101-106.